

Dissertation

**INFLUENCE OF SURFACE ROUGHNESS ON LEAKAGE OF
THE CORRUGATED METAL GASKET**

(波形金属ガスケットの漏れに及ぼす表面粗さの影響)

DIDIK NURHADIYANTO

**Graduate School of Science and Engineering
Yamaguchi University
Japan**

September 2014

CONTENTS

LIST OF FIGURE	
LIST OF TABLES	
ACKNOWLEDGMENT	
CHAPTER I INTRODUCTION	
1.1. Background	1
1.2. Research Purposes	6
1.3. Outline	10
CHAPTER II BASIC THEORY	
2.1. Asbestos History	12
2.2. Forces Acting on a Gasket Joint	15
2.3. Finite Element Analysis	21
2.4. Taguchi Method	31
2.5. Contact Mechanics Theories	35
2.5.1 Persson Theory for Elastic Contact Mechanics	35
2.5.2 Persson Theory for Elastoplastic Contact Mechanics	37
2.6. Percolation Theory	38
2.7. Contact between Two Rough Surfaces Model	45
2.8. Development of Gasket Asbestos Substitution	49
2.9. Contact Analysis Theory	74
2.10. Boundary Conditions of the Numerical Analysis	77
CHAPTER III OPTIMIZATION OF GASKET BASED ON CONTACT WIDTH CONSIDERING FORMING AND CONTACT STRESS EFFECT	
3.1 Gasket Optimization by Using Taguchi Method	80
3.2 Leakage Test for the 25-A Size Metal Gasket	95
3.2.1 Dies Design Analysis	95
3.2.2 Mold Press	100
3.2.3 Leak Quantity Measurement	102
3.3 Conclusion	109
CHAPTER IV INFLUENCE OF SURFACE ROUGHNESS ON LEAKGE OF THE 25-A SIZE METAL GASKET	
4.1 Surface Roughness Measurement	110
4.2 Simulation Analysis	112
4.2.1 Sinusoidal Model of Surface Roughness	120
4.2.2 Real Model of Surface Roughness	128
4.3 Leak Quantity Measurement	138
4.4 Conclusion	143
CHAPTER V CONTACT WIDTH ANALYSIS OF THE 25-A SIZE METAL GASKET BASED ON SURFACE ROUGHNESS	
5.1 Contact Width Simulation Analysis	145
5.2 Contact Width Experiment Analysis	154
5.2.1 Material and Method	155
5.2.2 Result and Discussion	157

5.3 Contact Area	165
5.4 Conclusion	169
CHAPTER VI DEFORMATION CHARACTERISTICS OF THIN STAINLESS GASKET MATERIAL		
6.1 Material and Method	171
6.1.1 Simulation Analysis	172
6.1.2 Experimental Analysis	173
6.2 Results and Discussion	178
6.3 Conclusion	185
CHAPTER VII CONCLUSION		
7.1. Summary of Results	187
7.2. Future Consideration	188
REFERENCES		

LIST OF FIGURE

Fig. 1.1	High local contact stress on corrugated metal gasket	4
Fig. 1.2	Layout of research step	9
Fig. 2.1	Types of asbestos	12
Fig. 2.2	Annual asbestos import to Japan and asbestos-related diseases in Japan (adapted from [21])	14
Fig. 2.3	Forces acting on a gasket joint (adapted from [22])	16
Fig. 2.4	Types of element (adapted from [23])	22
Fig. 2.5	A 3D body with displacement constraints, body and concentrated forces and surface traction (adapted from [24])	24
Fig. 2.6	(a) 3D state of stress (b) an eight-node hexahedron FE (c) the DOF at a typical node ($i = 1, 2, \dots, 8$) (adapted from [25])	30
Fig. 2.7	(a) axisymmetric state of stress (b) a four-node axisymmetric element and DOF at a typical node ($i = 1, 2, 3, 4$) (adapted from [25])	30
Fig. 2.8	A rubber block (dotted area) in adhesive contact with a hard rough substrate (dashed area) (adapted from [6])	35
Fig. 2.9	Stress distribution in the contact region between a rigid and an elastic substrate at increasing magnification (adapted from [6])	36
Fig. 2.10	Schematic of leakage occurring in a gasket pressed against a flange by a uniform pressure distribution	38
Fig. 2.11	Micro scale contact schematic approximated as square lattice grid	39
Fig. 2.12	Schematic of contact region at different magnifications	40
Fig. 2.13	Flow between parallel plates	41
Fig. 2.14	Pressure distribution of magnification	43
Fig. 2.15	Roughness motifs obtained (adapted from [36])	46
Fig. 2.16	Schematic illustrating indentation of a sinusoidal rough surface (adapted from [35])	48
Fig. 2.17	Construction of sum surface (adapted from [35])	49
Fig. 2.18	Schematic of the modified stub flange joint (adapted from [2])	50
Fig. 2.19	Over 3/4 of the contact between the gasket and the flange is lost (adapted from [32])	50
Fig. 2.20	Helium mass leak rate as a function of gasket stress (adapted from [5])	51
Fig. 2.21	Gasket deflection as a function of gasket stress (adapted from [5])	52
Fig. 3.22	Dimension of the flange and gasket used in the FEA (adapted from [3])	53
Fig. 2.23	Finite element mesh of bolted flange joint with spiral-wound gasket (adapted from [3])	53
Fig. 2.24	Bolted flange connections (left side) and MMC type (right side) flanged Joints (adapted from [4])	54
Fig. 2.25	Assembly situation of gaskets in MMC type flanged joints (schematics) (adapted from [4])	54
Fig. 2.26	Leakage rate of graphite filled spiral wound gasket depends on contact stress (adapted from [4])	55

Fig. 2.27	Leakage rate decreases with increasing gasket effective contact area (adapted from [41])	56
Fig. 2.28	The proposed new 25A size metal gasket appearance	57
Fig. 2.29	Helium leak result in Saeed studied (adapted from [13])	58
Fig. 2.30	Prevent leakage mechanism of the gasket (adapted from [14])	59
Fig. 2.31	Basic dimensions of the gasket (adapted from [14])	60
Fig. 2.32	Contact surface of the gasket (adapted from [14])	62
Fig. 2.33	Relationship between the contact area and contact stress in each axial force (adapted from [14])	63
Fig. 2.34	Basic dimensions of the gasket used in this research (adapted from [15])	64
Fig. 2.35	Schematic section of model	64
Fig. 2.36	Measurement procedure using pressure sensitive paper (adapted from [15])	65
Fig. 2.37	Red patches appeared on pressure sensitive paper after removing load (adapted from [15])	66
Fig. 2.38	Contact width measurement result produced by pressure sensitive paper (adapted from [15])	67
Fig. 2.39	Contact width measurement result produced by MSC.Marc simulation (adapted from [15])	67
Fig. 2.40	Position of convex portion (Adapted from [15])	68
Fig. 2.41	Value of position change every convex portion (Adapted from [15])	68
Fig. 2.42	Initial gasket cross section and design parameter (Adapted from [18])	69
Fig. 2.43	Gasket design with higher slope is choose as optimum design (Adapted from [18])	70
Fig. 2.44	Relationship between contact width and axial force (Adapted from [18])	72
Fig. 2.45	Comparison optimum design number 1 and number 2 (Adapted from [18])	72
Fig. 2.46	Distribution of contact stress at axial force 100 KN (Adapted from [18])	73
Fig. 2.47	Deformable body (Adapted from [39])	74
Fig. 2.48	Contact tolerance (Adapted from [39])	75
Fig. 2.49	Trial displacement with penetration (Adapted from [39])	76
Fig. 2.50	Coulomb friction model (Adapted from [39])	77
Fig. 2.51	Transformed system (2D) (Adapted from [39])	79
Fig. 2.52	Corner conditions (2D) (Adapted from [39])	79
Fig. 3.1	SUS304 stress-strain diagram	81
Fig. 3.2	Dimension of gasket	82
Fig. 3.3	Flow chart the stage of simulation and optimization the gasket	84
Fig. 3.4	Setting-up of gasket material, dies and flange before forming and tightening	85
Fig. 3.5	Forming simulation	85
Fig. 3.6	Tightening simulation	85
Fig. 3.7	Slope of the curve of relationship between contact width and axial force	87
Fig. 3.8	Simulation result of the model number 14	88
Fig. 3.9	Main effects of each factor for various levels at slope of curve	94
Fig. 3.10	Lack of die fills defect result on one of convex contact	96
Fig. 3.11	The changes process of the angle to reduce lack of die fills defect result on one of convex contact	97

Fig. 3.12 Gasket simulation to reduce lack of die fills defect	98
Fig. 3.13 Upper and lower dies design	99
Fig. 3.14 Upper and lower of dies	100
Fig. 3.15 Cold forming process	101
Fig. 3.16 Load for cold forming	102
Fig. 3.17 Photographs of 25-A size metal gasket	102
Fig. 3.18 General-purpose 25A flange	103
Fig. 3.19 Appearance of joint jig	103
Fig. 3.20 Four type of flange face configurations for gasket joints	104
Fig. 3.21 Schematic diagram of helium leakage measurement device	105
Fig. 3.22 Measurement of axial force	107
Fig. 3.23 Leakage measurement test result for gasket 0-MPa mode and 400-MPa mode	108
Fig. 3.24 Leakage measurement test result comparison for standard and forming consideration	108
Fig. 4.1 Surface roughness measurement setup	111
Fig. 4.2 Roughness curve	112
Fig. 4.3 Schematic of gasket tightening on rough flange	114
Fig. 4.4 Flowchart of various stages of simulation of gasket to obtain contact stress, contact width, and force per unit length	115
Fig. 4.5 Setting up of gasket material, dies, flange and curve before forming and tightening	116
Fig. 4.6 Forming simulation	117
Fig. 4.7 Tightening simulation	117
Fig. 4.8 Average contact stress in each axial force	118
Fig. 4.9 Maximum contact stress in each axial force	119
Fig. 4.10 Contact width in each axial force	120
Fig. 4.11 Average contact stress for gasket in 400-MPa mode	121
Fig. 4.12 Maximum contact stress for gasket in 400-MPa mode	122
Fig. 4.13 Contact width for gasket in 400-MPa mode	123
Fig. 4.14 Average contact stress for gasket in 0-MPa mode	125
Fig. 4.15 Maximum contact stress for gasket in 0-MPa mode	126
Fig. 4.16 Contact width for gasket in 0-MPa mode	127
Fig. 4.17 Average contact stress for gasket in 0-MPa mode	129
Fig. 4.18 Maximum contact stress for gasket in 400-MPa mode	130
Fig. 4.19 Contact width for gasket in 400-MPa mode	131
Fig. 4.20 Average contact stress for gasket in 0-MPa mode	132
Fig. 4.21 Maximum contact stress for gasket in 0-MPa mode	133
Fig. 4.22 Contact width for gasket in 0-MPa mode	134
Fig. 4.23 Comparison real and sinusoidal surface roughness model of average contact stress for gasket 0-MPa mode	135
Fig. 4.24 Comparison real and sinusoidal surface roughness model of maximum contact stress for gasket 0-MPa mode	135
Fig. 4.25 Comparison real and sinusoidal surface roughness model of contact width for gasket 0-MPa mode	136

Fig. 4.26 Comparison real and sinusoidal surface roughness model of average contact stress for gasket 400-MPa mode	136
Fig. 4.27 Comparison real and sinusoidal surface roughness model of maximum contact stress for gasket 400-MPa mode	137
Fig. 4.28 Comparison real and sinusoidal surface roughness model of contact width for gasket 400-MPa mode	137
Fig. 4.29 Leakage measurement result for gasket in 400-MPa mode	139
Fig. 4.30 Leakage measurement result for 0-MPa gasket mode	140
Fig. 4.31 Leakage measurement results for gaskets in 0-MPa and 400-MPa modes	140
Fig. 4.32 Helium leak measurement related to contact width for gasket 0-MPa mode	141
Fig. 4.33 Helium leak measurement related to contact width for gasket 400-MPa mode	142
Fig. 4.34 Changes of surface roughness after experiment	143
Fig. 5.1 Real contact width between gasket and flange	147
Fig. 5.2 Contact stress in X-position for gasket 0-MPa mode contact with flange having surface roughness 3.5 μ m	148
Fig. 5.3 Contact stress in X-position for gasket 0-MPa mode contact with flange having surface roughness 2.5 μ m	148
Fig. 5.4 Contact stress in X-position for gasket 0-MPa contact with flange having surface roughness 1.5 μ m	149
Fig. 5.5 Contact stress in X-position for gasket 400-MPa contact with flange having surface roughness 3.5 μ m	150
Fig. 5.6 Contact stress in X-position for gasket 400-MPa contact with flange having surface roughness 2.5 μ m	150
Fig. 5.7 Contact stress in X-position for gasket 400-MPa contact with flange having surface roughness 1.5 μ m	151
Fig. 5.8 Real contact width simulation result for all levels real surface roughness model of flange and all types of gasket when axial force 120 KN	152
Fig. 5.9 Real contact width simulation result for all levels real surface roughness model of flange and all types of gasket when axial force 100 KN	153
Fig. 5.10 Real contact width simulation result for all levels real surface roughness model of flange and all types of gasket when axial force 80 KN	153
Fig. 5.11 Real contact width simulation result for all levels real surface roughness model of flange and all types of gasket when axial force 60 KN	154
Fig. 5.12 Digital microscope VH-Z250	155
Fig. 5.13 Gasket and flange in contact and after contact condition	156
Fig. 5.14 Grooves formed conditions for gasket 400-MPa mode	158
Fig. 5.15 Grooves formed conditions for gasket 0-MPa mode	160
Fig. 5.16 Real contact width experiment result for all levels surface roughness of flange and all types of gasket	162
Fig. 5.17 Basic dimension of surface roughness	164
Fig. 5.18 Contact width	164
Fig. 5.19 Real contact width	165

Fig. 5.20 Gasket in tightening process	166
Fig. 5.21 Free body diagram for tightening process	166
Fig. 5.22 Phenomena of sliding contact on the convex contact of the gasket	167
Fig. 5.23 The value of position change on the convex contact	168
Fig. 6.1 Dimensions of thin stainless gasket material	171
Fig. 6.2 FEM simulation model	173
Fig. 6.3 Tightening simulation	173
Fig. 6.4 Experimental apparatus	174
Fig. 6.5 Dies to produce a gasket	175
Fig. 6.6 Thin metal gasket	175
Fig. 6.7 The sandwiching silicone rubber	176
Fig. 6.8 Rubber deformation	177
Fig. 6.9 Deformation mode for gasket having flat portion of 4.0 mm	179
Fig. 6.10 Deformation mode for gasket having flat portion of 2.0 mm	180
Fig. 6.11 Deformation mode for gasket having flat portion of 1.5 mm	181
Fig. 6.12 Deformation map for thin stainless gasket material	182
Fig. 6.13 Load–displacement curve	183
Fig. 6.14 Displacement-contact stress curve	184
Fig. 6.15 Displacement-contact width curve	185

LIST OF TABLES

Table 1.1	Comparison of heat resistance, pressure resistance, and minimum axial force	3
Table 2.1	Gasket materials and contact facing (adapted from [22])	19
Table 2.2	Effective Gasket Width (adapted from [22])	20
Table 2.3	Array selectors all pairs of combinations	33
Table 2.4	Micro-geometrical roughness and waviness parameters of the surface roughness (adapted from [30])	47
Table 2.5	Optimum design levels in Saeed studied (adapted from [13])	57
Table 2.6	Comparison of Helium Leak Quantity and Water Pressure Test Result (adapted from [14])	61
Table 2.7	Initial basic dimensions of the gasket (adapted from [18])	69
Table 2.8	Factor and level description (adapted from [18])	71
Table 2.9	Optimum gasket design at number 1 and number 2 (adapted from [18])	73
Table 3.1	Characteristic of the SUS304	81
Table 3.2	Factors and levels description	89
Table 3.3	L18 test matrix	90
Table 3.4	Result of L18 Taguchi method	91
Table 3.5	Optimum design of gasket for 0-MPa and 400-MPa mode	95
Table 3.6	Optimum dimensions of dies for 0-MPa and 400-MPa modes	99
Table 5.1	Contact width result for 400-MPa gasket mode	159
Table 5.2	Contact width result for 0-MPa gasket mode	161
Table 5.3	Differences of contact width between simulation result and experimental result	163
Table 5.4	average radius of contact width	168

ACKNOWLEDGEMENT

It would have been impossible to make this thesis without the help and support of several persons:

First of all, I would like to express my deepest appreciation and thanks to my supervisor, Professor Ken KAMINISHI and Professor Shigeyuki HARUYAMA, for his excellent guidance throughout this work. Thank you for your patience, time for discussions, and critical review of my work. I receive generous scientific and practical knowledge as well as for letting me become a PhD student in such interesting field. I also thank the examiner committee, Professor Koichi GODA, Professor Xian CHEN and Associate Professor Tsuyoshi KOGA for their suggestions and reviews during the examination.

Mr. Kazuya USHIJIMA and Mr. Mitsuata YUDAI as teamwork of new metal gasket project have given great contributions and inputs to my work, I really appreciate for those. Dear friends and members of Strength of Material laboratory Yamaguchi University Japan, thank you for contributing to a very pleasant working environment. I also would like to thank all lecturers in Mechanical Engineering Department for a nice education atmosphere. Appreciation to Mr. OKAJIMA and Mr. KADOTA for good administration helps.

I am grateful to all my friends in Ube city for our friendships. Thanks to all Indonesian students during living in Japan for our togetherness and all member of PPI Yamaguchi. Appreciation is also addressed to Indonesian Embassy for great helps. Gratitude is given to my colleagues in Yogyakarta State University for their great encouragement and support during my study in Japan. I am very gratefully to Director General of Higher Education, Ministry of National Education Republic of Indonesia for giving chance to pursuing study in Japan with scholarship financial support on Batch 6 since 2011 until 2014.

Finally, I would like to especially thank my dear wife, Sri Katon Indah Wijaya and my dear daughter, Fadhila Fathin Zahra, for great understanding during difficult times and a fare away love.

Didik NURHADIYANTO
Ube city, September 2014

ABSTRACT

Asbestos—containing sealing material, and as a sealing material which is excellent in preventing superior leak prevention of piping, it has been used in many industries, is extremely dangerous chemicals asbestos, and it is causing serious illnesses problems. Therefore, in the country, the production of asbestos and its usage was banned from 2008. However, the use environment is harsh sealing material, Replacement of asbestos-containing sealing material of conventional (expanded graphite, Glass fibers, ceramic fibers, fluorocarbon resin, etc.), is expensive, and moreover There is a problem does not have a function of the extent of asbestos-containing sealing material, and life is short. For the development of alternative sealing material containing asbestos sealing material is a very important social issues, As leak-proof seal material anew, and uses elastic deformation of metal (spring effect), Low-cost sealing member having the same or better performance and asbestos sealing material has been proposed. The sealant, in asymmetrical front and back surfaces of the axial direction, Although it is very simple shape of only having a plurality of projections, as leakage prevention function, the projections are arranged on one side a plurality of asymmetrically is a very important feature, if you bolted the seal material, entire seal is elastically deformed by the projection of the plurality, it is possible to prevent leakage tip of the projection to contact and firmly attached to the contact surface. Studies have been made on the optimal shape given to the leakage characteristics by many researchers therefore. Saeed et al. have proposed an optimal shape considering the effect of the geometry parameter that gives the gasket shape for increasing the contact width is focused on the contact area to provide the leakage characteristics. In addition, from the experimental and theoretical analysis of the finite element method, Haruyama et al. revealed the relationship between the axial force and the contact width for the allowable limit of the contact width for water leakage does not occur. Choiron et al revealed that the gasket contact width is important as a design parameter of the experiment using pressure sensitive paper and a theoretical analysis by the finite element method focused on the stress distribution of the elastic-plastic contact region. Further, Widder indicates that the function of the leakage is increased by considering the relationship of the leak and the surface roughness, the surface roughness becomes larger because the surface roughness is actually occurring at the contact portion. However, various studies have been made by prior investigators, the study of surface roughness and the parameters affecting the leakproof based on the stress distribution in the contact area have been made, the leakage prevention based on the stress distribution in the contact area studies revealed optimal shape from consideration and surface roughness parameters affects not made.

In this study, the metal gasket using the spring effect, we found the optimum shape from consideration of the surface roughness and the parameters affecting the leakage prevention. 1. It is also revealed the outline of the research in this paper shows the problems in previous studies and research on performance and the scope of application of the various gaskets (Chapter 1). 2. The asbestos material historical background and the danger show a strong need for a newly gasket. While the influence of surface roughness in leakage is big, process design for obtaining the optimal shape has become clear when factors that affect

the leakage performance of 25A-size metal gasket has been clarified (Chapter 2). 3. In designing the SUS304, 25A metal gasket, the conditions of contact stress has been clarified using numerical analysis, especially the area/boundary of plasticity and elasticity. In addition, leakage performance and axial force relationship also has been clarified through leakage test (Chapter 3). 4. From the examination of each conditions of contact stress using numerical analysis which has been mentioned in previous chapter, it is clear that flange surface roughness give effect to the contact area and contact stress. Other than that, effect on the leakage performance and axial force is examined by flange surface roughness, which indicates that optimal shape during contact stress with plasticity area is less affected (Chapter 4). 5. Based on the real measurement result, area when surface roughness is considered and regional(local) contact stress have been examined through numerical analysis and the distribution of contact stress has been clarified. Then, the gap between result of contact area measurement through surface observation and the result of numerical analysis is proved to be small (Chapter 5). 6. In order to examine the local deformation of contact area, numerical analysis on deformation mode of thin metal gasket and actual evaluation test are carried out. From the tests, it is clarified that there are all 1~3 deformation modes and mode map can be clarified (Chapter 6). 7. To summarize the result, even though it is known that flange surface roughness is hardly affect the optimal shape conditions in the leakage performance of corrugated metal gasket, in the future it is essential to examine it with considering the surface disposition effect and creep property in high temperature environment (final Chapter).

CHAPTER I

INTRODUCTION

1.1 Background

Gasket is one of the seals used in the small gap on the static component. The function of the gasket is to prevent or stop leakage of fluid, such as gas, water and oil. Usually the gasket put between the two flanges used in plumbing systems. Flanges that contact with the gasket surface must be flat, no scratches, clean and dry. In every change in temperature, the gasket must withstand pressure, heat and chemical resistant. Axial force to tighten the two surfaces always based on the specification of torque to prevent leakage.

Gasket containing asbestos is a good gasket to prevent leakage. It was notable for their wide temperature range and resistance to chemicals, but it is extremely chemical substance dangerous, which causing serious illnesses. In Japan as scheduled for 2008, production of asbestos and usage was prohibited [1]. It is extremely urgent to develop materials to replace asbestos gasket because it is an important social issue.

Researcher has a challenge of finding alternative materials after asbestos banned. These materials expected have good performance as same as asbestos material. Most of researcher has been investigated new materials or developed a new seal system that optimizing by different design parameter for leakage performance. There is no ideal product that can replace gasket asbestos, so different materials are required to developed for various applications.

The performance of gaskets fabricated using various materials have been investigated. Glass Fiber Reinforced Plastic (GFRP) materials are used because their resistance to corrosion [2] and [3]. However, this material is expensive and low in operating pressure compare than carbon steel. This material is suitable for ClO_2 , HCl , H_2O_2 , NaClO_3 , NaOH , and H_2SO_4 . Exfoliated graphite material, when used as filler for metal based designs such as a Spiral wound Gasket (SWG), is appropriate for use in high-temperature and high-pressure conditions [3] and [4]. However, this material has problems associated with purity, fragility, and storage. Polytetrafluoroethylene (PTFE) exhibits extreme chemical

resistance, but it lacks creep resistance [3] and [5]. In fact, the performance of the substitutes of asbestos used to fabricate gaskets is inferior to that achieved by asbestos and the substitutes have a short period of utilization.

Persson et al. [6] and [7] studied the contact stress distribution. They compared the contact stress distribution result obtained using an analytical model with the (exact) numerical result obtained for contact between cylinder and a nominal flat substrate with surface roughness having many different length scales and found good agreement between the two. Specially, the theory predicted that the area of contact in most cases varies linearly with the load and that it depends on the magnification; both predictions showed excellent agreement with the (exact) numerical results.

Contact mechanics theory to determine the leak-rate of static seals investigated by Persson et al. [8]. Case for rubber gaskets, they assumed that merely elastic deformation occurs in the solid. Plastic deformation often occurs in the contact region for metal gaskets. Based on the percolation theory, they presented a theory of the leak-gaskets to predict the apparent contact area as a function of the magnification. It shows some interfacial surface, the increasing of the magnification effect on decreasing the contact area. In the next study, Lorenz et al. [9] calculated the volume-flow per unit time of leak-rate (Q) on the rubber gasket. The calculated leak-rate is in good agreement with experiment.

In the study above, they assumed that only elastic deformation occurs. However, the theory can be generalized to the case that plastic deformation occurs simply by replacing the boundary condition, which describes that plastic deformation occurs in the contact area when the local stress has reached σ_Y [10].

The use of metal gaskets might appropriate. It preferred because of certain advantages such as chemical resistance, capability in wide temperature range, capability to withstand pressure, recyclability, low cost and most importantly its reliability in critical situations. The comparison of heat resistance, pressure resistance, and minimum axial force work condition between metal and other gasket materials shown in Table 1.1 [11]. However, disadvantage of metal gasket is the axial forces need to be high to deform the solid metal gasket and the loss of tightness of bolted flange due to the relaxation of the joint. Gasket

and bolt are the joint members that give the largest bolt load relaxation ratio over time. In general, bolted joints relax extensively during the first few hours of service due to the excessive short term creep of the gasket. However, in the long term, the contribution of the bolt creeps becomes significant, especially at high temperature [12].

Table 1.1 Comparison of heat resistance, pressure resistance, and minimum axial force

Seal Material	Heat Resistance [$^{\circ}$ C]	Pressure resistance [MPa]	Minimum axial force [MPa]
Asbestos	~ 1000	14.7	11
Metal	~ 520	14.0	200
Graphite	$-240 \sim 400$	2.0	20
Resin	$-50 \sim 150$	1.0	20
Gum	$-60 \sim 120$	0.5	1.4

Decrease the axial forces for solid metal gasket and the loss of tightness of bolted flange due to the relaxation of the joint, the researcher using corrugated metal gasket. Saeed et al. [13] proposed super seal gasket, a new 25A size metal gasket that incorporates strategically placed circumferential annular lips. These lips, owing to the spring effect of the metal, form seal line with flanges. The circumferential annular lips provided on the upper and lower of the gasket. When the flange is tightened by bolts, it can be generated high local contact stress on a convex portion of the gasket to obtain a low loading metal gasket as shown in the Fig. 1.1. Also, the elastic regions on the flat sections (denoted by blue line) produce the spring effect of metal gasket, and it can reduce the effect of the occurring of loosening of bolts.

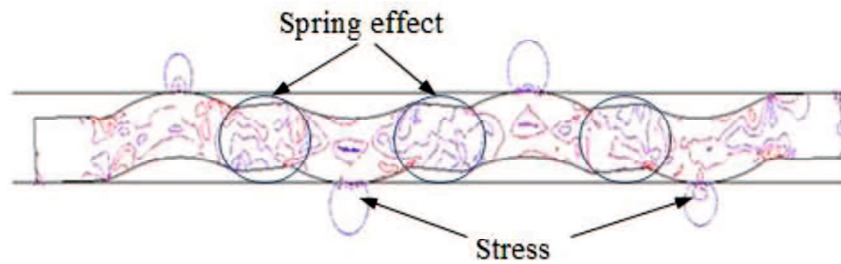


Fig. 1.1 High local contact stress on corrugated metal gasket

The contact stress and contact width were considered important design parameters for optimizing the gasket performance. However, the value of the contact width as design for no leak has not yet been defined. Also, the research justified the helium leak rate condition, but the condition leak or not leak not clarified yet. Haruyama et al. investigated the allowable limits of the contact width for no leak [14]. A contact width for which no leakage occurs in the newly developed gasket was determined by comparing the evaluation results of the relationship between the axial force of the flange and the contact width as obtained using finite element method (FEM) analysis with the experimental results of the axial force and the leakage. These results were used to obtain the optimum contact width. The contact width shows a relationship with helium leakage; increasing the contact width results in a decrease the leakage. The contact width which has no leak in the new 25A-size metal gasket clarified, which is above 0.8 mm. Choiron et al. [15] studied a method for validating the contact width measurement by using a simulation-based analysis. They compared the simulation result with experimental one obtained using pressure-sensitive paper and found good agreement between the two. In the increasing of axial force value, the helium leak quantity is decreasing, and the contact width is increasing. Based on this circumstance, it can be concluded that the contact width has a relationship with the helium leakage quantity. This fact is very useful if used in the evaluation of gasket performance. The result of the present study shows that the contact width can be employed to evaluate the sealing performance. Convex portion 1 and 4 will sliding and convex portion 2 and 3 will move very small and work primarily to reduce leakage and convex portion 1 and 4 support to realize it.

All new 25A size metal gasket models on the previous study use the assumption exclude forming effect. It was known that the forming process produced residual forming data, such as characterizing geometric imperfections and residual stresses [16]. The use of simulation is beneficial in the design of metal forming operations because it is more cost effective than trial and error. The development of hardware and software support the metal forming simulation to define the shape and initial material. It also predicted the forces and stresses necessary to execute the forming operation [17]. Press forming is performed to produce gasket shape by a punch forces the initial material to slide into a die. Therefore, the forming effect is considered in gasket design modeling assessment. By using forming effect, the limit of contact width on the previous model which excluded forming effect for no leakage will be evaluated.

All new 25A size metal gasket models on the previous study use the assumption an elastic contact stress. In fact, plastic deformation occurs in the contact area when the local stress has been reached. The use of simulation is beneficial in the design of metal forming operations because it is more cost effective than trial and error. The development of hardware and software support the metal forming simulation to define an elastic and plastic contact stress. It also predicted the forces and stresses necessary to execute the forming operation. Gasket elastic mode, the contact width having elastic contact stress is longer than plastic contact stress. Gasket plastic mode, the contact width having plastic contact stress is longer than elastic contact stress [18].

An important characteristic to consider in the development of new metal gasket is a function to prevent leakage depending on the surface roughness standard used. Leakage is a function of surface roughness for molded rubber sealing [19] —it increases with the surface roughness. Person et al. [8] and Lorenz et al. [9] studied theory leak-rate of seals, which is the case of rubber seals. They have presented a theory of the leak-rate of seal, which based on percolation theory and developed contact mechanics theory. They have presented numerical results for the leak-rate \dot{Q} , and for surface roughness lateral size λ_c and the height u_c of the critical construction. They have presented results for how leak-rate depended on lateral size and the height surface roughness and on the pressure with which

the rubber squeezed against the rough counter-surface.

Previous studies on the design of a new metal gasket used models that did not include the surface roughness effect. The main problem in this regard is the fact that a suitable surface roughness for which no leakage occurs did not yet well understood.

For that reason, this study is the gasket shape was produced by using forming and tightening simulation to ensure the limited size of contact width. Press forming is performed to produce gasket shape by a punch forces the initial material to slide into a die. In this study, they founded the optimum design of New 25A-size metal gasket includes forming effect according to the elastic and plastic condition respectively derived from FEM analysis. The optimum design of the simulation result was tested using helium leak test. Here, they have been known the gasket performance based on the elastic and plastic design.

In this light, this study aims to determine the surface roughness of a flange contact that minimizes leakage in the newly developed 25A-size metal gasket. The surface roughness determined through a comparison between simulation and experimental results. The simulation investigates the contact stress, contact width, and force per unit length according to the surface roughness of the flange. The experiment involves a helium leakage test using two new metal gaskets having different surface roughness levels.

1.2 Research Purposes

Based on the explanation above, we developed the optimum metal gasket. The real contact area and contact stress are affected by the load. The quantity of leakage paths reduced under increasing compression. This assumption connected with previous studies that contact area and contact stress as the main parameter affected the leakage. In this study, a new metal gasket evaluation method is investigated based assumption different surface roughness due to the leakage mechanism theory on the metal gasket did not be provided yet. The surface roughness is set to fulfill the JIS standard. Therefore, the leakage test is used to obtain a performance evaluation method on the new metal gasket. It is not possible to decide whether there was a leakage or no leakage from the helium leakage test.

Saeed et al. [13] results justify the selection of contact area as reasonable

performance evaluation criteria, but the limited size of contact area for no leak as design parameter did not define yet. The leakage can be reduced with increasing the contact width. Choiron et al. [15] justify that the contact width validation is provided by using Finite Element Analysis (FEA) and the result is compared to experimental using pressure sensitive paper. The quantitative evaluation of helium leakage rate and the contact width of the gasket that has no leakage by the water pressure test are carried out as design concept.

Choiron et al. [18] justify that the optimum design of new metal gasket considering plastic contact stress is realized by using Taguchi method. They studied, that the optimum design use seven parameters, and it is chosen due to assume that the better sealing performances are desirable because the large contact stress creates sealing lines on contact width. Based on plastic contact stress consideration of contact width, the optimized gasket is determined by deleting contact width with contact stress below of 400MPa. The optimum design of new 25A-size metal gasket has been obtained. By using forming effect, the limit of contact width on the previous model which excluded forming effect for no leakage was evaluated. Initial blank thickness is varied by adding 0% ($t_{0\%}$), 5% ($t_{5\%}$) and 10% ($t_{10\%}$) of the final thickness of the gasket. The result shows that the final design shapes produced the defect occurred in the radius shape of convex contact. The lack of the die fill defect decreased with increasing initial blank thickness. The $t_{0\%}$ forming model provides contact width trend as similar to the non-forming model. The forming models show a higher contact stress than it's the non-forming models due to residual stress of forming effect. The increasing initial blank thickness will need extra force to forming process. This treatment will change the characteristic of material gasket. We need another treatment to decrease lack of the die fill defect.

Widder [19] studied the surface finish effect in static sealing. Leakage is a function of surface roughness—it increases with the surface roughness. Previous studies on the design of a new metal gasket used models that did not include the surface roughness effect. The main problem in this regard is the fact that a suitable surface roughness for which no leakage occurs did not yet well understood. Person et al. [8] and Lorenz et al. [9] studied theory leak-rate of seals, which is the case for rubber seals. They have presented numerical

results for the leak-rate and for surface roughness. They have presented results for how leak-rate depended on lateral size and the height surface roughness and on the pressure with which the rubber squeezed against the rough counter-surface. In this study, we will investigate the influence of surface roughness on contact stress and contact width by simulation. Beside that we will investigate the influence of surface roughness on contact width and leakage by experiment that is the case for flange contact with 25A-size metal gasket.

Based on the explanation above, the purpose of this study are:

1. Investigate the optimum design of the corrugated 25A-size metal gasket based on contact width considering forming and contact stress effect.
2. Investigate the influence of the surface roughness of a flange on contact stress, contact width and leakage of the corrugated 25A-size metal gasket. To measure a contact width by simulation and experimental.
3. Investigate the deformation mode in apply other size metal gasket which is a thin stainless gasket.

The layout of research step is shown in Fig.1.2. The work is divided based on three stages as follows:

1. **First Stage:** The optimum design based on contact width considering forming and contact stress effect. Gasket divided into two gaskets, which are 400-MPa mode for the gasket designed based on plastic contact stress and 0-MPa mode for the gasket designed based on elastic contact stress. The lack of the die fill defect decreased with increasing the angle of inner radius. It means will increase an inner lip height of convex and decrease the radius of convex. A new approach of leakage test is developed by using the amount of helium leakage rate using a helium leakage test.

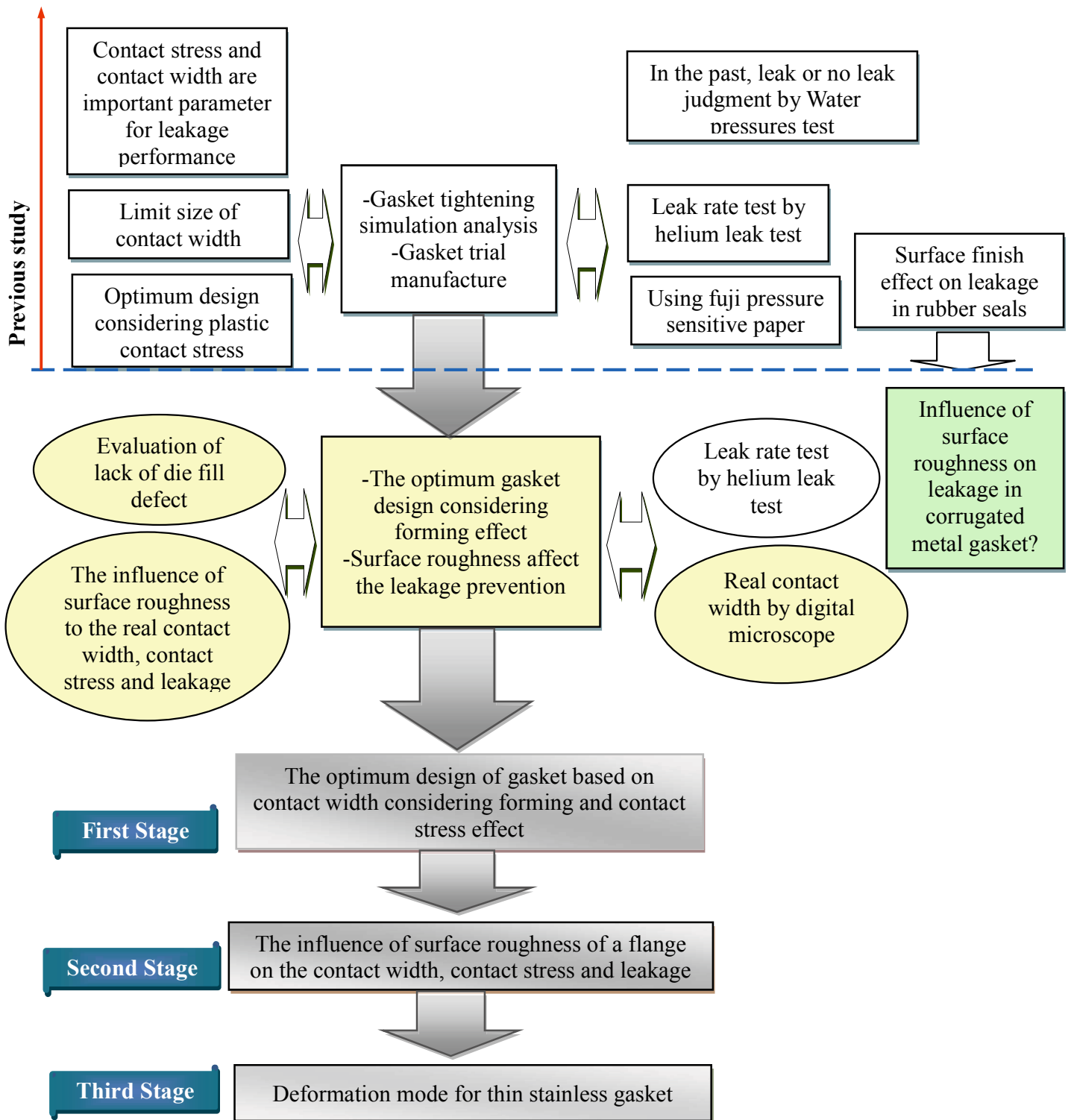


Fig. 1.2 layout of research step

2. **Second Stage:** Previous studies on the design of a new metal gasket used models that did not include the surface roughness effect. In this stage, the surface roughness of a flange contact that minimizes leakage in the newly developed 25A-size metal gasket. The surface roughness influence determined through a comparison between simulation and experimental results. An experimental analysis by measuring the leakage and a simulation analysis result based on contact stress and contact width.
3. **Third Stage:** Application to other size metal gasket which is a thin stainless gasket. This gasket material for low-pressure fluid flow. The metal gaskets tend to corrode easily, so we use the stainless. In this study, we examined the deformation mode of a thin stainless gasket using an FEM analysis. A final evaluation was made using a compression examination.

1.3 Outline

The dissertation outline described as bellow. This dissertation contains seven chapters. The first chapter describes the introduction, which consist of motivation and background of this research. Descriptions of a metal gasket as an asbestos substitution in relation to the asbestos banned in Japan since 2008, as well as the health impact caused by the use of asbestos, are reviewed. The basic theory used as a base for this project given in the Chapter 2. The asbestos history, forces acting on a gasket joint, FEA, Taguchi Method, contact mechanics theory, leakage theory, and contact between two surface roughness model describes completely in this chapter. A new approach of leak test method was used to evaluate the leakage of the metal gasket using helium leak and water pressure tests continuously. FEM analysis was used to analyze the contact width, and it is validated using pressure sensitive paper. By using the results of the FEM analysis and the leak measurement results, the design concept of the 25A-size metal gasket was realized; the design was developed by using the relationship between the contact width and leakage. By using this design concept, the limits of contact width for no leakage can be chosen. In the Chapter 3, the optimum design of new 25A-size metal gasket is developed by using Taguchi method. The optimum design as a second stage was done based on the increasing contact width with considering forming and contact stress effect. The lack of the die fill

defect decreased with increasing the angle of inner radius. Dies design, mold press and the leakage measurement for the optimum design of 25-A size metal gasket as described in this chapter. Chapter 4 has investigated the influence of surface roughness on contact stress and contact width by simulation of 25-A size new metal gasket. Beside that the influence of surface roughness on leakage explained in this chapter. The surface roughness was analyzed using an FEM model and experimental analysis. Chapter 5 investigated the real contact width of a flange contact with the newly developed 25A-size metal gasket based on surface roughness. The contact width determined through a comparison between simulation and experimental results. The simulation investigates the real contact width according to the surface roughness of the flange. The experiment involves a microscope using a new metal gasket having different surface roughness levels to investigate a real contact width. In the Chapter 6, we discussed the other application of corrugated gasket we used a thin stainless gasket. Thin stainless gasket used in the low fluid pressure. Beside that the aim of using this gasket is to reduce the axial force for tightening. Stainless material used for corrosion decreased. Finally, conclusions and suggestions for future studies are presented in Chapter 7.

CHAPTER II

LITERATURE STUDY

2.1. Asbestos History

Asbestos is a mineral form of silica fibers belonging to the serpentine group that occurs in the environment naturally. The serpentine group consist of chrysotile, which is a magnesium silicate hydroxide with the composition $Mg_6(OH)_6(Si_4O_{11})H_2O$, and amphibole of rock-forming minerals, including actinolite, amosite (brown asbestos, cummingtonite, grunerite), anthophyllite, chrysotile (white asbestos), crocidolite (blue asbestos), tremolite, or a mixture containing at least one of these minerals. All forms of asbestos are hazardous and can cause cancer. Amphibole forms of asbestos are more hazardous to health than chrysotile (see Fig. 2.1) [20].

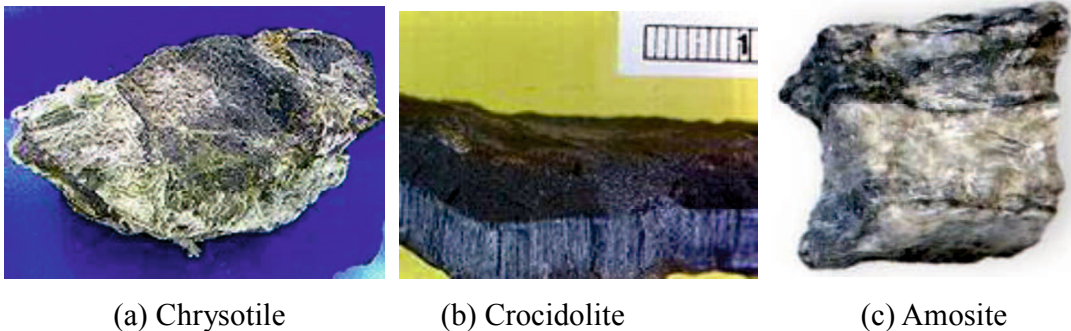


Fig. 2.1 Types of asbestos

Asbestos fibers do not dissolve in water or evaporate into the air. Nevertheless, pieces of fibers can enter the air and water. Fiber-containing particles and small diameter fibers may remain suspended in the air. It is happening for a long time and be carried long distances by water or wind currents before settling. Asbestos dust is asbestos particles floating in the air or deposited asbestos particles that can be scattered into the air as dust in the working environment. Larger diameter fibers and particles tend faster to settle. Fibers of asbestos are not competent to move through soil. They are remained virtually unchanged

over long periods and will not react with other compounds in the environment. Nevertheless, chrysotile may have some minor mineral loss in acidic environments. Fibers of asbestos can break into shorter due to the physical processes. When fibers of asbestos are breathed in, they may be trapped in the lungs. Levels of fibers in the lung tissue will accumulate over time. However some fibers, particularly chrysotile fibers, can be degraded in the lung with time [20].

Asbestos is resistant to chemicals, fire or water so that asbestos can't be destroyed. If dust is inhaled or swallowed asbestos, dust will enter the lungs and stick. The dust can't be destroyed by the body, causing various diseases as mentioned above.

Asbestos dust poisoning due process is not instantaneous. Toxins contained chrysotile asbestos in the base material accumulatively attack. Humans are constantly exposed to asbestos dust sucking cancer that can cause death. Inhaled asbestos fibers will enter into the lungs and cause connective tissue, inflammation, and adhesions in the chest cavity. If we breathe asbestos fibers into our lungs, some of the fibers will be deposited in the air passages and on the cells that make up our lungs. Most fibers are removed from our lungs by being carried away or coughed up in a layer of mucus to the throat, where they are swallowed into the stomach. This usually takes place within a few hours. Fibers deposited in the deepest parts of the lung are removed more slowly. In fact, some fibers may move through our lungs and can remain in place for many years and may never be removed from your body. If we swallow asbestos fibers (either those present in water or those that are moving to our throat from your lungs), nearly all of the fibers pass along our intestines within a few days and are excreted in the feces. A small number of fibers may penetrate into cells that line our stomach or intestines, and a few penetrate all the way through and get into our blood. Some of these become trapped in other tissues, and some are removed in our urine. If we get asbestos fibers on our skin, very few of these fibers, if any, pass through the skin into our body [20].

Asbestos workers have increased chances of getting two principal types of cancer: cancer of the lung tissue itself and mesothelioma, a cancer of the thin membrane that surrounds the lung and other internal organs. These diseases do not develop immediately

following exposure to asbestos, but appear only after a number of years. There is also some evidence from studies of workers that breathing asbestos can increase the chances of getting cancer in other locations (for example, the stomach, intestines, esophagus, pancreas, and kidneys), but this is less certain. Members of the public who are exposed to lower levels of asbestos may also have increased chances of getting cancer, but the risks are usually small and are difficult to measure directly. Lung cancer is usually fatal, while mesothelioma is almost always fatal, often within a few months of diagnosis. Some scientists believe that early identification and intervention of mesothelioma may increase survival [20].

Coming to the forms of asbestos, they are basically three in number, which are divided into two groups called serpentine group and amphibole group. In 2005, 2.2 million tons of asbestos were mined worldwide. Russia was the largest producer with about 40% world share followed by China and Kazakhstan.

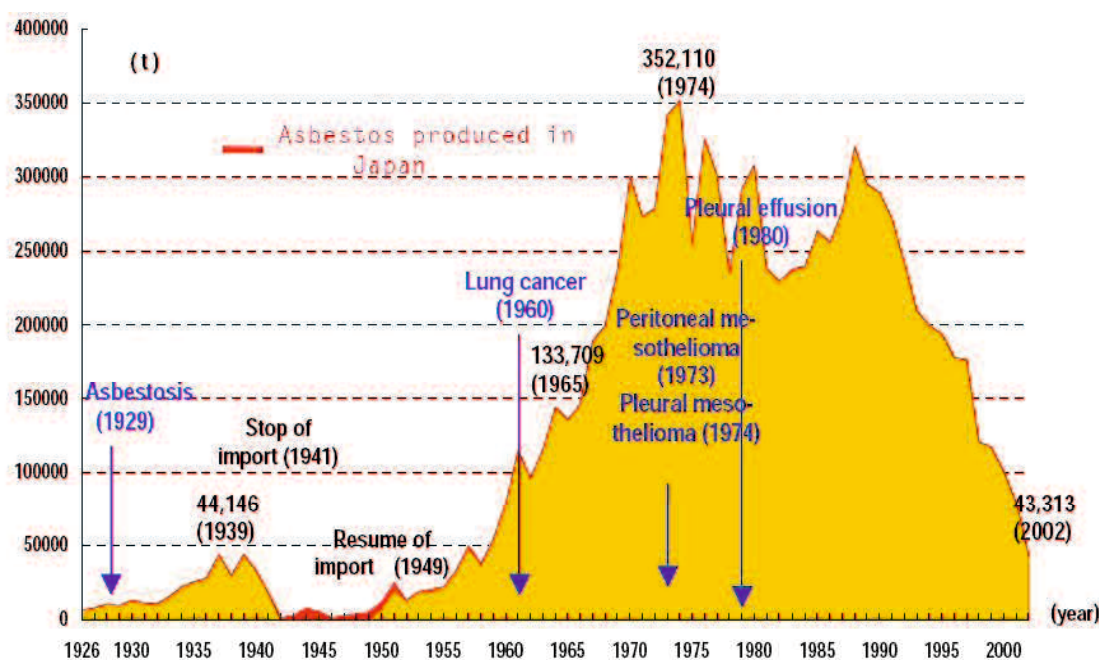


Fig. 2.2 Annual asbestos import to Japan and asbestos-related diseases in Japan (adapted from [21])

Japan is one of the biggest importer countries of asbestos in the world, particularly after World War II. In this period, the amount of use asbestos expanded with the economic growth rapidly. It was necessary for the electric power, shipbuilding, and heavy chemical industries. Asbestos imports increased during the period of Japan industrial growth in the 1960s and 1970s. In 1974, annual imports reached a peak at 352,110 tons (Fig. 2.2). Thus, the figure for 1988 represents the second peak in the use of asbestos in Japan. But following the global trend, Japanese asbestos industry stopped importing crocidolite (blue asbestos) since 1988 and amosite (brown asbestos) since 1993. Thereafter only chrysotile (white) asbestos has been used in Japan. On 28 June 2002, the Minister of Health, labor and Welfare announced that the Japanese Government was thinking about the ban of chrysotile [21].

2.2. Forces Acting on a Gasket Joint

Gasket is one of the seals used in the small gap on the static component. The function of the gasket is to prevent or stop leakage of fluid, such as gas, water and oil. Usually the gasket put between the two flanges used in plumbing systems. Flanges that contact with the gasket surface must be flat, no scratches, clean and dry. In every change in temperature, the gasket must withstand pressure, heat and chemical resistant. Axial force to tighten the two surfaces always based on the specification of torque to prevent leakage.

There are three principal forces acting on pipe-gasket-bolt system, which are [22]:

1. Bolt load and/or other means of applying the initial axial force that it will prevent or stopping the leakage to form a seal.
2. The hydrostatic end force, tending to separate flanges when the system is pressurized.
3. Internal pressure acting on the portion of the gasket. This pressure tending to blow the gasket out of the joint and/or to bypass the gasket under operating conditions.

Figure 2.3 indicates the three primary forces acting upon a pipe-gasket-bolt system. The initial axial force applied to a joint must serve some purposes [22].

- It must be sufficient to initially seat the gasket and flow the gasket into the imperfections on the gasket seating surfaces regardless of operating conditions.

- Initial axial force must be strong enough to compensate for the total hydrostatic end force.
- It must be sufficient to maintain a residual load on the gasket/flange interface.

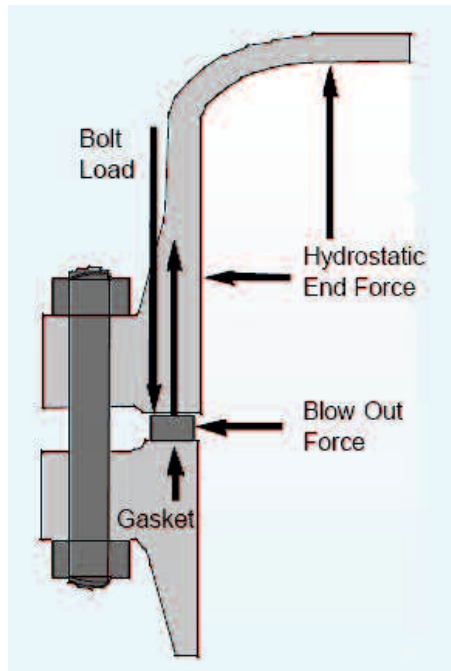


Fig. 2.3 Forces acting on a gasket joint (adapted from [22])

From a practical standpoint, residual gasket load must be "X" times internal pressure if a tight joint is to be maintained. This unknown quantity "X" is what is known as the "m" factor in the ASME boiler and pressure vessel code [22] and will vary depending upon the type of gasket being used as shown in the Table 2.1. Actually the "m" value is the ratio of residual unit stress (bolt load minus hydrostatic end force) on gasket (psi) to internal pressure of the system. The larger the number used for "m," the more conservative the flange design would be, and the more assurance the designer has of obtaining a tight joint.

The initial bolt load required to seat a gasket sufficiently is defined as:

$$W_{m2} = \pi b G y \quad (2-1)$$

The required operating bolt load must be at least sufficient, under the most severe operating conditions, to contain the hydrostatic end force and, in addition, to maintain a residual compression load on the gasket that is sufficient to assure a tight joint. ASME defines this bolt load as:

$$W_{m1} = \frac{\pi}{4} G^2 P + 2b\pi GmP \quad (2-2)$$

After W_{m1} and W_{m2} are calculated, then the minimum required bolt area A_m is determined:

$$\begin{aligned} A_{m1} &= \frac{W_{m1}}{S_b} \\ A_{m2} &= \frac{W_{m2}}{S_a} \\ A_m &= A_{m1} \text{ if } A_{m1} \geq A_{m2} \quad \text{or} \quad A_m = A_{m2} \text{ if } A_{m2} \geq A_{m1} \end{aligned} \quad (2-3)$$

Bolts are then selected so that the actual bolt area A_b is equal to or greater than A_m

$$A_b = (\text{Number of Bolts}) \times (\text{Minimum Cross-Sectional area of bolts in inches}^2)$$

$$A_b \geq A_m \quad (2-4)$$

The maximum unit load $Sg_{(\max)}$ on the gasket bearing surface is equal to the total maximum bolt load in pounds divided by the actual sealing area of the gasket in inches².

$$Sg_{(\max)} = \frac{A_b S_a}{\frac{\pi}{4} [(OD - 0.125)^2 - (ID)^2]} \quad \left. \vphantom{\frac{A_b S_a}{\frac{\pi}{4} [(OD - 0.125)^2 - (ID)^2]}} \right\} \text{ Spiral wound gasket}$$

$$Sg_{(\max)} = \frac{A_b S_a}{\frac{\pi}{4} [(OD)^2 - (ID)^2]} \quad \left. \vphantom{\frac{A_b S_a}{\frac{\pi}{4} [(OD)^2 - (ID)^2]}} \right\} \text{ All other types of gasket} \quad (2-5)$$

Except as noted, the symbols and definitions below are:

A_b = actual total cross-sectional area of bolts at root of thread or section of least diameter under stress (inches²).

A_m = total required cross-sectional area of bolts, taken as the greater of A_{m1} or A_{m2} , (inches²).

A_{m1} = total cross-sectional area of bolts at root of thread or section of least diameter under stress, required for the operating conditions.

A_{m2} = total cross-sectional area of bolts at root of thread or section of least diameter under stress, required for gasket seating.

b = effective gasket or joint-contact-surface seating width (inches) in Table 2.2

b_o = basic gasket seating width (inches) as shown in Table 2.2

G = diameter at location of gasket load reaction as shown in Table 2.2

When $b_o \leq 1/4$ in., G = mean diameter of gasket contact face (inches).

When $b_o > 1/4$ in., G = outside diameter of gasket contact face less $2b$ (inches).

m = gasket factor as shown in the Table 2.1.

N = width, in inches, used to determine the basic gasket seating width b_o , based upon the possible contact width of the gasket (Table 2.2)

P = design pressure (lbf/inch²).

S_a = allowable bolt stress at ambient temperature (lbf/inch²).

S_b = allowable bolt stress at operating temperature (lbf/inch²).




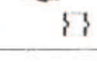
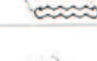





S_g = Actual unit load at the gasket bearing surface (lbf/inch²).

W_{m1} = required bolt load for operating conditions (lbf).

W_{m2} = minimum required bolt load for gasket seating ((lbf)

y = gasket or joint-contact-surface unit seating load, minimum design seating stress, PSI (Table 2.1).

Table 2.1 Gasket materials and contact facing (adapted from [22])

Gasket material		Gasket factor m	Min. design seating stress y (psi)	Sketches and notes	Use facing sketch	Use column	
Self-Energizing types O Rings, Metallic, Elastomer other gasket types considered as self-sealing		0	0	—	—	—	
Elastomers without fabric. Below 75 Shore Durometer 75 or higher Shore Durometer		0.50 1.00	0 200		1 (a, b, c, d) 4, 5		
Elastomers with cotton fabric insertion		1.25	400				
Vegetable fiber		1.75	1100				
Spiral-wound metal, with nonmetallic filler		Carbon Stainless or Monel	3.00	10000		1 (a, b)	II
Corrugated metal, double jacketed with nonmetallic filler	Soft Aluminum	2.50	2900		1 (a, b, c, d)		
	Soft copper or brass	2.75	3700				
	Iron or soft steel	3.00	4500				
	Monel or 4-6% chrome	3.25	5500				
	Stainless steels	3.50	6500				
Corrugated metal	Soft aluminum	2.75	3700		1 (a, b, c, d)		
	Soft copper or brass	3.00	4500				
	Iron or soft steel	3.25	5500				
	Monel or 4-6% chrome	3.50	6500				
	Stainless steels	3.75	7600				
Flat metal jacketed with nonmetallic filler	Soft aluminum	3.25	5500		1a, 1b, 1c*, 1d*, 2*		
	Soft copper or brass	3.50	6500				
	Iron or soft steel	3.75	7600				
	Monel	3.50	8000				
	4-6% chrome Stainless steels	3.75 3.75	9000 9000				
Grooved metal	Soft aluminum	3.25	5500		1 (a, b, c, d) 2, 3		
	Soft copper or brass	3.50	6500				
	Iron or soft steel	3.75	7600				
	Monel or 4-6% chrome	3.75	9000				
	Stainless steels	4.25	10100				
Solid flat metal	Soft aluminum	4.00	8800		1 (a, b, c, d) 2, 3, 4, 5		
	Soft copper or brass	4.75	13000				
	Iron or soft steel	5.50	18000				
	Monel or 4-6% chrome	6.00	21800				
	Stainless steels	6.50	26000				
Ring joint	Iron or soft steel Monel or 4-6% chrome Stainless steels	5.50 6.00 6.50	18000 21800 26000		6	I	

*The surface of a gasket having a lap should be against the smooth surface of the facing and not against the nubbin.

Reprinted with permission of ASME

Notes:

This table gives a list of many commonly used gasket materials and contact facings with suggested design values of m and y that have generally proved satisfactory in actual service when using effective gasket seating width b given in the table on the next page. The design values and other details given in this table are suggested only and are not mandatory.

Table 2.2 Effective Gasket Width (adapted from [22])

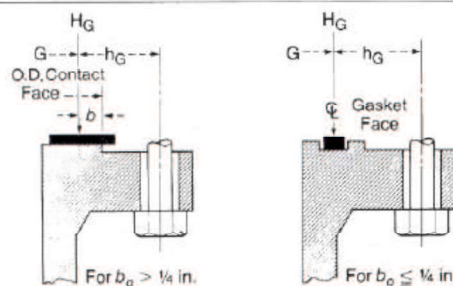
	Facing Sketch Exaggerated	Basic Gasket Seating Width, b_o	
		Column I	Column II
1a			
1b*		$\frac{N}{2}$	$\frac{N}{2}$
1c			
1d*		$\frac{w + T}{2}, \left(\frac{w + N}{4} \max\right)$	$\frac{w + T}{2}, \left(\frac{w + N}{4} \max\right)$
2		$\frac{w + N}{4}$	$\frac{w + 3N}{8}$
3		$\frac{N}{4}$	$\frac{3N}{8}$
4*		$\frac{3N}{8}$	$\frac{7N}{16}$
5*		$\frac{N}{4}$	$\frac{3N}{8}$
6		$\frac{w}{8}$	

Effective Gasket Seating Width, "b"

$b = b_o$, when $b_o \leq \frac{1}{4}$ in.

$b = \frac{\sqrt{b_o}}{2}$, when $b_o > \frac{1}{4}$ in.

Location of Gasket Load Reaction



NOTE: The gasket factors listed only apply to flanged joints in which the gasket is contained entirely within the inner edges of the bolt holes.

*Where serrations do not exceed 1/64 in. depth and 1/32 in. width spacing, sketches 1b and 1d shall be used.

Reprinted with permission of ASME

2.3. Finite Element Analysis

In the finite element method, the actual continuum or body of matter is represented as an assemblage of subdivisions called finite elements. The body of matter can be applied on solid, liquid, or gas. The type of element can be shown in the Fig. 2.4. These elements are considered to be interconnected at specified joints called nodes or nodal points. The nodes usually lie on the element boundaries where adjacent elements are considered to be connected. Since the actual variation of the field variable (e.g., displacement, stress, temperature, pressure, or velocity) inside the continuum is not known, we assume that the variation of the field variable inside a finite element can be approximated by a simple function. These approximating functions (also called interpolation models) are defined in terms of the values of the field variables at the nodes. When field equations (like equilibrium equations) for the whole continuum are written, the new unknowns will be the nodal values of the field variable. By solving the field equations, which are generally in the form of matrix equations, the nodal values of the field variable will be known. Once these are known, the approximating functions define the field variable throughout the assemblage of elements. The solution of a general continuum problem by the finite element method always follows an orderly step-by-step process [23].

The finite element analysis method requires the following major steps [23]:

1. Discretization or meshing of the domain into a finite number of sub domains (elements).
2. Selection of interpolation functions.
3. Development of the element matrix for the sub domain (element).
4. Assembly of the element matrices for each sub domain to obtain the global matrix for the entire domain,
5. Imposition of the boundary conditions.
6. Solution of equations.
7. Additional computations (if desired).

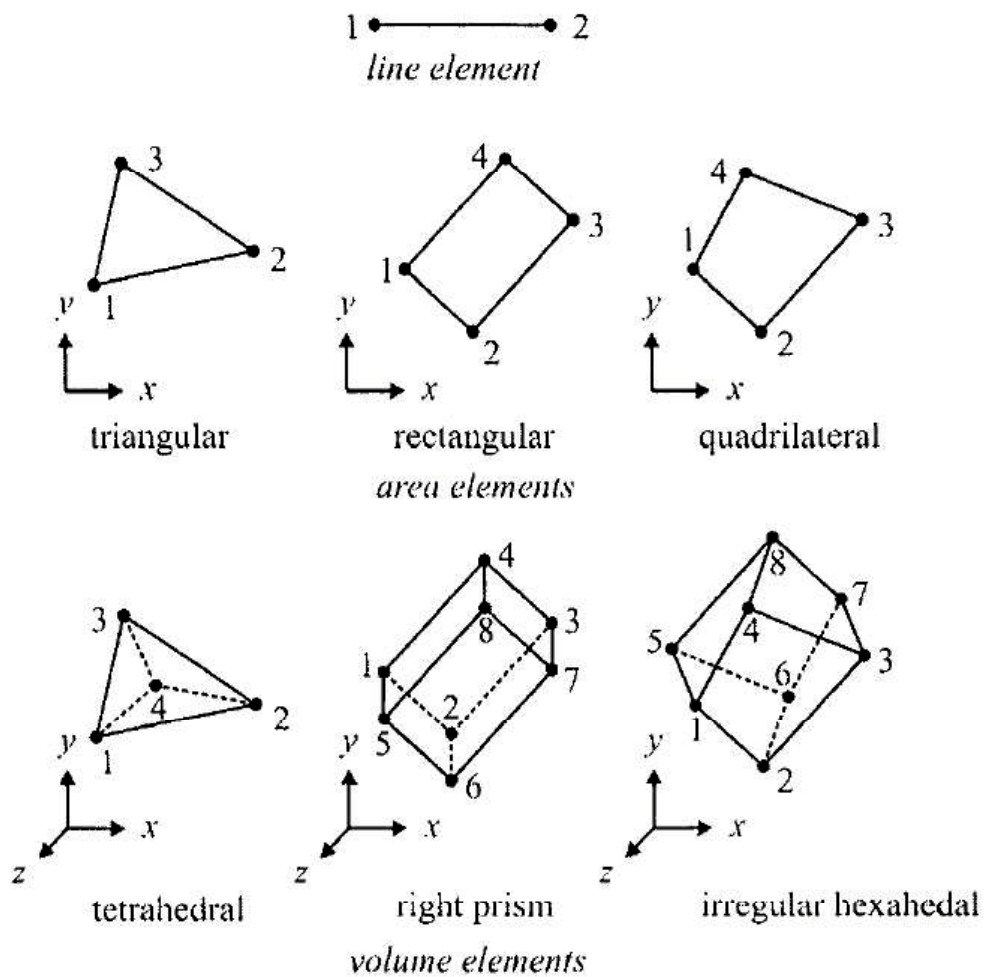


Fig. 2.4 Type of element (adapted from [23])

There are three main approaches to constructing an approximate solution based on the concept of FEA [24]:

1. Direct Approach

This approach is used for relatively simple problems, and it usually serves as a means to explain the concept of FEA and its important steps.

2. Weighted Residuals

This is a versatile method, allowing the application of FEA to problems which

functional cannot be constructed. This approach directly utilizes the governing differential equations, such as those of heat transfer and fluid mechanics.

3. Variational Approach

This approach relies on the calculus of variations, which involves extremizing a functional. This functional corresponds to the potential energy in structural mechanics

In solid mechanics, this is known as the principle of minimum potential energy, which states that among all compatible displacement fields satisfying the boundary conditions, the correct displacement field satisfying the equilibrium equations is the one that renders the potential energy an absolute minimum. A solution satisfying both equilibrium equations and boundary conditions is, of course, "exact"; however, such solutions are difficult, if not impossible, to construct for complex problems. Therefore, approximate solutions are obtained by assuming admissible displacement fields with unknown coefficients. The values of these coefficients are determined in such a way that the total potential energy of the system is a minimum. The principle of virtual work is applicable for any material behavior, whereas the principle of minimum potential energy is applicable only for elastic materials. However, both principles yield the same element equations for elastic materials. The total potential energy of the structural system shown in Fig. 2.5 is defined as [24]:

$$\pi_p = W + Q \quad (2-6)$$

where W = the strain energy

Q = the potential energy arising from the presence of body forces, surface tractions, and the initial residual stresses.

Strain energy is the capacity of the internal forces (or stresses) to do work through strains in the structure. For a linear elastic material, the strain energy of the deformed structure is given by [24]

$$W = \frac{1}{2} \int_V (\boldsymbol{\varepsilon} - \boldsymbol{\varepsilon}^*)^T \boldsymbol{\sigma} dV \quad (2-7)$$

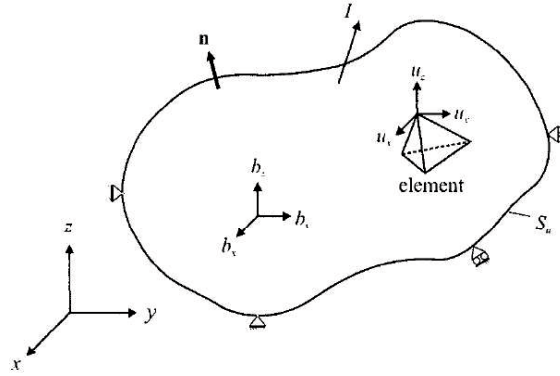


Fig. 2.5 A 3D body with displacement constraints, body and concentrated forces and surface traction (adapted from [24])

where $\boldsymbol{\sigma}$ is the vector of stress components arising from the difference between the total strains, $\boldsymbol{\varepsilon}$, and initial strains, $\boldsymbol{\varepsilon}^*$. It can be expressed as

$$\boldsymbol{\sigma} = \mathbf{D} (\boldsymbol{\varepsilon} - \boldsymbol{\varepsilon}^*) \quad (2-8)$$

in which

$$\boldsymbol{\sigma}^T = \{\sigma_{xx} \quad \sigma_{yy} \quad \sigma_{zz} \quad \sigma_{xy} \quad \sigma_{yz} \quad \sigma_{zx}\}$$

$$\boldsymbol{\varepsilon}^T = \{\varepsilon_{xx} \quad \varepsilon_{yy} \quad \varepsilon_{zz} \quad \gamma_{xy} \quad \gamma_{yz} \quad \gamma_{zx}\}$$

And the material property matrix

$$D = \frac{E}{(1+\nu)(1-2\nu)} \begin{bmatrix} 1-\nu & \nu & \nu & 0 & 0 & 0 \\ \nu & 1-\nu & \nu & 0 & 0 & 0 \\ \nu & \nu & 1-\nu & 0 & 0 & 0 \\ 0 & 0 & 0 & \frac{(1-2\nu)}{2} & 0 & 0 \\ 0 & 0 & 0 & 0 & \frac{(1-2\nu)}{2} & 0 \\ 0 & 0 & 0 & 0 & 0 & \frac{(1-2\nu)}{2} \end{bmatrix} \quad (2-9)$$

where σ_{ij} and ε_{ij} represent the stress and strain components, with $i,j = x,y,z$ being the Cartesian coordinates. The elastic modulus and Poisson's ratio are denoted by E and ν , respectively.

The potential energy arising from the presence of body forces, b , surface tractions, T , and the initial residual stresses, σ^* , is given by

$$\pi_p = -\int_V u^T b dV - \int_{S_\sigma} u^T T dS - \int_V \varepsilon^T \sigma^* dV \quad (2-10)$$

$$b^T = \{b_x \quad b_y \quad b_z\}$$

$$T^T = \{T_x \quad T_y \quad T_z\}$$

$$u^T = \{u_x \quad u_y \quad u_z\}$$

in which b_x , b_y , and b_z are the components of body force (in units of force per unit volume), and T_x , T_y , and T_z represent the components of the applied traction vector (in units of force per unit area) over the surface defined by S_σ . The entire surface of the body having a volume of V is defined by S , with segments S_u and S_σ subjected to displacement and traction conditions, respectively. The displacement components are given by u_x , u_y , and u_z in the x-, y-, and z-directions, respectively. Also, included in the expression for the total potential is the initial residual stresses denoted by σ^* . The initial stresses could be measured, but their prediction without full knowledge of the material's history is impossible. After partitioning the entire domain occupied by volume V into E number of elements with volume V^e , the total potential energy of the system can be rewritten as [24]

$$\pi_p(u_x, u_y, u_z) = \sum_{e=1}^E \pi_p^{(e)}(u_x, u_y, u_z)$$

in which

$$\pi_p^{(e)} = \frac{1}{2} \int_{V^{(e)}} \varepsilon^T D \varepsilon dV - \int_{V^{(e)}} \varepsilon^T D \varepsilon^* dV + \frac{1}{2} \int_{V^{(e)}} \varepsilon^{*T} D \varepsilon^* dV - \int_{V^{(e)}} u^T b dV - \int_{S_\sigma^{(e)}} u^T T dS + \int_{V^{(e)}} \varepsilon^T \sigma^* dV \quad (2-11)$$

where the superscript e denotes a specific element. Based on kinematical considerations, the components of the total strain vector ε , in terms of the displacement components are expressed as:

$$\begin{Bmatrix} \varepsilon_{xx} \\ \varepsilon_{yy} \\ \varepsilon_{zz} \\ \gamma_{xy} \\ \gamma_{yz} \\ \gamma_{zx} \end{Bmatrix} = \begin{bmatrix} \frac{\partial}{\partial x} & 0 & 0 \\ 0 & \frac{\partial}{\partial y} & 0 \\ 0 & 0 & \frac{\partial}{\partial z} \\ \frac{\partial}{\partial y} & \frac{\partial}{\partial x} & 0 \\ 0 & \frac{\partial}{\partial z} & \frac{\partial}{\partial y} \\ \frac{\partial}{\partial z} & 0 & \frac{\partial}{\partial x} \end{bmatrix} \begin{Bmatrix} u_x \\ u_y \\ u_z \end{Bmatrix}, \text{ or } \varepsilon = L \cdot u \quad (2-12)$$

in which L is the differential operator matrix.

The finite element process seeks a minimum in the potential energy based on the approximate form of the dependent variables (displacement components) within each element. The greater the number of degrees of freedom associated with the element (usually means increasing the number of nodes), the more closely the solution will approximate the true equilibrium position. Within each element, the approximation to the displacement components can be expressed as [24]

$$u_x^{(e)} \approx \tilde{u}_x^{(e)} = \sum_{r=1}^n N_r^{(e)} u_{x_r}^{(e)} \quad u_y^{(e)} \approx \tilde{u}_y^{(e)} = \sum_{r=1}^n N_r^{(e)} u_{y_r}^{(e)} \quad u_z^{(e)} \approx \tilde{u}_z^{(e)} = \sum_{r=1}^n N_r^{(e)} u_{z_r}^{(e)}$$

with n representing the number of nodes associated with element e . The nodal unknowns and shape functions are denoted by $u_{x_r}^{(e)}, u_{y_r}^{(e)}, u_{z_r}^{(e)}$ and $N_r^{(e)}$, respectively. In matrix form, the approximate displacement components can be expressed as [24]

$$\tilde{\mathbf{u}}^{(e)} = \mathbf{N}^{(e)T} \mathbf{U}^{(e)} \quad (2-13)$$

in which

$$\begin{aligned} \tilde{\mathbf{u}}_x^{(e)T} &= \{ \tilde{u}_x^{(e)} \quad \tilde{u}_y^{(e)} \quad \tilde{u}_z^{(e)} \} \\ \mathbf{N}^{(e)T} &= \begin{bmatrix} N_1 & 0 & 0 & N_2 & 0 & 0 & \dots & N_n & 0 & 0 \\ 0 & N_1 & 0 & 0 & N_2 & 0 & \dots & 0 & N_n & 0 \\ 0 & 0 & N_1 & 0 & 0 & N_2 & \dots & 0 & 0 & N_n \end{bmatrix}_{3 \times 3n} \\ \mathbf{U}^{(e)T} &= \{ u_{x_1}^{(e)} \quad u_{y_1}^{(e)} \quad u_{z_1}^{(e)} \quad u_{x_2}^{(e)} \quad u_{y_2}^{(e)} \quad u_{z_2}^{(e)} \quad \dots \quad u_{x_n}^{(e)} \quad u_{y_n}^{(e)} \quad u_{z_n}^{(e)} \} \end{aligned}$$

With the approximate form of the displacement components, the strain components within each element can be expressed as

$$\boldsymbol{\varepsilon} \approx \mathbf{B}^{(e)} \mathbf{U}^{(e)} \quad (2-14)$$

Where

$$\mathbf{B}^{(e)} = \mathbf{L} \mathbf{N}^{(e)T} \quad (2-15)$$

leading to the expression for the total potential in terms of element nodal displacements, U

$$\pi_p^{(e)} = \frac{1}{2} \mathbf{U}^{(e)T} \mathbf{k}^{(e)} \mathbf{U}^{(e)} - \mathbf{U}^{(e)T} \mathbf{p}^{(e)} + \frac{1}{2} \int_{V^{(e)}} \boldsymbol{\varepsilon}^{*T} \mathbf{D} \boldsymbol{\varepsilon}^* dV \quad (2-16)$$

in which the element stiffness matrix, k, and the element force vector, p, are defined as

$$\mathbf{k}^{(e)} = \int_{V^{(e)}} \mathbf{B}^{(e)T} \mathbf{D} \mathbf{B}^{(e)} dV \quad (2-17)$$

$$\mathbf{p}^{(e)} = \mathbf{p}_b^{(e)} + \mathbf{p}_\Gamma^{(e)} + \mathbf{p}_{\varepsilon^*}^{(e)} + \mathbf{p}_{\sigma^*}^{(e)}$$

with $\mathbf{p}_b^{(e)}$, $\mathbf{p}_\Gamma^{(e)}$, $\mathbf{p}_{\varepsilon^*}^{(e)}$, and $\mathbf{p}_{\sigma^*}^{(e)}$ representing the element load vectors due to body forces, surface tractions (forces), initial strains, and initial stresses, respectively, defined by

$$\begin{aligned}
\mathbf{p}_b^{(e)} &= \int_{V^{(e)}} N^{(e)} b \, dV \\
\mathbf{p}_T^{(e)} &= \int_{S_\sigma^{(e)}} N^{(e)} T \, dS \\
\mathbf{p}_{\varepsilon^*}^{(e)} &= \int_{V^{(e)}} B^{(e)} D\varepsilon^* \, dV \\
\mathbf{p}_{\sigma^*}^{(e)} &= \int_{V^{(e)}} B^{(e)T} \sigma^* \, dV
\end{aligned}$$

Evaluation of these integrals results in the statically equivalent nodal forces in the elements affected by the body force, the surface tractions, and the initial strains and initial stresses. In the presence of external concentrated forces acting on various nodes, the potential energy is modified as [24]:

$$\pi_p = \frac{1}{2} U^T \left\{ \sum_{e=1}^E k^{(e)} \right\} U - U^T \left\{ \sum_{e=1}^E \left(\mathbf{p}_b^{(e)} + \mathbf{p}_T^{(e)} + \mathbf{p}_{\varepsilon^*}^{(e)} - \mathbf{p}_{\sigma^*}^{(e)} \right) - \mathbf{p}_c \right\} + \frac{1}{2} \sum_{e=1}^E \int_{V^{(e)}} \varepsilon^{*T} D\varepsilon^* \, dV \quad (2-18)$$

where \mathbf{P}_c is the vector of nodal forces and U represents the vector of nodal displacements for the entire structure. Note that each component of the element nodal displacement vector, $U^{(e)}$ appears in the global (system) nodal displacement vector, U . Therefore, the element nodal displacement vector $U^{(e)}$ can be replaced by U with the appropriate enlargement of the element matrices and vectors in the expression for the potential energy by adding the required number of zero elements and rearranging. The summation in the expression for the potential energy implies the expansion of the element matrices to the size of the global (system) matrix while collecting the overlapping terms. Minimization of the total potential energy requires that

$$\left\{ \frac{\partial \pi_p}{\partial U} \right\} = 0 \quad (2-19)$$

leading to the system (global) equilibrium equations in the form

$$K U = P$$

in which K and P is the assembled (global) stiffness matrix and the assembled (global) nodal load vector, respectively, defined by

$$K = \sum_{e=1}^E k^{(e)}$$

$$K = \sum_{e=1}^E \left(p_b^{(e)} + p_T^{(e)} + p_{\varepsilon^*}^{(e)} - p_{\sigma^*}^{(e)} \right) - p_c \quad (2-20)$$

This global equilibrium equation cannot be solved unless boundary constraints are imposed to suppress the rigid-body motion. Otherwise, the global stiffness matrix becomes singular. After obtaining the solution to the nodal displacements of the system equilibrium equations, the stresses within the element can be determined from

$$\sigma = D B^{(e)} U^{(e)} - D \varepsilon^* + \sigma^* \quad (2.21)$$

The global stiffness matrix and the load vector require the evaluation of the integrals associated with the element stiffness matrix and the element nodal load vector [24].

The term “3D solid” is used to mean a three-dimensional solid that is unrestricted as to shape, loading, material properties, and boundary conditions [25]. A consequence of this generality is that all six possible stresses (three normal and three shears) must be taken into account, see Fig. 2.6. Also, the displacement field involves all three possible components, u , v , and w . Typical finite elements for 3D solids are tetrahedral and hexahedra, with three translational degree of freedom (DOF) per node. Fig. 2.7b shows a hexahedral element.

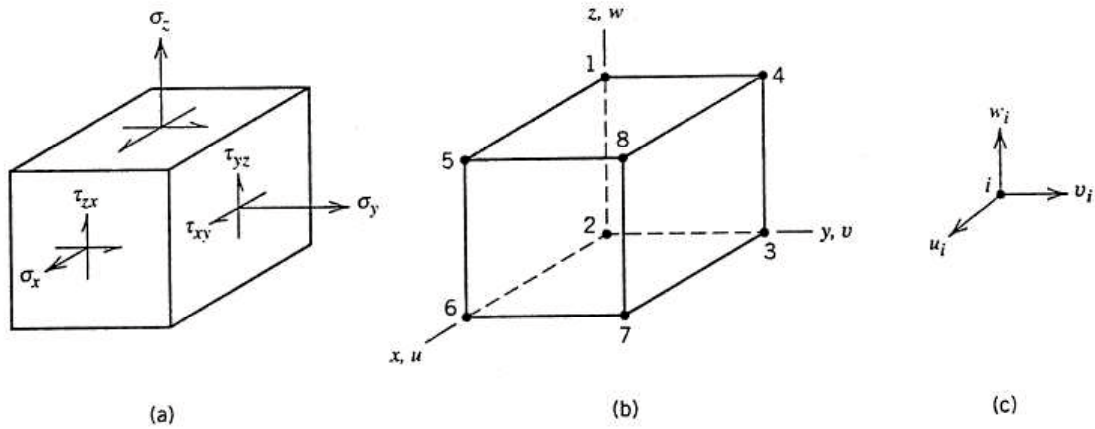


Fig. 2.6 (a) 3D state of stress (b) an eight-node hexahedron FE (c) the DOF at a typical node ($i = 1, 2, \dots, 8$) (adapted from [25])

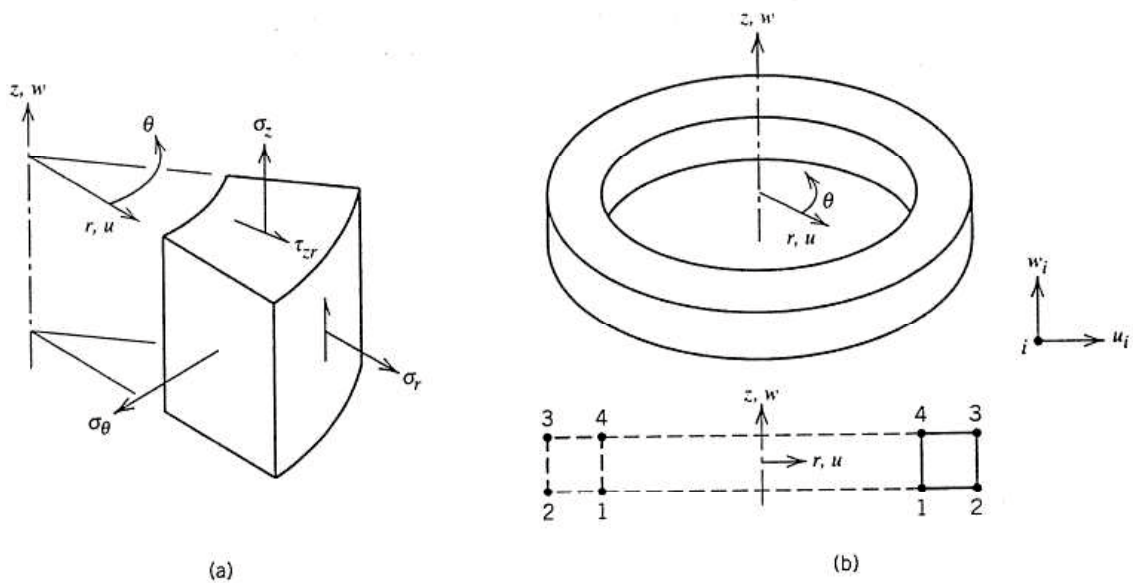


Fig. 2.7 (a) Axisymmetric state of stress (b) a four-node axisymmetric element and DOF at a typical node ($i = 1, 2, 3, 4$) (adapted from [25])

A solid of revolution, also called an axisymmetric solid, is generated by revolving a plane figure about an axis in the plane [25]. Common examples include a hose nozzle and a light bulb, although the light bulb has a very thin wall and would be properly classed as a shell of revolution for stress analysis purposes. Loads and supports may or may not have

axial Symmetry. In the case where geometry, elastic properties, loads, and supports are all axisymmetry, consequently, nothing varies with the circumferential coordinate θ , material points displace only radially and axially, and shear stresses $\tau_{r\theta}$ and $\tau_{\theta z}$ are both zero. Thus the analysis problem is mathematically two-dimensional. Axisymmetric finite elements are often pictured as plane triangles or quadrilateral, but these plane shapes are actually cross sections of annular elements, and what appear to be nodal points are actually nodal circles (Fig. 2.7).

2.4. Taguchi Method

This method is development of the Design of Experiment (DoE) used to improve the quality of products and processes as well as is being able to minimize the cost and resources. This method is extremely helpful in off-line quality control. The target of Taguchi Method is to render the product robust against noise, because it often referred to as robust design.

According to Taguchi's definition of quality is accepted by the public loss since the product was delivered. Genichi Taguchi [26] distinguishes three conditions, namely larger the better as a result of the chemical reaction. Smaller the better as the resultant flue gases by motor vehicles. The target is minimum variation such parts or components of the product.

Taguchi contribution on quality is:

1. Loss function is a function of the losses incurred by the society (producers and consumers) due to the quality produced. For producers, namely the emergence of quality costs, while for consumers is that there is dissatisfaction or disappointment over the products purchased or consumed due to poor quality.
2. Orthogonal array is used to design efficient experiments and to analyze experimental data. Orthogonal array is used to determine the minimum number of experiments that can provide as much information as possible all factors affecting parameter. The most important part of the orthogonal array lies in the selection of a combination of the level of input variables for each experiment.

3. Robustness to minimize the sensitivity of the system to the sources of variation.

These measures are divided into three main phases which include the overall experimental approach. The three phases are (1) the planning phase, (2) the implementation phase, and (3) the analysis phase. Planning phase is the most important phase of the experiment is expected to provide the information. Planning phase is the phase when the factors and levels selected. The second important phase is the implementation phase, the phase when the experimental results have been obtained. If the experiment is planned and executed well, the analysis will be easier and less likely to be able to produce information that is positive about the factors and levels. Analysis phase is when the positive or negative information relating to the factors and levels that have been generated by two previous phases. Analysis phase is the last thing which is important if researchers will be able to produce positive results.

Taguchi method is a robust design approach, which uses many ideas from statistical experimental design for evaluating and implementing improvement in product, processes, and equipment. The fundamental principle of Taguchi method is to improve the quality of a product by minimizing the effect of the causes of variation without eliminating the inevitable causes. The two major tools used in the Taguchi method are Orthogonal Arrays (OA) which are used to study many design parameters simultaneously and Signal-to-Noise Ratio (SNR) which measures quality.

A full factorial experiment conducts all possible combinations of the factor levels and therefore can reach the overall optimum setting, but it becomes overwhelming in the number of the design's parameters or levels increases. For example, if a new design involves 8 three-level parameters, the experiment needs to conduct 6561 ($=3^8$) settings. Therefore, the approach is only practical for a limited number of parameters and levels.

An orthogonal array has two major requirements. The first is that the levels of any factor occur with the same frequency. The second is that, for any two factors, each possible combination of levels takes place with the same frequency. If all factor have q levels, an orthogonal arrays is usually expressed as $LM(qm)$ where m is the number of factors and M represents the number of rows in the array (a multiple of q^2).

Table 2.3 Array selectors all pairs of combinations

		Number of Levels			
		2	3	4	5
Number of Parameters (P)	2	L4	L9	L'16	L25
	3	L4	L9	L'16	L25
	4	L8	L9	L'16	L25
	5	L8	L18	L'16	L25
	6	L8	L18	L'32	L25
	7	L8	L18	L'32	L50
	8	L12	L18	L'32	L50
	9	L12	L27	L'32	L50
	10	L12	L27	L'32	L50
	11	L12	L27		L50
	12	L16	L27		L50
	13	L16	L27		
	14	L16	L36		
	15	L16	L36		
	16	L32	L36		
	17	L32	L36		
	18	L32	L36		
	19	L32	L36		
	20	L32	L36		
	21	L32	L36		
	22	L32	L36		
	23	L32	L36		
	24	L32			
	25	L32			
	26	L32			
	27	L32			
	27	L32			
	29	L32			
	30	L32			
	31	L32			

In the study of orthogonal arrays, Taguchi [26] explored the entire design space with a few experiments and suggested several standard orthogonal arrays. He classified them into three types: 2-level arrays ($L_4, L_8, L_{16}, L_{32}, L_{64}$), 3-level arrays (L_9, L_{27}, L_{81}), and

mixed 2-and-3-level arrays (*L18*, *L36*, *L54*). For example, if one has 12 three-level parameters, Taguchi chooses the *L27* design and so only conducts 27 specified settings. In this way, for design containing many parameters and levels, a fractional factorial approach could determine a feasible parameter setting with much less effort and time because of using the orthogonal array.

The question is can we get similar information with fewer test? Because each setting requires a gasket to product and test, so it means a significant high cost. Therefore option number 2, Taguchi method is chosen as shown in Table 2.3. The motivation is instead of testing all possible combinations of factors, it can test all pairs of combinations in some more efficient way. The key feature is comparing any pairs of factors across all experiments and it can be seen that each combination is represented.

The second tool of Taguchi method, the SNR, is used to find which level is suitable for each factor. In communication engineering parlance, the SNR means the measure of signal quality, which corresponds to the solution quality in Taguchi method. While conducting each experiment as per the orthogonal array, the objective function value is computed. A level of a particular factor, which gives the maximum effect in contribution to the objective function value, is optimal for the concerned factor. As the effect of this level, it is said to have maximum influence or the maximum SNR and so considered as the optimal level for the factor. With the conduct of all the experiments as per the orthogonal arrays, the solution obtained with optimal level for each factor, is the optimum solution for the given optimization problem. From the SNR, the optimum conditions of factors are selected. There are several SNR available, depending on the type of characteristic; lower is better (eq. 2-22), nominal is best (Eq. 2-23), or higher is better (Eq. 2-24) [26].

$$\text{SNR} = 10 \log \left(\frac{1}{n} \sum_{i=1}^n y_i^2 \right) \quad (2-22)$$

$$\text{SNR} = 10 \log \left(\frac{1}{n} \sum_{i=1}^n (y_i - S)^2 \right) \quad (2-23)$$

$$\text{SNR} = 10 \log \left(\frac{1}{n} \sum_{i=1}^n \frac{1}{y_i^2} \right) \quad (2-24)$$

Where y_i = the value each of the better quality characteristic

S = the target value

N = the number of measurements in a trial

2.5. Contact Mechanics Theories

Surface roughness on many different length scales, even a highly polished surface. Surface roughness has an important influence on many important physical phenomena such as contact mechanics, sealing, adhesion, and friction. When two bodies with nominally flat surfaces are brought into contact, real contact will only occur in small randomly distributed area. We can visualize the contact region as small areas where asperities from one solid are squeezed against asperities of the other solid. It depending on the conditions the asperities may deform elastically or plastically [6].

2.5.1 Persson Theory for Elastic Contact Mechanics

When a surface roughness is studied at low magnification ($\zeta = 1$) it looks as if complete contact occurs between the solid at many *macroasperity* contact region explained by Persson et al. [6]. The contact between two solids, which are a rubber and a hard rough substrate, at increasing magnification ζ is shown in Fig. 2.8.

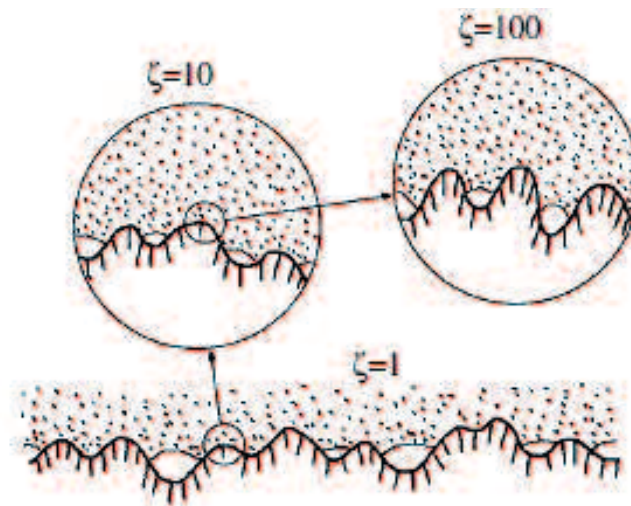


Fig. 2.8 A rubber block (dotted area) in adhesive contact with a hard rough substrate (dashed area) (Adapted from [6])

In normal condition, no magnification, no surface roughness can be observed and the block makes contact with the substrate everywhere in the nominal contact area. Increasing the magnification and smaller length scale roughness detected, it can be observed that only partial contact occurs at the asperities. There is observed the contact and no contact regions. In fact, if there was no short distance cut-off the true contact area would eventually vanish. In reality, a short distance cut-off always exists, e.g., the interatomic distance. In many cases the local pressure in the contact regions at the asperities may become so high that the material yields plastically before reaching the atomic dimension. In these cases the size of the real contact area will be determined mainly by the yield stress of the solid [6].

The magnification ζ refers to some (arbitrary) chosen reference length scale. This could be, e.g., the lateral size L of the nominal contact area in which case $\zeta = \frac{L}{\lambda} = q/q_L$, where λ is the shortest wavelength roughness which can be resolved at magnification ζ .

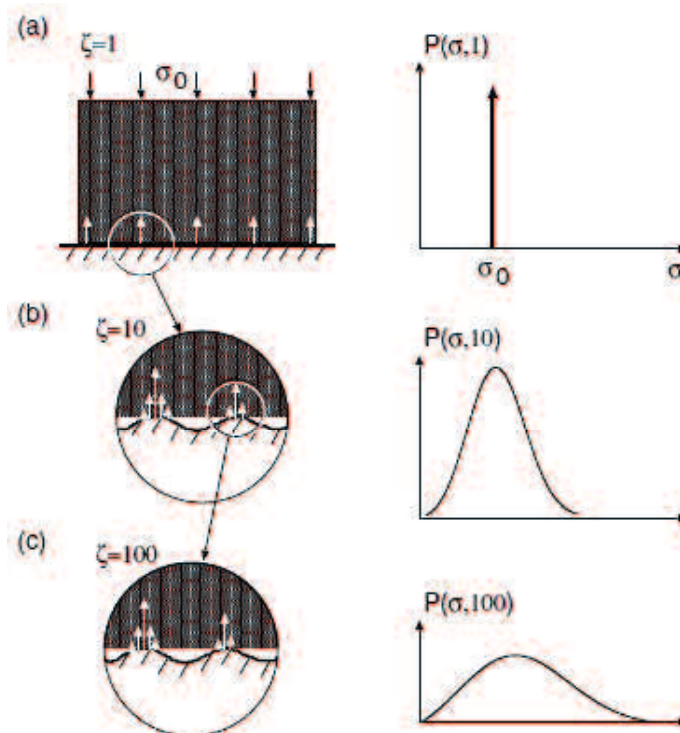


Fig. 2.9 Stress distribution in the contact region between a rigid and an elastic substrate at increasing magnification (Adapted from [6])

When the system is studied at the lowest magnification $\zeta = 1$ no surface roughness can be observed and the block makes (apparent) contact with the substrate everywhere in the nominal contact area. In this case, if we neglect friction at the interface, the stress at the interface will everywhere equal the applied stress σ_0 —see Fig. 2.9(a)—so the distribution will initially be delta function like, $P(\sigma, 1) = \delta(\sigma - \sigma_0)$. Increasing the magnification, we include surface roughness with wavelength down to $\lambda = L/\zeta$, and here one may observe some non-contact regions as shown in Fig. 2.15(b). Since the stress must go continuously to zero at the edges of the boundary between the contact and non-contact regions, it follows that the stress distribution $P(\sigma, \zeta)$ will have a tail extending the whole way down to zero stress as indicated in Fig. 2.9(b) (right). There will also be a tail toward larger stresses $\sigma > \sigma_0$ because the average stress must be equal to σ_0 . This distribution broadens as in a diffusion problem. With increasing magnification, the stress distribution will broaden further and without limit as indicated in Fig. 2.15(c) (right).

2.5.2 Persson Theory for Elastoplastic Contact Mechanics

In the study above we assumed that only elastic deformation occurs. However, the theory can be generalized to the case in where also plastic deformation occurs simply by replacing the boundary condition $P(0, \zeta) = 0$ with $P(\sigma_Y, \zeta) = 0$, which describes that plastic deformation occurs in the contact area when the local stress has reached σ_Y . Increasing magnification the contact area diffuses over the $\sigma = 0$ boundary into non-contact, and over the $\sigma = \sigma_Y$ boundary into plastic contact. Let us to introduce the function $P_{non}(\zeta)$ and $P_{pl}(\zeta)$ which describe the fraction of the original (for $\zeta = 1$) macro-contact area where, under the magnification ζ , non-contact, and contact with plastic yield has occurred, respectively [10]. Thus we have

$$P_{el}(\zeta) + P_{non}(\zeta) + P_{pl}(\zeta) = 1 \quad (2.25)$$

where $P_{el}(\zeta) = P(\zeta)$ describes the fraction of the macro-contact area where elastic contact occurs on the length scale L/ζ .

The statement about conservation of area (projected on xy-plane) [27]:

$$A_{el}(\zeta) + A_{pl}(\zeta) + A_{non}(\zeta) = 0$$

Or after integration

$$A_{el} + A_{pl} + A_{non} = A_0 \quad (2.26)$$

2.6. Percolation Theory

Surface roughness is an important factor which influences the rate of leakage through seals. The exact mechanism of roughness induced leakage is not well understood. Practically all macroscopic bodies have surfaces with roughness on many different length scales. When two bodies with nominally flat surfaces are brought into contact, the real (atomic) contact will only occur in small randomly distributed areas and the area of real contact is usually extremely small fraction on nominal contact area.

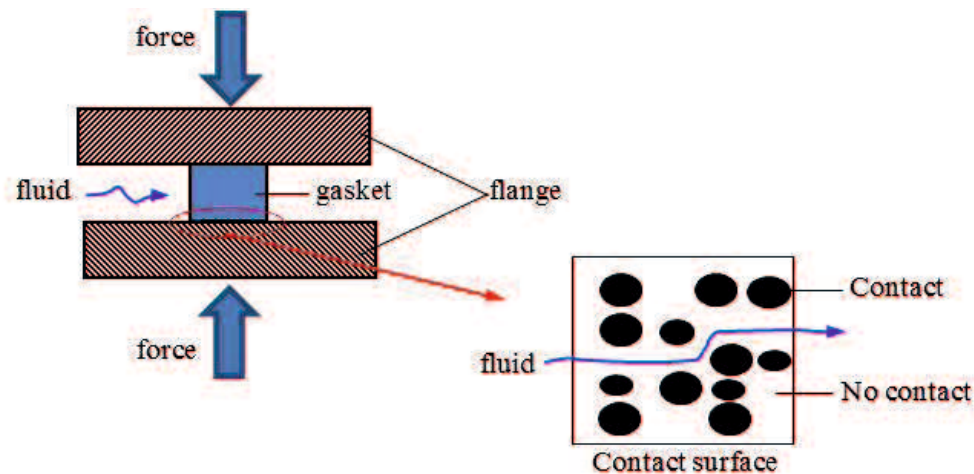


Fig. 2.10 Schematic of leakage occurring in a gasket pressed against a flange by a uniform pressure distribution

Most engineering surfaces have a surface roughness that lies in a wide range of length scales and this roughness strongly influences the leakage rate. In other side, accounting for the whole range of surface roughness is impossible using standard numerical methods such as FEM. Fig. 2.10 shows a schematic of how surface roughness leads to imperfect contact between a gasket and a flange. Here, the black and white areas respectively indicate the contacting and non-contacting surfaces. Clearly, the fluid can easily find a path through which to percolate, thus causing leakage to occur.

A micro scale contact schematic in the Fig. 2.10 can be approximated as square lattice grid as shown in the Fig 2.11.

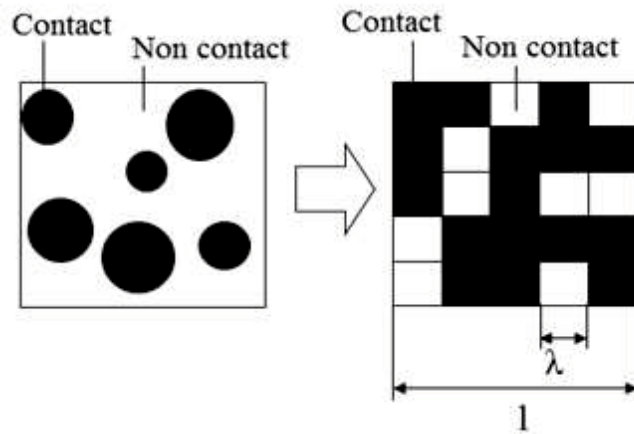


Fig. 2.11 Micro scale contact schematic approximated as square lattice grid

Persson et al. [6] uses percolation theory to predict the apparent contact area as a function of the magnification. The definition on magnification is described in Eq. (2-27). It shows some interfacial surface is observed, the increasing of magnification effect on decreasing contact area.

$$\zeta = \frac{l}{\lambda} \quad (2-27)$$

Where ζ = magnification

λ = length of one side of the square lattice grid

l = length of the apparent contact area

When a contact area is studied at low magnification it appears as if complete contact occurs, but when the magnification is increased it is observed that in actual only partial contact occurs as shown in the Fig. 2.12.

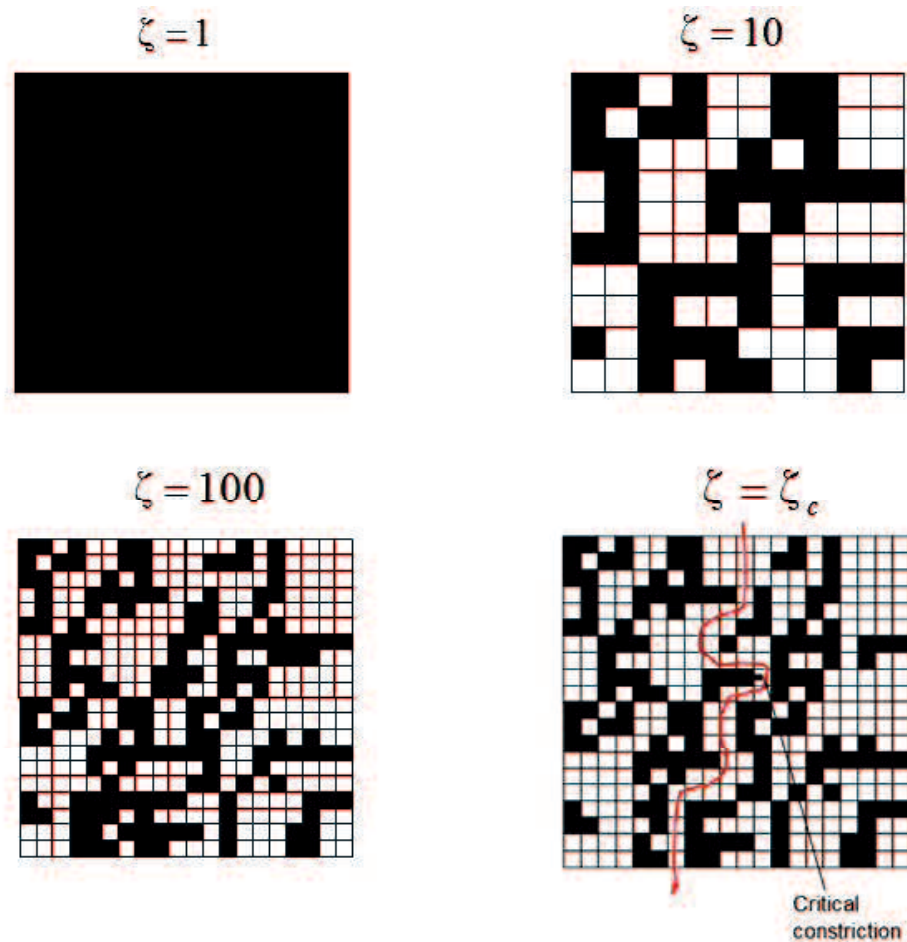


Fig 2.12 Schematic of contact region at different magnifications

When a surface roughness is studied at low magnification, no surface roughness and the block makes contact with the substrate everywhere in the nominal contact area. Increasing the magnification, here one may observe some non-contact regions. At high enough magnification, a percolating path of non-contact area (white square lattice) will eventually be observed at the percolation threshold ($\zeta = \zeta_c$). The non-contact area will

percolate as describe by probabilities; $P(\zeta_c)$ in Eq. (2-28) and the leakage will be occurring (red line in the Fig. 2.12) [7] and [9]. If the contact of gasket system produces a higher percolation threshold, it means the low leakage in the system.

$$P(\zeta_c) = 1 - \frac{A(\zeta_c)}{A_0} \quad (2-28)$$

Where $A(\zeta_c)$ = the noncontact area at the percolation threshold

A_0 = the apparent contact area

Derivation of the expression amount of leakage between parallel plates can explain from Fig. 2.13.

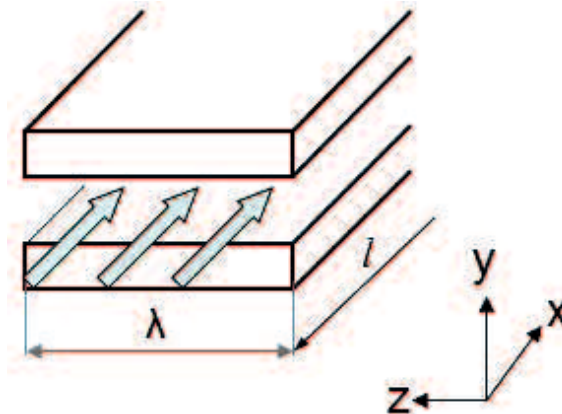


Figure 2.13 Flow between parallel plates

Assuming that only the-x direction of flow

$$u \neq 0 \quad v = w = 0 \quad (2-29)$$

When you assign to this equation of continuity

$$\frac{\partial u}{\partial x} + \frac{\partial v}{\partial y} + \frac{\partial w}{\partial z} = 0 \text{ then}$$

$$\frac{\partial u}{\partial x} = 0 \quad (2-30)$$

And also to assign to the Navier-stokes equations

$$\frac{\partial u}{\partial t} + u \frac{\partial u}{\partial x} + v \frac{\partial u}{\partial y} + w \frac{\partial u}{\partial z} = -\frac{1}{\rho} \frac{\partial p}{\partial x} + \nu \left(\frac{\partial^2 u}{\partial x^2} + \frac{\partial^2 u}{\partial y^2} + \frac{\partial^2 u}{\partial z^2} \right) \quad \text{than}$$

$$\frac{\partial u}{\partial t} + u \frac{\partial u}{\partial x} = -\frac{1}{\rho} \frac{\partial p}{\partial x} + \nu \left(\frac{\partial^2 u}{\partial x^2} + \frac{\partial^2 u}{\partial y^2} + \frac{\partial^2 u}{\partial z^2} \right) \quad (2-31)$$

When you assign equation (2-30) to (2-31)

$$\frac{\partial u}{\partial t} = -\frac{1}{\rho} \frac{\partial p}{\partial x} + \nu \left(\frac{\partial^2 u}{\partial y^2} + \frac{\partial^2 u}{\partial z^2} \right) \quad (2-32)$$

When a two-dimensional steady flow

$$\frac{\partial u}{\partial t} = 0 \quad \frac{\partial}{\partial z} = 0$$

Then equation (2-32)

$$0 = -\frac{1}{\rho} \frac{\partial p}{\partial x} + \nu \frac{\partial^2 u}{\partial y^2}$$

$$\frac{\partial^2 u}{\partial y^2} = \frac{1}{\mu} \frac{\partial p}{\partial x} \quad (2-34)$$

when the integral equation once

$$\frac{\partial u}{\partial y} = \frac{y}{\mu} \frac{\partial p}{\partial x} + C_1$$

integrating one more time

$$u = \frac{y^2}{2\mu} \frac{\partial p}{\partial x} + C_1 y + C_2$$

Boundary condition

From $u = 0$ at $y = 0, y = h$

$$C_2 = 0 \quad C_1 = -\frac{h}{2\mu} \frac{\partial p}{\partial x}$$

$$\text{So } u = \frac{y^2 - hy}{2\mu} \frac{\partial p}{\partial x} \quad (2-35)$$

Formula derivation of the amount of leakage

Than Q flow rate this

$$Q = \int_0^h u \lambda dy \quad (2-36)$$

$$Q = \frac{\lambda}{2\mu} \frac{\partial p}{\partial x} \int_0^h (y^2 - hy) dy$$

$$Q = \frac{\lambda}{2\mu} \frac{\partial p}{\partial x} \left[\frac{y^3}{3} - \frac{hy^2}{2} \right]_0^h$$

$$Q = -\frac{\lambda h^3}{12\mu} \frac{\partial p}{\partial x}$$

$$Q = \frac{\lambda h^3}{12\mu} \frac{p_2 - p_1}{\lambda}$$

$$Q = \frac{\lambda h^3}{12\mu} (p_2 - p_1) \quad (2-37)$$

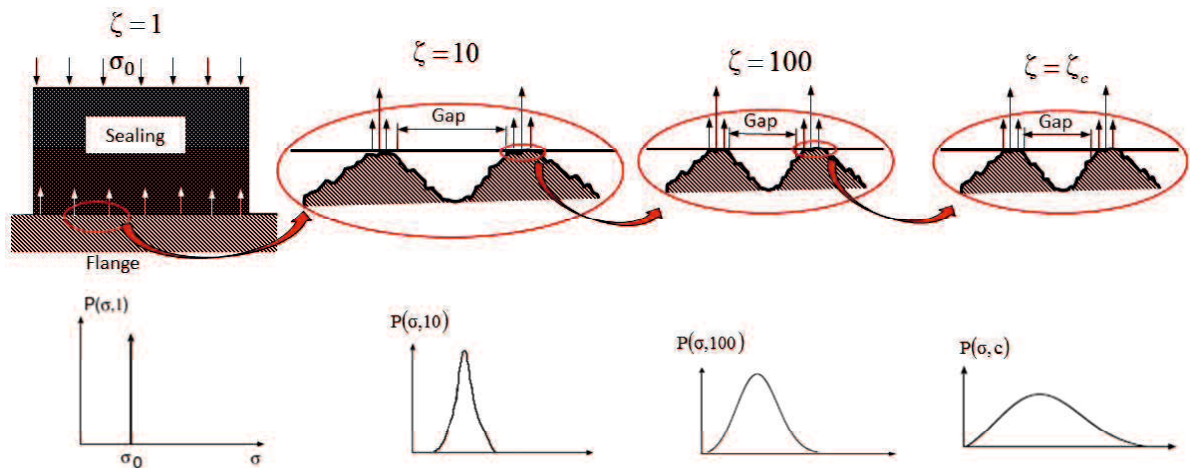


Fig. 2.14 Pressure distribution of magnification

Pressure distribution of magnification can explain using equation (2.62) and Fig. 2.14

[6]. When a surface roughness is studied at low magnification, no surface roughness, the stress at the interface will everywhere equal the applied stress σ_0 . Increasing the magnification, there will be a tail toward larger stresses $\sigma > \sigma_0$ because the average stress must be equal to σ_0 . The contact stress distribution $P(\sigma, \zeta)$ is investigated [7]. The theory predicts that the area of contact in most cases varies linearly with the load, and that it depends on the magnification.

Derivation of the contact area (no elastic deformation bonding), contact area depends on the magnification of the scale to observe ζ also depends on the stress distribution of the contact area $P(\sigma, \zeta)$. Diffusion equation can be represented by

$$\frac{\partial P}{\partial \zeta} = f(\zeta) \frac{\partial^2 P}{\partial \sigma^2} \quad (2.38)$$

Here the $f(\zeta) = G'(\zeta)\sigma_0^2$ is

Paper “Theory of rubber friction and contact mechanics” derivation is

$$G(\zeta) = \frac{\pi}{4} \left(\frac{E^*}{\sigma} \right)^2 \int_{q_L}^{\zeta q_L} dq q^3 C(q)$$

with $E^* = E/(1-\nu^2)$.

$$G'(\zeta) = \frac{\pi}{4} E^{*2} q_L q^3 C(q)$$

The effective contact ratio $P(\zeta)$ is

$$P(\zeta) = \int_0^\infty d\sigma P(\sigma, \zeta)$$

$$P(\zeta) = \frac{2}{\pi} \int_0^\infty dx \frac{\sin x}{x} e^{-x^2 G(\zeta)} = \text{erf} \left(\frac{1}{2\sqrt{G}} \right)$$

With the number of Hurst, derivation of expression of the contact area

$$P(\zeta) = \frac{4\sigma_0(1-\nu^2)}{q_0 h_0 E} \left(\frac{1-H}{\pi H} \right)^{1/2} \zeta^{H-1} \quad (2-39)$$

Which σ_0 = the appearance contact stress

q_0 = roll-of wavelength

h_0 = rms roughness

$$P(\zeta) = 1 - \frac{A(\zeta)}{A_0} \quad (2-40)$$

$$\text{Percolation probability } P(\zeta_c) = 1 - \frac{A(\zeta_c)}{A_0}$$

We find that the percolation channel is formed when $\zeta = \zeta_c$, where $\frac{A(\zeta_c)}{A_0} = 0.4$, in accordance with percolation theory [27]

$$\text{so} \quad 0.6 = \frac{4\sigma_0(1-\nu^2)}{q_0 h_0 E} \left(\frac{1-H}{\pi H} \right)^{1/2} \zeta_c^{H-1} \quad (2-41)$$

$$\text{Critical magnification } \zeta_c = \left(\frac{4\sigma_0(1-\nu^2)}{0.6q_0 h_0 E} \right)^{\frac{1}{1-H}} \left(\frac{1-H}{\pi H} \right)^{\frac{1}{2(1-H)}} \quad (2-42)$$

Bottiglione et al. [28] calculated the critical path height (u_c).

$$u_c = \langle h^2 \rangle^{1/2} \frac{1}{\zeta_c^H} \left(\frac{\zeta_m^{2H} - \zeta_c^{2H}}{\zeta_m^{2H} - 1} \right)^{1/2} = q_0^{-2H} \frac{1}{\zeta_c^H} \left(\frac{\zeta_m^{2H} - \zeta_c^{2H}}{\zeta_m^{2H} - 1} \right)^{1/2} \quad (2-43)$$

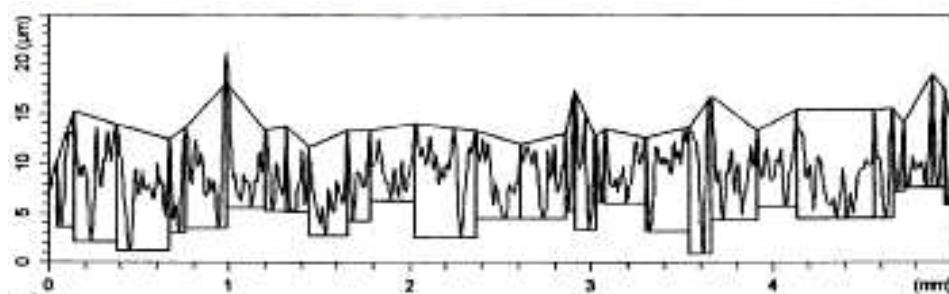
where $\langle h^2 \rangle = \int d^2q C(q_1, q_2) = 2\pi \int_0^\infty dq q C(q) \approx q_0^{-2H}$

In the next study, Persson et.al [8] calculated the volume-flow per unit time of leak-rate (Q) on rubber gasket. The calculated leak-rate is in good agreement with experiment.

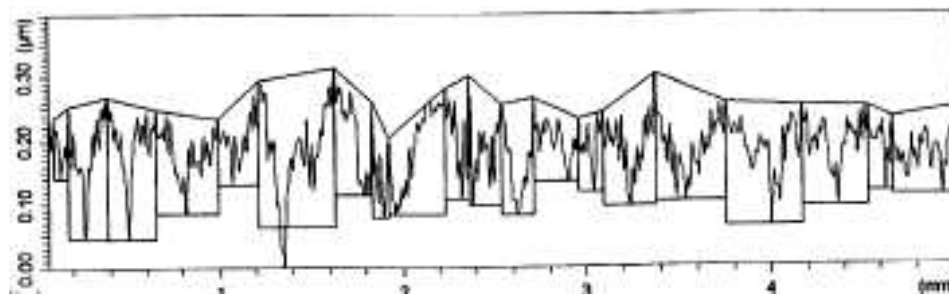
2.7. Contact between Two Rough Surfaces Model

In practice, all engineering surfaces show some surface roughness. Engineering surfaces often exhibit micro-geometric defect termed roughness and waviness. The actual

extent of these defects varies, depending on the machining processes, but they are always present. This fact causes the contact between two engineering surfaces to be located at only a limited number of asperities although the surfaces apparently have a high degree of surface conformity. A variation in the normal load applied through the contact modifies the deformation of the contact asperities and thus changes the number of asperities in contact. The relation between the number of contact asperities and the applied load has raised an exceedingly difficult problem [29].



(a) shot-peening



(b) polishing surfaces

Fig. 2.15 Roughness motifs (Adapted from [30])

The classical standard for roughness and waviness parameter determination uses filtering techniques; these allow the measurement to be decomposed into two profiles called roughness and waviness profiles. Each of these profiles is separately treated to obtain roughness or waviness parameters. The methodology adopted here draws upon the recent ISO standardized method (ISO 12085, 1996). With this method, signal processing is

obtained by a graphic technique and uses the called “motif” concept a motif being defined as that part of the profile which lies between two significant peaks. Because the profiles of engineering surfaces are often very jagged, it is necessary to combine elementary motifs to identify the main asperities and valleys which can describe roughness. The present method defines four conditions for a reproducible determination of the elementary motifs of roughness. They may be identified as follows: the width condition, the envelope condition, the magnification condition and the relationship condition. They, respectively, eliminate low altitude peaks, proximate peaks or valleys and significantly low asperities. After every possible combination has been performed the procedure furnishes the so-called roughness motif of which an example is given in Fig. 2.15 [30].

Roughness parameters can be deduced from the dimensions of the motifs:

- R_m is the mean value of the height R_i of each roughness motif.
- R_{rms} is the root mean square of the R_i values.
- S_m is the mean value of the width S_i of the motif.
- S_{rms} is the root mean square of the S_i values.

Only the first two are used in the micro-geometry model and the notation adopted is, respectively, H_m and H_{rms} referring to the mean and the root mean square value for amplitude of submit altitudes. Table 2.4 recapitulates the values for roughness and waviness parameters deduced from the motif procedure for the three surfaces described previously.

Table 2.4 Micro-geometrical roughness and waviness parameters of the surface roughness
(Adapted from [30])

Surface machining	Roughness				Waviness	
	R_m (μm)	R_{rms} (μm)	S_m (μm)	S_{rms} (μm)	H_m (μm)	H_{rms} (μm)
Shot peening	9.4	2.9	185	105	5.8	1.90
Grinding	1.2	0.43	130	100	0.51	0.24
Polishing	0.19	0.12	150	120	0.30	0.14

The surfaces of most materials are rough and contain irregular geometric features or asperities with sizes ranging over many length scales. Many models follow the approach proposed by Greenwood and Williamson [31], who chose to idealize a rough surface as a collection of asperities with spherical tips having the same curvature but varying heights. However, their model has proved difficult to apply to surfaces in practice because it is impossible to accurately measure the average curvature of asperities on real surfaces. This is because most surfaces have an approximate fractal or self-affine geometry over a wide range of length scales. Gao et al. [29] analyzed in detail the behavior of an elastic-perfectly plastic solid with a sinusoidal rough surface that is subjected to contact loading, see Fig. 2.16.

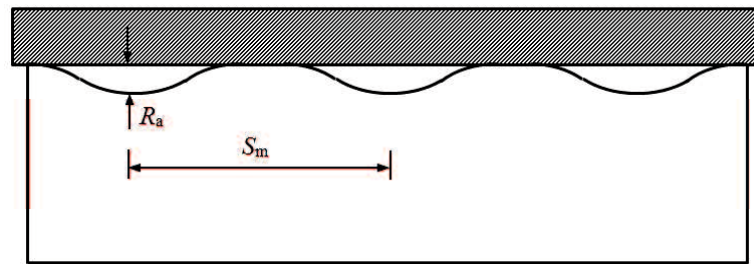


Fig. 2.16 Schematic illustrating indentation of a sinusoidal rough surface
(Adapted from [29])

When two nominally flat surfaces are in contact, the actual area of contact is usually only small fraction of the nominal area—only the peaks or asperities on the surface are in contact—and therefore, the real contact stress is higher than the nominal one. When the function of two surfaces is to prevent the leakage of a liquid, this roughness characteristic assumes great importance.

It is difficult to directly analyze the contact between two rough surfaces. Many researchers transform the contact between two rough deformable surfaces into contact between a smooth surface and a rough deformable surface; this is also called as a sum surface [30] and [32]. The micro-geometric parameters of each surface are combined to

obtain the parameters of the sum surface, as shown in Fig. 2.17.

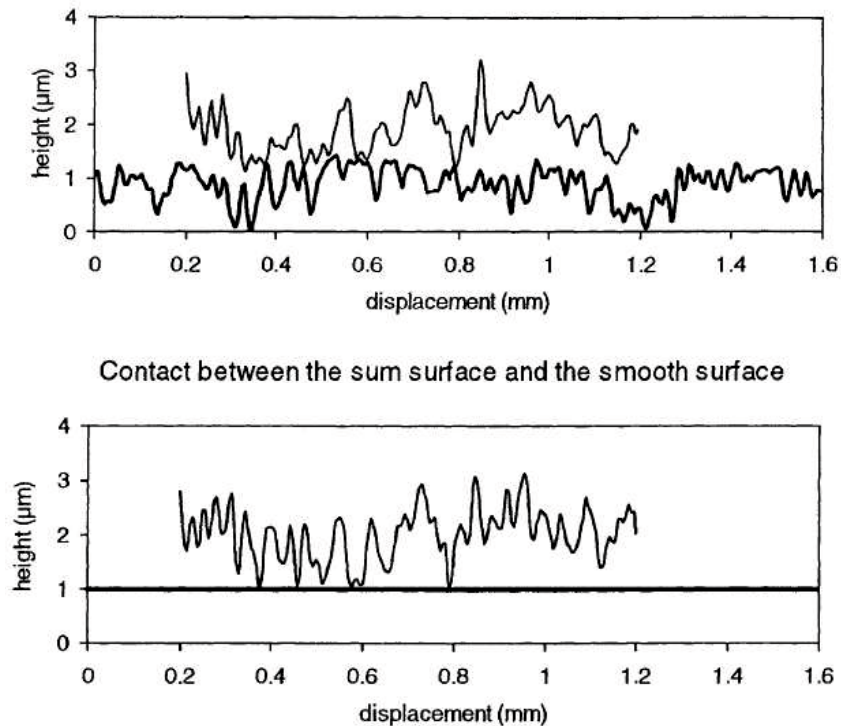


Fig. 2.17 Construction of sum surface (Adapted from [35])

2.8. Development of Gasket Asbestos Substitution

Estrada et al [2] developed a detailed strength and leakage three-dimensional and axisymmetric finite element analysis of the joint leakage on glass fiber reinforced plastic (GRFP). They use a contact formulation to allow loss of contact between the mating flange and the gasket as the internal pressure increases. Also, in the axisymmetric model, they allow fluid penetration into the space where this contact loss occurs; however, this type of loading is not supported in three-dimensional analysis.

The analysis was performed on a modified stub flanged joint, see Fig. 2.18. The pipe and hub is filament wound as an integral unit. The metallic backing ring is used to connect the joint to other members. The results shows that over 3/4 of the contact between the

gasket and the flange is lost as shown in the Fig. 2.19. However, the pressure on the portion of the gasket that remains in contact is greater than the internal pressure, and the minimum required gasket pressure to keep the joint leak tight.

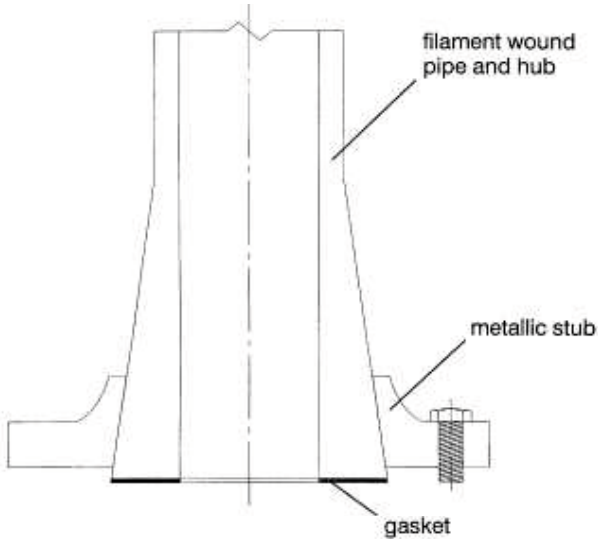


Fig. 2.18 Schematic of the modified stub flange joint (Adapted from [2])

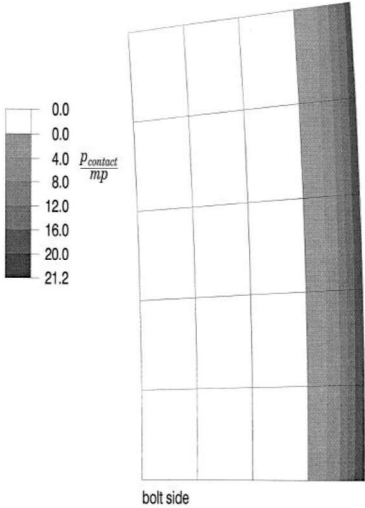


Fig. 2.19 Over 3/4 of the contact between the gasket and the flange is lost (Adapted from [2])

Huang et al. [5] used the room temperature tightness test (ROTT), developed by the pressure vessel research council (PVRC) to provide critical information on sealing performance and mechanical behavior of a polytetrafluoroethylene (PTFE) gasket material. This research used the helium mass leak rate and gasket deflection measurements. The result shows of helium leak rate as a function of gasket stress see Fig. 2.20. Fig. 2.21 showing the deflection results is a collection of the 15-min incremental measurements during the test.

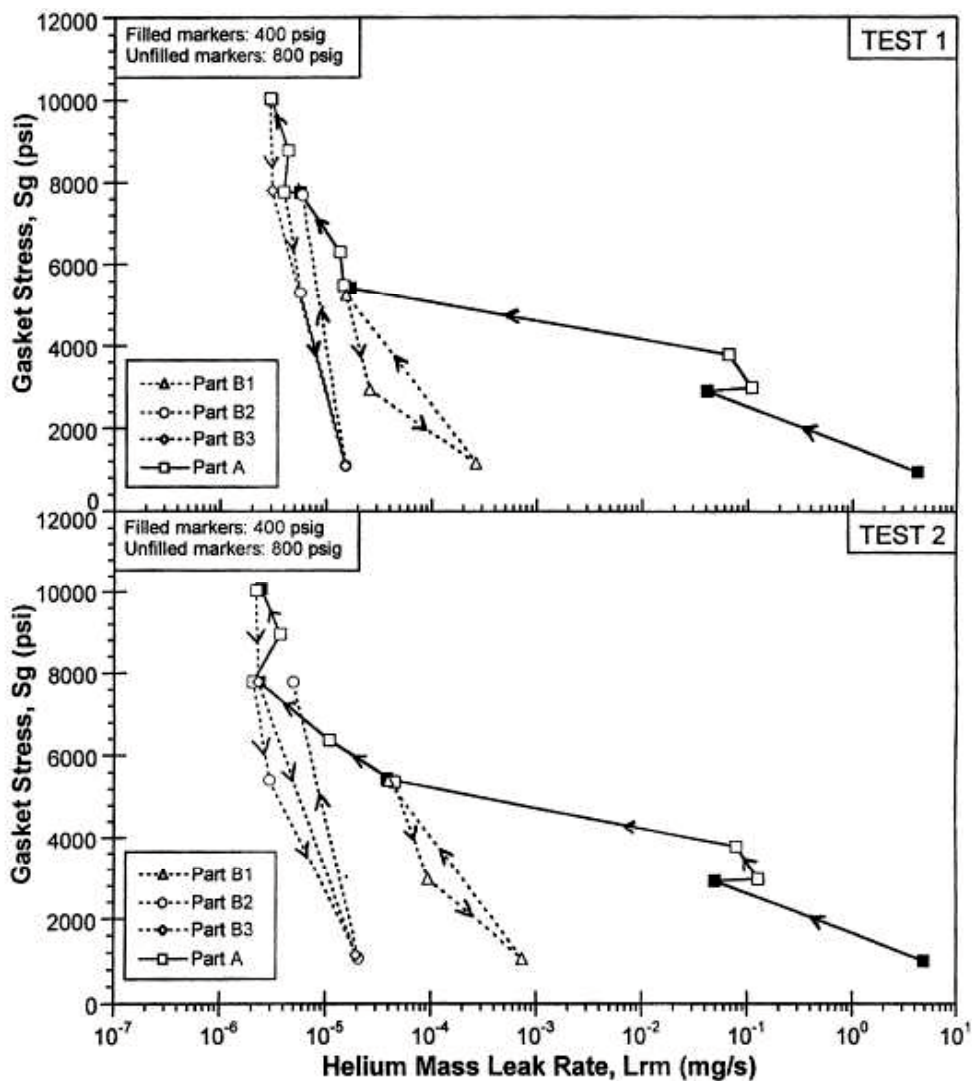


Fig. 2.20 Helium mass leak rate as a function of gasket stress (Adapted from [5])

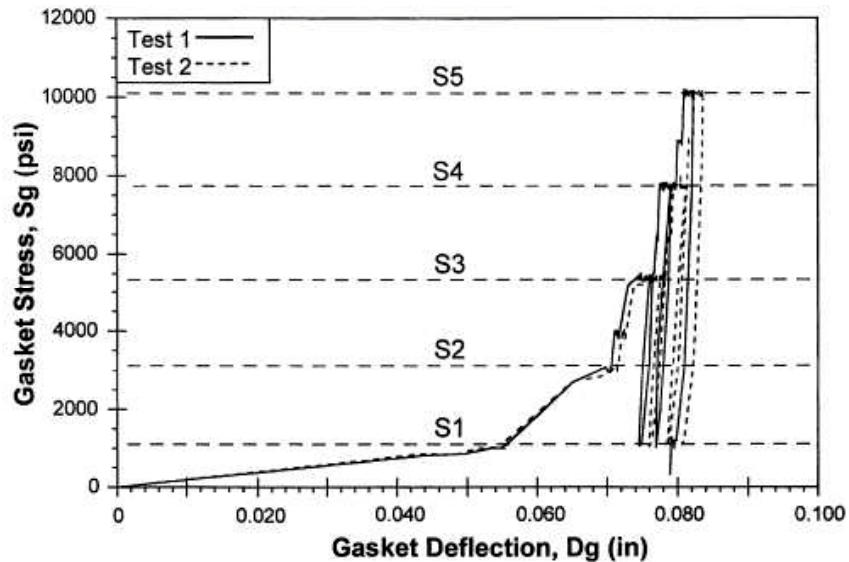


Fig. 2.21 Gasket deflection as a function of gasket stress (Adapted from [5])

Krishna et al [3] studied a three dimension finite element analysis of bolted flange joints on spiral wound gasket for finding the contact stresses 2.22. Nonlinearity and hysteresis of the gasket under various loading and operating conditions are taken into account. Three types of gaskets namely asbestos filled (AF), Graphite filled (GF), and PTFE filled (TF). Fig. 2.23 shows the dimensions of the pipe flange and the spiral wound gasket used in the finite element analysis. The results shows that the distribution of contact stress has a more dominant effect on sealing performance than the limit on flange rotation specified by ASME. The variation in contact stress distribution in the radial direction is found to be highest in GF spiral-wound gasket and the least for TF spiral-wound gaskets. The FE method is very useful during the design process for the selection of gasket, pretension of bolts and number of bolts.

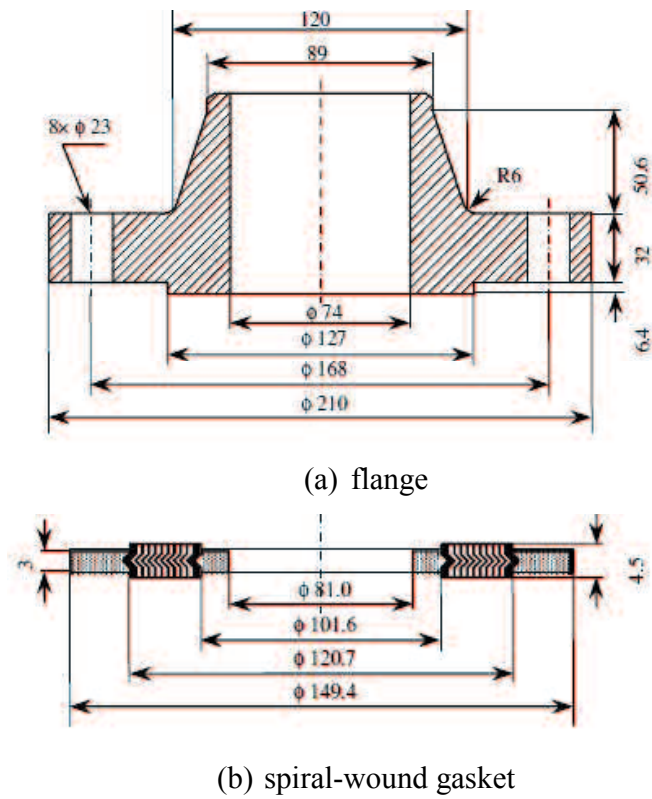


Fig. 3.22 Dimension of the flange and gasket used in the FEA (Adapted from [3])

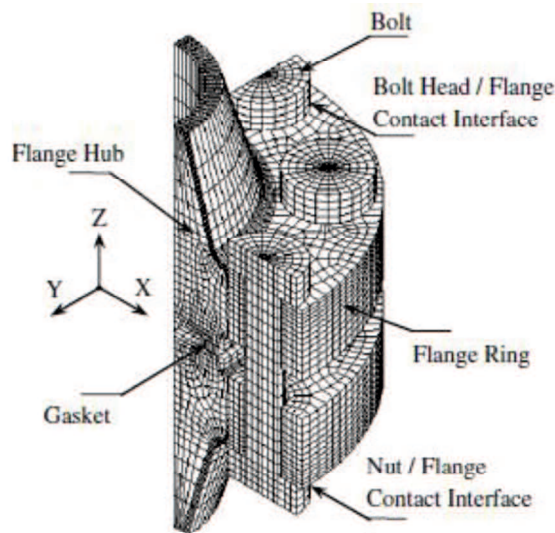


Fig. 2.23 Finite element mesh of bolted flange joint with spiral-wound gasket (Adapted from [3])

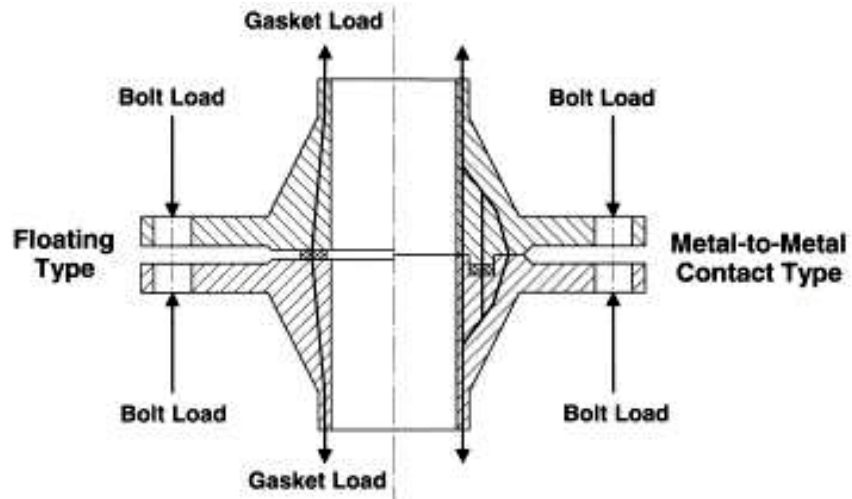


Fig. 2.24 Bolted flange connections (left side) and MMC type (right side) flanged joints
(Adapted from [4])

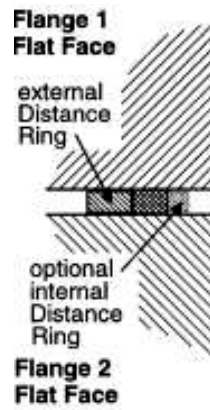


Fig. 2.25 Assembly situation of gaskets in MMC type flanged joints (schematics)
(Adapted from [4])

Roos et al [4] discuss the gasket characteristic for the design of bolted flange connection of metal-to-metal contact (MMC) type. In this study, flat face flanges and a gasket with a sealing element and distance ring (e.g. graphite SWG with outer distance ring) is used, see Fig. 2.24 and Fig. 2.25. Tightening of the bolts leads to contact between the flanges and the distance ring. Depending on the width of the gasket the required gasket stress for MMC can be too high. The optimum width with respect to adequate MMC stress and tightness is about 10 mm or less. This type of gasket shows excellent tightness or low leakage rate. The leakage rate of graphite filled spiral wound gasket depends on contact stress as shown in the Fig. 2.26.

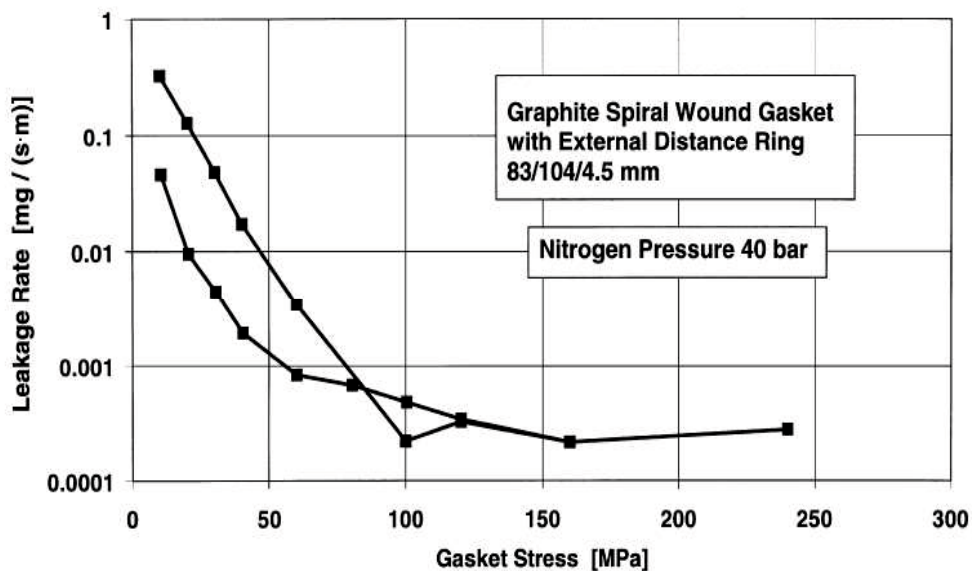


Fig. 2.26 Leakage rate of graphite filled spiral wound gasket depends on contact stress
(Adapted from [4])

On flat solid gasket, Toshimichi F. [33] presented a three-dimensional FEM for estimating the scatter in bolt preloads and achieving the uniform bolt preloads when tightening each bolt one by one in an arbitrary order. Zou [34] studied on an octagonal metal gasket. Research indicates that the gasket actual contact stress distributes

non-uniformly. The leakage rate decreases with increasing gasket effective contact area and gasket average contact stress as shown in Fig. 2.27.

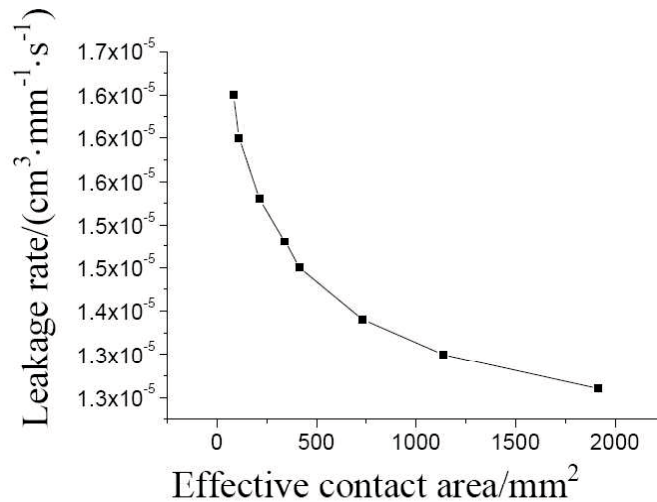


Fig. 2.27 Leakage rate decreases with increasing gasket effective contact area (Adapted from [34])

Gasket flat shape design needed high axial force for tightening. Saeed, *et al* [13], investigated the optimum corrugated shape metal gasket. The gasket selected due to the advantage of metal properties and can solve the problem of the flat metal gasket. Corrugated shape metal gaskets produce high contact stress that can reduce the axial force and produce a spring effect that can reduce gasket relaxation. The contact stress and contact width are an important design parameter to control the 25A size metal gasket performance. The gasket has a metal spring effect and produces high local contact stress to create a sealing line with flanges. A new 25A size metal gasket, with corrugation has been proposed as show in Fig. 2.28.



Fig. 2.28 The proposed new 25A size metal gasket appearance

The optimum levels for the two evaluation criteria are summarized in Table 2.5. It is obvious that with the exception of material and lip height, both evaluation criteria suggest the same optimum conditions.

Table 2.5 Optimum design levels in Saeed studied (adapted from [13])

Design factor	Evaluation criterion	
	Contact stress	Contact area
Material	Mat 2	Mat 1
Lip height h [mm]	0.2	0.4
Lip number	2 x 2	2 x 2
Pitch p [mm]	3	3
Overhang OH [mm]	3	3
Thickness t [mm]	1.5	1.5

Performance of the optimum design with 2 x 2 lips based on contact area was verified experimentally using helium leak test. This decision was based on our assumption that a larger contact area is more beneficial than a larger contact stress as it can counter the roughness of the contact surfaces; because it can be argued that provided the contact stress is greater than internal pressure of the contained fluid, there should be no leakage. Higher slope for “Optimized” design shows a higher functionality of leakage performance as

shown in the Fig. 2.29.

In this study, the evaluation method of 25A size metal gasket was determined by using a new approach for leak measurement. Leak measurement was performed continuously to evaluate the 25A size metal gasket performance at the condition of the gasket was tightened to the flanges. The leak evaluation was carried out by using a water pressure test and a helium leak test. FEM analysis was used to analyze the relationship between contact width and axial force and is validated using pressure sensitive paper. By using the results of the FEM analysis and the leak measurement results, the design concept of the 25A size metal gasket was realized; the design was developed by using the relationship between the contact width and leakage. By using this design concept, the limits of contact width for no leakage can be chosen.

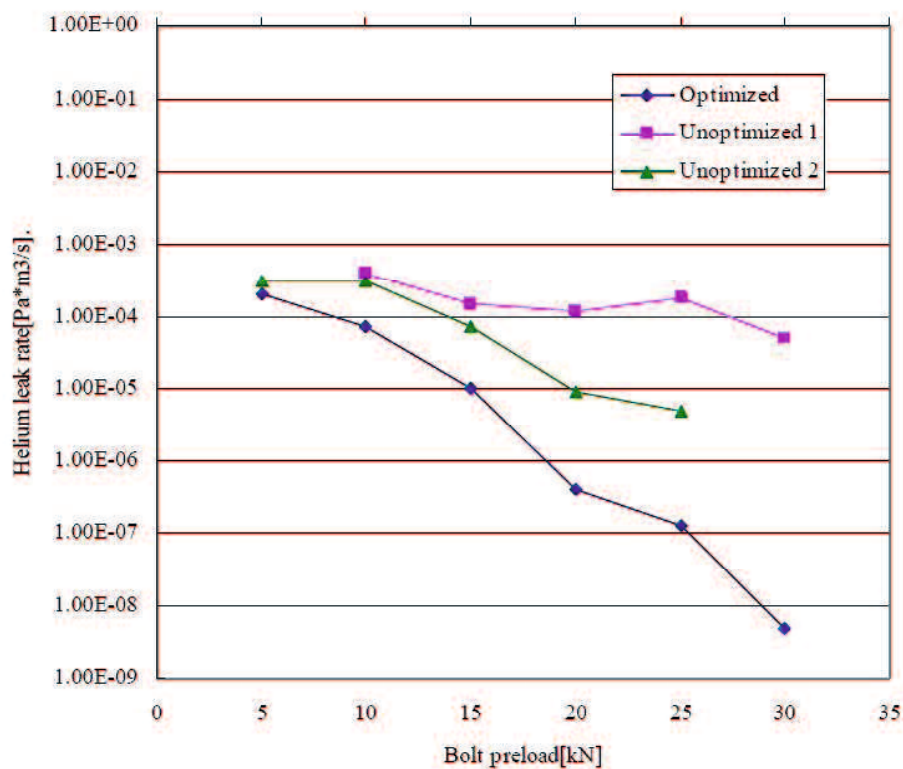


Fig. 2.29 Helium leak result in Saeed studied (Adapted from [13])

The results justify that parameter factors affect the gasket performance is contact area.

However, the limits size of contact width as a design parameter is not yet defined. Also justify the helium leak rate, but the leak or no leak condition not clarified yet.

Haruyama, *et al* [14] investigated the limits size of contact width as 25A size metal gasket design parameter. In this study, the quantitative evaluation of helium leak rate and contact width of gasket which has no leak by water pressure test had been cleared. From the above matter, contact width can be used as a main parameter to optimize the gasket design. The leakage can be reduced with increasing the contact width.

The gasket which was used in this research as shown in Fig. 2.30 is in the shape of circumference beads is placed on both front and back sides of a sealing surface alternately. By the tightening of the seal materials to the flange, each bead of both sides surface of gasket contacted the flange and produced high local contact stresses to prevent leakage. The Schematic diagram in figure 40 shows the prevent leakage mechanism of the all-metal gasket.

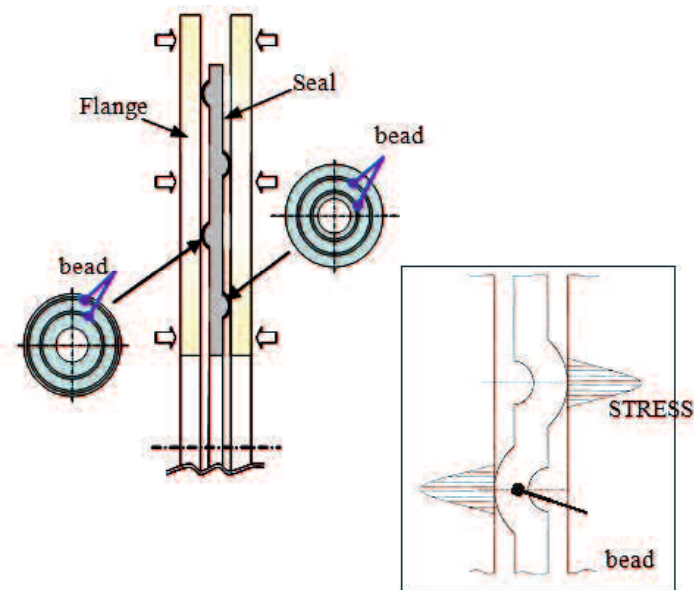


Fig. 2.30 Prevent leakage mechanism of the gasket (Adapted from [14])

Basic dimensions of the gasket that was evaluated is prescribed in JISB2404 and the flange shape is corresponds to 20K pressure and 25A diameter with 1.5 mm thickness. The material selected were SUS304 which could be applied for high-temperature. Nominal

stress is $\sigma = 398.83\text{MPa}$ and modulus of the elasticity is 210GPa . The shape of the gasket is produced by a mold press. Fig. 2.31 shows the basic dimensions of the gasket used in this research.

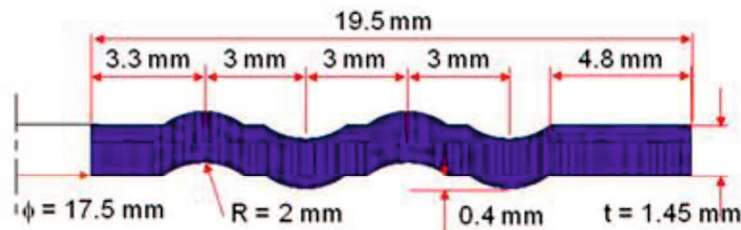


Fig. 2.31 Basic dimensions of the gasket (Adapted from [14])

The condition of the leak occurrence from water pressure test was judged using the quantitative measurement by helium leak test. Therefore, in this research, the method as below is used. In the state that the axial force of the flange is fixed (in this case 20, 25 and 30KN), an experiment of helium leak quantity evaluation was done and helium leak quantity was measured. After that, for every axial force, at the state that the axial force was being loaded, the joint of vacuum piping of helium leak test was exchanged to the water pressure test machine and the water pressure test was performed. Under that circumstance, for 5, 10, 15, 20MPa of water pressure and 600s of maintenance time the leak judgment was done by viewing the presence of leak and the changing of pressure gauge. From this method, it is possible to evaluate axial force of each flange, helium leak quantity and the presence of leak by water test by the same test specimen and axial force.

Table 2.6 shows the experiment results of the helium leak quantity and the presence of leak under the changing of axial force. The helium leak flow is $1.0 \times 10^{-6}\text{ Pa}\cdot\text{m}^3/\text{s}$ at the axial force 120 KN, it is observed that the leak by water pressure test did not occurred. Furthermore, it is known that at the helium leak quantity near $1.0 \times 10^{-6}\text{ Pa}\cdot\text{m}^3/\text{s}$ and the internal pressure 10MPa, the leak did not occur. From above matter, for the gasket used in this research, for a quantitative decision criteria to prevent the leak, it is possible to take the condition of helium leak quantity below the $1.0 \times 10^{-6}\text{ Pa}\cdot\text{m}^3/\text{s}$ as a decision criteria for the evaluation of the performance of the gasket design. It also became possible to evaluate the

performance of the gasket by quantitative measurement of helium leak quantity and water pressure test result.

Table 2.6 Comparison of Helium Leak Quantity and Water Pressure Test Result
(Adapted from [14])

Axial Force [KN]	Helium leak quantity [Pa · m ³ /s]	Pressure [MPa]		Result
		0 [s]	600 [s]	
80	5.6×10 ⁻⁵	5	5	No leakage
		10	8.5	Leak
		15	12	Leak
		20	14	Leak
100	9.6×10 ⁻⁶	5	5	No leakage
		10	10	No leakage
		15	15	No leakage
		20	18	Leak
120	1.0×10 ⁻⁶	5	5	No leakage
		10	10	No leakage
		15	15	No leakage
		20	20	No leakage

In previous research, it is clear that contact area and contact stress of the gasket is an important decision criterion for the performance of the gasket, but contact stress and contact area for the presence of leak examination are not sufficient. Therefore, in this study, using the relation of axial force of gasket, leak quantity and the presence of leak gotten from helium leak test and water pressure test, the relation of contact stress and contact area of gasket is examined by FEM analysis.

In this research, from the crush analysis of gasket, the examination of the relation of flange axial force to the contact width of seal material salient part and to the contact stress was done.

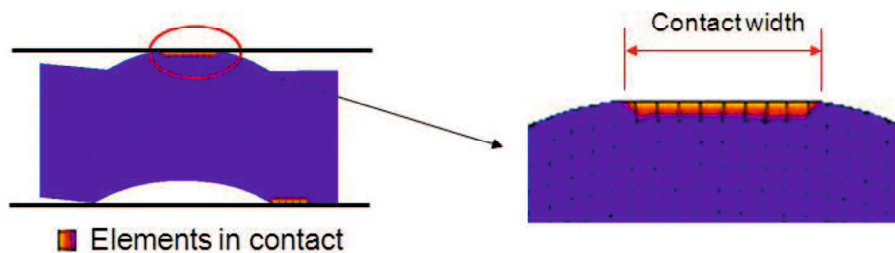
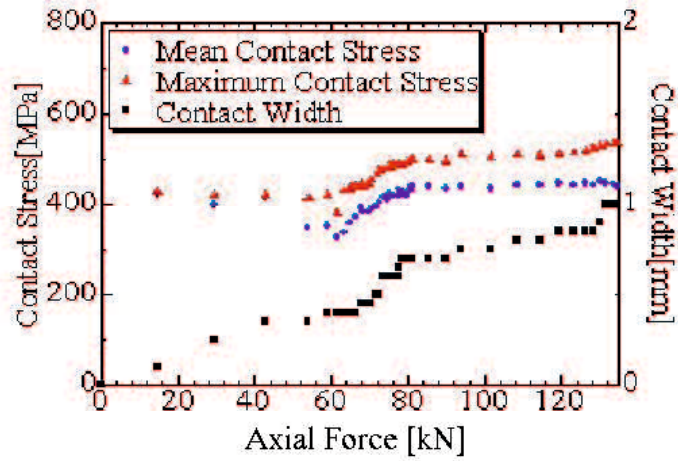


Fig. 2.32 Contact surface of the gasket (Adapted from [14])

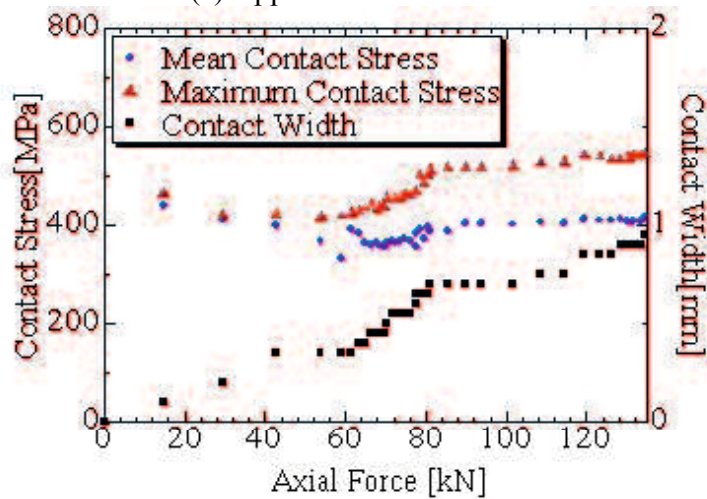
For contact area, only at the beads (convex part) of gasket which is effective for avoiding leak is taken as evaluation part. The top surface and bottom surface of contact area increased step by step due to the increment of the axial force to the gasket. From above matter, as shown in Figure 2.32, with the increment of axial force, not only the convex section of gasket surface, but also the edge of external and internal circumference of gasket becomes contacted.

In addition, it is known that the leak quantity has decreased due to the rise of the contact area at the value near 80KN, 100KN and 120KN. Furthermore, Figure 2.33 shows relationship between the contact area and stress in each convex and contact stress. As seen from the figure, contact stress becomes an approximately constant value at the contact part. However, the contact area increased due to the increment of axial force. Moreover, contact stress is in average value at the beads contact part. For the relation of contact area and contact stress from leak quantity, in the state of high contact stress, the contact width became bigger with the axial force. Therefore, as used in this research, for the general-used flange which corresponds to JISB2220 and the gasket, even in the state that the internal pressure exists, for the state that the contact stress occurs because of the internal pressure, it is possible to put an aim for the gasket design condition that if the contact width is above 0.8 mm, the leak by water pressure test will not occur.

In this research, the quantitative evaluation of helium leak quantity and the relation of contact area and contact stress of gasket which has no leak by water test pressure had been cleared. From the above matter, by improving the performance, the optimize designing of gasket become possible.



(a) Upper convex section



(b) Lower convex section

Fig. 2.33 Relationship between the contact area and contact stress in each axial force

(Adapted from [14])

Choiron, et al [15] provided the contact width validation by using simulation analysis and the result is compared to experimental using pressure sensitive paper. The gasket used in this research is circumference beads gasket as illustrated in Fig. 2.34. The shaped of the gasket is produced by a mold press. When the gasket is tightened to the flange, each bead of both surfaces of gasket created elastic effect and produced high local contact stresses to

prevent leakage. This circumference made the range of conventional axial force could be possible to use.

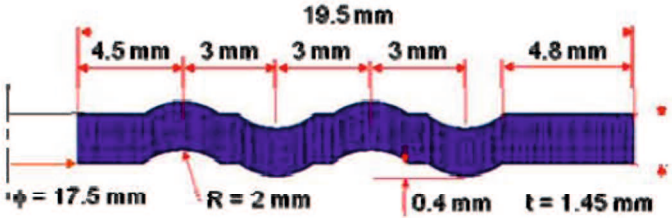
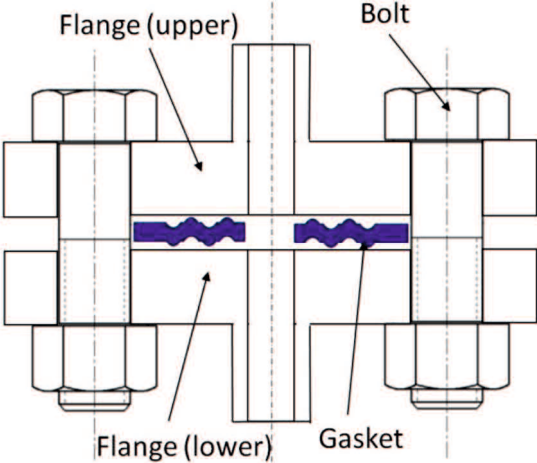
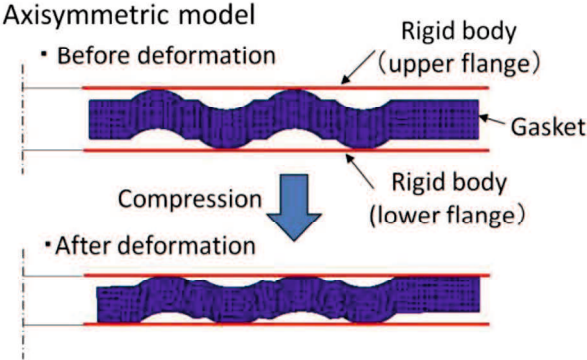


Fig. 2.34 Basic dimensions of the gasket used in this research (Adapted from [15])



(a) Physical model



(b) Axisymmetric model

Fig. 2.35 Schematic section of model

From the tensile test result, nominal stress (σ_Y) of SUS304 was 398.83MPa, the modulus of the elasticity (E) was 210GPa and the tangent modulus was 1900.53MPa. In this study, the model material follows the linear hardening law which divides into two equations for elastic region and plastic region. The flange was assumed as a rigid body on both the sides. Using two-dimensional assumptions, an axisymmetric model was made to implement compression displacement in the axial direction on the gasket in between the top and the bottom of the flange (Fig. 2.35).

Lee et al. [35] used Fuji pressure sensitive paper to measure the contact width and the pressure profile of the lip seal due to its accuracy, speed, and economic cost. To validate contact width parameter of the proposed new gasket directly, Fuji pressure sensitive paper was used. Due to the ease of application, validation method using pre-scale pressure sensitive paper is one of most popular methods used in contact area and pressure in joint measurement for industrial purpose. Pre-scale pressure sensitive paper is able to produce an accurate and economic permanent high resolution surface topography of contact pressure distribution [36].

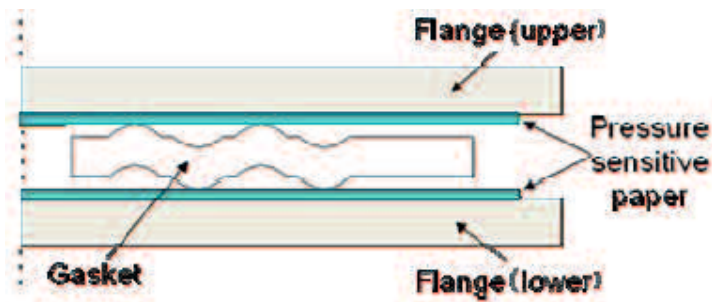


Fig. 2.36 Measurement procedure using pressure sensitive paper (Adapted from [15])

The first procedure of validation method is to form the paper into the designed form. The designed form is furthermore placed in between the joining parts of gasket and flange as shown in Fig. 2.36. The tightening process is carried out based on the axial force. After the load is applied, red patches will be stamped in the paper as illustration of pressure

distribution profile that occurred between the two surfaces. A CMOS camera was used to zoom in on the patch. The contact width measurement was performed on eight points located along the contact zone. The measurements using the pressure sensitive paper was compared with the simulation results [15]. The focus of this research is to observe red patches stamped in the paper and measure contact width of the gasket directly. The points of measurement are performed at four point of contact width as depicted in Fig. 2.37.

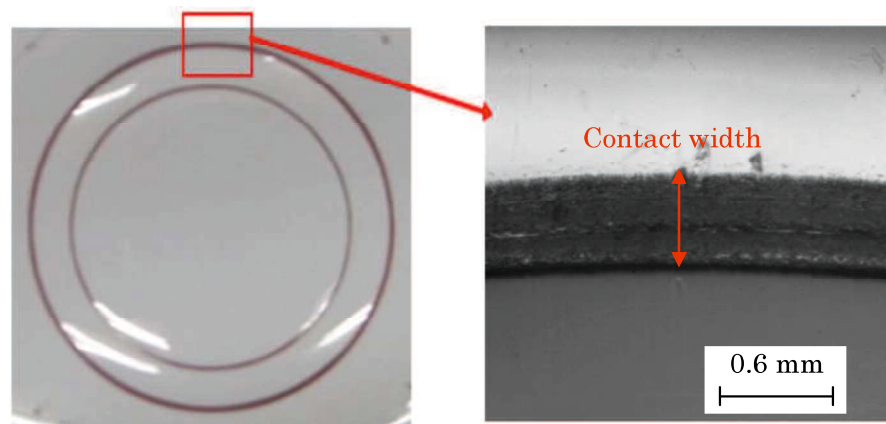


Fig. 2.37 Red patches appeared on pressure sensitive paper after removing load
(Adapted from [15])

The value of contact width could be seen in Fig. 2.38 as a result of measurement using pressure sensitive paper. On the other hand Fig. 2.39 illustrated result produced by MSC.Marc simulation. As shown in both graphs, the axial load affected the contact width significantly. With the more value of axial load, the more the value of contact width. The increase of contact width effect started at axial load value of 60KN. This value is furthermore taken as decision criteria for the evaluation of the performance of the gasket design.

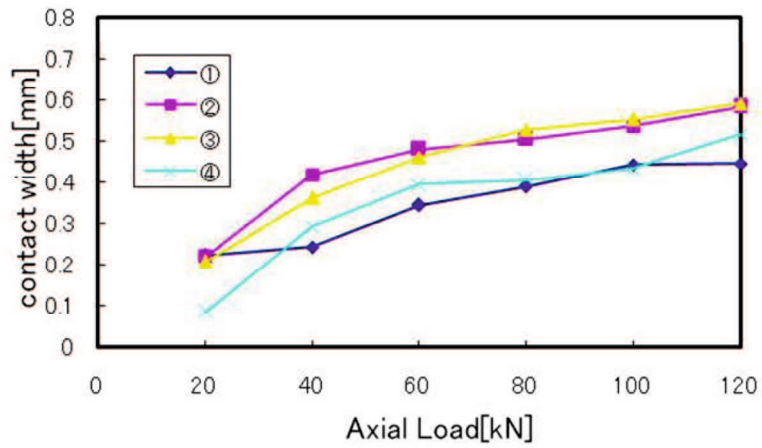


Fig. 2.38 Contact width measurement result produced by pressure sensitive paper
(Adapted from [15])

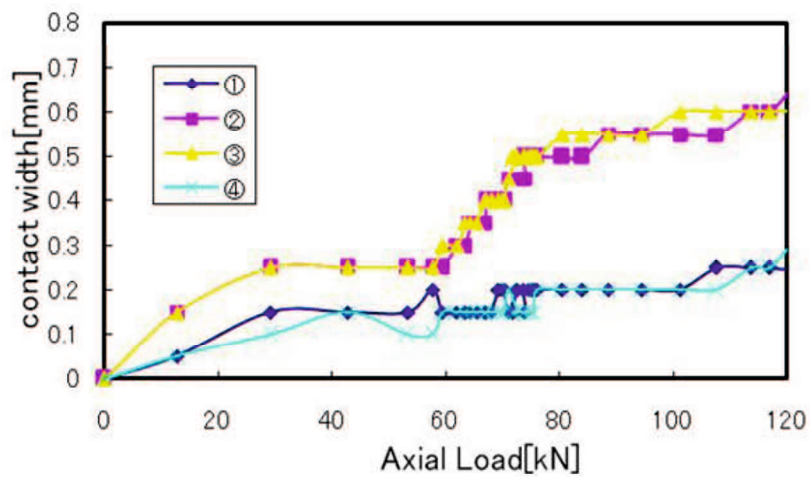


Fig. 2.39 Contact width measurement result produced by MSC.Marc simulation
(Adapted from [15])

Figure 2.40 and 2.41 shows the position of convex portion change when the axial force given. Changes of convex portion 1 and 4 were greater than changes of convex portion 2 and 3. The convex portion 2 and 3 moved very small and work primarily to reduce the leakage, and convex portion 1 and 4 will support to realize it. The contact width of convex portion 1 and 4 experimental result, tend to be larger than simulation result due

to the displacement of convex portion.

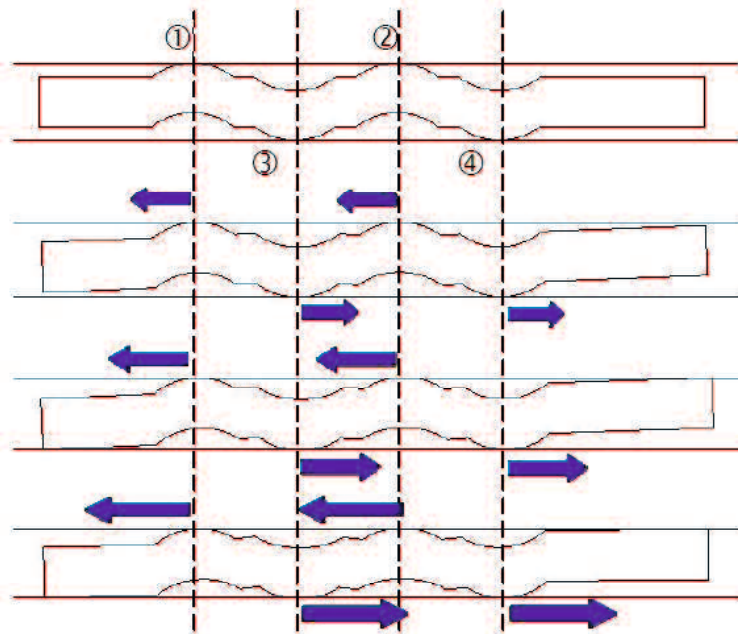


Fig. 2.40 Position of convex portion (Adapted from [15])

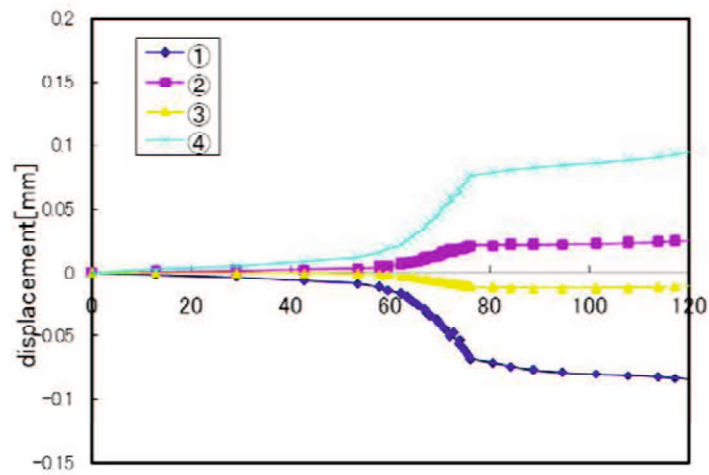


Fig. 2.41 Value of position change every convex portion (Adapted from [15])

Choiron, et al [18] investigated the optimum 25A-size metal gasket design based on plastic contact stress consideration on contact width. The optimized gasket is determined by

deleting contact width with contact stress below of 400MPa. Optimum gasket is chosen by using balancing between contact width and contact stress. The design of experiments (DoE) Taguchi method is used to investigate the factor effect on the contact width and predict the optimal design. The seven factors are overhang (OH), pitch 1 (p_1), pitch 2 (p_2), pitch 3 (p_3), thickness (t), radius (R), and lip height (h). The L18 orthogonal array was built to design experimental matrix for seven factors with three levels.

Gasket used in this study was circumference beads gasket as illustrated in Fig. 2.42. When the gasket is tightened to the flange, each bead of both surfaces of gasket created elastic effect and produced high local contact stress for preventing leakage. This circumstance made the range of conventional axial force could be possible use. Table 2.7 shows the initial basic dimension of the gasket. The gasket material was SUS304 due to its effectiveness in high-temperature and high-pressure environment.

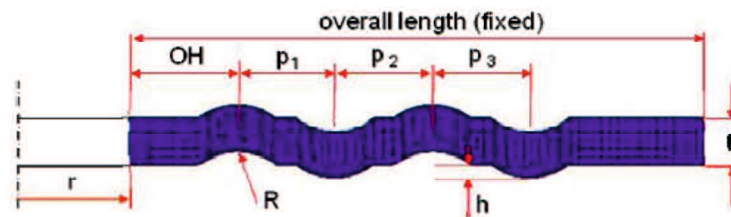


Fig. 2.42 Initial gasket cross section and design parameter (adapted from [18])

Table 2.7 Initial basic dimensions of the gasket (adapted from [18])

Design Parameter	Dimension [mm]
1. Inner radius (r)	17.5
2. Overall length (fixed)	19.5
3. Over hang (OH)	4.5
4. Lip height (h)	0.4
5. Thickness (t)	1.45
6. Convex radius (R)	2
7. Pitch ($p_1 = p_2 = p_3$)	3

The contact width modeling was undertaken using FEM analysis software MSC.Marc. The flange was assumed as a rigid body in both sides. Using two dimensional assumptions axisymmetric model was made to adopt compression displacement in axial direction on gasket in between the top and the bottom of the flange. Based on previous study, the plastic contact stress built sealing lines between flange and gasket to avoid leakage, although the value is not yet defined clearly. The optimization design based on the increasing contact width is combined with considering contact stress. The optimum design also determined based on reducing the axial force. It can be denote by using the slope or gradient of the curve of relationship between contact width and axial force. The slope of curve is increased; it will be reduce the axial force. Due to the optimization design based on increasing contact width is combined with considering contact stress. The gasket design with higher slope is choose as optimum design as shown in Fig. 2.43.

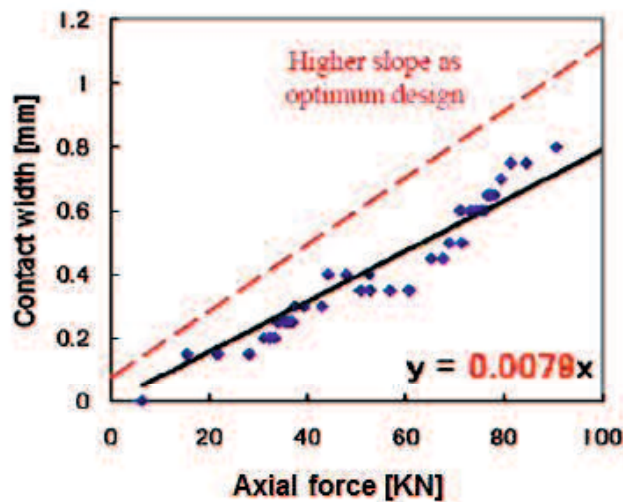


Fig. 2.43 Gasket design with higher slope is choose as optimum design

(Adapted from [18])

From MSC Marc result, the contact width is determined based on contact status. Contact status values are 1 and 0 which mean contact and no contact, respectively. This status is done without considering the distribution of the contact stress. This condition is called as gasket design number 1. Moreover, the gasket design number 2 is done by

deleting the contact stress value below of 400MPa. It was found from the material properties, the yield stress is 398.83MPa. Therefore, contact width value is more reduced due to contact width with contact stress below of 400MPa is deleted. This procedure is done based on assumption which the large contact stress creates sealing lines on contact width [37].

In this study, the Taguchi DOE method was used to evaluate the effect of each parameter design and predict optimal design of new 25A-size metal gasket. Taguchi method uses a special set of arrays called orthogonal arrays. These standard arrays stipulate the way of conducting the minimal number of experiments, which could give the full information of all factors that affect the performance parameters [38]. The following Table 2.8 shows the Taguchi test matrix for the tests. To design experimental matrix for eight factors with three levels, the L18 orthogonal array was most applicable.

Table 2.8 Factor and level description (adapted from [18])

Factor	Factor description	Level 1	Level 2	Level 3
A	Over Hang (OH)	3.0	4.0	-
B	Pitch 1 (p_1)	3.5	4.0	4.5
C	Pitch 1 (p_2)	3.5	4.0	4.5
D	Pitch 1 (p_3)	3.5	4.0	4.5
E	Thickness (t)	1.2	1.5	1.8
F	Radius (R)	1.5	2.5	3.5
G	Lip height (h)	0.30	0.35	0.40
H	Error	1	2	3

The result of relationship between the contact width and axial force, both of optimum design number 1 and initial design are shown in Fig. 2.44. The higher slope of the curve for the optimized design at number 1 provides a marked improvement on the initial design [18]. The level range of load between 80KN and 100KN shows that the optimum design at number 1 can reduce the axial force. The level range of load is improved compared with the initial design which the condition of no leak occurred on 100KN axial force.

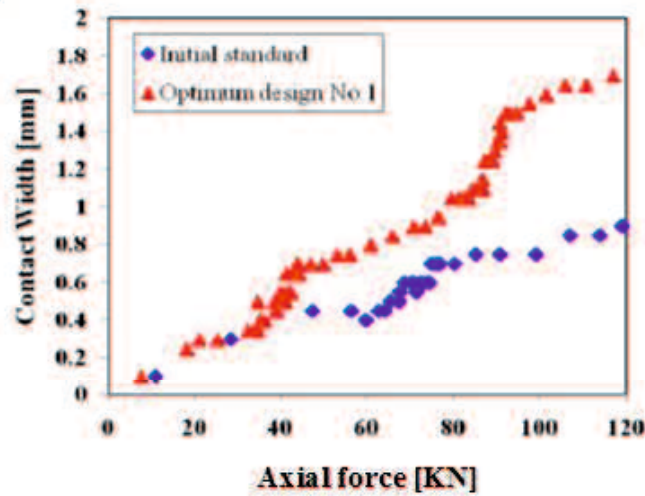


Fig. 2.44 Relationship between contact width and axial force (Adapted from [18])

Fig. 2.45 shows comparison optimum design number 1 and number 2 by condition that contact width with contact stress below of 400MPa is deleted. Based on assumption which the large contact stress creates sealing lines on contact width, slope of the curve for optimized design number 2 is higher than the optimized design number 1.

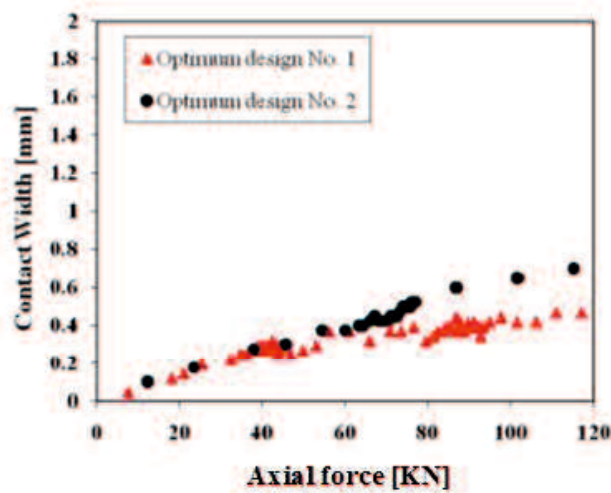


Fig. 2.45 Comparison optimum design number 1 and number 2 (Adapted from [18])

In addition, the optimum design of gasket based on results of each of the observed values is illustrated in Table 2.9. Optimum design No. 1 called elastic mode, the optimum design based on contact width using elastic and plastic contact stress. Optimum design No. 2 called plastic mode, the optimum design based on contact width using plastic contact stress only. The condition of contact stress bellow 400MPa deleted because the nominal stress of material is 398,83MPa. The contact width in elastic contact stress was longer than plastic contact stress for optimum design No. 1. The contact width in plastic contact stress was longer than elastic contact stress for optimum design No. 2 see Fig. 2.46.

Tables 2.9 Optimum gasket design at number 1 and number 2 (Adapted from [18])

Factor	Level Description	
	Optimum design No. 1	Optimum design No. 2
OH	4.0 mm	3.0 mm
p ₁	3.5 mm	3.5 mm
p ₂	4.0 mm	4.5 mm
p ₃	4.0 mm	4.5 mm
t	1.2 mm	1.8 mm
R	3.5 mm	1.5 mm
h	0.4 mm	0.3 mm

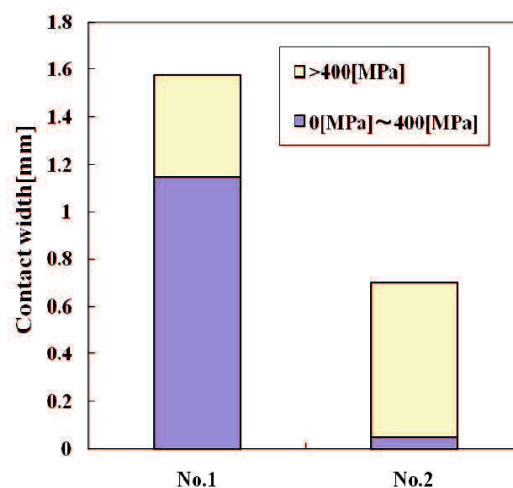


Fig. 2.46 Distribution of contact stress at axial force 100 kN (Adapted from [18])

2.9.Contact Analysis Theory

The simulation of many physical problems requires the ability to model the contact phenomena. The analysis of contact behavior is complex because of the requirement to accurately track the motion of multiple geometric bodies, and the motion due to the interaction of these bodies after contact occurs. This includes representing the friction between surfaces and heat transfer between the bodies if required. The numerical objective is to detect the motion of the bodies, apply a constraint to avoid penetration, and apply appropriate boundary conditions to simulate the frictional behavior and heat transfer [39].

There are two types of contact bodies in Marc —deformable and rigid. Deformable bodies are simply a collection of finite elements as shown in Fig. 2.47. This body has three key aspects to it 1) the elements which make up the body 2) the nodes on the external surfaces which might contact another body or itself 3) the edges (2D) or faces (3D) which describe the outer surface which a node on another body (or the same body) might contact. Rigid bodies are composed of curves (2D) or surface (3D). The most significant aspect of rigid bodies is that they do not deform. Deformable bodies can contact rigid bodies, but contact between rigid bodies is not considered [39].

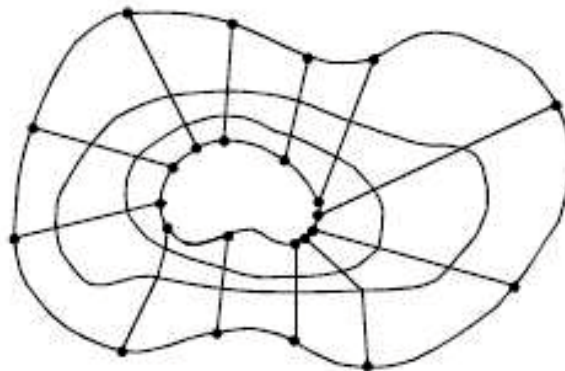


Fig. 2.47 Deformable body (adapted from [39])

The motion of deformable bodies is prescribed using the conventional method of applying displacements, force or distributed load to the bodies. It is advantageous to not apply displacement or point loads which might come into contact with other rigid bodies. If

a prescribed displacement is to be imposed, it is better to introduce another rigid body and apply the motion to the rigid body. There are four ways to prescribe the motion of rigid surfaces, which are velocity, position, load and scaling [39].

During the incremental procedure, each potential contact node is first checked to see whether it is near a contact segment. The contact segments are either edges of other 2D deformable bodies, faces of 3D deformable bodies or segment from rigid bodies. By default, each node could contact any other segment including segments on the body that belongs to. This allows a body to contact itself. During the iteration process, the motion of the node is checked to see whether it has penetrated a surface by determining whether it has crossed a segment. During the contact process, it is unlikely that a node exactly contacts the surface. For this reason, a contact tolerance (Fig. 2.48) is associated with surface. If a node is within the contact tolerance, it is considered to be in contact with the segment. The default contact tolerance is calculated by the program [39].

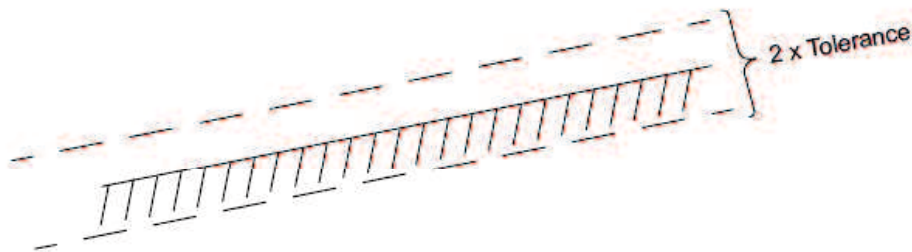


Fig. 2.48 Contact tolerance (adapted from [39])

During an increment, if node A moves from $A^{(t)}$ to $A^{(t+\Delta)}$, where $A^{(t+\Delta)}$ is beyond the contact tolerance, the node is considered to have penetrated (Fig. 2.49). In such a case, a special procedure is invoked to avoid this penetration.

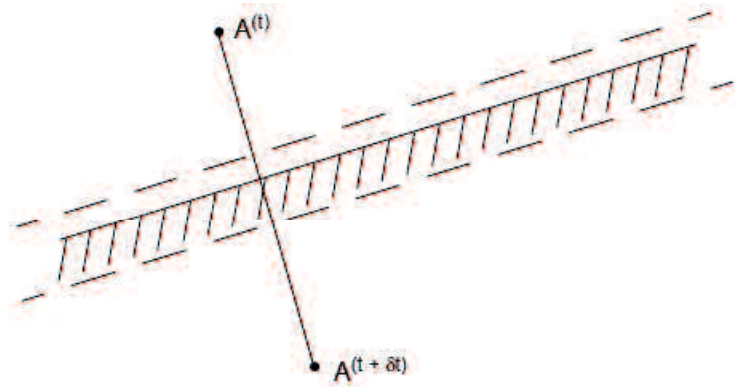


Fig. 2.49 Trial displacement with penetration (adapted from [39])

Friction is a complex physical phenomenon that involves the characteristic of the surface roughness, temperature, normal stress and relative velocity. An example of this complexity is that quite often in contact problems neutral lines develop. This means that along a contact surface, the material flows in one direction in part of the surface and in the opposite direction in another part of the surface. Such neutral lines are, in general, not known a priori. The most popular friction model is the adhesive friction or coulomb friction model. This model is used for most applications with the exception of bulk forming such as forging. For such applications the shear friction model is more appropriate. The coulomb model can be characterized by:

$$\|\sigma_t\| < \mu\sigma_n \text{ (stick) and } \sigma_t = -\mu\sigma_n \cdot t \text{ (slip)} \quad (2.44)$$

Where

σ_n is the normal stress

σ_t is the tangential (friction) stress

μ is the friction coefficient

t is the tangential vector in the direction of the relative velocity

$$t = \frac{v_r}{|v_r|}, \text{ in which } v_r \text{ is the relative sliding velocity}$$

Similarly, the Coulomb model can also be written in term of nodal forces instead of stresses:

$$\|f_t\| < \mu f_n \text{ (stick) and } f_t = -\mu f_n \cdot t \text{ (slip)} \quad (2.45)$$

Where

f_t is the tangential (friction) force

f_n is the normal force

For a given normal stress or normal force, the friction stress or force has a step function behavior based upon the value of the relative sliding velocity v_r or the tangential relative incremental displacement Δu_t , as outlined in Fig. 2.50 for a 2D case, where the relative velocity and incremental displacement are scalar values [39].

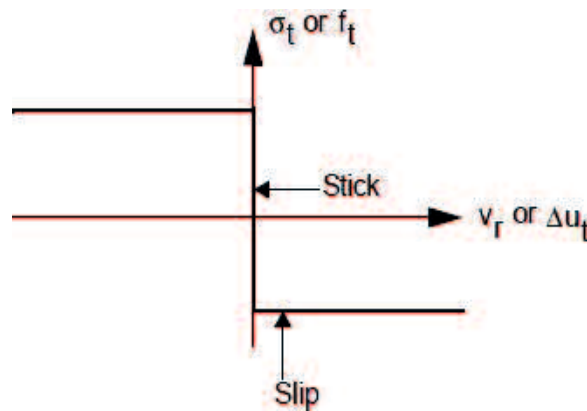


Fig. 2.50 Coulomb friction model (adapted from [39])

2.10. Boundary Conditions of the Numerical Analysis

Marc is based on the stiffness method and deals primarily with force-displacement relations. In a linear elastic system, force and displacement are related through the constant stiffness of the system; the governing equation of such a system can be expressed as

$$K u = F \quad (2.46)$$

Where K is the stiffness matrix and u and F are nodal displacement and nodal force vectors, respectively. Equation (2.46) can be solved either for unknown displacements subjected to prescribed forces or for unknown forces (reactions) subjected to prescribed displacements. In general, the system is subjected to mixed (prescribed displacement and force) boundary conditions, and Marc computes both the unknown displacements and reactions. Obviously, at any nodal point, the nodal forces and nodal displacements cannot be simultaneously prescribed as boundary conditions for the same degree of freedom. We must prescribe at least a minimum number of boundary conditions to ensure that rigid body motion does not occur. The prescribed force boundary conditions are often referred to as loads and the prescribed displacement boundary conditions as boundary conditions [39].

For contact between a deformable body and a rigid surface, the constraint associated with no penetration is implemented by transforming the degrees of freedom of the contact node and applying a boundary condition to the normal displacement. This can be considered solving problem [39]:

$$\begin{bmatrix} K_{\hat{a}\hat{a}} & K_{\hat{a}b} \\ K_{b\hat{a}} & K_{bb} \end{bmatrix} \begin{Bmatrix} u_{\hat{a}} \\ u_b \end{Bmatrix} = \begin{Bmatrix} f_{\hat{a}} \\ f_b \end{Bmatrix} \quad (2.47)$$

where \hat{a} represent the nodes in contact which have a local transformation, and b represents the nodes not in contact and, hence, not transformed. Of the nodes transformed, the displacement in the normal direction is then constrained such that $\delta u_{\hat{a}n}$ is equal to the incremental normal displacement of the rigid body at the contact point.

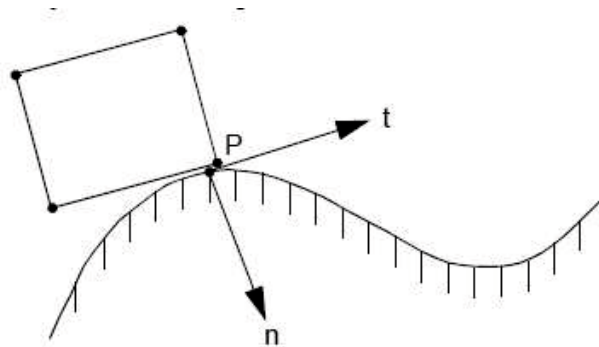
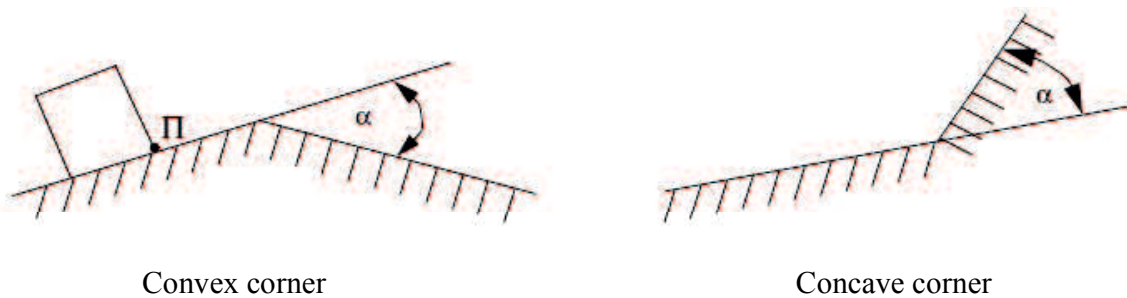


Fig. 2.51 Transformed system (2D) (adapted from [39])

As a rigid body can be represented as either a piecewise linear or as an analysis surface, two procedures are used. For piecewise linear representations, the normal is constant until node P comes to the corner of two segments as shown in Fig. 2.65. During the iteration process, one of three circumstances occurs. If the angle α is small ($-\alpha_{smooth} < \alpha < \alpha_{smooth}$), the node P slides to the next segment. In such a case, the normal is updated based upon the new segment. If the angle α is large ($\alpha > \alpha_{smooth}$ or $\alpha < -\alpha_{smooth}$) the node separates from the surface if it is a convex corner, or stick if it is a concave corner. The value of α_{smooth} is important in controlling the computational cost. A larger value α_{smooth} reduces the computational costs, but might lead to inaccuracies. The default values are 8.625° for 2D [39].



Convex corner

Concave corner

Fig. 2.52 Corner conditions (2D) (adapted from [39])

CHAPTER III

OPTIMIZATION OF GASKET BASED ON CONTACT WIDTH CONSIDERING FORMING AND CONTACT STRESS EFFECT

The new 25A-size metal gasket models on the previous study use the assumption exclude forming effect. It was known that the forming process produced residual stresses and a geometric imperfections characteristic. Press forming is performed to produce gasket shape by a punch forces the initial material to slide into a die. The plastic deformation occurs in the contact area when the local stress has reached. The use of simulation is beneficial in the design of metal forming operations because it is more cost effective than trial and error. The development of hardware and software support the metal forming simulation to define an elastic and plastic contact stress. It also predicted the forces and stresses necessary to execute the forming operation. The plastic contact stress was built sealing lines between flange and gasket to avoid leakage [37]. Previous study gasket design based on elastic and plastic contact width produced the contact width having elastic contact stress was longer than plastic contact stress. The gasket design based on plastic contact width produced the contact width having plastic contact stress was longer than elastic contact stress [18].

In this study, we investigated the optimum design of new 25A-size metal gasket based on contact width considering include forming effect and an elastic and plastic condition respectively derived from FEM analysis. The simulation is built include forming effect appropriate as the reality process. The plastic contact stress built sealing lines between flange and gasket to avoid the leakage [37]. The optimum design of the simulation result was tested using helium leakage test. Here we will be known the gasket performance based on the elastic and plastic design.

3.1 Gasket Optimization by Using Taguchi Method

SUS304 was used as a gasket material because of its effectiveness in a

high-temperature and high-pressure environment. Its material properties were first determined through a tensile test carried out based on JIS Z2241 [40] —the nominal stress, modulus of elasticity (E), and tangent modulus was respectively found to be 398.83MPa, 210GPa, and 1900.53MPa. Fig. 3.1 shows the stress-strain diagram of SUS304 material. The characteristic of material SUS304 is shown in Table 3.1.

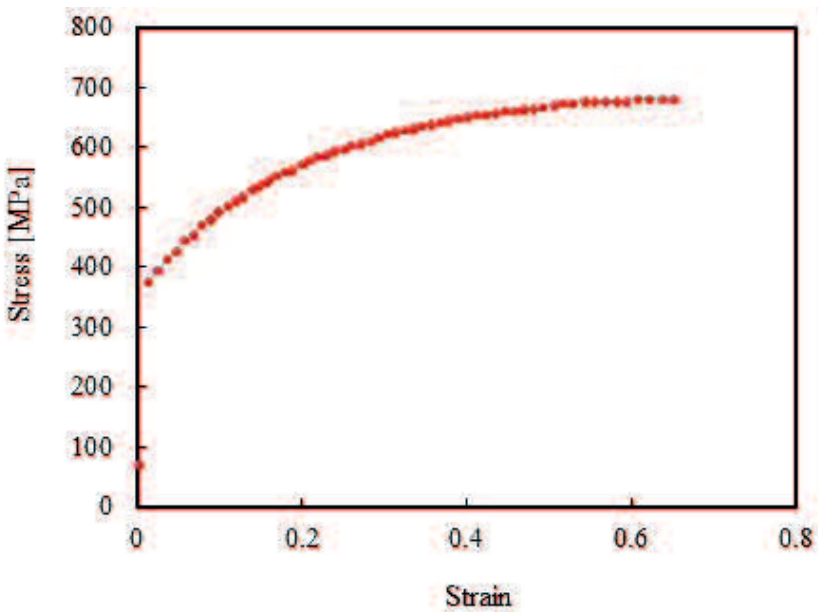


Fig. 3.1 SUS304 stress-strain diagram

Table 3.1 Characteristic of the SUS304

Properties	Value
Nominal stress (σ)	398.83 [MPa]
Modulus of the elasticity (E)	210 [GPa]
Tangent modulus	1900.53 [MPa]
Poisson Ratio	0.3

In the previous study [18], the gasket design based on contact status, which is contact and no contact, without considering the distribution of the stress called 0-MPa mode. In the other hand, the gasket design by deleting the contact stress value below of 400MPa called 400-MPa mode. It found from the material properties; the yield stress is 398.83MPa. In this study, the gasket design based on an elastic condition we call 0-MPa mode while it based on a plastic condition is 400-MPa mode.

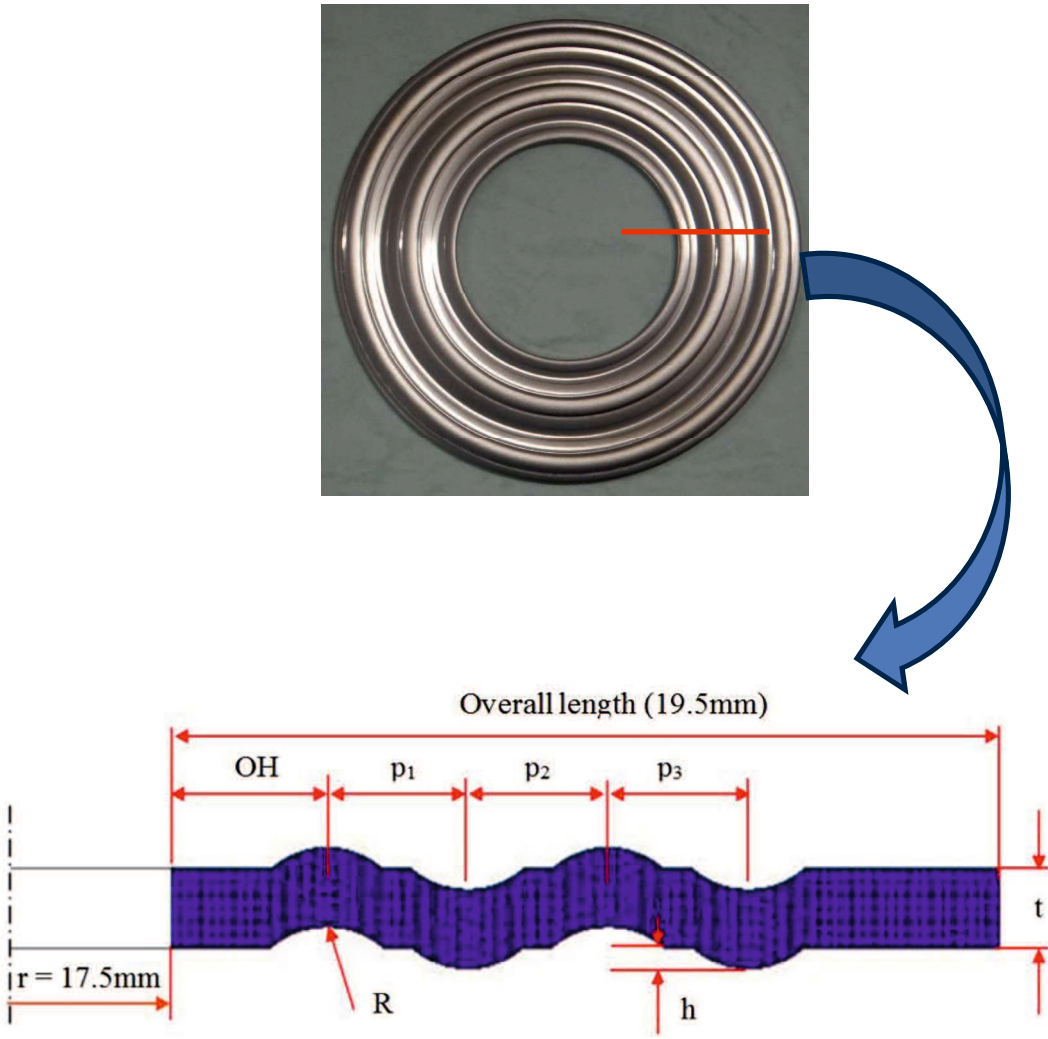


Fig. 3.2 Dimension of gasket

This study investigated the optimization design of the gasket based on contact width and considering forming effect and contact stress effect. The dimension of gasket optimization is shown in Fig. 3.2. The optimization applied to gasket shape. Eight factors is a maximum number of the gasket shape variation. The overall length of gasket is fixed due it was regulated for inner radius and outer radius by using JIS B 2040. The upper figure shows a metal gasket and the lower figure shows 2D section of metal gasket.

A gasket model is divided into two simulation stages by using two pressing model which is forming and tightening simulation. Both stages were modeled using finite element method analysis software MSC. Marc [39]. Flowchart the stage of simulation and optimization the gasket considering forming effect as shown in Fig.3.3. The virtual gasket model with various designs was generated by using four basic steps. They were the parameterization the models, automatic meshing, computation of preprocessing and post-processing in batch mode and optimization. Firstly, 2-D parameter model is built by utilizing the Solid work software. To connect drawing data from Solid work (IGES file) and automatic meshing by using Hypermesh software, batch command file built, and an NAS file produced with this procedure. Then the procedure file was configured to obtain preprocessing and running the model on MSC.Marc software. The graphic user interface (GUI) did not appear, and the program run command in the background. After the FEM analysis was complete, the output file including analysis results could be generated in TXT file. The TXT result file was transformed to Microsoft excel by using MACRO command. The output result contains the contact status, stress value, and body force at each time at every convex position. Calculation of the contact width versus axial force on convex position number 1 until 4 produced with several step of MACRO command.

Figure 3.4 shows the simulation setting up before forming and tightening simulation. Material gasket in this study was circumference and deformable. The dies and flanges were assumed as rigid body in both sides. In the first stage, using two-dimensional assumptions, the axis-symmetric model was adopting a forming process simulation in the axial direction on gasket material between the top and the bottom of the dies see Fig. 3.5. Forming simulation will produce the circumference beads gasket. The second stage was the gasket

shape produced by mold press was continuity compressed in the axial direction to adopt tightening of the gasket on the flanges, see Fig. 3.6. When the gasket tightened by the flanges, each of beads of both surfaces of the gasket created elastic effect and produced high local contact stress for preventing leakage. This circumstance made the range of conventional axial force could be possible to use.

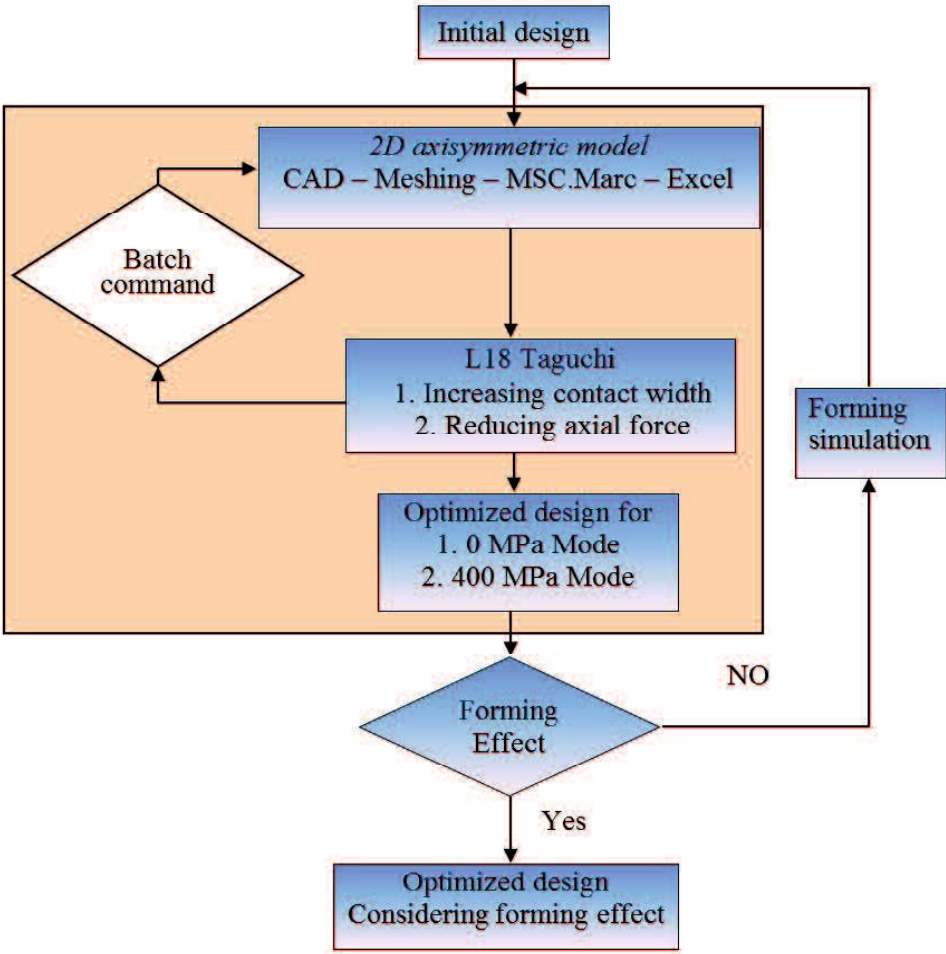


Fig. 3.3 Flow chart the stage of simulation and optimization the gasket

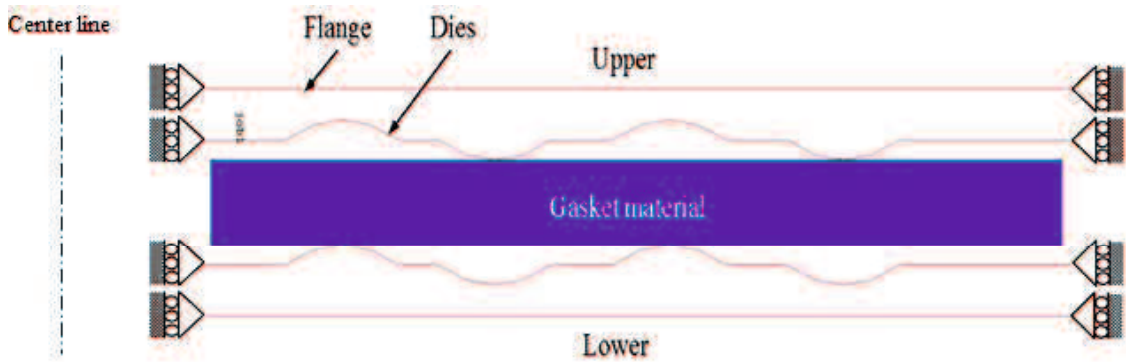


Fig. 3.4 Setting-up of gasket material, dies and flange before forming and tightening

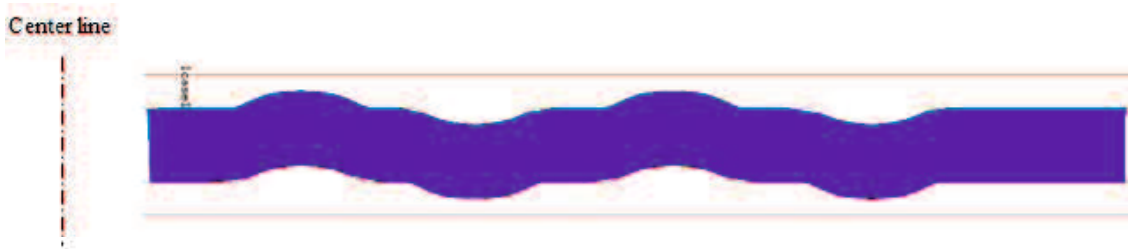


Fig. 3.5 Forming simulation

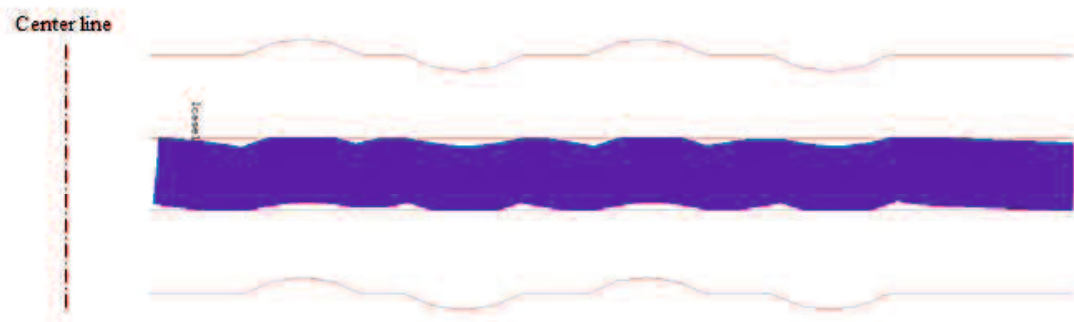


Fig.3.6 Tightening simulation

From MSC Marc result, the contact width is determined based on contact status. Contact status values are 1 and 0 which mean contact and no contact, respectively. This

status did without considering the distribution of the contact stress. This condition called as gasket 0-MPa mode or elastic gasket design. Moreover, the gasket 400-MPa or plastic gasket design is done by deleting the contact stress value below of 400-MPa. It found from the material properties; the yield stress is 398.83MPa. Therefore, contact width value is more reduced due to contact width with contact stress below of 400-MPa deleted. This procedure is done based on the assumption that the large contact stress creates sealing lines on contact width.

The Taguchi method was used to evaluate the effect of each parameter design and predict the optimal design of 25A-size metal gasket. Taguchi method uses a special set of arrays called orthogonal arrays. These standard arrays stipulate the way of conducting the minimal number of experiments, which could give the full information of all the factors that affect the performance parameters. Present study, we used eight factors and three levels, using full factorial experiment, it needs $3^8 = 6561$ settings. Using Taguchi Methods we need only 18 settings. The graph of main effect can describe that the trial setting, although 18 trials, give the full information of all the factors that the effect of the performance parameters [38]. The Taguchi method applied on simulation experiment, is becoming as a popular as actual experiments. Simulation result yields no error in repeatability but has a problem with error modeling. Analysis of the means study of experiment result reveals the effect of design parameters that are used to determine the optimal level of the parameter. A visual summary of the experiment is the plot of the means by factor levels. In this plot, the optimum setting for each factor can be easily can be identified.

The optimum design determined based on reducing the axial force. It could be denote by using the slope or gradient of the curve of relationship between contact width and axial force, see Fig.3.7. The upper and lower contact width was the value of convex portion number 3 and 2, respectively. The slope of the curve increased; it will reduce the axial force. Due to the optimization design based on increasing contact width is combined with considering forming effect and contact stress effect [43]. The gasket design with higher slope is chosen as the optimum design as shown in Fig. 3.7.

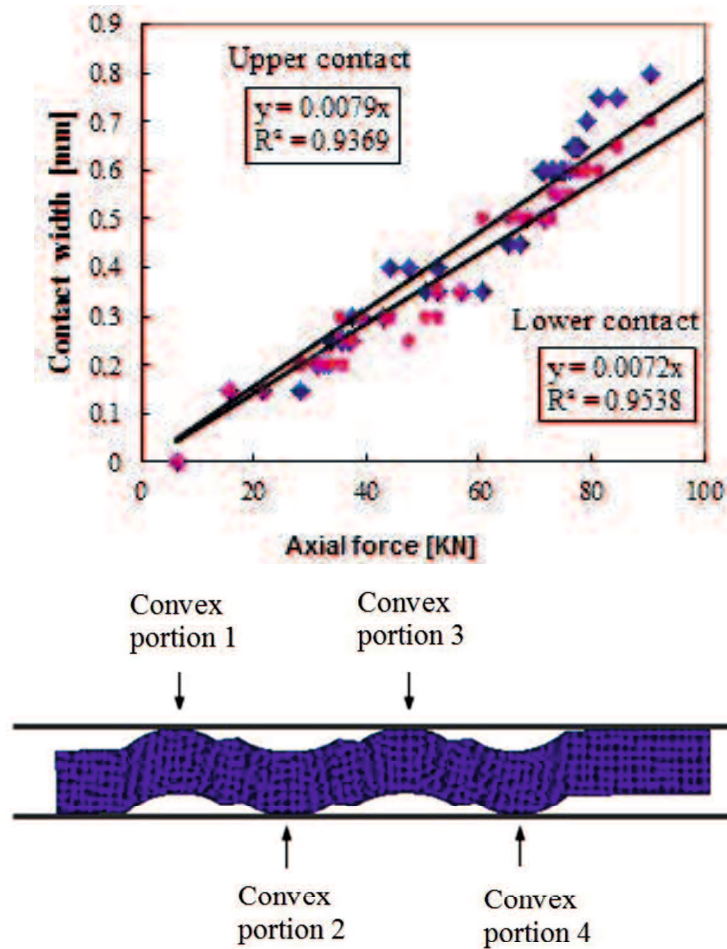
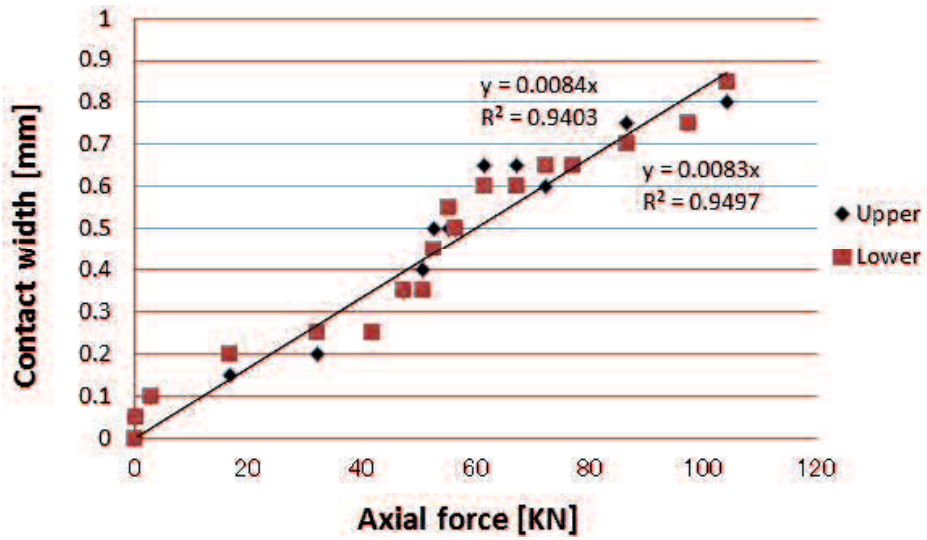
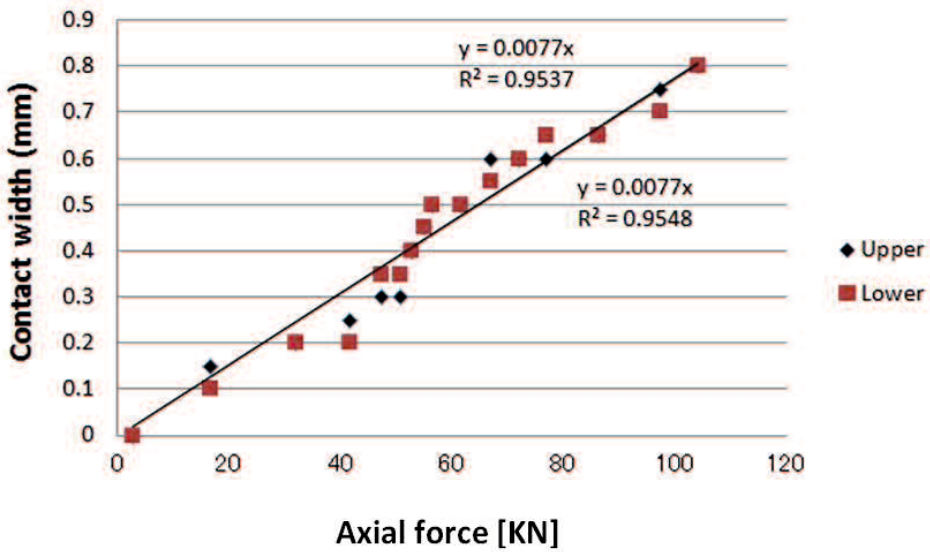


Fig 3.7 Slope of the curve of relationship between contact width and axial force

The slope of the curve increased; it would reduce the axial force. The slope of the curve was built manually by using trend line command in Microsoft Excel software. The process of optimization using L18 Taguchi illustrated as a circulating loop. Due to the optimization design based on increasing contact width combined with considering contact stress, and optimized design divided as two modes design that are 0-MPa and 400-MPa modes. The next circulating loop was generated to fulfill the forming effect by adding forming simulation before the tightening simulation. Finally, the optimized design considering forming effect could be achieved.



(a) Gasket in 0-MPa mode



(b) Gasket in 400-MPa mode

Fig. 3.8 Simulation result of the model number 14

The simulation result of one of the models in upper and lower contact for 0-MPa and 400-MPa modes particularly in 1st simulation shown in the Fig. 3.8. The figure shows that for increasing axial force increase the contact width. There are 18 data for upper and lower

contact, respectively. The contact width for convex contact portion 2 and 3 were higher than those for convex contact portion 1 and 4 because the reaction normal force for the former peaks is higher than that for the latter peaks. The figure shows that the contact width was similar for convex contact portion 2 and 3 as well as for convex contact number 1 and 4. Therefore, we focused our analysis on convex contact portion 2 and 3, which we respectively called as the lower and upper contacts. Convex portion 2 and 3 worked primarily to reduce leakage and convex portion 1 and 4 support to realize it. The space between the convex portion 1 and 3 or between the convex portion 2 and 4 are not the major attention, but the flat portion in that space are important to produce spring effect. The limit of contact width in the convex portion 2 is important in the upper contact surface of gasket. Moreover the limit of contact width in the convex portion 3 is important in the lower contact surface of the gasket.

Design experimental matrix for eight factors with three levels, the L18 orthogonal array was most applicable. The following Table 3.2 shows the factor and levels description of gasket design. Table 3.3 shows the L18 test matrix of optimization design of the new 25A-size metal gasket.

Table 3.2 Factors and levels description

Factor	Factor Description	Level 1	Level 2	Level 3
A	Over Hang (OH)	3	4	-
B	Pitch 1 (p_1)	3.5	4	4.5
C	Pitch 2 (p_2)	3.5	4	4.5
D	Pitch 3 (p_3)	3.5	4	4.5
E	Thickness (t)	1.2	1.5	1.8
F	Radius (R)	1.5	2.5	3.5
G	Lip height (h)	0.3	0.35	0.4
H	Error	1	2	3

Table 3.3 L18 test matrix

Trial	Factor							
	A	B	C	D	E	F	G	H
1	1	1	1	1	1	1	1	1
2	1	1	2	2	2	2	2	2
3	1	1	3	3	3	3	3	3
4	1	2	1	1	2	2	3	3
5	1	2	2	2	3	3	1	1
6	1	2	3	3	1	1	2	2
7	1	3	1	2	1	3	2	3
8	1	3	2	3	2	1	3	1
9	1	3	3	1	3	2	1	2
10	2	1	1	3	3	2	2	1
11	2	1	2	1	1	3	3	2
12	2	1	3	2	2	1	1	3
13	2	2	1	2	3	1	3	2
14	2	2	2	3	1	2	1	3
15	2	2	3	1	2	3	2	1
16	2	3	1	3	2	3	1	2
17	2	3	2	1	3	1	2	3
18	2	3	3	2	1	2	3	1

The L18 matrix conducted and the slope of the curve of relationship between contact width and axial force as observed values (Y) was calculated for both models 0-MPa mode and 400-MPa mode as shown in the Table 3.3. The slope of the curve has been obtained by the slope average of upper and lower contact.

Table 3.4 Result of L18 Taguchi method

Run#	Factor	Slope of curve	
		0-MPa mode	400-MPa mode
1	A ₁ B ₁ C ₁ D ₁ E ₁ F ₁ G ₁ H ₁	0.00835	0.0077
2	A ₁ B ₁ C ₂ D ₂ E ₂ F ₂ G ₂ H ₂	0.0089	0.0077
3	A ₁ B ₁ C ₃ D ₃ E ₃ F ₃ G ₃ H ₃	0.0085	0.0075
4	A ₁ B ₂ C ₁ D ₁ E ₂ F ₂ G ₃ H ₃	0.008	0.0071
5	A ₁ B ₂ C ₂ D ₂ E ₃ F ₃ G ₁ H ₁	0.00805	0.00575
6	A ₁ B ₂ C ₃ D ₃ E ₁ F ₁ G ₂ H ₂	0.0095	0.0057
7	A ₁ B ₃ C ₁ D ₂ E ₁ F ₃ G ₂ H ₃	0.01165	0.0042
8	A ₁ B ₃ C ₂ D ₃ E ₂ F ₁ G ₃ H ₁	0.0076	0.00545
9	A ₁ B ₃ C ₃ D ₁ E ₃ F ₂ G ₁ H ₂	0.00705	0.0059
10	A ₂ B ₁ C ₁ D ₃ E ₃ F ₂ G ₂ H ₁	0.00675	0.0061
11	A ₂ B ₁ C ₂ D ₁ E ₁ F ₃ G ₃ H ₂	0.0108	0.005
12	A ₂ B ₁ C ₃ D ₂ E ₂ F ₁ G ₁ H ₃	0.00765	0.0069
13	A ₂ B ₂ C ₁ D ₂ E ₃ F ₁ G ₃ H ₂	0.00565	0.00475
14	A ₂ B ₂ C ₂ D ₃ E ₁ F ₂ G ₁ H ₃	0.01075	0.00435
15	A ₂ B ₂ C ₃ D ₁ E ₂ F ₃ G ₂ H ₁	0.0092	0.007
16	A ₂ B ₃ C ₁ D ₃ E ₂ F ₃ G ₁ H ₂	0.0096	0.0056
17	A ₂ B ₃ C ₂ D ₁ E ₃ F ₁ G ₂ H ₃	0.00555	0.0048
18	A ₂ B ₃ C ₃ D ₂ E ₁ F ₂ G ₃ H ₁	0.0102	0.0045

To calculate the main effect of each factor, the result for trials of the factor added and then divides by the number of such trials [41]. In the example for gasket A₁, the column for A is observed that the level 1 occurs in the experiment number 1 until 9. The main effect of A₁ is calculated by adding the results (Y) of those nine trials and then divides by nine as a number of trials.

For 0-MPa gasket mode:

$$A_1 = (0.00835+0.0089+0.0085+0.008+0.00805+0.0095+0.01165+0.0076+0.00705)/9 \\ = 0.008622$$

$$A_2 = (0.00675+0.0108+0.00765+0.00565+0.01075+0.0092+0.0096+0.00555+0.0102)/9 \\ = 0.008461$$

$$B_1 = (0.00835+0.0089+0.0085+0.00675+0.0108+0.00765)/6 = 0.008492$$

$$B_2 = (0.008+0.00805+0.0095+0.00565+0.01075+0.0092)/6 = 0.008525$$

$$B_3 = (0.01165+0.0076+0.00705+0.0096+0.00555+0.0102)/6 = 0.008608$$

$$C_1 = (0.00835+0.008+0.01165+0.00675+0.00565+0.0096)/6 = 0.008333$$

$$C_2 = (0.0089+0.00805+0.0076+0.0108+0.01075+0.00555)/6 = 0.008608$$

$$C_3 = (0.0085+0.0095+0.00705+0.00765+0.0092+0.0102)/6 = 0.008683$$

$$D_1 = (0.00835+0.008+0.00705+0.0108+0.0092+0.00555)/6 = 0.008158$$

$$D_2 = (0.0089+0.00805+0.01165+0.00765+0.00565+0.0102)/6 = 0.008683$$

$$D_3 = (0.0085+0.0095+0.0076+0.00675+0.01075+0.0096)/6 = 0.008783$$

$$E_1 = (0.00835+0.0095+0.01165+0.0108+0.01075+0.0102)/6 = 0.010208$$

$$E_2 = (0.0089+0.008+0.0076+0.00765+0.0092+0.0096)/6 = 0.008492$$

$$E_3 = (0.0085+0.00805+0.00705+0.00675+0.00565+0.00555)/6 = 0.006925$$

$$F_1 = (0.00835+0.0095+0.0076+0.00765+0.00565+0.00555)/6 = 0.007383$$

$$F_2 = (0.0089+0.008+0.00705+0.00675+0.01075+0.0102)/6 = 0.008608$$

$$F_3 = (0.0085+0.00805+0.01165+0.0108+0.0092+0.0096)/6 = 0.009633$$

$$G_1 = (0.00835+0.00805+0.00705+0.00765+0.01075+0.0096)/6 = 0.008575$$

$$G_2 = (0.0089+0.0095+0.01165+0.00675+0.0092+0.00555)/6 = 0.008592$$

$$G_3 = (0.0085+0.008+0.0076+0.0108+0.00565+0.0102)/6 = 0.008458$$

$$H_1 = (0.00835+0.00805+0.0076+0.00675+0.0092+0.0102)/6 = 0.008358$$

$$H_2 = (0.0089+0.0095+0.00705+0.0108+0.00565+0.0096)/6 = 0.008583$$

$$H_3 = (0.0085+0.008+0.01165+0.00765+0.01075+0.00555)/6 = 0.008683$$

For 400-MPa gasket mode:

$$A_1 = (0.0077+0.0077+0.0075+0.0071+0.00575+0.0057+0.0042+0.00545+0.0059)/9$$

$$= 0.006333$$

$$A_2 = (0.0061+0.005+0.0069+0.00475+0.00435+0.007+0.0056+0.0048+0.0045)/9 \\ = 0.005444$$

$$B_1 = (0.0077+0.0077+0.0075+0.0061+0.005+0.0069)/6 = 0.006817$$

$$B_2 = (0.0071+0.00575+0.0057+0.00475+0.00435+0.007)/6 = 0.005775$$

$$B_3 = (0.0042+0.00545+0.0059+0.0056+0.0048+0.0045)/6 = 0.005075$$

$$C_1 = (0.0077+0.0071+0.0042+0.0061+0.00475+0.0056)/6 = 0.005908$$

$$C_2 = (0.0077+0.00575+0.00545+0.005+0.00435+0.0048)/6 = 0.005508$$

$$C_3 = (0.0075+0.0057+0.0059+0.0069+0.007+0.0045)/6 = 0.00625$$

$$D_1 = (0.0077+0.0071+0.0059+0.005+0.007+0.0048)/6 = 0.00625$$

$$D_2 = (0.0077+0.00575+0.0042+0.0069+0.00475+0.0045)/6 = 0.005633$$

$$D_3 = (0.0075+0.0057+0.00545+0.0061+0.00435+0.0056)/6 = 0.005783$$

$$E_1 = (0.0077+0.0057+0.0042+0.005+0.007+0.0045)/6 = 0.005683$$

$$E_2 = (0.0077+0.0071+0.00545+0.0069+0.007+0.0056)/6 = 0.006625$$

$$E_3 = (0.0075+0.00575+0.0059+0.0061+0.00475+0.0048)/6 = 0.0058$$

$$F_1 = (0.0077+0.0057+0.00545+0.0069+0.00475+0.0048)/6 = 0.005883$$

$$F_2 = (0.0077+0.0071+0.0059+0.0061+0.00435+0.0045)/6 = 0.005942$$

$$F_3 = (0.0075+0.00575+0.0042+0.005+0.007+0.0056)/6 = 0.005842$$

$$G_1 = (0.0077+0.00575+0.0059+0.0069+0.00435+0.0056)/6 = 0.006033$$

$$G_2 = (0.0077+0.0057+0.0042+0.0061+0.007+0.0048)/6 = 0.005917$$

$$G_3 = (0.0075+0.0071+0.00545+0.005+0.00475+0.0045)/6 = 0.005717$$

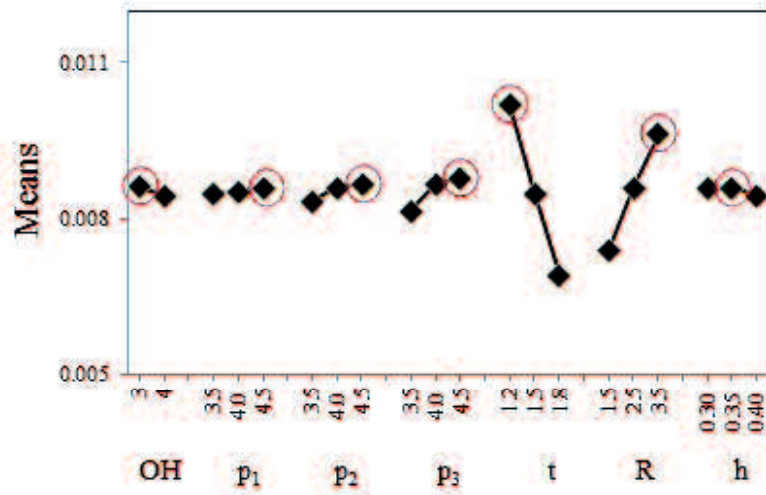
$$H_1 = (0.0077+0.00575+0.00545+0.0061+0.007+0.0045)/6 = 0.006083$$

$$H_2 = (0.0077+0.0057+0.0059+0.005+0.00475+0.0056)/6 = 0.005775$$

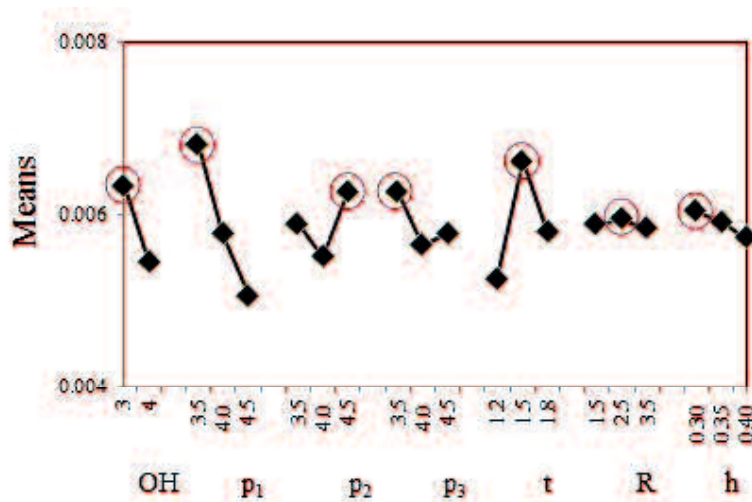
$$H_3 = (0.0075+0.0071+0.0042+0.0069+0.00435+0.0048)/6 = 0.005808$$

Based on the calculation above, the main effect is plotted for visual inspection of each factor for various level conditions at 0-MPa and 400-MPa mode is shown in Fig. 3.9. The highest value for the slope of the curve is supposed as the axial force reducing. The main factor of the design is providing a larger contact width and reducing the axial force. For Fig.

3.8 (a) the higher value of OH is 3, p_1 is 4.5, p_2 is 4.5, p_3 is 4.5, t is 1.2, R is 3.5, and h is 0.35. As well as for Fig. 3.8 (b) the higher value of OH is 3, p_1 is 3.5, p_2 is 4.5, p_3 is 3.5, t is 1.5, R is 2.5, and h is 0.3.



(a) 0-MPa modes



(b) 400-MPa modes

Fig. 3.9 Main effects of each factor for various levels at slope of curve

Finally, this study suggests the optimum gasket design based on results of each model shown in Table 3.5.

Table 3.5 Optimum design of gasket for 0-MPa and 400-MPa mode

Factor	Forming model	
	0-MPa mode	400-MPa mode
OH	3.0 mm	3.0 mm
p ₁	4.5 mm	3.5 mm
p ₂	4.5 mm	4.5 mm
p ₃	4.5 mm	3.5 mm
t	1.2 mm	1.5 mm
R	3.5 mm	2.5 mm
h	0.35 mm	0.3 mm

3.2 Leakage Test for the 25-A Size Metal Gasket

After the optimum design of a new 25- size metal gasket obtained, the next step is the leakage experiment. The helium leakage test was used to check the performance of the gasket. These are the step after optimum design of the gasket was obtained: dies design, dies production, mold press for the product a gasket, leakage measurement.

3.2.1 Dies design analysis

The pressing process is a manufacturing method that provides a work piece with the shape, certain dimensional and capability, through the die forcing component to suffer plastic deformation. The pressing process is having a series of advantages such as the ability of processing complex shapes, lower cost, high production efficiency, and steady quality. The pressing die as an important basic technique will become increasingly more useful with the development of industrial products and the improvement of production technology. Metal sheet pressing forming has been applied widely in fields such as

automation, aviation, ship, instrumental and home appliances. It is one of the important processing methods [42].

Sheet pressing plastic forming is a very complex process. Many factors affect the resulting shape. Production of press die depended on previous experience and repetitive debugging. After design have done needs a continuous test die. Thus, this prolongs the design cycle and increases die cost. It is necessary to find a scientific sheet material forming analysis system to explore the forming status of the press part, which can act as the references of die design. So, we are using the finite element method to simulate the process of metal plasticity forming.

After the optimum dimension of the gasket obtained, the design of the punch and dies should design too. Fig. 3.10 shows the lack of die fills defect happen as a result of forming simulation. The defect is tending occurred on the radius shape of convex contact, both on 0-MPa and 400-MPa modes. In the forming simulation, the lack of the die fill defect is not allowed. We should design the punch and dies which decreased the lack of the die fill defect [43-44]. The lack of the die fill defect will decrease the contact width.

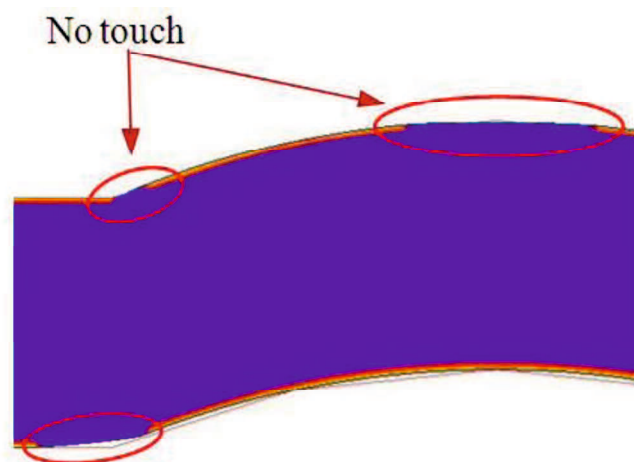


Fig. 3.10 Lack of die fills defect result on one of convex contact

Using MSC Marc Software analysis founded that the lack of the die fill defect is decreased with increasing the angle of inner radius. The changes in the angle will change

the radius and lip height, see Fig. 3.11. It means will increase an inner lip height of convex and decrease the radius of convex. The increased of angle is varied by 0% ($\theta_{0\%}$), 5% ($\theta_{5\%}$) and 10% ($\theta_{10\%}$) from the initial angle, see Fig.3.12. The adding 10% of the angle showed the best reduction of the lack of the die fill defect. There is no the lack of die fill in this condition. The addition of the angle inner radius did not affect the characteristic of the gasket because there is no contact with a flange for the inner radius.

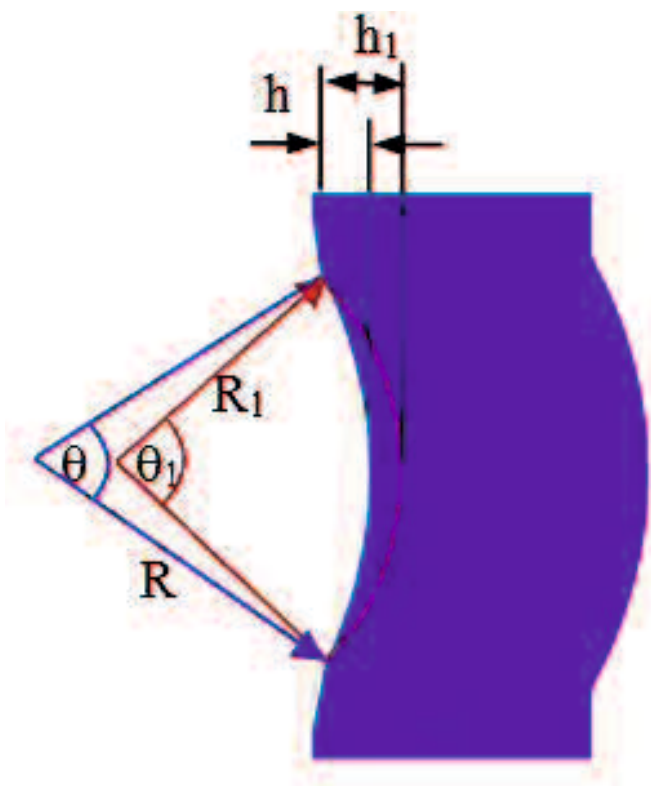


Fig. 3.11 The changes process of the angle to reduce lack of die fills defect result on one of convex contact

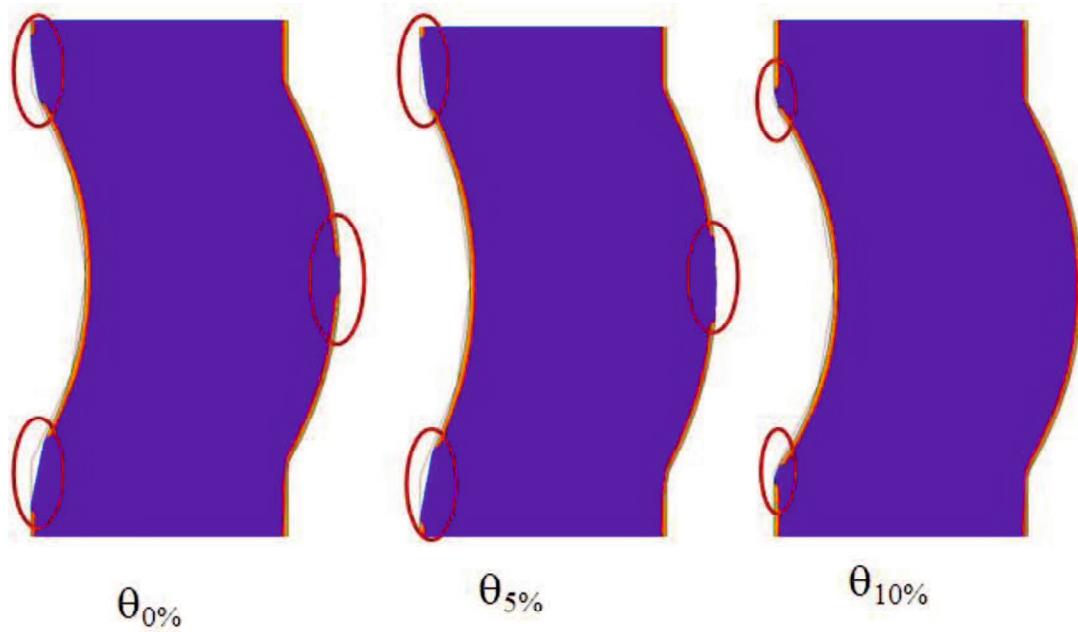


Fig.3.12 Gasket simulation to reduce lack of die fills defect

The optimum dimension of dies to forming a metal gasket has obtained. Fig. 3.13 and Table 3.6 show the optimum dimension of dies. The initial lip high is h , and the initial radius is R . For the inner radius, the radius was changed from R to R_1 , and the lip high was changed from h to h_1 . There is no change for the outer radius with a gasket dimension, but there is a change for the inner radius. The change of inner radius will not change the performance of the gasket because contact between gasket and flange will happen for the outer radius of gasket [43].

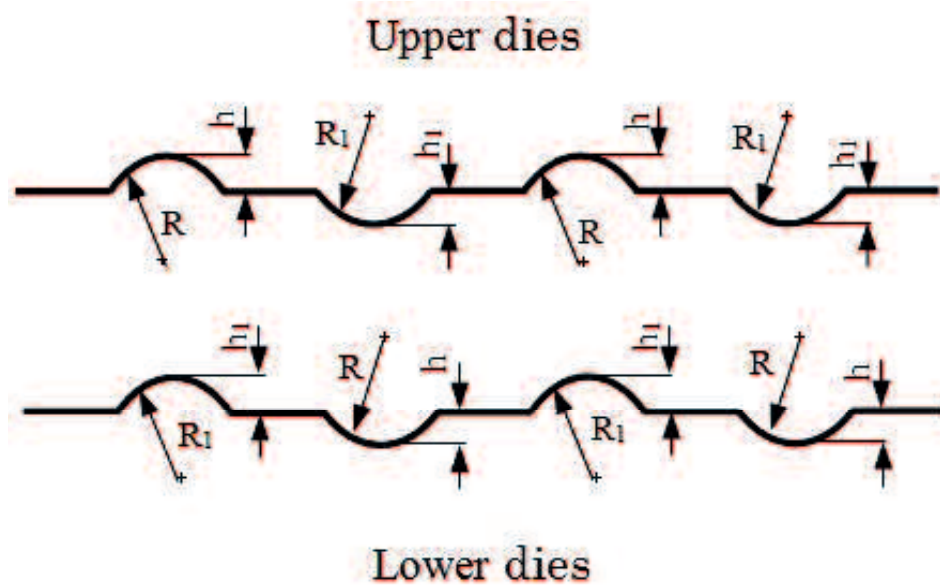


Fig.3.13 Upper and lower dies design

Table 3.6 Optimum dimensions of dies for 0-MPa and 400-MPa modes

Gasket	h	R	h_1	R_1
0-MPa Mode	0.35	3.50	0.39	3.20
400-MPa Mode	0.30	2.50	0.33	2.30

Finally, based on the dimensions of dies design in the Table 3.6, the dies used to forming material gasket can be produced. The dimension of dies design shows in Table 3.5, but the dimension of lip height for inner radius change from h to h_1 and the dimension of radius for inner radius change from R to R_1 , respectively. Fig 3.14 shows the upper and lower dies after manufactured.

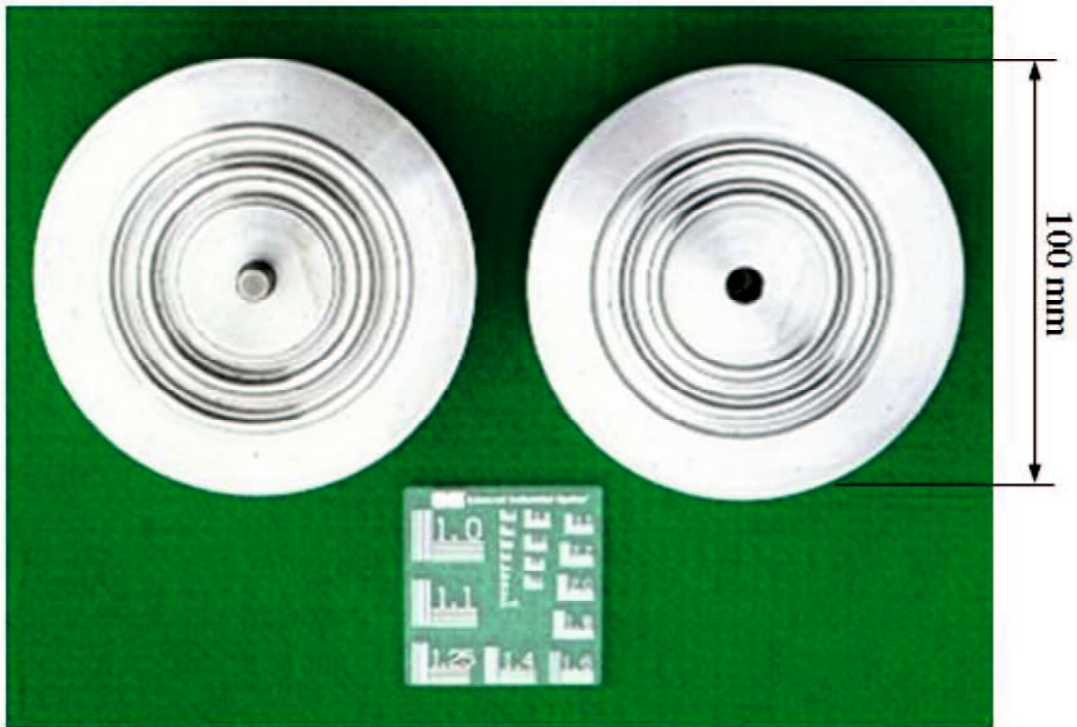


Fig. 3.14 Upper and lower of dies

3.2.2 Mold Press

The gasket was manufactured using a mold press. This process called forming process in simulation analysis. The shape of the gasket is realized by using a punch to force the initial material to slide into a die. Hence, the forming effect was considered for assessing the modeling of gasket design. A UH-1000 KNI universal testing machine was used to perform the forming process. Fig. 3.15 shows the press forming process for manufacturing a gasket. Lower dies has a fixed boundary condition. The upper dies moved in a downward direction and pressed gasket material and lower dies. Firstly, we put the lower dies in bottom based. Next, the material gasket put in the center of lower dies. The upper dies put in the above of material gasket. Make sure that the position of lower dies, material gasket, and upper dies in one center line. Finally, the upper punch moved downward and pressed the upper dies.

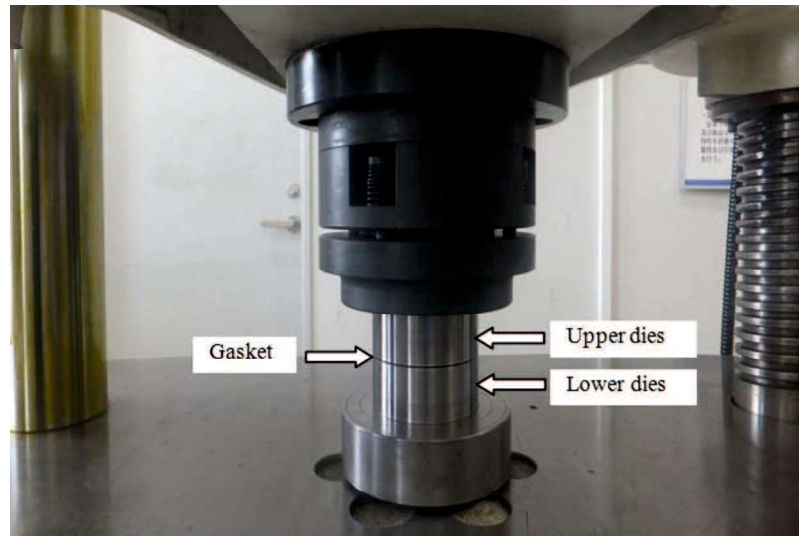


Fig. 3.15 Cold forming process

The deformation in the thickness direction for sheet pressing forming is very small in contrast with that in other directions. The deformation mode of sheet forming mainly has the following kinds: bi-directional stretching, plane stress, stretching, depths extending, bending and counter-bending. However, the procedure of sheet forming can be considered as virtually static so that velocity and acceleration can be ignored. Elastic forming and spring-back are involved in plastic forming. Therefore, they must be considered in any analysis [42]. The load for pressing process is shown in Fig. 3.16. We pressed the gasket material minimum three times. It is very important due to the spring back effect. The load gave to gasket material was 950 KN. This load was enough to shape the material gasket to be gasket. The time from initial load until 950 KN was 60 minutes. The material gasket before forming process and gasket after forming process are shown in Fig. 3.17.

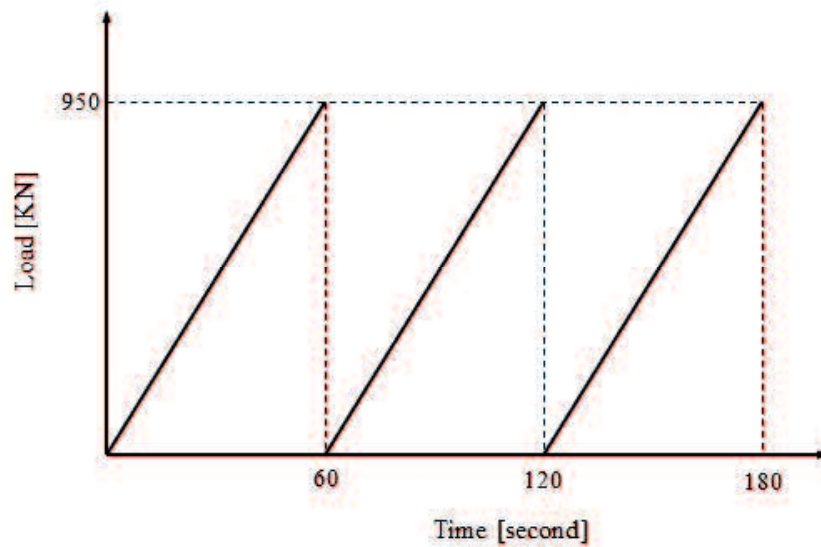


Fig. 3.16 Load for cold forming



(a) Material gasket (b) gasket

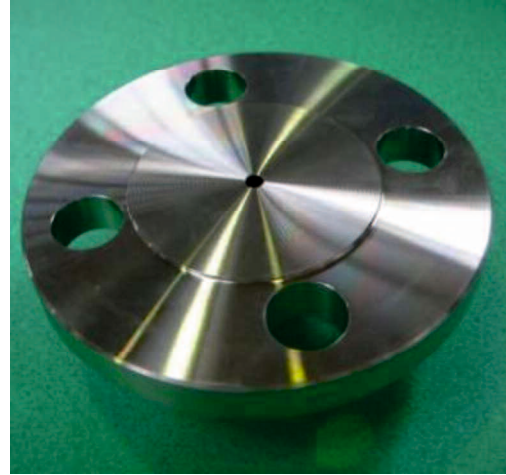
Fig. 3.17 Photographs of 25-A size metal gasket

3.2.3 Leak Quantity Measurement

Fig. 3.18(a) and (b) shows a general-purpose flange based on JIS B2220 [45] with 10 K pressure and 25A diameter used in this test. The upper flange and the joint welded carefully to avoid distortions. To avoid the experiment result error due to the leakage from the joint of the flange and pipe, the leakage flow quantity of the joint part calibrated. The axial force has been produced by the bolt as shown in Fig.3.19.



(a) Lower flange



(b) Upper flange

Fig. 3.18 General-purpose 25A flange



Fig. 3.19 Appearance of joint jig

There are a many varieties of flange configuration and styles, as shown in Fig. 3.20, but only four types of facing are widely used, which are raised face, flat face, ring-joint and lap-joint flange. In this study, flat face flange is used due to the same flange in Saeed study. The flange used in this test was a general-purposed flange prescribed in JIS B 2220. Flat faced flanges used with a gasket that the outer diameter equals that of the flange. In this case, the gasket is relatively easy to install and remove. It becomes a challenge for other research to explore another type of flange.

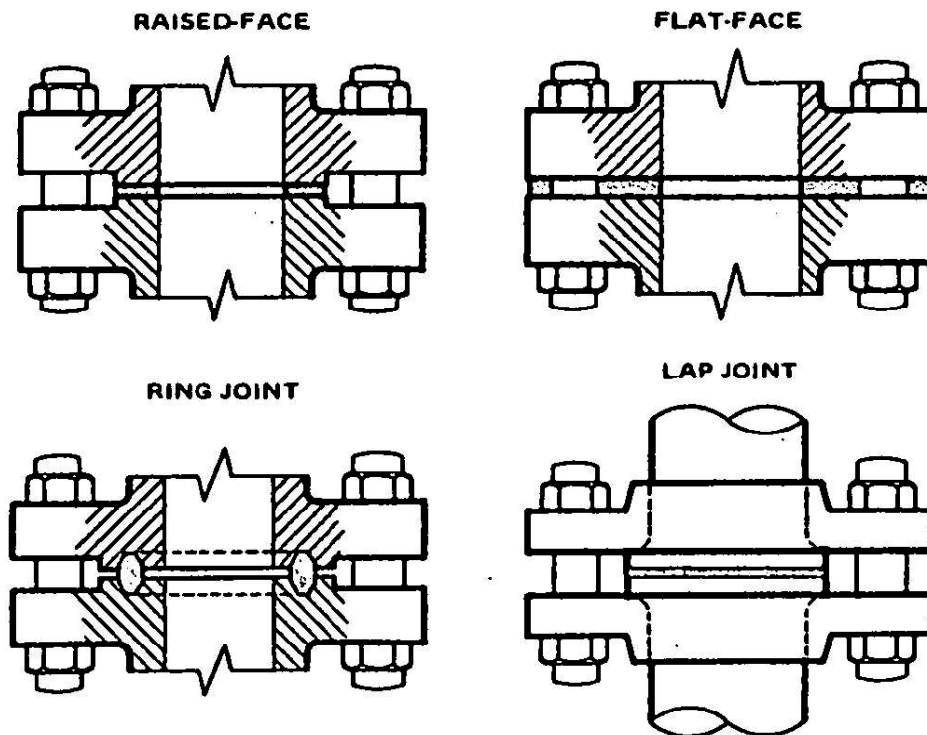


Fig. 3.20 Four type of flange face configurations for gasket joints

In the previous study [42], the gasket design based on contact status, which is contact and no contact, without considering the distribution of the stress called 0-MPa mode. In the other hand, the gasket design by deleting the contact stress value below of 400MPa called 400-MPa mode. It was found from the material properties; the yield stress is 398.83MPa. In this study, the gasket design based on an elastic condition, we called 0-MPa mode while it based on a plastic condition is 400-MPa mode.

In the past, leak or no leak judgment is done by using water pressure test. Now, many researchers have been performing leak test by using the helium test [5] and [16]. Helium used for leak detection due to the several reasons as below:

- Helium is better test sensitivity.
- It's not harmful when used adequate ventilation.
- It's inexpensive.

- It's light. Helium will dissipate rapidly allowing fast cleanups and ultimately shorter test times.

Evaluate the axial force and leakage quantity; the leakage quantity was measured using helium leakage measurement. Fig. 3.21 shows a schematic diagram of the helium leakage measurement device that developed for the leakage quantity evaluation test. The helium flow leakage quantity was quantitative. The highest detection ability in the helium leakage measurement was chosen based on the JIS Z2330 [46] and JIS Z2331 standard [47]. The measurement method employed is called the vacuum method. First, gas from the test tube and the internal part of the chamber was evaluated using vacuum pumps. The helium gas was injected into the outer part of the gasket in the chamber, and the residual air was measured by using an oxygen density sensor. The helium density could be calculated in the outer part of the gasket.

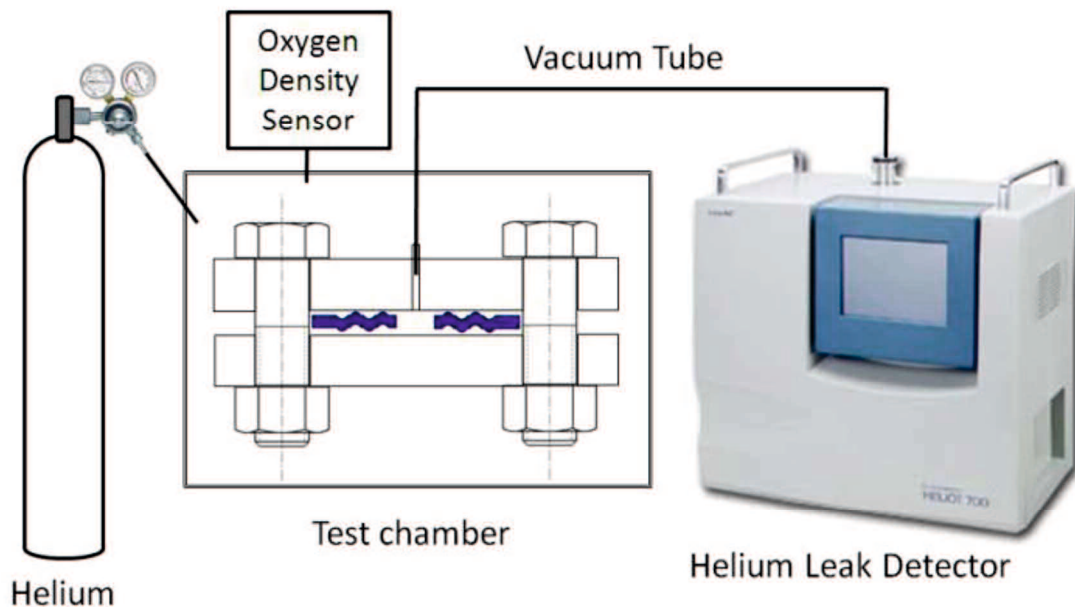


Fig. 3.21 Schematic diagram of helium leakage measurement device

During the experiment, helium gas was substituted in the test chamber; and the residual air was measured by an oxygen density sensor. The helium density measured when the oxygen density was below 0.2 % and the helium density was above 99 % under atmospheric condition. The helium density at the outer part of the gasket was calculated by using a helium leakage detector (HELIOT 702D1, ULVAC); in particular, the minimum leakage quantity could be detected. The helium leakage measurement system is built to measure approximately 1.0×10^{-09} Pa m³/s. The minimum and maximum leakage quantity detectable using this device was $1.0E^{-11}$ Pa m³/s and approximately $1.0E^{-0.3}$ Pa m³/s, respectively. To avoid the influence of leakage flow fluctuation at stages, measurement was performed between 300 to 500 s. The leakage flow quantity of the joint part was calibrated to avoid experimental errors due to the leakage from the joint of the flange and the pipe.

Gasket performance is evaluated by using the relationship between axial force and helium leak rate. An axial force was produced on the flange by the tightening of the flange using bolts. Approximate the axial force, the tightening torque of the bolt commonly converted into an axial load. Nevertheless, the axial force could not be predicted accurately owing to the different friction coefficients of each bolt and nut used in the clamping as well as the variation of the axial force due to the clamping order of the bolt. Overcome these problems, in this study, the axial force was directly measured by embedding a strain gage into the bolts as shown in Fig. 3.22. Using data acquisition, the axial force every bolt can be obtained. The leakage quantity was measured based on the measurement of the helium flow leakage quantity. Axial force levels of 10, 15, 20, 25, and 30 KN measured for every bolt. The axial force of every bolt monitored in order to adjust the axial force error to below 3%. For bolts were used to clamp the flange, therefore, we also tested axial force of 40, 60, 80, 100, and 120 KN.

In the previous study [18], the qualitative explanation produced by water pressured test was transformed into a quantitative value using helium leak test. Therefore, quantitative decision criterion to prevent the leak is determined under the condition of helium leak quantity below the 1.0×10^{-6} Pa.m³/s, and it observed that the leak by water pressure test did not occur.

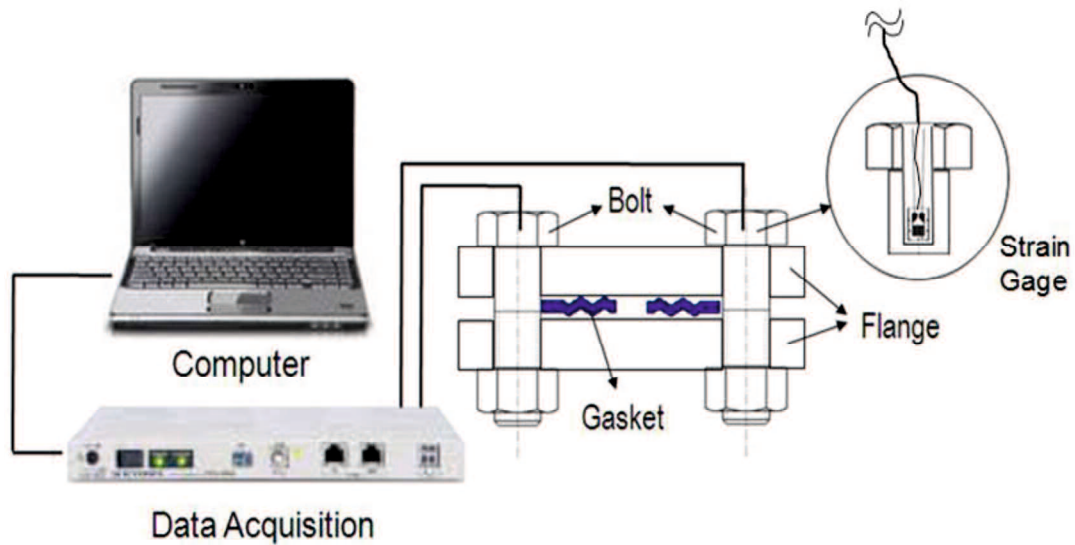


Fig. 3.22 Measurement of axial force

The leakage measurement result of the proposed metal gasket is shown in Fig. 3.23. Previous study [14], the leak by water pressure test did not occurred on 1.0×10^{-6} Pa.m³/s of the helium leak rate. Figure shows that the gasket 0-MPa mode did not leakage start on the 100 KN axial loads while the gasket 400-MPa mode leakage did not occur start on the 80 KN axial loads. Both types of gaskets show good performance, because it did not leakage at certain axial load. The gasket 400-MPa shows better sealing performance than gasket 0-MPa mode. Therefore, the gasket design 400-MPa mode is chosen due to the better sealing performances are desirable because the large contact stress [43].

Fig. 3.24 shows the leakage measurement test result comparison for non-forming and forming consideration. Gasket 0-MPa mode and 400-MPa mode is gaskets design based on forming consideration [43]. Gasket non-forming, in this Fig. we called as a standard model is gasket design did not use forming in simulation [18]. Figure shows that the gasket standard model did not leakage on the 120 KN axial loads while the gasket 0-MPa mode leakage did not occur in the 100 KN axial forces and the gasket 400-MPa mode leakage did not occur in the 80 KN axial forces. The gasket 0-MPa mode and 400-MPa shows better sealing performance than gasket standard model.

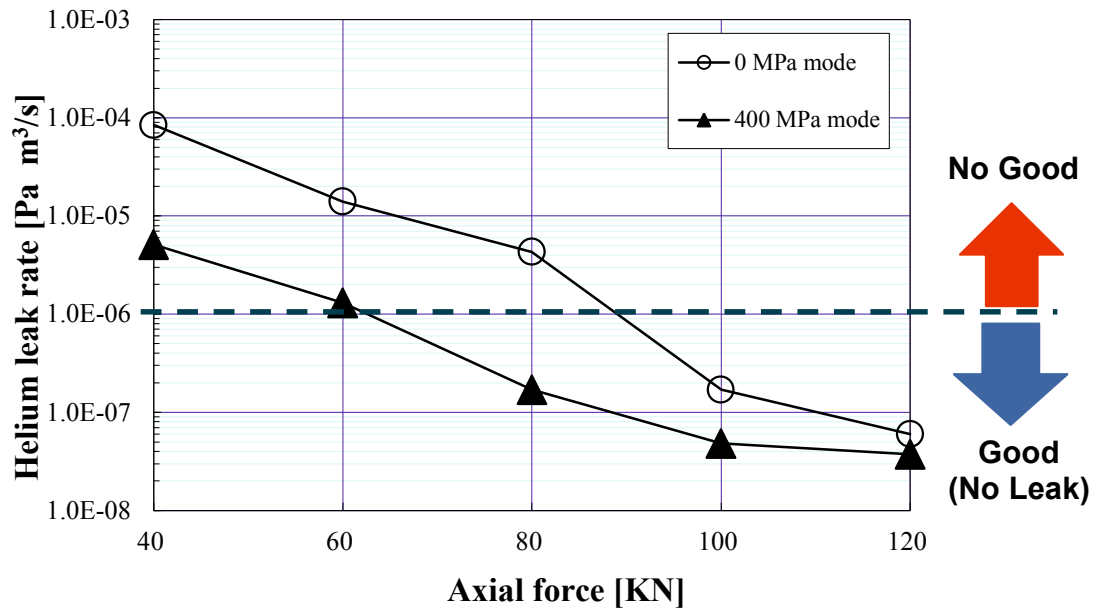


Fig. 3.23 Leakage measurement test result for gasket 0-MPa mode and 400-MPa mode

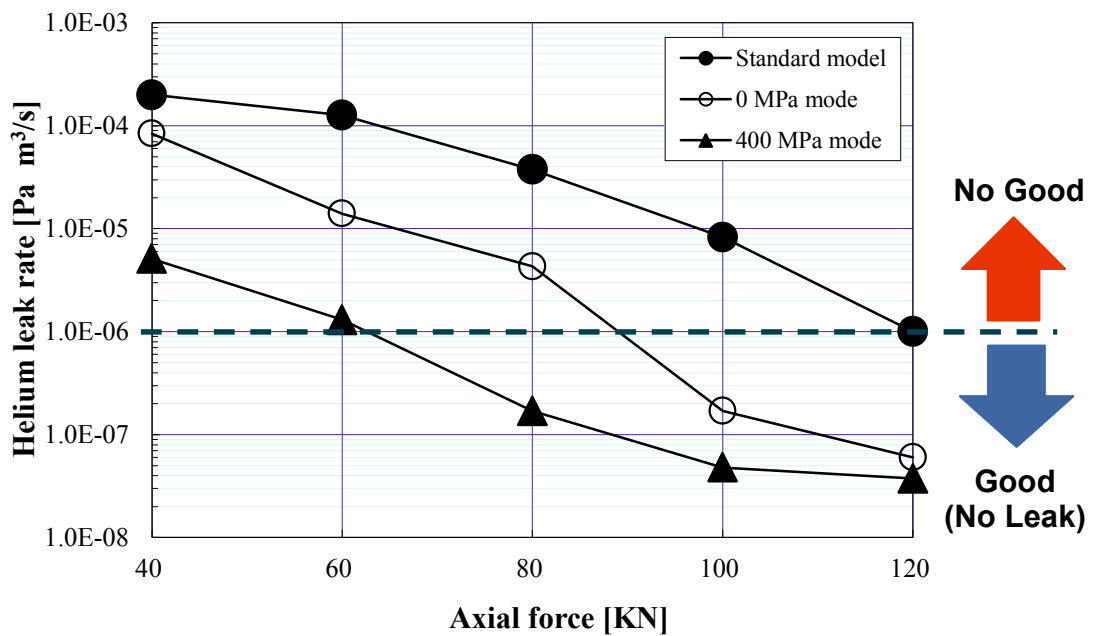


Fig. 3.24 Leakage measurement test result comparison for standard and forming consideration

3.3 Conclusion

This study investigates the optimum design of the 25A-size metal gasket by a simulation using FEM based on contact width considering forming effect and contact stress effect. The helium leak rate measured using a helium leakage test. The following conclusions derived from this study:

1. The optimum design of the 25A-size metal gasket by simulation was founded.
2. Forming process for both metal gaskets mode can be done well.
3. Final evaluation is determined by helium leak quantity to check leakage performance of both types of gaskets.
4. According to the leaks that occurred, we find that the gasket 400-MPa mode was better sealing performances than 0-MPa mode. Both types of gasket can be used as a seal because it did not leak in the helium leak test.
5. The gasket 0-MPa mode and 400-MPa shows better sealing performance than gasket standard model.

CHAPTER IV

INFLUENCE OF SURFACE ROUGHNESS ON LEAKAGE OF THE 25-A SIZE METAL GASKET

An important characteristic to consider in the development of new metal gasket is a function to prevent or to stop the leakage depending on the surface roughness standard used. Person et al. [8] and Lorenz et al. [9] studied theory leak-rate of seals, which is the case for rubber seals. They have presented a theory of the leak-rate of seal, which based on percolation theory and developed contact mechanics theory. They have presented numerical results for the leak-rate, and for surface roughness lateral size and the height size of the critical construction. They have presented results for how leak-rate depended on lateral size and the height surface roughness and on the pressure with which the rubber is squeezed against the rough counter-surface. Leakage is a function of surface roughness [19] —it increases with the surface roughness. Previous studies on the design of corrugated metal gasket used models that did not include the surface roughness effect. The main problem in this regard is the fact that a suitable surface roughness for which no leakage occurs did not yet well understood.

In this light, this study aims to determine the surface roughness of a flange contact that minimizes leakage in the newly developed 25A-size metal gasket. The surface roughness determined through a comparison between simulation and experimental results. The simulation investigates the contact stress and contact width according to the surface roughness of the flange. The experiment involves a helium leakage test using two new metal gaskets having different surface roughness levels.

4.1 Surface Roughness Measurement

In reality, all engineering surfaces show some surface roughness. Engineering surfaces often showed micro-geometric defect called roughness and waviness. These defects always present; they are usually varies depending on the machining processes. This

fact causes the contact between two engineering surfaces to be located at only a limited number of asperities, even though the surfaces seem to be tightly sealed. A variation of normal load applied through the contact modifies the deformation of the contact asperities. It changes the number of asperities in the contact area.

The flange surface roughness measurement based on the JISB0601-2001 standard [48]. Fig.4.1 shows the experimental setup of the surface roughness measurement. A Handysurf E-35B was used to measure the surface roughness. The equipment calibrated first, to avoid experimental error due to the surface roughness. Using this device, all functions automatically set the ideal values for the measurement range, evaluation length, the cut-off value, and recording magnification according to the measurement conditions. This setup allows the conditions of measurement, parameter values and data of the profile curve to be directly transmitted to a personal computer.

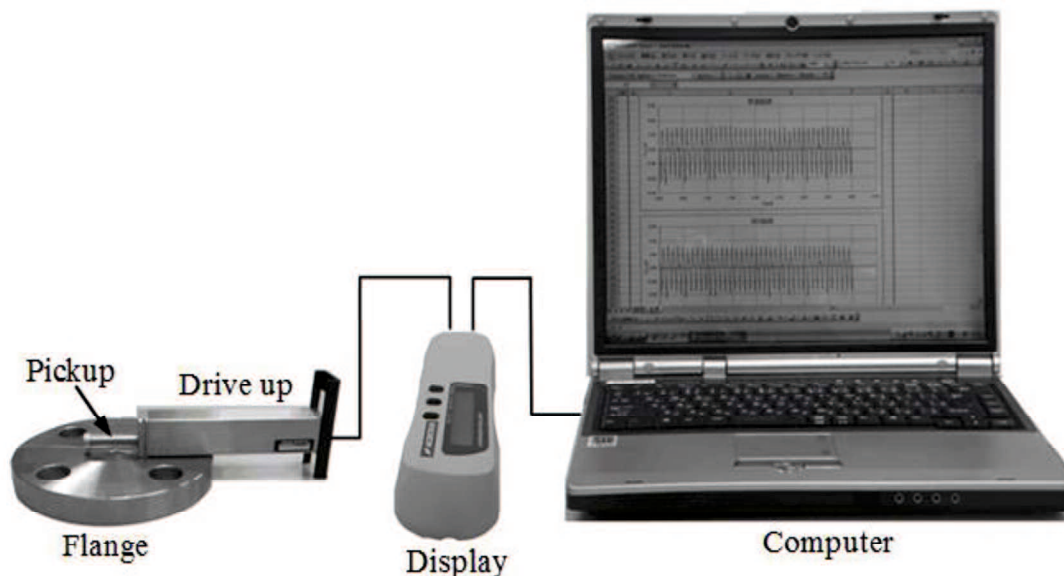


Fig. 4.1 Surface roughness measurement setup

The data processing transformed into Microsoft Excel software. The output result contains the average surface roughness R_a , maximum surface roughness R_z , and another

parameter. Furthermore, the output result can be obtained in the form of a roughness curve. Fig. 4.2 shows an example of the surface roughness measurement result. Flanges with three different average surface roughness (Ra) values—1.5, 2.5, and 3.5 μm —were used. This data was used to draw the real flange surface roughness using Solid Work software.

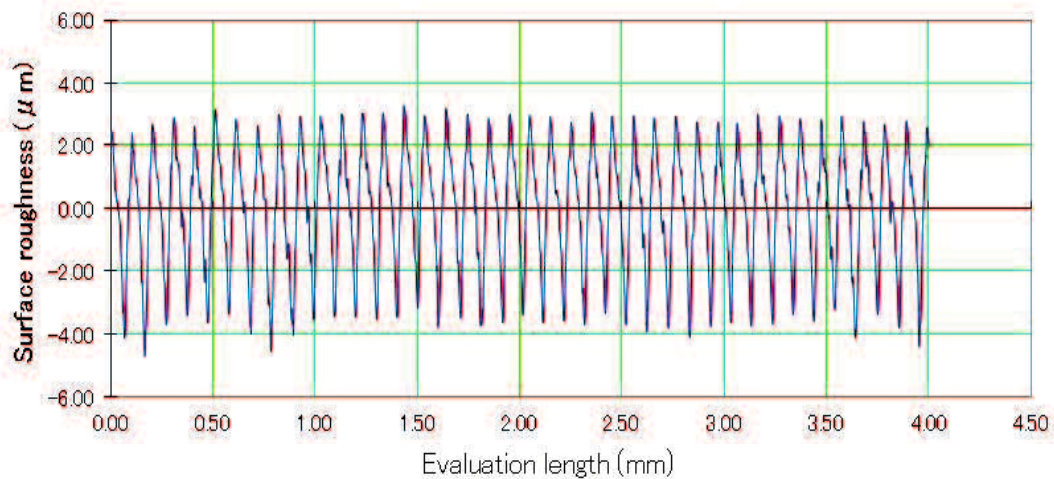


Fig. 4.2 Roughness curve

4.2 Simulation Analysis

A simulation analysis was performed to describe the contact mechanism of the 25A-size metal gasket and the rough flange. By using this approach, the relationship between the surface roughness parameter to the contact stress and contact width was determined. The gasket used in this study was manufactured using a mold press. It had beads along its circumference. When the gasket was tightened to the flange, the beads on both surfaces of the gasket created an elastic effect. The flange was assumed to have a rough surface on both sides. The gasket was in contact with both the lower and the upper sides of the flange. The flange pressed the gasket along an axial direction. SUS304 was used as a gasket and flange material because of its effectiveness in a high-temperature and high-pressure environment. Its material properties were first determined through a tensile test carried out based on JIS Z2241 [40] —the nominal stress, modulus of elasticity (E),

and tangent modulus was respectively found to be 398.83MPa, 210GPa, and 1900.53MPa.

Tightening the flange using bolts can lead to high local contact stress on the convex section of the gasket, realizing a low loading metal gasket. The contact stress distribution for a corrugated metal gasket is higher than that for a flat metal gasket. This is because the contact stress distributed in the convex section. Furthermore, the elastic regions in the flat sections produce the spring effect of metal gasket, and this can be used to reduce the effect caused by the loosening of bolts. Therefore, the new metal is preferred for realizing a low loading metal gasket.

Fig.4.3 shows a schematic of gasket tightening in consideration of the surface roughness at the flange and gasket contact area under analysis, where the gasket is shown to have corrugated shape and the flange, flat shape. When the gasket was tightened to the flange, each bead of both surfaces of the gasket created elastic effect.

In this study, we analyze a flange having three different surface roughness values: 1.5, 2.5, and 3.5 μm . According to the explanation above, the surface roughness was modeled as a sinusoidal rough surface and a real rough surface. We compared the result of surface roughness based on sinusoidal model and real model. The sinusoidal model suitable with the theory of Gao [29], which analyzed in detail the behavior of an elastic-perfectly plastic solid with a sinusoidal rough surface that is subjected to contact loading. The real surface roughness of the flange was measured using a Handysurf E-35B as described in Section 4.2. Through the surface roughness measurements, we obtained the average roughness (Ra) and the mean spacing of profile irregularities (RSM). Then, both Ra and RSM were used to model the surface roughness of the flange. The average roughness describes height asperities and RSM describes the wavelength of the surface roughness.

A flange with the best surface roughness is one that shows minimum leakage. Accordingly, the standard surface roughness for a flange with no leakage can be chosen. It can be denoted by using the slope of the curve of the relationships among the contact width and the axial force or contact stress and axial force. The surface roughness is thus selected based on an increase in the contact width and contact stress.

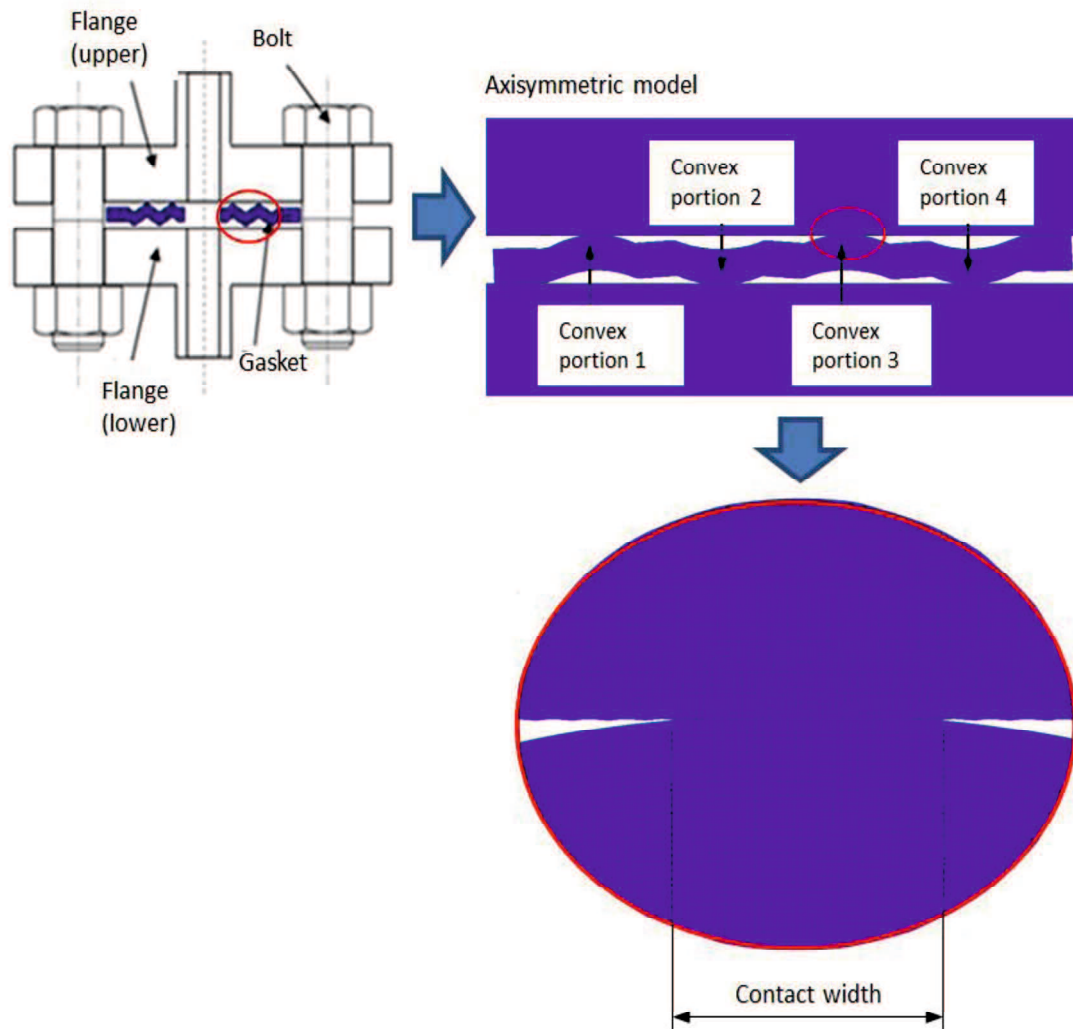


Fig. 4.3 Schematic of gasket tightening on rough flange

Fig. 4.4 shows a flowchart of the various stages of the simulation of the gasket considering the surface roughness effect. These stages were modeled using the MSC's MARC FEM analysis software [39]. We have two types of gasket, which are 0-MPa mode and 400-MPa mode. Gasket 0-MPa mode is optimum design gasket based on elastic and plastic contact stress. Gasket 400-MPa mode is optimum design gasket based on plastic contact stress. Flanges have three types of surface roughness, which are 1.5, 2.5, and 3.5 μm for gasket 0-MPa mode and 400-MPa mode respectively. We assumed the gasket is

flawless because forming product.

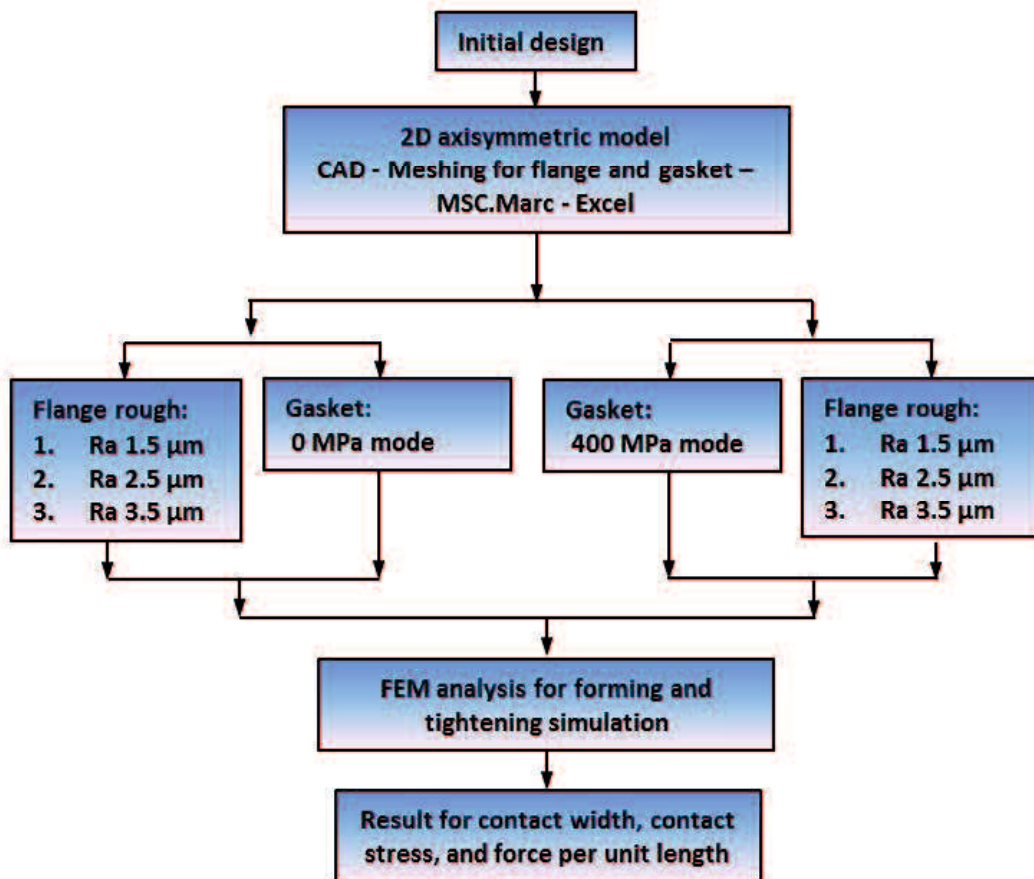


Fig. 4.4 Flowchart of various stages of simulation of gasket to obtain contact stress, contact width, and force per unit length

A virtual gasket model with various designs generated through four basic steps as described in [43]. Forming and tightening analysis were conducted to obtain the contact stress, contact width, and force per unit length. First, 2-D parameter models of the flange and the gasket were built using Solid work software. To connect the drawing data obtained from Solid work (IGES file) and the automatic meshing performed using Hypermesh, a batch command file was developed, using which an NAS file generated. We used a quadrilateral mesh for the gasket and flange material because it has a rectangular section.

The procedure file was configured to perform the pre-processing and run the model on MARC. The graphic user interface (GUI) does not appear; instead, the program runs commands in the background. After the FEM analysis completed, the output file, including the analysis results can be generated in TXT file that can be converted to a Microsoft Excel file. The output result contains the contact status, contact width, and contact stress force at each time at every peak position. The calculation of the contact width versus the axial force at peak position 1 —4 are performed using a multi-step MACRO command.

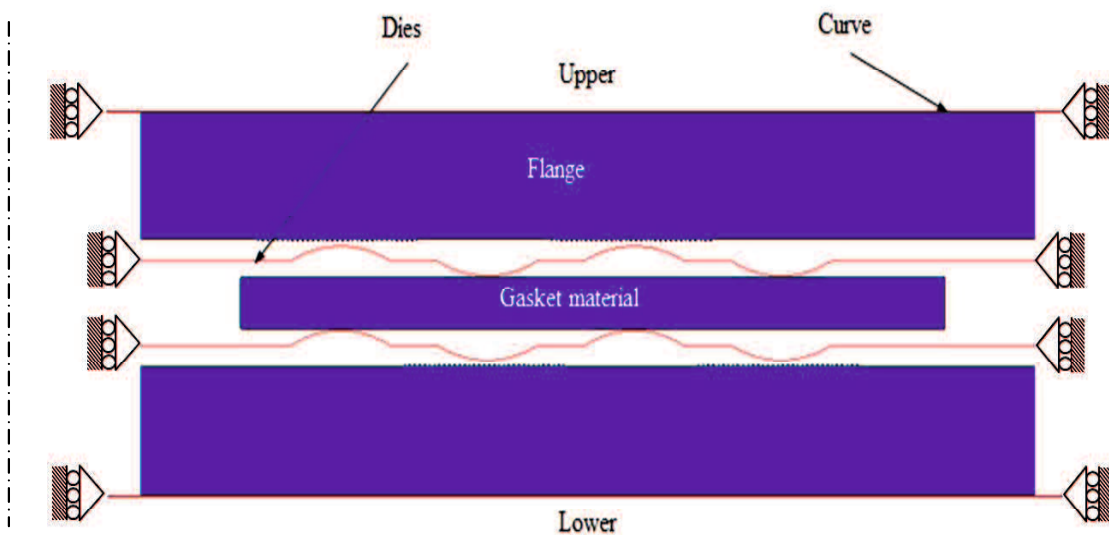


Fig. 4.5 Setting up of gasket material, dies, flange and curve before forming and tightening simulation

In this study, the gasket model was investigated through a forming simulation and a tightening simulation. Fig. 4.5 shows the setting for gasket material, flange, dies and curve. In the first stage, the dies were assumed as rigid bodies on both sides. Using two-dimensional (2D) assumptions, in the axisymmetric model, a forming process simulation conducted along the axial direction for the initial gasket material between the top and the bottom of the dies, see Fig. 4.6. We used quadrilateral meshing for gasket

material and flange. We used the meshing control based on the input number of element for different surface roughness. The element size of meshing will adjust for each surface roughness. The element size was smaller than the size of roughness spacing. In the second stage, the gasket shape produced by mold press was continually compressed the axial direction to tighten the gasket and the flanges, see Fig. 4.7. Both the gasket and the flange assumed as deformable bodies on both sides.



Fig. 4.6 Forming simulation

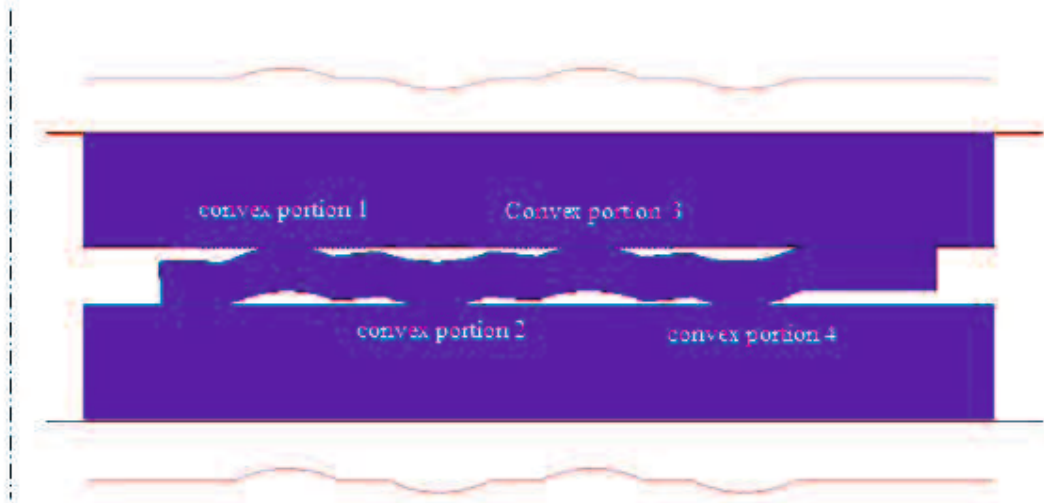


Fig. 4.7 Tightening simulation

Based from the simulation design, there were two types of gasket, which are 0-MPa mode and 400-MPa mode. Using MSC Marc software, the contact width is determined based on contact status and contact stress. The contact and no contact condition between gasket and flange described by contact status values, which are 1 and 0, respectively. This status was done without considering the distribution of the contact stress. This condition called as gasket 0-MPa mode or elastic gasket design. Moreover, the gasket 400-MPa mode or plastic gasket design is done by deleting the contact stress value below of 400MPa. It founded from the SUS304 material properties; the yield stress is 398.83MPa. Consequently, contact width value is more reduced because of contact width with which has contact stress below of 400MPa deleted. This procedure was done based on the assumption that the large contact stress creates sealing lines on contact width [37].

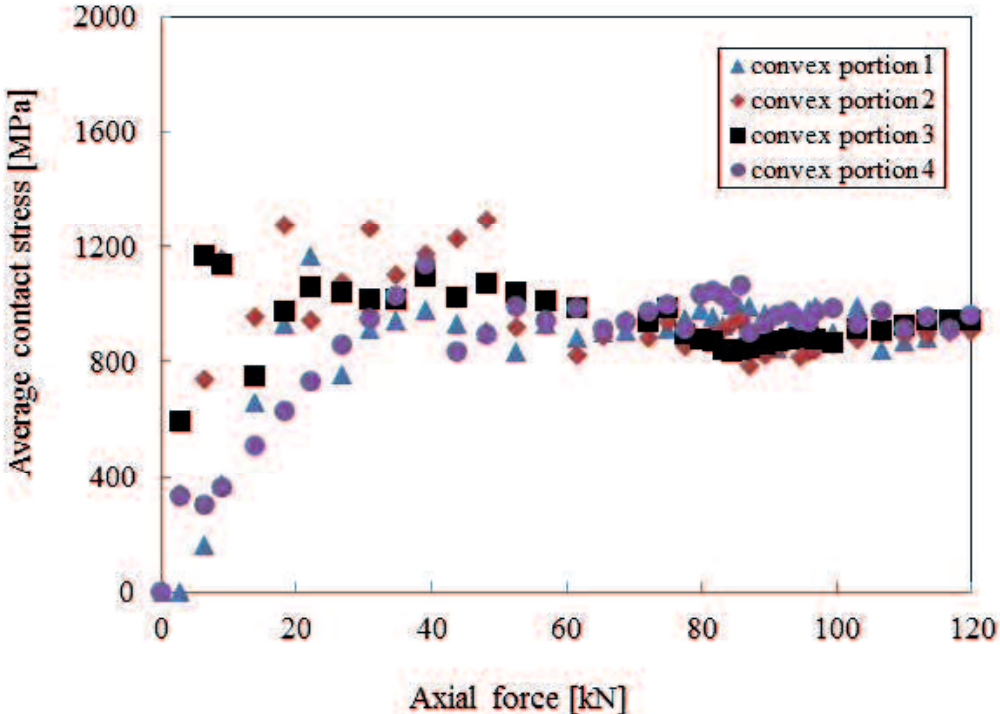


Fig. 4.8 Average contact stress in each axial force

The Fig. 4.8 shows the average contact stress for convex portion 1, 2, 3, and 4 are similar. The maximum contact stress in Fig. 4.9, contact width in Fig. 4.10 for convex portion 2 and 3 were higher than those for convex portion 1 and 4 because the reaction normal force for the former peaks is higher than that for the latter peaks. The figure shows that the maximum contact stress and contact width were similar for convex portion 2 and 3 as well as for convex portion 1 and 4. Therefore, we focused our analysis on convex portion 2 and 3, which we respectively called as the lower and upper contacts [49] and [50].

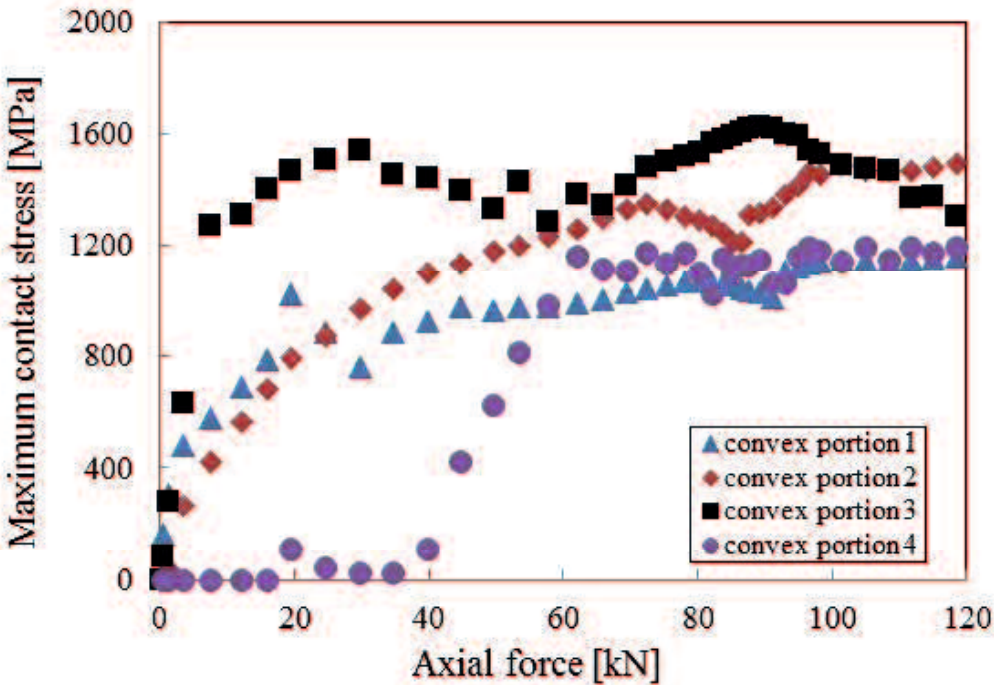


Fig. 4.9 Maximum contact stress in each axial force

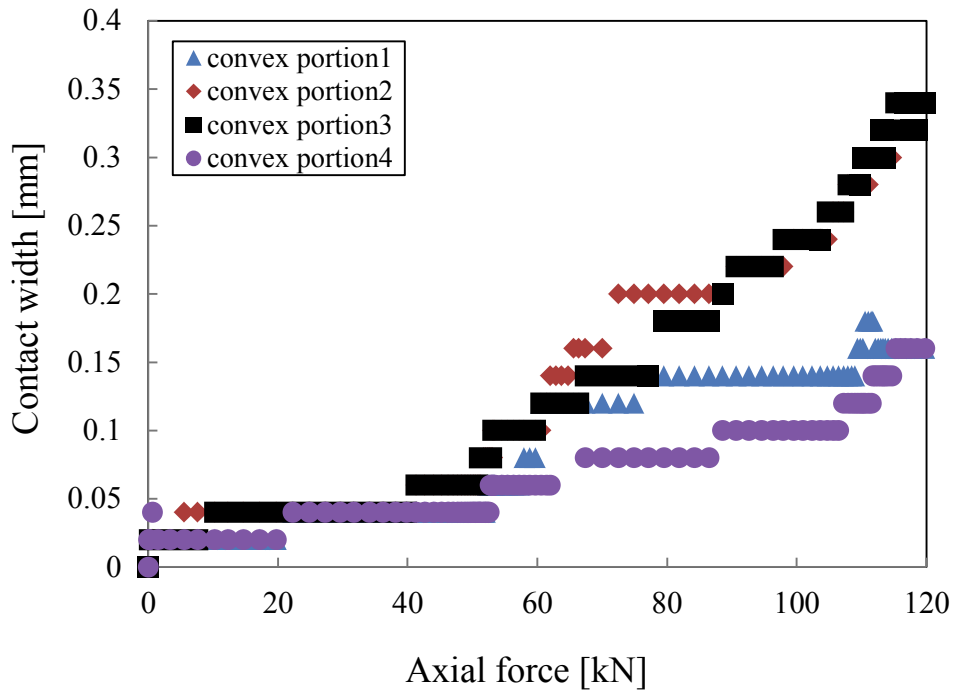
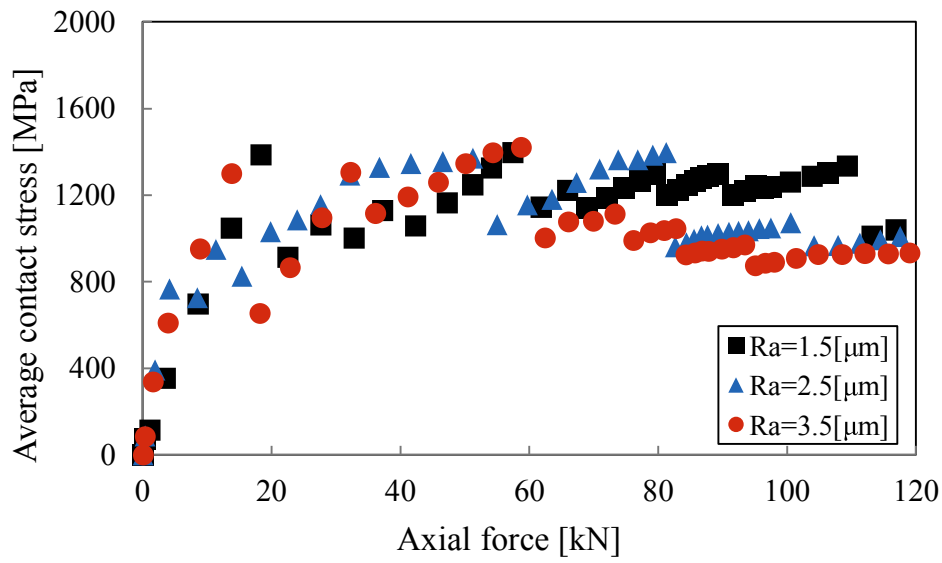


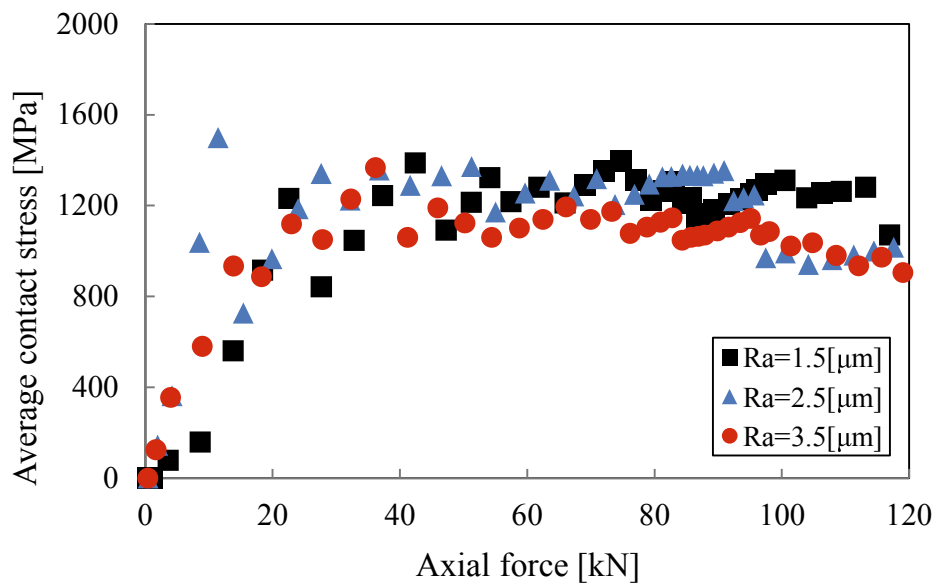
Fig. 4.10 Contact width in each axial force

4.2.1. Sinusoidal Model of Surface Roughness

Fig. 4.11 shows the simulation sinusoidal model result for the upper and lower contacts of a gasket in the 400-MPa mode for the average contact stress. The contact stress for a gasket in contact with flanges having surface roughness values of 1.5, 2.5, and 3.5 μm was similar for both the upper and the lower contacts. But, the flange having surface roughness 1.5 μm showed the highest propensity than 2.5 μm and 3.5 μm . This figure shows that the average contact stress increases significantly with the axial force in the initial axial force. The average contact stress for flange having surface roughness 3.5 μm was lowest than others.

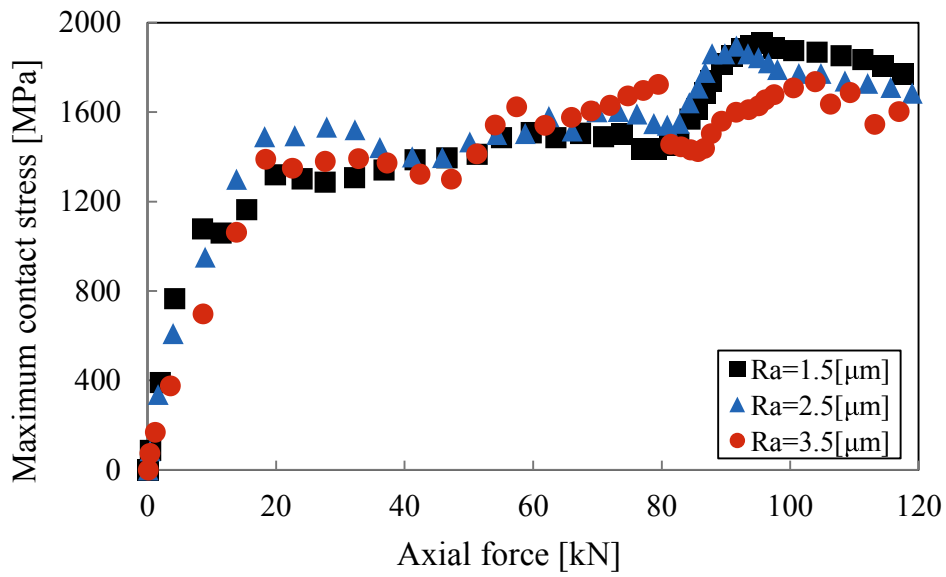


(a) Upper contact

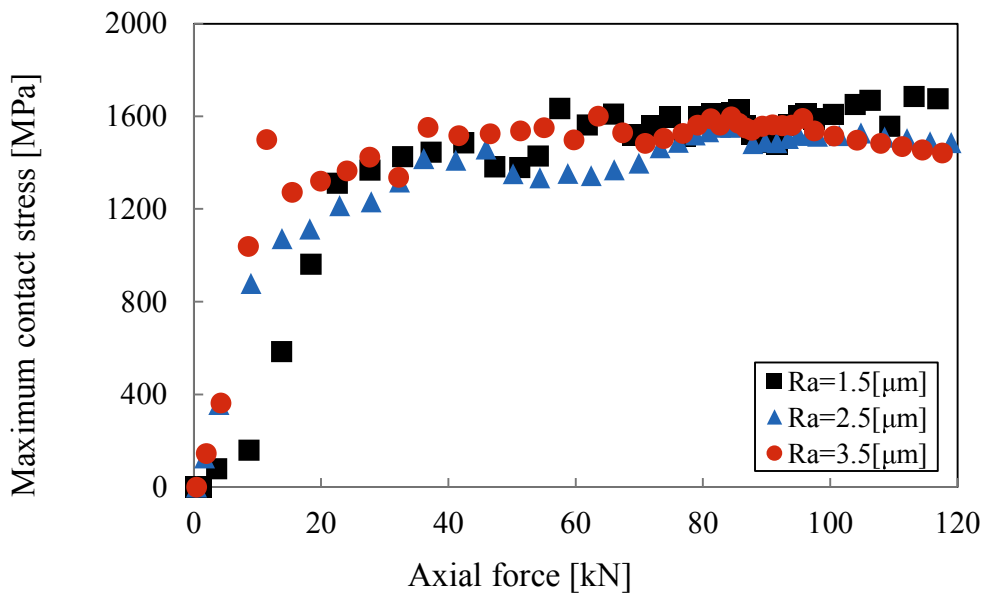


(b) Lower contact

Fig. 4.11 Average contact stress for gasket in 400-MPa mode



(a) Upper contact

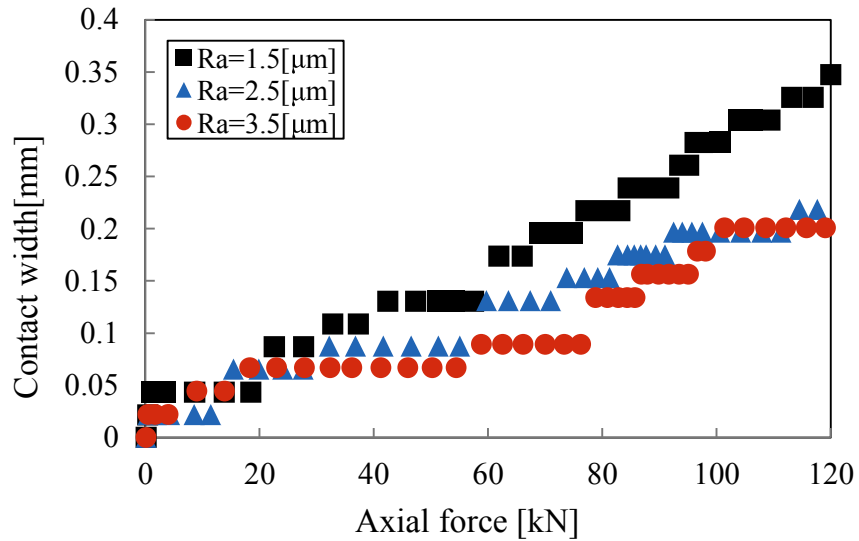


(b) Lower contact

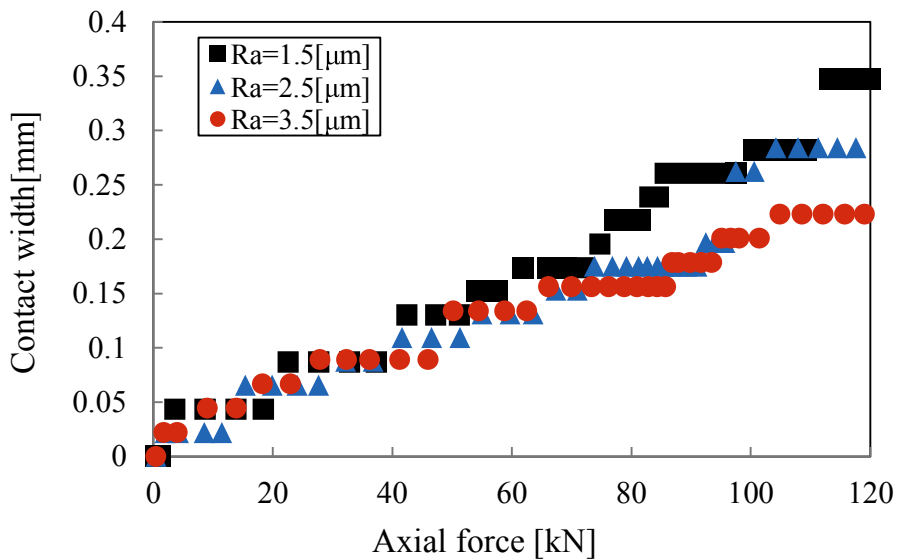
Fig. 4.12 Maximum contact stress for gasket in 400-MPa mode

Fig. 4.12 shows the simulation result for the upper and lower contacts of a gasket in the 400-MPa mode for the maximum contact stress. The contact stress for a gasket in

contact with flanges having surface roughness values of 1.5, 2.5, and 3.5 μm was similar for both the upper and the lower contacts. But, the flange having surface roughness 1.5 μm showed the highest propensity than 2.5 μm and 3.5 μm . This figure shows that the maximum contact stress increases significantly with the axial force.



(a) Upper contact



(b) Lower contact

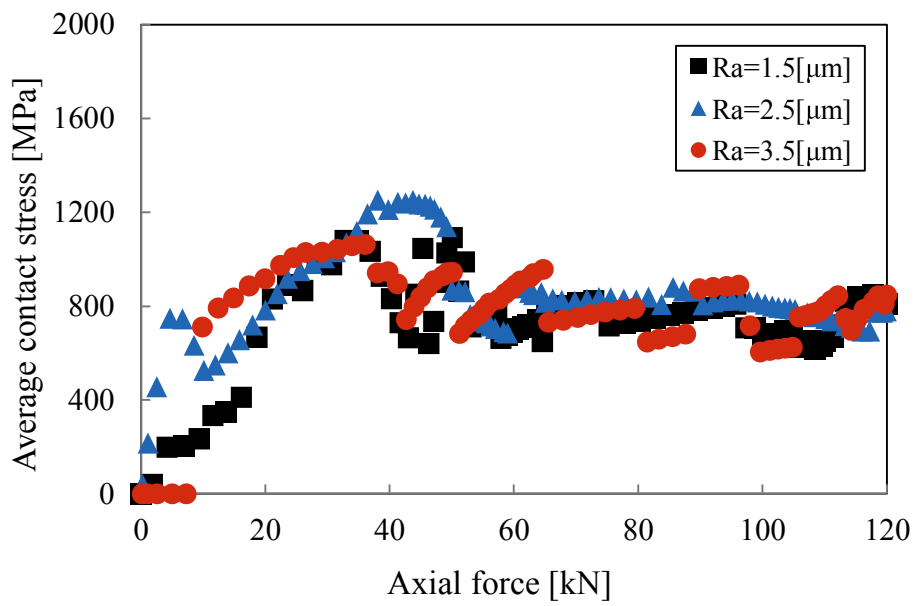
Fig. 4.13 Contact width for gasket in 400-MPa mode

Fig. 4.13 shows the simulation result for upper and lower contacts width of the gasket in the 400-MPa mode for the contact width. This figure shows that the contact width increases significantly with the axial force. There is no dent occurs in convex portion for all surface roughness. The contact width in a gasket in contact with a flange having a surface roughness of 3.5 and 1.5 μm had the lowest and the highest slope, respectively.

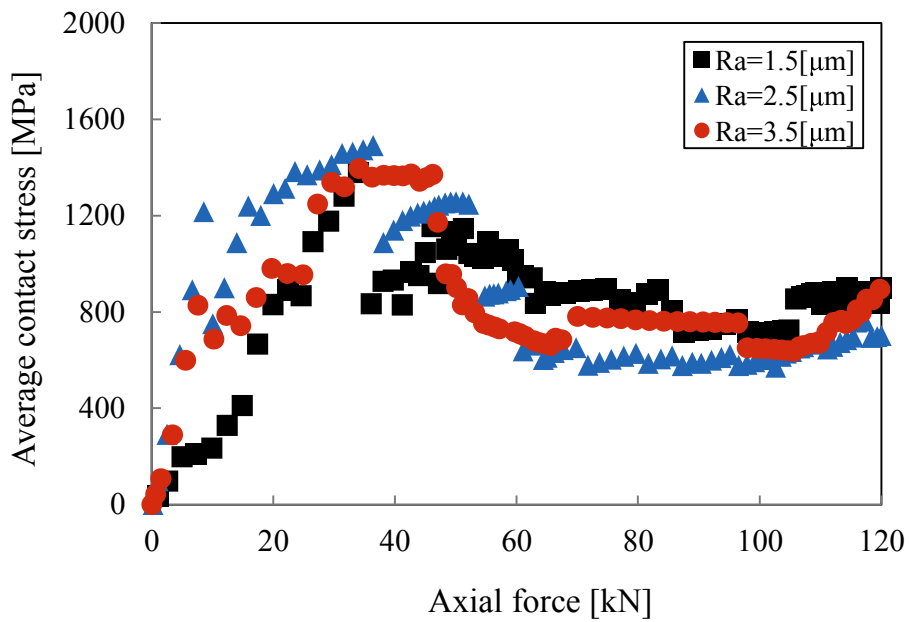
Fig. 4.14 shows the simulation results for the upper and lower contact for a gasket in 0-MPa mode for the average contact stress. For both contacts, the average contact stress between the gasket and flanges having surface roughness value of 1.5, 2.5, and 3.5 μm were similar. But, the flange having surface roughness 1.5 μm showed the highest propensity than 2.5 μm and 3.5 μm . The average contact stress for flange having surface roughness 3.5 μm was lowest than others. Start for axial force 60KN, the elastic stress distribution in the region between convex portion produced the spring effect that it reduces the value of contact stress, and then the graph of the contact stress tend to go down.

Fig. 4.15 shows the simulation results for the upper and lower contact for a gasket in 0-MPa mode for the maximum contact stress. For both contact, a flange having a surface roughness of 3.5 μm showed the lowest contact stress. The highest slope of the maximum contact stress observed for a flange having a surface roughness of 1.5 μm .

Fig. 4.16 shows the simulation result for the upper and lower contacts for a gasket in 0-MPa mode for the contact width. This figure shows that the contact width increases with the axial force. The contact width in a gasket in contact with a flange having surface roughness 3.5 μm and 1.5 μm had the lowest and highest slope, respectively.

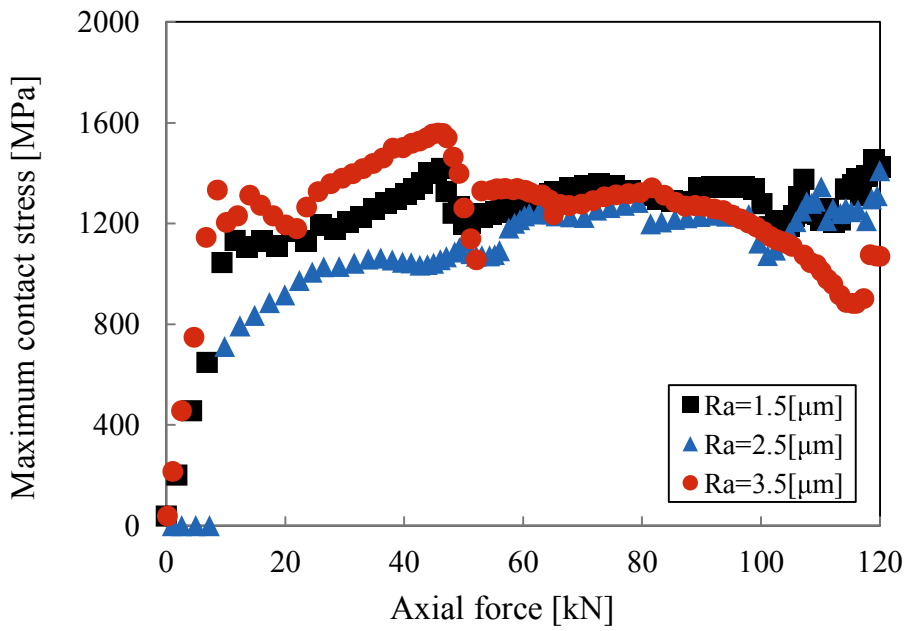


(a) Upper contact

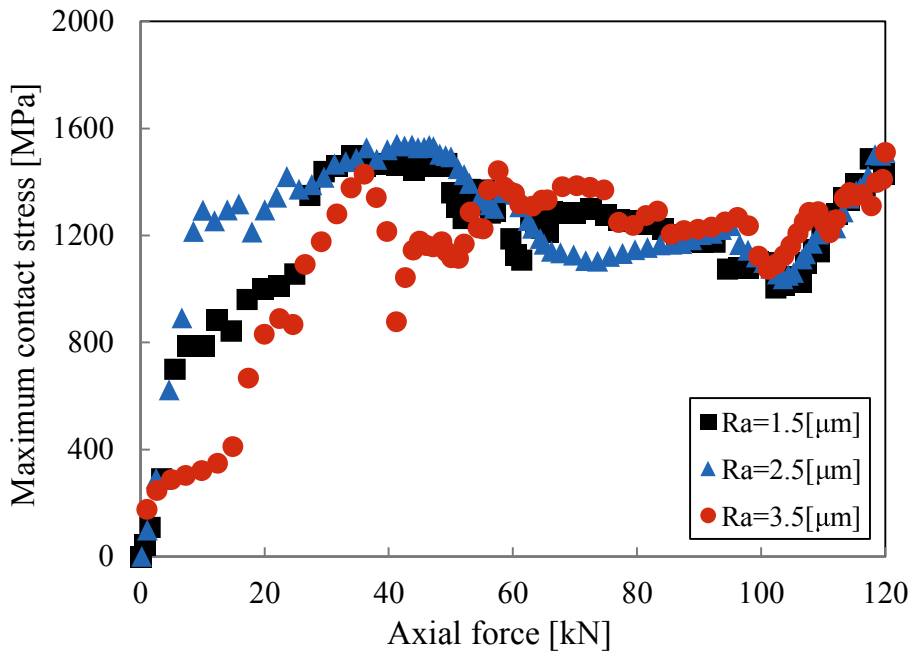


(b) Lower contact

Fig. 4.14 Average contact stress for gasket in 0-MPa mode

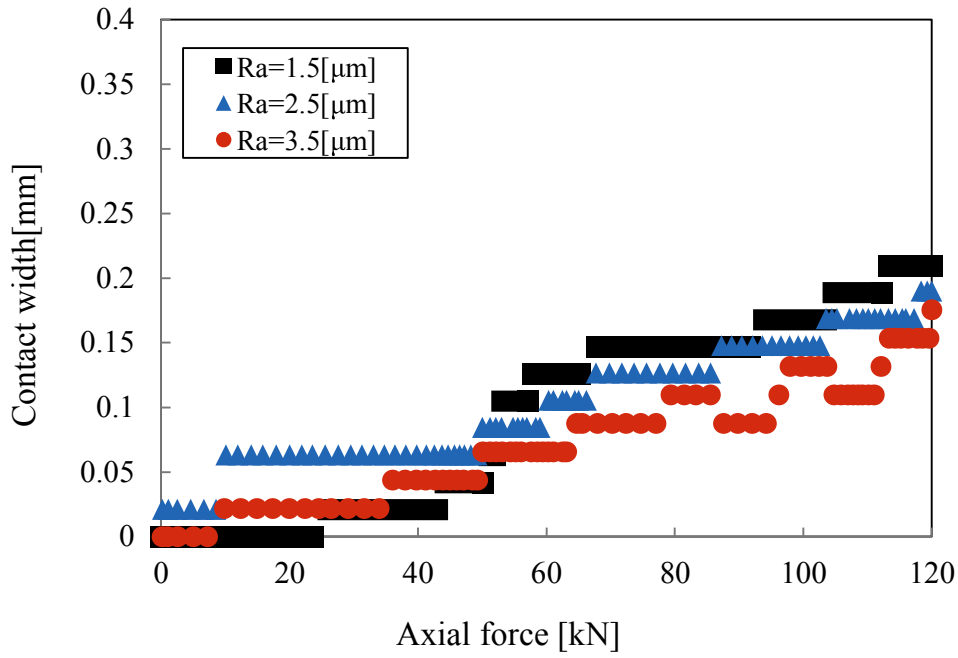


(a) Upper contact

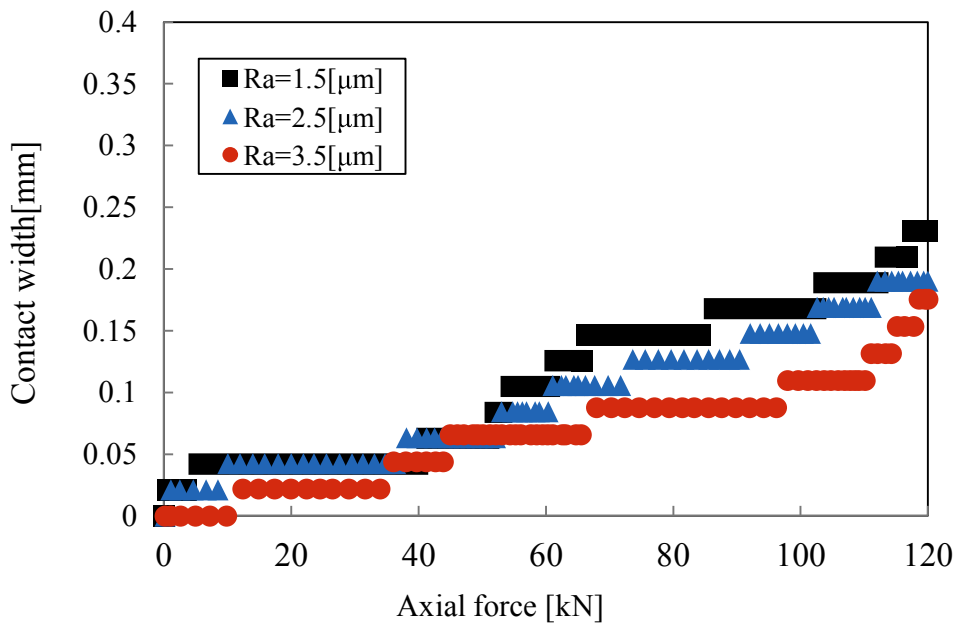


(b) Lower contact

Fig. 4.15 Maximum contact stress for gasket in 0-MPa mode



(a) Upper contact



(b) Lower contact

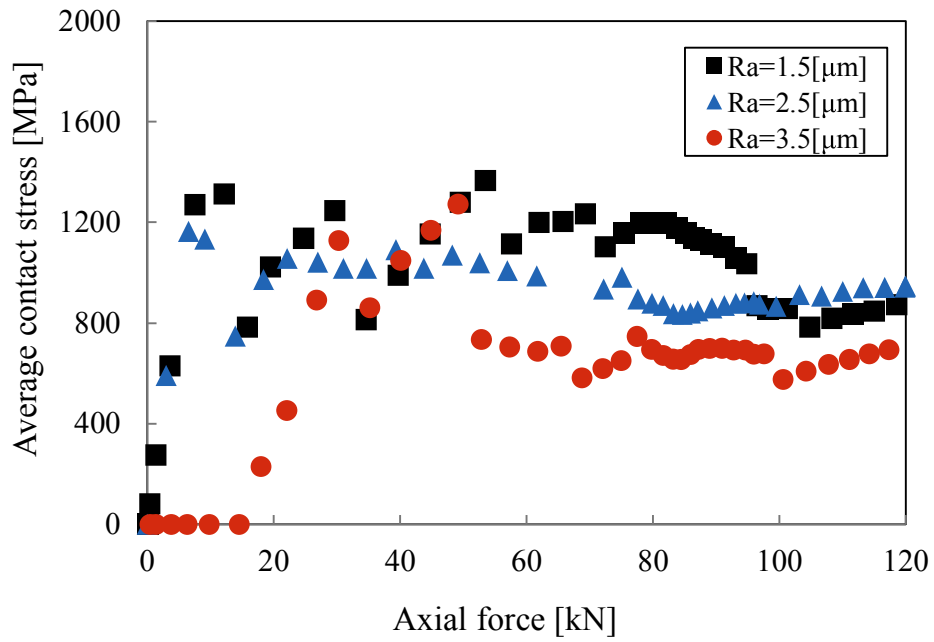
Fig. 4.16 Contact width for gasket in 0-MPa mode

4.2.2. Real Model of Surface Roughness

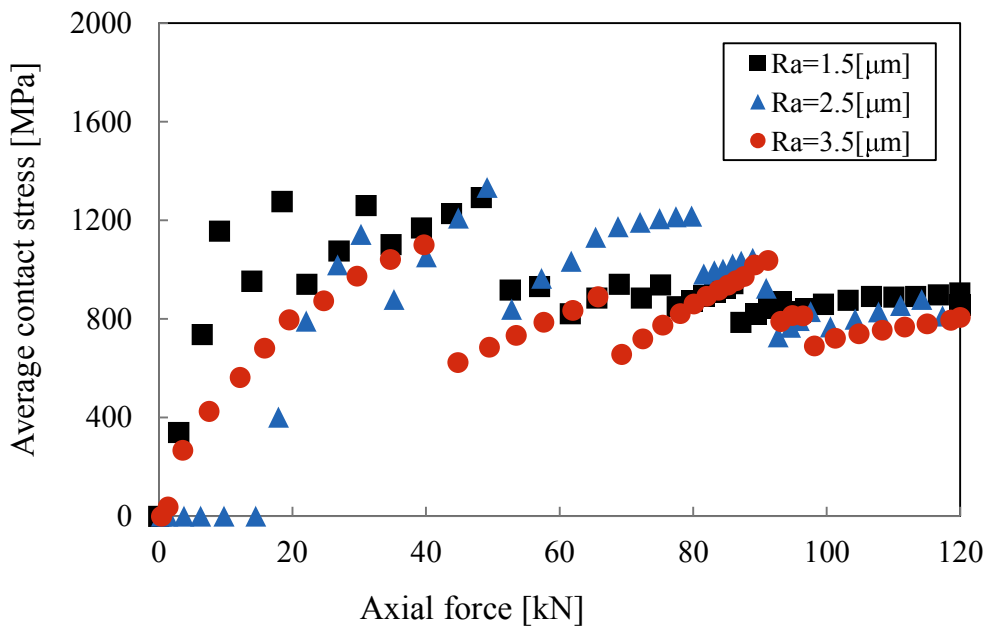
Fig. 4.17 shows the simulation result for the upper and lower contacts of a gasket in the 400-MPa mode for the average contact stress. The contact stress for a gasket in contact with flanges having surface roughness values of 1.5, 2.5, and 3.5 μm was similar for both the upper and the lower contacts. But, the flange having surface roughness 1.5 μm showed the highest propensity than 2.5 μm and 3.5 μm . This figure shows that the average contact stress increases significantly with the axial force. The average contact stress for flange having surface roughness 3.5 μm was lowest than others. To maintain seal integrity, the effective compressive pressure on the gasket must be greater than the internal pressure by some multiple. Usually, the value of the internal pressure in the piping system is around 10MPa. Figure 4.17 denoted that the contact stress value was around 800MPa; therefore, it is larger enough to reduce the internal pressure effect, which is 80 times internal pressure.

Fig. 4.18 shows the simulation result for the upper and lower contacts of a gasket in the 400-MPa mode for the maximum contact stress. The contact stress for a gasket in contact with flanges having surface roughness values of 1.5, 2.5, and 3.5 μm was similar for both the upper and the lower contacts. But, the flange having surface roughness 1.5 μm showed the highest propensity than 2.5 μm and 3.5 μm . This figure shows that the maximum contact stress increases significantly with the axial force.

Fig. 4.19 shows the simulation result for upper and lower contacts width of the gasket in the 400-MPa mode for the contact width. This figure shows that the contact width increases with the axial force. The contact width in a gasket in contact with a flange having a surface roughness of 3.5 and 1.5 μm had the lowest and the highest slope, respectively. The slope of relationship between axial force and contact width shows increase significantly start from the axial force 60 KN-80 KN, both for upper and lower contact. In this range, the value of contact stress is elastic distribution, and the phenomena still fulfill the elastic stress condition. However, for values of the axial force from 80 KN to 120 KN, the contact width was still increase. In this range, the distribution of stress is mixing the elastic and the plastic region.

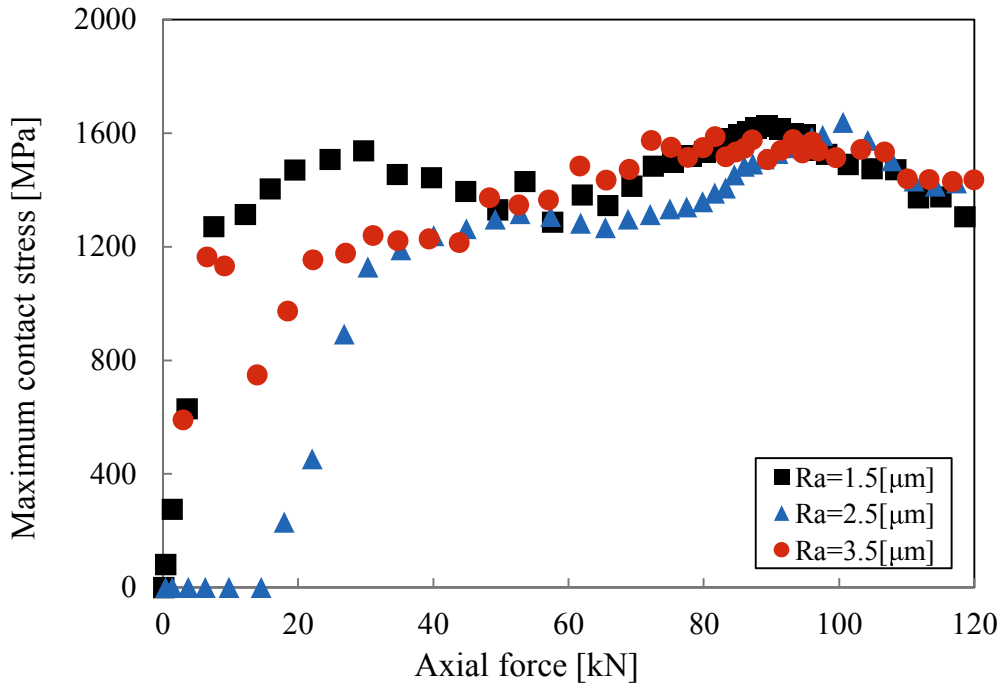


(a) Upper contact

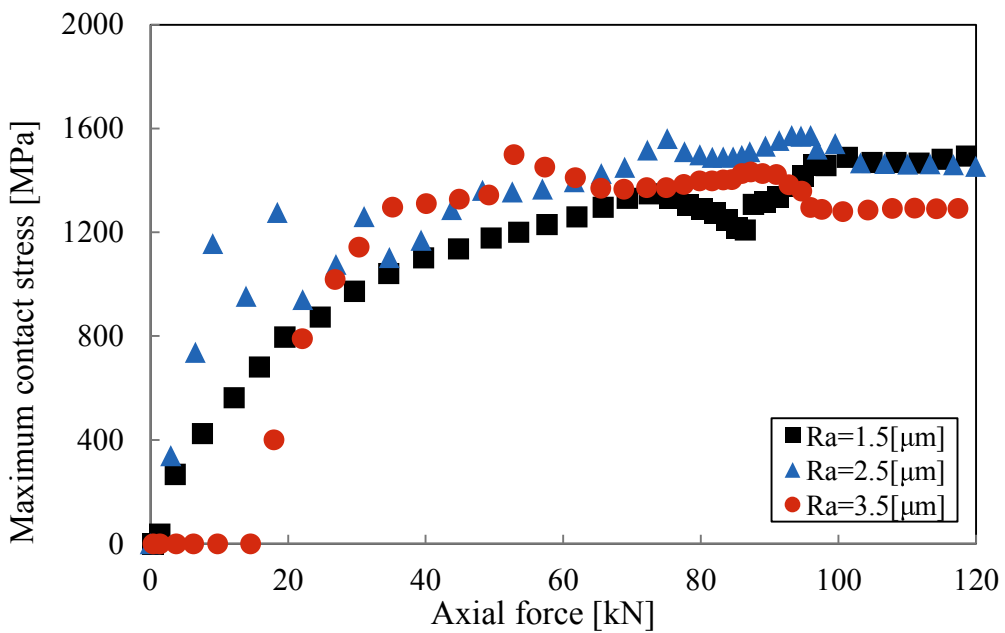


(b) Lower contact

Fig. 4.17 Average contact stress for gasket in 400-MPa mode

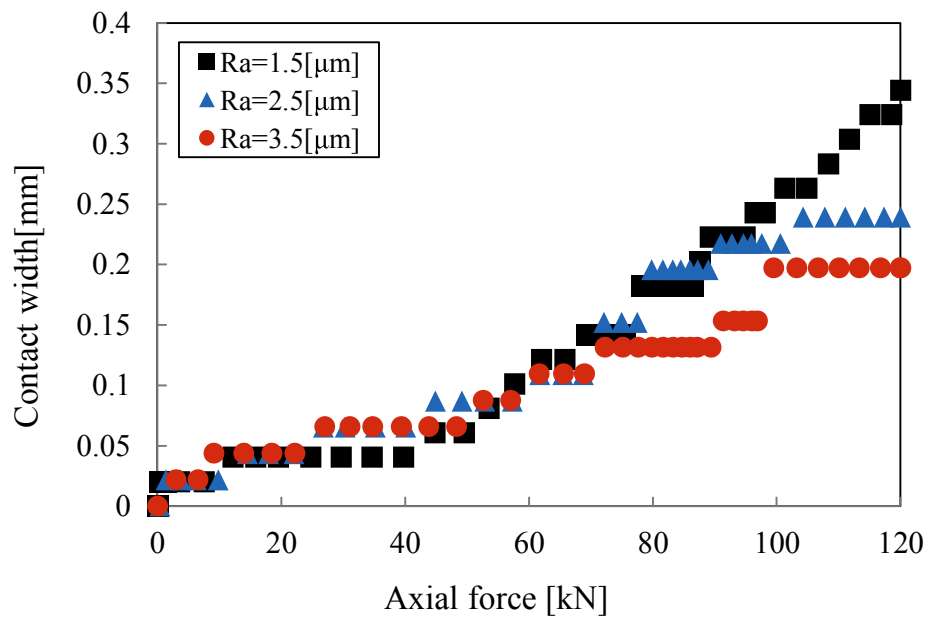


(a) Upper contact

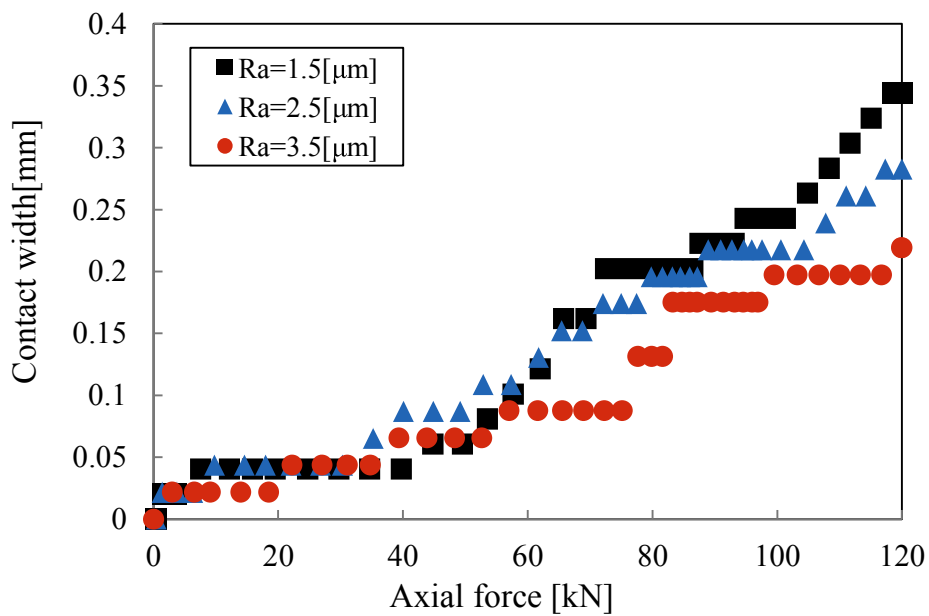


(b) Lower contact

Fig. 4.18 Maximum contact stress for gasket in 400-MPa mode



(a) Upper contact

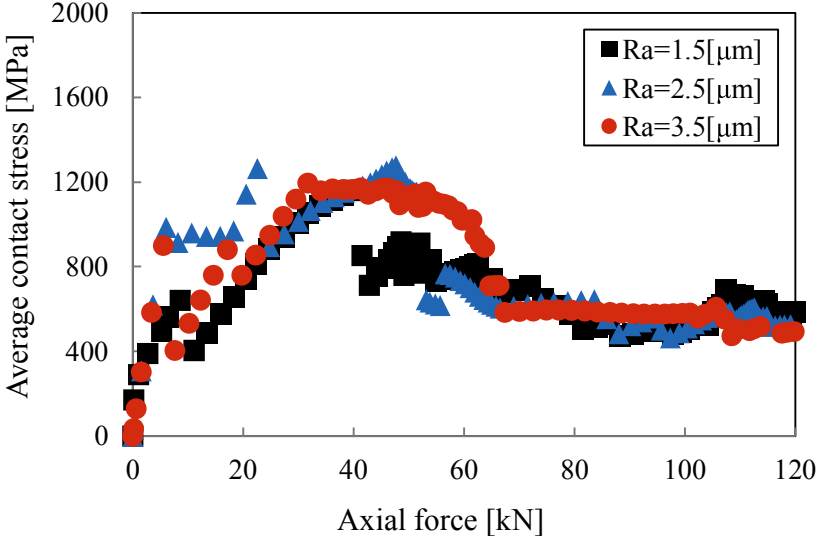


(b) Lower contact

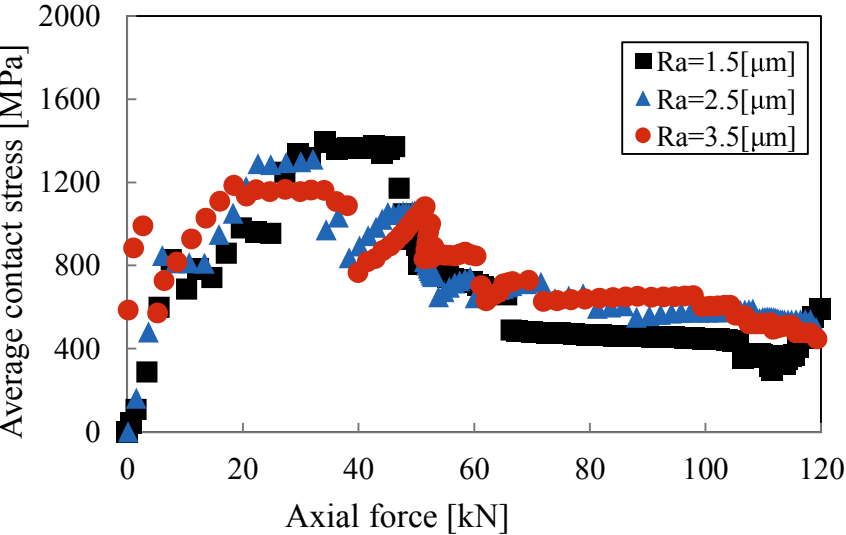
Fig. 4.19 Contact width for gasket in 400-MPa mode

Fig. 4.20 shows the simulation results for the upper and lower contact for a gasket in

0-MPa mode for the average contact stress. For both contacts, the average contact stress between the gasket and flanges having surface roughness value of 1.5, 2.5, and 3.5 μm were similar. Figure 4.20 denoted that the contact stress value was around 400MPa; therefore, it is larger enough to reduce the internal pressure effect, which is 40 times internal pressure.



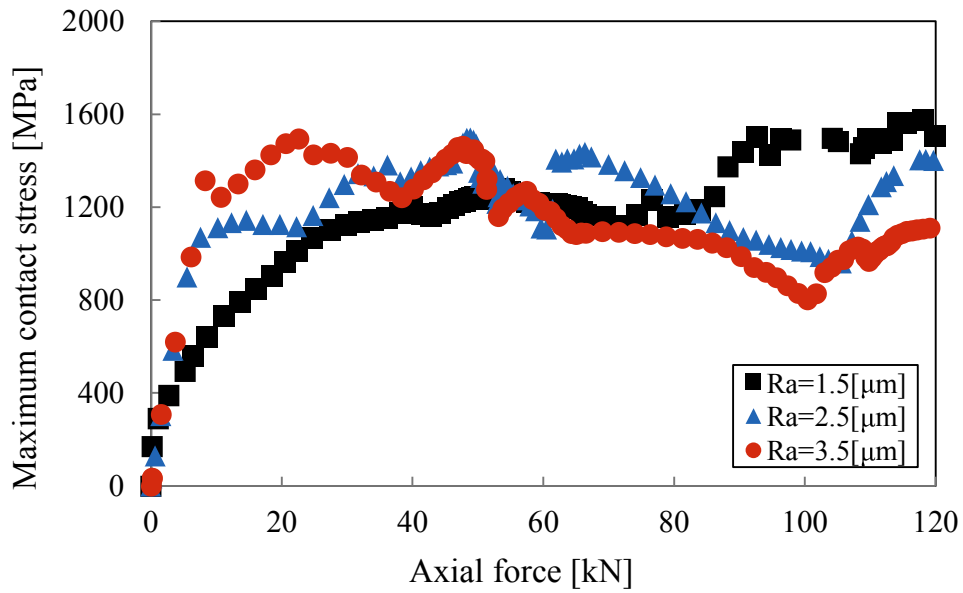
(a) Upper contact



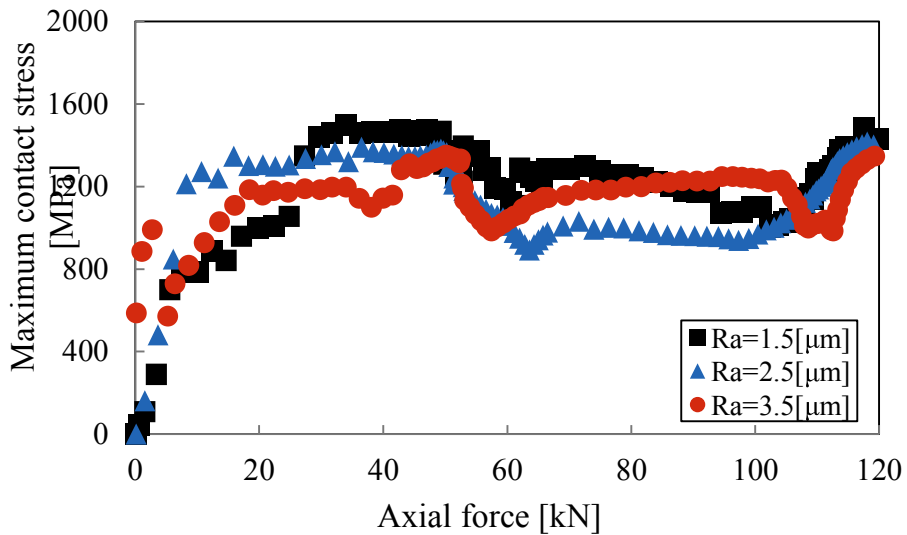
(b) Lower contact

Fig. 4.20 Average contact stress for gasket in 0-MPa mode

Fig. 4.21 shows the simulation results for the upper and lower contact for a gasket in 0-MPa mode for the maximum contact stress. For both contact, a flange having a surface roughness of $3.5\mu\text{m}$ showed the lowest contact stress. The highest slope of the maximum contact stress observed for a flange having a surface roughness of $1.5\mu\text{m}$.



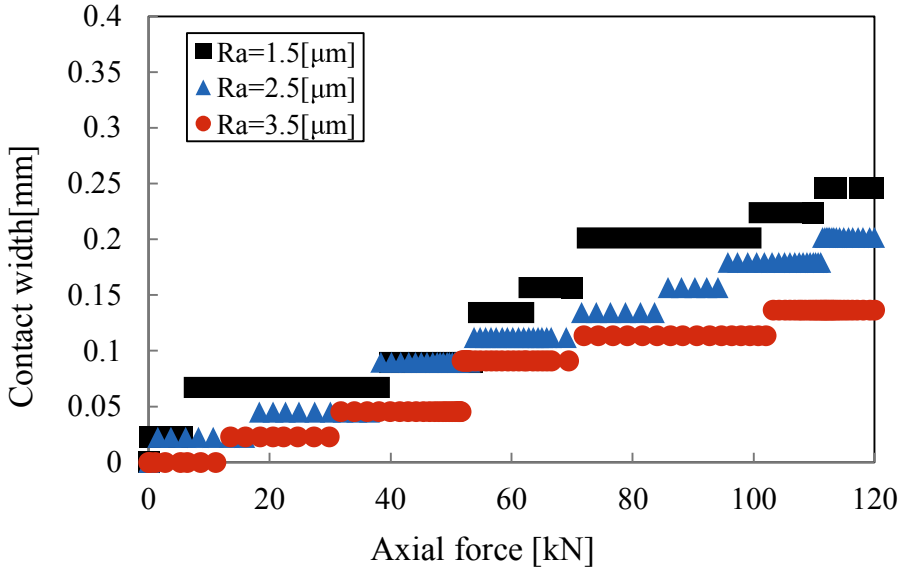
(a) Upper contact



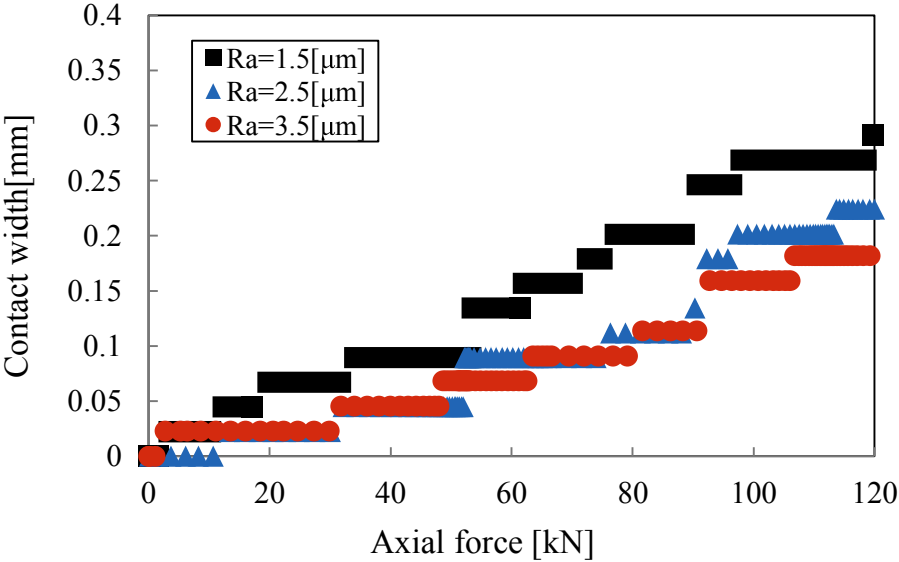
(b) Lower contact

Fig. 4.21 Maximum contact stress for gasket in 0-MPa mode

Fig. 4.22 shows the simulation result for the upper and lower contacts for a gasket in 0-MPa mode for the contact width. This figure shows that the contact width increases with the axial force. The contact width in a gasket in contact with a flange having surface roughness $3.5\mu\text{m}$ and $1.5\mu\text{m}$ had the lowest and highest slope, respectively.



(a) Upper contact



(b) Lower contact

Fig. 4.22 Contact width for gasket in 0-MPa mode

The simulation results showed that the average contact stress for the gasket in 0-MPa mode was lower than for a gasket in 400-MPa mode. The contact width for the former gasket was lower than that for the latter one. Consequently, the former gasket is superior to the later one.

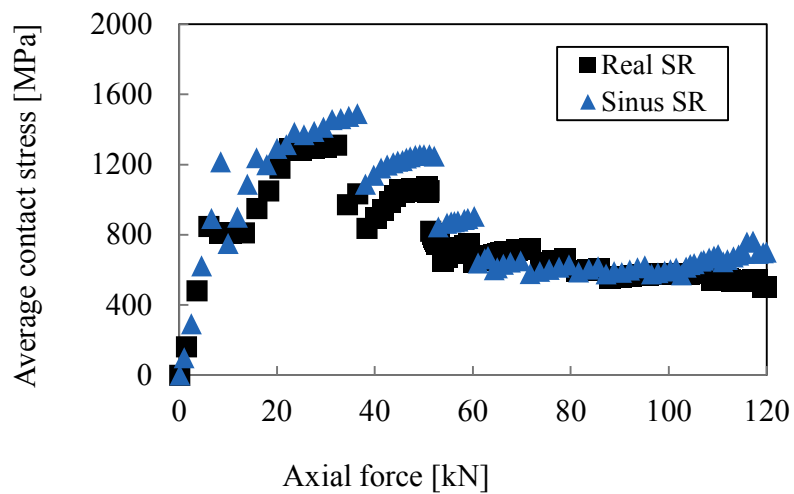


Fig. 4.23 Comparison real and sinusoidal surface roughness model of average contact stress for gasket 0-MPa mode

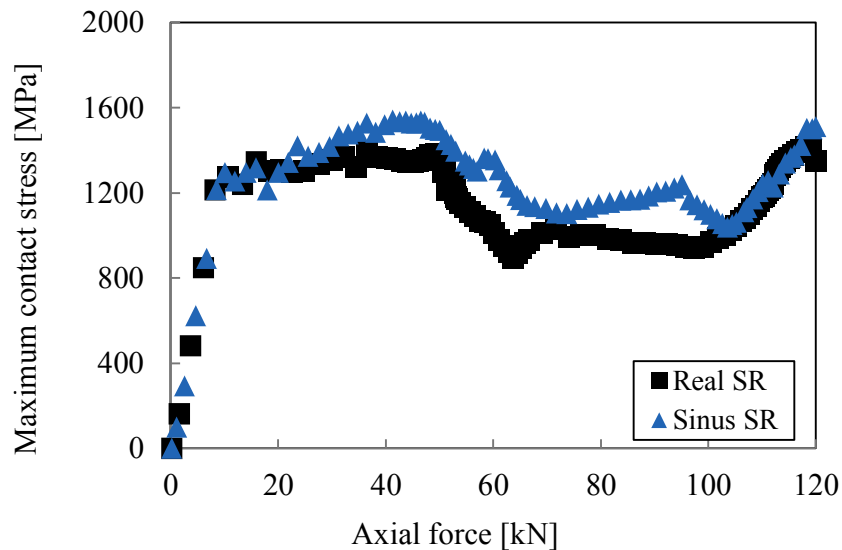


Fig. 4.24 Comparison real and sinusoidal surface roughness model of maximum contact stress for gasket 0-MPa mode

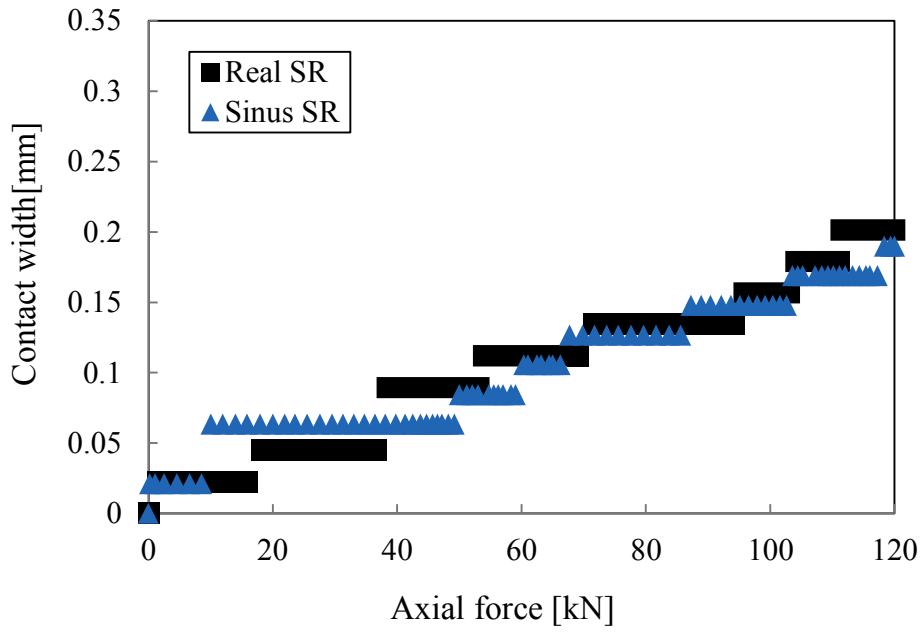


Fig. 4.25 Comparison real and sinusoidal surface roughness model of contact width for gasket 0-MPa mode

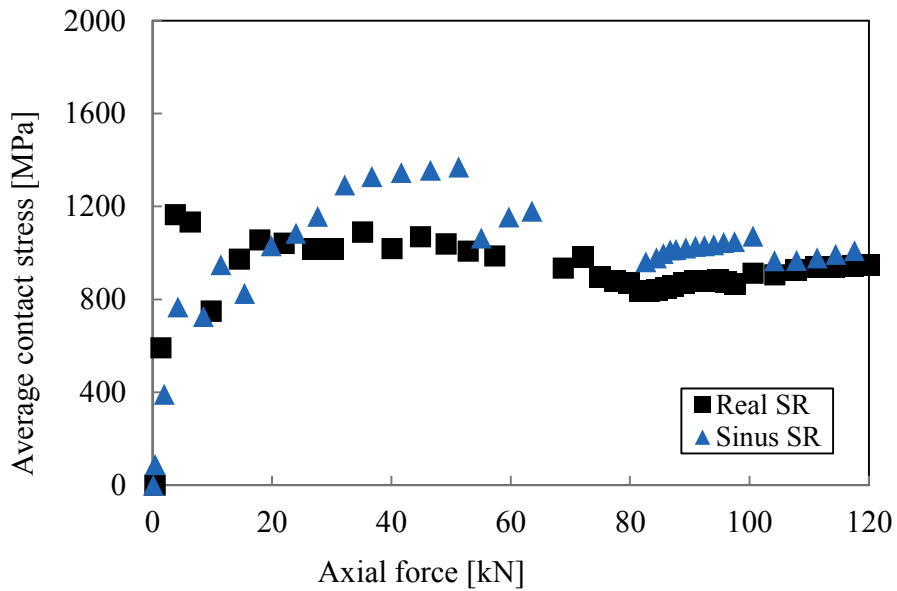


Fig. 4.26 Comparison real and sinusoidal surface roughness model of average contact stress for gasket 400-MPa mode

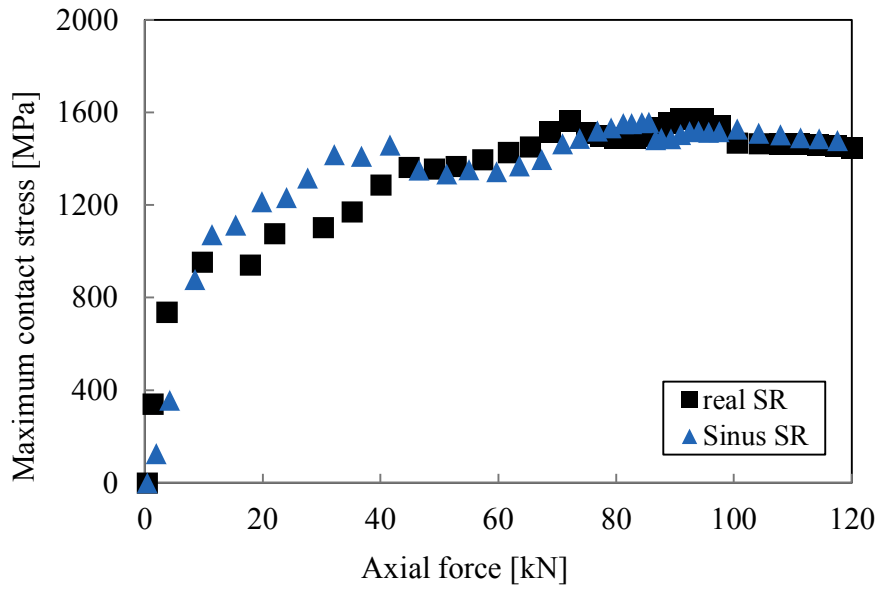


Fig. 4.27 Comparison real and sinusoidal surface roughness model of maximum contact stress for gasket 400-MPa mode

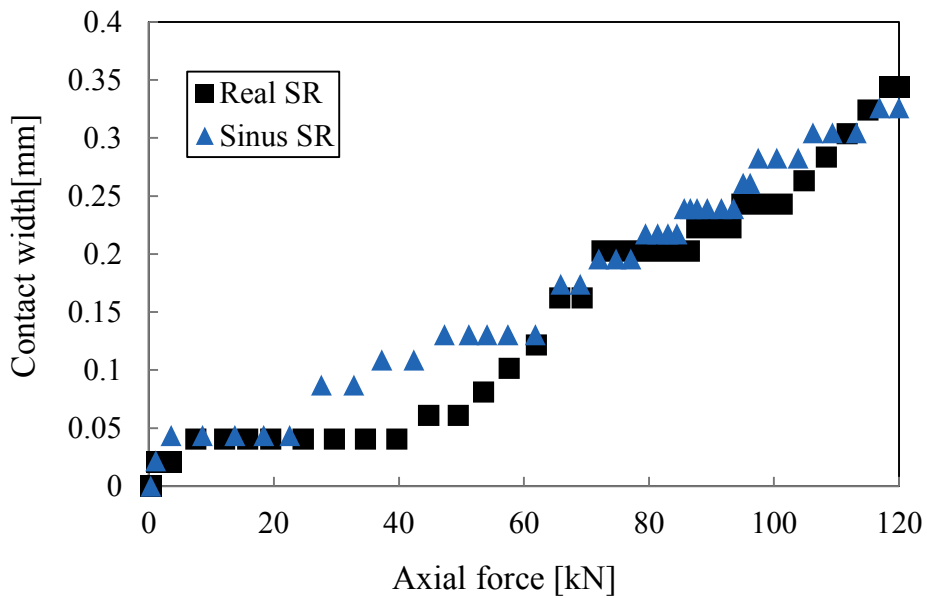


Fig. 4.28 Comparison real and sinusoidal surface roughness model of contact width for gasket 400-MPa mode

The simulation result of average contact stress, maximum contact stress and contact width for real surface roughness model and sinusoidal surface roughness model shows a similar, see Fig. 4.23-4.28. Of course, the real surface roughness model is better than the sinusoidal surface roughness model because the sinusoidal surface roughness model just approach model for the surface roughness. But based the result above, we can be modeled the surface roughness using the sinusoidal model.

4.3 Leak Quantity Measurement

To evaluate the axial force and leak quantity, the leakage quantity was measured based on the measurement of that of a helium flow. A schematic diagram of the helium leakage measurement device explained in section 3.2.3. The helium flow leakage quantity was quantitatively measured to evaluate the surface roughness of the flange. The highest detection ability in the helium leakage measurement was chosen based on the JIS Z2330 [46] and JIS Z2331 [47] standard. The measurement method employed is called the vacuum method.

In this study, two types of gaskets—elastic (0-MPa mode) and plastic (400-MPa mode) design [43]—and three flange surface roughness levels—1.5, 2.5, and 3.5 μm —were investigated.

In the previous study [15], a qualitative explanation obtained using water pressure test transformed into a quantitative value using a helium leak test. The quantitative decision criterion for preventing leakage determined under the condition that the helium leakage quantity was below $1.0 \times 10^{-6} \text{ Pa}\cdot\text{m}^3/\text{s}$ and it observed that the leakage did not occur in the water pressure test.

Fig. 4.29 shows the result of the helium leakage test for a gasket in 400-MPa mode. A gasket in contact with a flange of all roughness levels did not show leakage for a certain axial force. For a low axial force, changes in surface roughness caused significant changes in the leakage; the same did not observe for high axial force. Flange having surface roughness 1.5 and 2.5 μm did not leakage for the axial force start from 80kN, but flange having surface roughness 3.5 μm did not leakage for the axial force start from 100kN. Based

from the result we can use the flange having surface roughness 3.5, 2.5 and 1.5 μm contact with the gasket 400-MPa mode.

Fig. 4.30 shows the result of the helium leakage test for a gasket in 0-MPa mode. A gasket in contact with a flange having a surface roughness of 3.5 μm showed leakage at all axial force, making this roughness level an unsuitable choice for this gasket. On the other hand, a gasket in contact with a flange having a surface roughness of 1.5 and 2.5 μm did not show leakage for a certain axial force. A flange having surface roughness 1.5 μm contact a gasket 0MPa model did not leakage for the axial force start from 80kN but the flange having surface roughness 2.5 μm did not leakage for the axial force start from 100kN. For a low axial force, changes in surface roughness caused significant changes in the leakage; the same did not observe for high axial force.

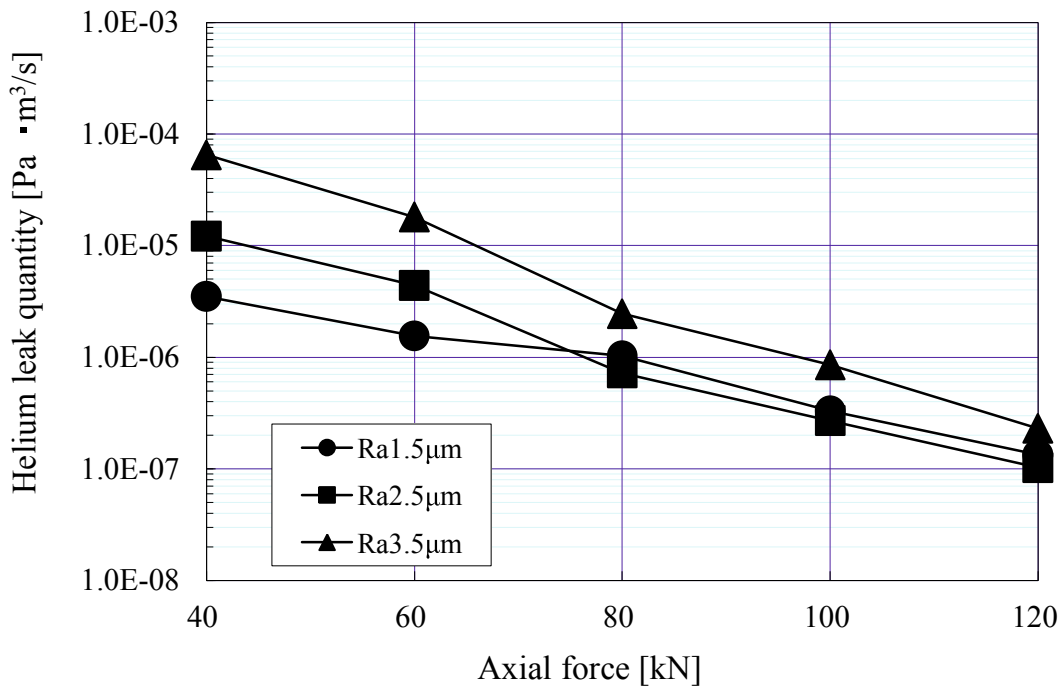


Fig. 4.29 Leakage measurement result for gasket in 400-MPa mode

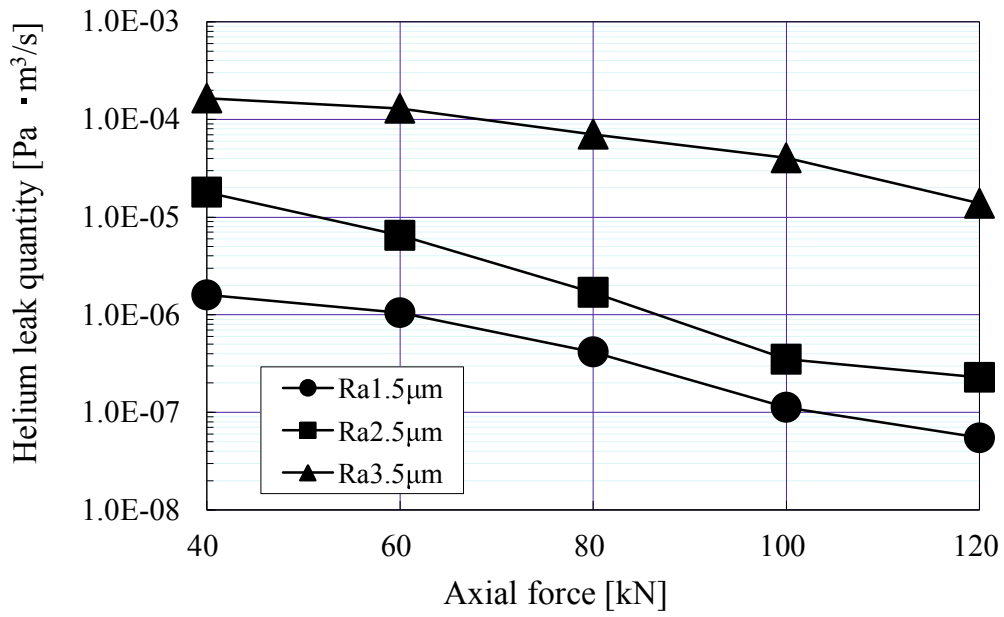


Fig. 4.30 Leakage measurement result for 0-MPa gasket mode

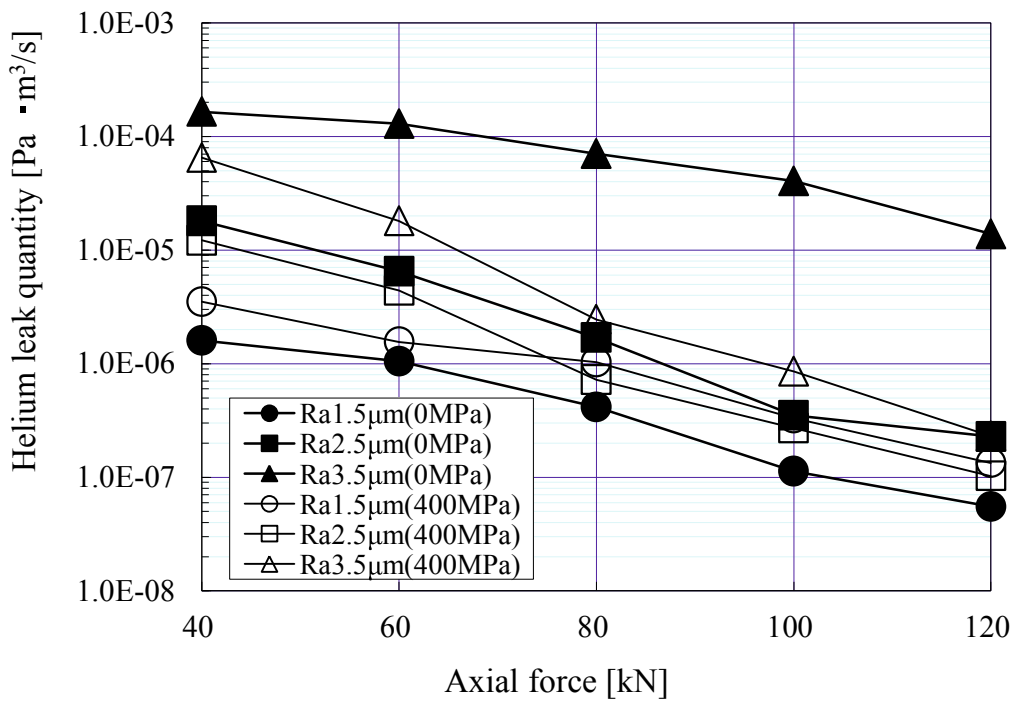


Fig. 4.31 Leakage measurement results for gaskets in 0-MPa and 400-MPa modes

Fig. 4.31 shows the relationship between axial force and the helium leakage quantity for gaskets with two different modes. For a low axial force, changes in surface roughness caused significant changes in the leakage; the same did not observe for high axial force. A gasket in 400-MPa mode is superior to one in 0-MPa mode especially for surface roughness $2.5\mu\text{m}$ and $3.5\mu\text{m}$. The slope changes for the former gasket are greater than those for the latter one.

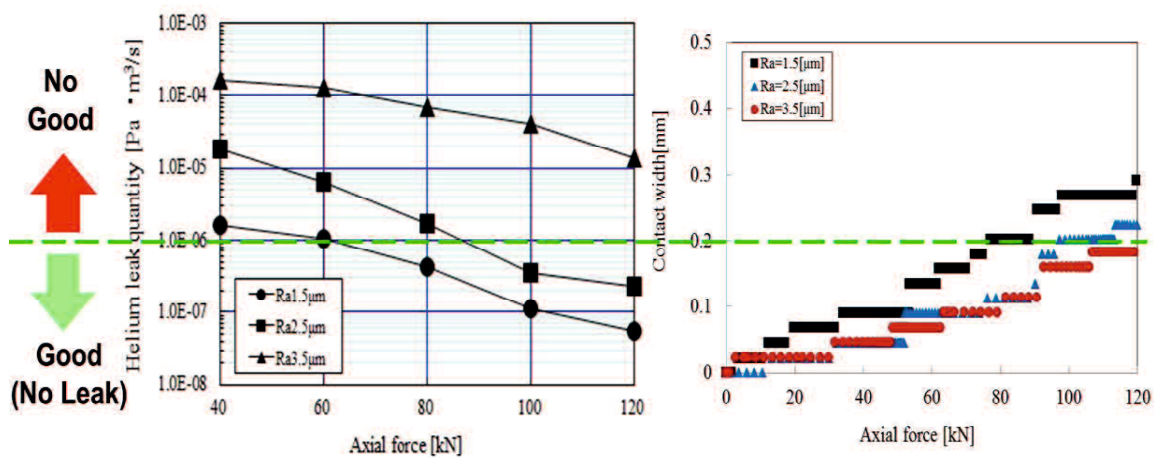


Fig. 4.32 Helium leak measurement related to contact width for gasket 0-MPa mode

Fig. 4.32 shows the helium leak measurement related to contact width for gasket 0-MPa mode. In the previous study [14], the helium leak rate $1.0\text{E-}06 \text{ Pa}\cdot\text{m}^3/\text{s}$, it was observed that the leakage by water pressure test did not occur. Gasket contact with flange having surface roughness $3.5\mu\text{m}$ was leak for all axial force value. Gasket contact flange having surface roughness $2.5\mu\text{m}$ the leakage did not occur when the axial force 100 KN. In that time, the real contact width for simulation result is 0.20 mm. Gasket contact flange having surface roughness $1.5\mu\text{m}$ the leakage did not occur when the axial force 80 KN. In that time, the real contact width for simulation result is 0.20 mm.

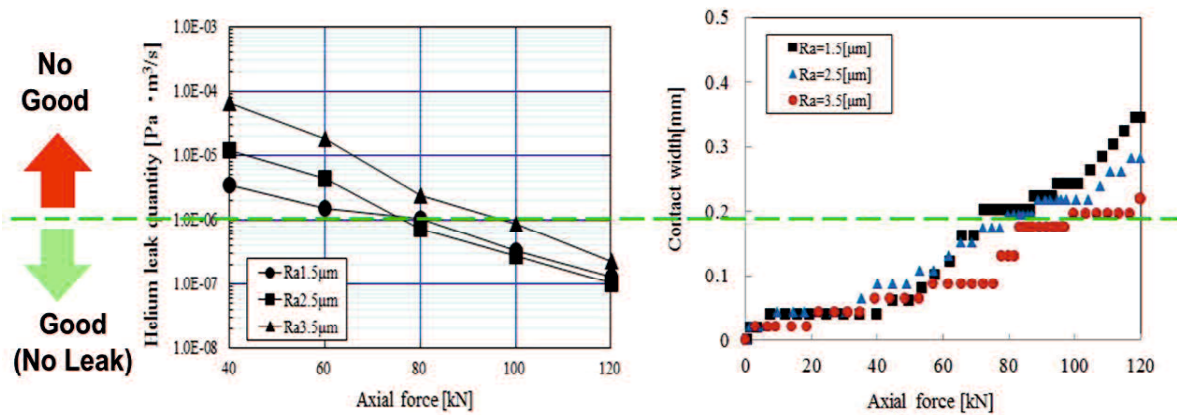


Fig. 4.33 Helium leak measurement related to contact width for gasket 400-MPa mode

Fig. 4.33 shows the helium leak measurement related to contact width for gasket 400-MPa mode. From the previous study [14], the helium leak rate $1.0\text{E-}06 \text{ Pa}\cdot\text{m}^3/\text{s}$, it was observed that the leakage by water pressure test did not occur. Gasket contact with flange having surface roughness $3.5 \mu\text{m}$ the leakage did not occur when the axial force 100 kN. In that time, the real contact width for simulation result is 0.195 mm. Gasket contact flange having surface roughness $2.5 \mu\text{m}$ the leakage did not occur when the axial force 80 kN. In that time, the real contact width for simulation result is 0.195 mm. Gasket contact flange having surface roughness $1.5 \mu\text{m}$ the leakage did not occur when the axial force 80 kN. In that time, the real contact width for simulation result is 0.20 mm.

Small changes were observed in the surface roughness after the experiment completed. Furthermore, the flange was smoother than before after use. Both of these observations are attributable to small deformations that occur during the experiment. Fig. 4.34 shows the changes in surface roughness after the experiment.

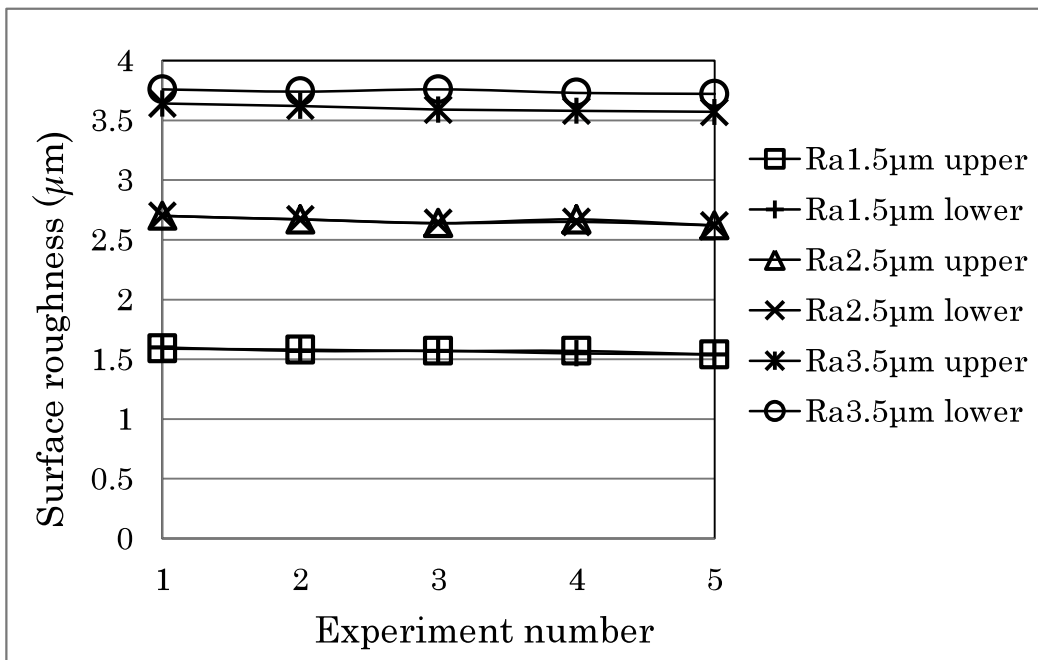


Fig. 4.34 Changes of surface roughness after experiment

A comparison of the simulation results and experimental data showed good agreement, suggesting that the theoretical analysis of the surface roughness is correct and will give an accurate prediction. In theory, helium leakage will decrease with an increase in the contact stress and contact width. The slope of the force per unit length for a gasket in 400-MPa mode is higher than that for a gasket in 0-MPa mode. Furthermore, the helium leakage test result suggests that the gasket in 400-MPa mode is superior to that in 0-MPa mode.

4.4 Conclusion

This study investigates the helium leakage quantity for a flange with different surface roughness values through a simulation analysis using FEM and a leakage test. The following conclusions derived from this study:

1. Simulation results suggest that the average contact stress for a gasket in 0-MPa mode is lower than for one in 400-MPa mode. The contact width for the former gasket was lower than that for the latter one.

2. The average contact stress for a flange having surface roughness values of 1.5, 2.5, and 3.5 μm was similar. The contact width is a function of surface roughness of flange—it decreases when the surface roughness increases.
3. The helium leakage test shows that the gasket in 400-MPa mode shows better sealing performances than the gasket in 0-MPa mode.
4. For a gasket in 400-MPa mode in contact with the flange, leakage did not occur for all surface roughness value for a certain axial force.
5. For a gasket in 0-MPa mode in contact with the flange, leakage occurred for a surface roughness of 3.5 μm , but not for 2.5 and 1.5 μm , for a certain axial force. Leakage is a function of surface roughness—it increases with the surface roughness.
6. The leakage did not occur when real contact width is 0.195 mm.
7. For a low axial force, changes in surface roughness caused a significant change in the leakage; the same did not observe for high axial force.

CHAPTER V

CONTACT WIDTH ANALYSIS OF THE 25-A SIZE METAL GASKET BASED ON SURFACE ROUGHNESS

An important characteristic to consider in the development of new metal gasket is a function to prevent leakage depending on the surface roughness standard used. Leakage is a function of surface roughness [19] —it increases with the surface roughness. A smoother of surface roughness has a higher slope for contact width-axial force relationship. The higher slope suggests that the gasket and flange are pressed together strongly. Previous studies on the design of a new metal gasket used models that did not include the surface roughness effect. The main problem in this regard is the fact that a suitable surface roughness for which no leakage occurs did not yet well understood.

In this light, this study aims to determine the real contact width of a flange contact with the newly developed 25A-size metal gasket based on surface roughness. The contact width determined through a comparison between simulation and experimental results. The simulation investigates the real contact width according to the surface roughness of the flange. The experiment involves a microscope using a new metal gasket having different surface roughness levels to investigate a real contact width.

5.1 Contact Width Simulation Analysis

A simulation analysis was performed to describe the contact mechanism of the 25A-size metal gasket and the rough flange. By using FEM analysis, the relationship between the surface roughness parameter and contact width was determined. The gasket used in this study was manufactured using a mold press. It had beads along its circumference. When the gasket was tightened to the flange, the beads on both surfaces created an elastic effect. The flange was assumed to have a rough surface on both sides. The gasket was in contact with both the lower and the upper sides of the flange. The flange pressed the gasket along an axial direction. SUS304 was used as a gasket material and

flange material because of its effectiveness in a high-temperature and high-pressure environment. Its material properties were first determined through a tensile test carried out based on JIS Z2241 [40] —the nominal stress, modulus of elasticity (E), and tangent modulus was respectively found to be 398.83MPa, 210GPa, and 1900.53MPa.

A schematic of gasket tightening in consideration of the surface roughness at the flange and gasket contact area under analysis, where the gasket is shown to have corrugated shape and the flange, a flat shape is discussed in section 4.1. In this study, we analyze a flange having three different surface roughness values: 1.5, 2.5, and 3.5 μm . According to the explanation above, the surface roughness was modeled as a sinusoidal rough surface and real surface roughness. A flowchart of the various stages of the simulation of the gasket considering the surface roughness effect discussed in section 4.1. These stages were modeled using the MSC's MARC FEM analysis software. There were two types of gasket, which are 0-MPa mode and 400-MPa mode.

As a mentioned above, we measured two places of gasket, which are convex portion 2 and convex portion 3, because both convex portions were similar character and very influence for leakage process. Both of these convex portions have the higher contact stress and wider contact width compare with convex portion 1 and convex portion 4 [51].

Fig. 5.1 shows the real contact width for simulation result. When a contact width studied at low magnification its look, complete contact occurs between gasket and flange. When the magnification increased and smaller length scale roughness detected, it can be observed that only partial contact occurs at the asperities. In reality, a short distance cut-off always exists, e.g., the interatomic distance. In many cases, the local pressure in the contact regions at the asperities may become so high that the material yields plastically before reaching the atomic dimension. In these cases, the size of a real contact area will be determined mainly by the yield stress of the solid.

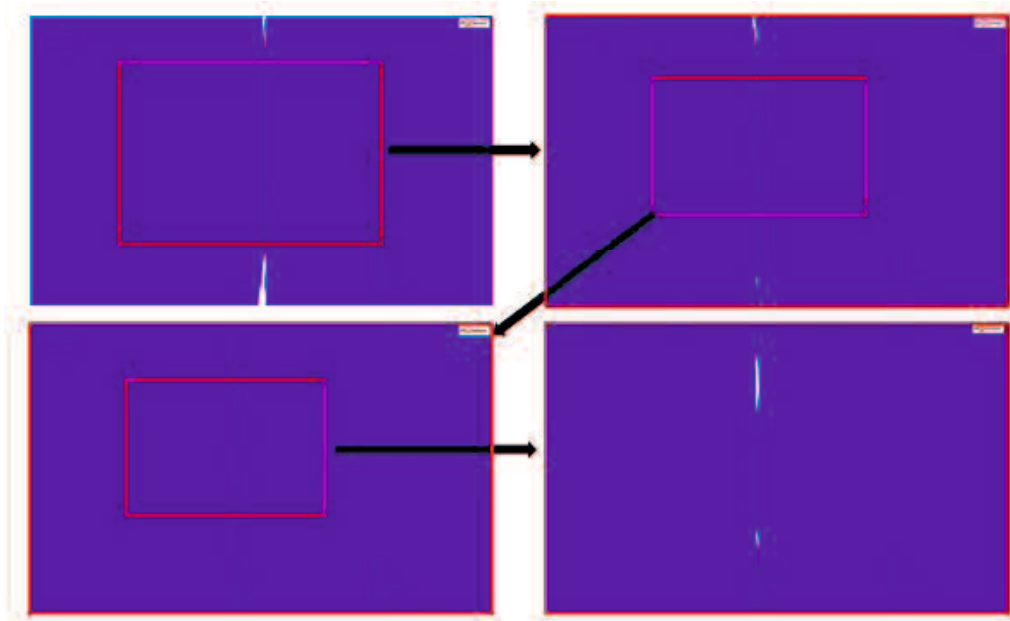


Fig. 5.1 Real contact width between gasket and flange

The real contact width can be modeled using contact stress value in a horizontal position. The contact stress value 0 is no contact condition, the contact stress value between 0-400 is elastic contact condition and the contact stress value up to 400 is plastic contact stress. The contact width is the number of nodes that contact with flange times element width. The width of an element in this simulation varied, because a meshing control based on the input number of an element for different surface roughness. The elastic contact stress can't deform the gasket.

Fig. 5.2 shows the contact stress for gasket 0-MPa mode contact with flange having surface roughness $3.5\mu\text{m}$ when the axial force 120 KN. The width of an element in this simulation was 0.02273667 mm. Figure shows that numbers of total contacts are nine nodes, consist of elastic contact are eight nodes and plastic contact is one node. Based from the theory above, the contact width of this figure is 0.2046 mm which is 0.1819 mm plastic contact and 0.0227 mm elastic contact. The X-position 0 is the initial convex curve of gasket.

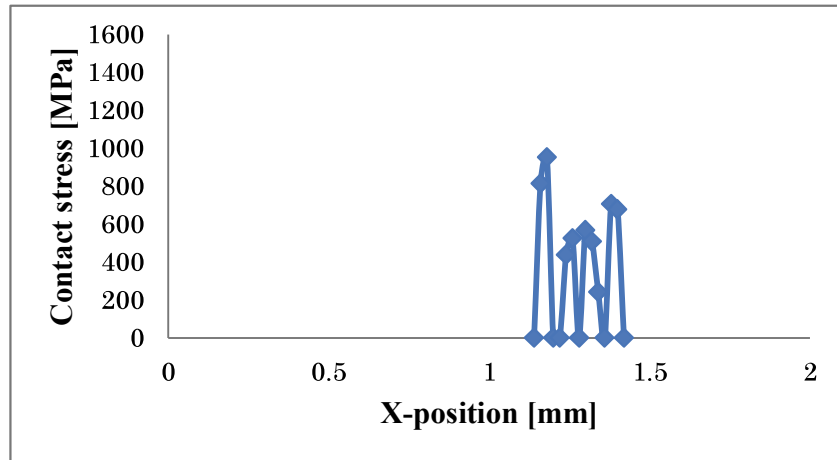


Fig. 5.2 Contact stress in X-position for gasket 0-MPa mode contact with flange having surface roughness 3.5µm

Fig. 5.3 shows the contact stress for gasket 0-MPa mode contact with flange having surface roughness 2.5µm when the axial force 120 KN. The width of the element in this simulation was 0.02238667 mm. Figure shows that numbers of total contacts are thirteen nodes, consist of elastic contact are three nodes and plastic contact is ten nodes. Based from the theory above, the contact width of this figure is 0.291 mm which is 0.067 mm elastic contact and 0.224 mm plastic contact.

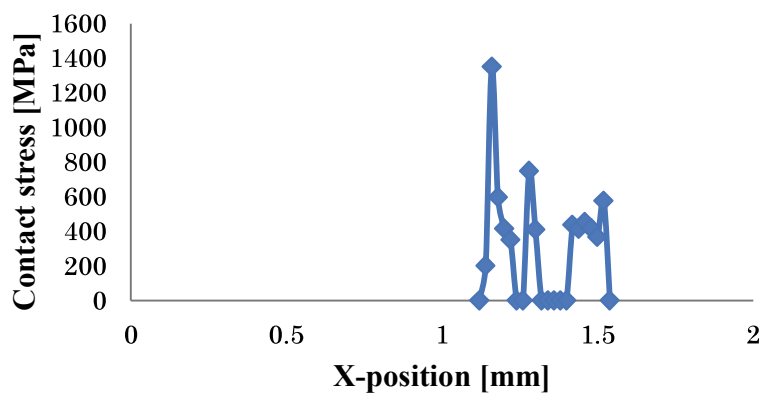


Fig. 5.3 Contact stress in X-position for gasket 0-MPa mode contact with flange having surface roughness 2.5µm

Fig. 5.4 shows the contact stress for gasket 0-MPa mode contact with flange having surface roughness $1.5\mu\text{m}$ when the axial force 120 KN. The width of the element in this simulation was 0.02238 mm. Figure shows that numbers of total contacts are fourteen nodes, consist of elastic contact are three nodes and plastic contact is eleven nodes. Based from the theory above, the contact width of this figure is 0.3133 mm which is 0.0671 mm elastic contact and 0.2462 mm plastic contact.

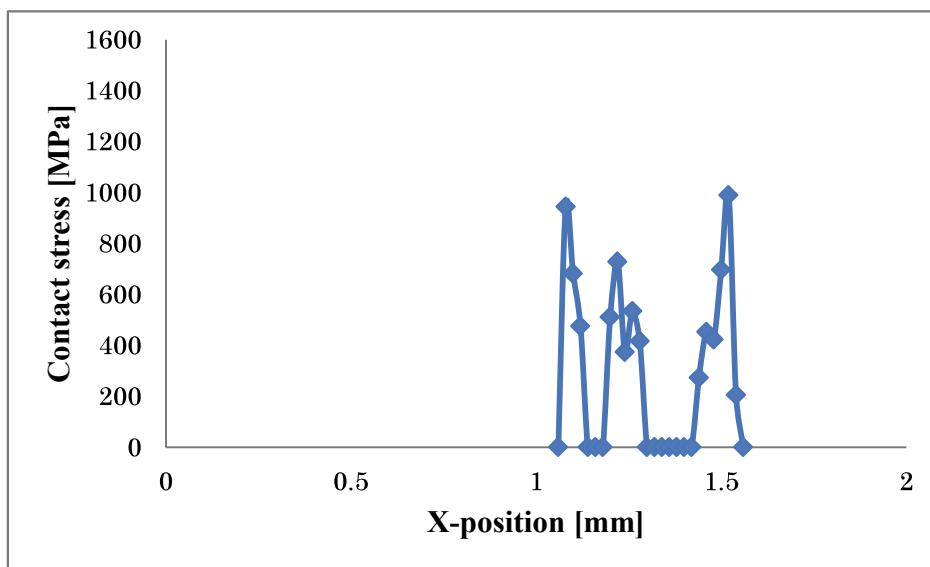


Fig. 5.4 Contact stress in X-position for gasket 0-MPa contact with flange having surface roughness $1.5\mu\text{m}$

Fig. 5.5 shows the contact stress for gasket 400-MPa mode contact with flange having surface roughness $3.5\mu\text{m}$ when the axial force 120 KN. The width of the element in this simulation was 0.02173 mm. Figure shows that numbers of total contact are thirteen nodes, consist of elastic contacts are two nodes and plastic contact is eleven nodes. Based from the theory above, the contact width of this figure is 0.285 mm which is 0.044 mm elastic contact and 0.241 mm plastic contact.

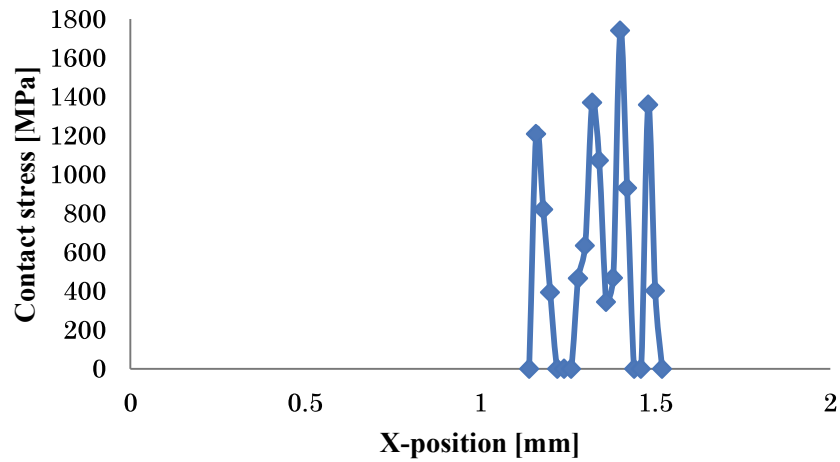


Fig. 5.5 Contact stress in X-position for gasket 400-MPa contact with flange having surface roughness 3.5µm

Fig. 5.6 shows the contact stress for gasket 400-MPa mode contact with flange having surface roughness 2.5µm when the axial force 120 KN. The width of the element in this simulation was 0.021666 mm. Figure shows that numbers of total contacts are thirteen nodes, consist of elastic contact are two nodes and plastic contact is eleven nodes. Based from the theory above, the contact width of this figure is 0.2828 mm which is 0.0438 mm elastic contact and 0.239 mm plastic contact.

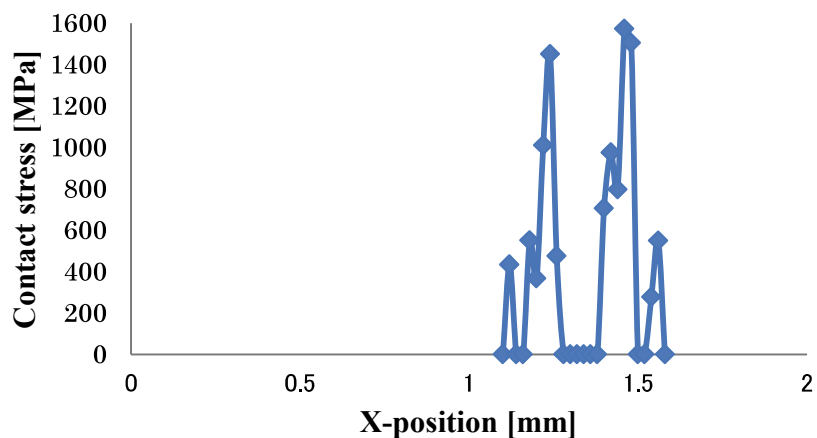


Fig. 5.6 Contact stress in X-position for gasket 400-MPa contact with flange having surface roughness 2.5µm

Fig. 5.7 shows the contact stress for gasket 400-MPa mode contact with flange having surface roughness $1.5\mu\text{m}$ when the axial force 120 KN. The width of the element in this simulation was 0.02025333 mm. Figure shows that numbers of total contacts are seventeen nodes, consist of elastic contact are two nodes and plastic contact is fifteen nodes. Based from the theory above, the contact width of this figure is 0.3443 mm which is 0.0405 mm elastic contact and 0.3038 mm plastic contact.

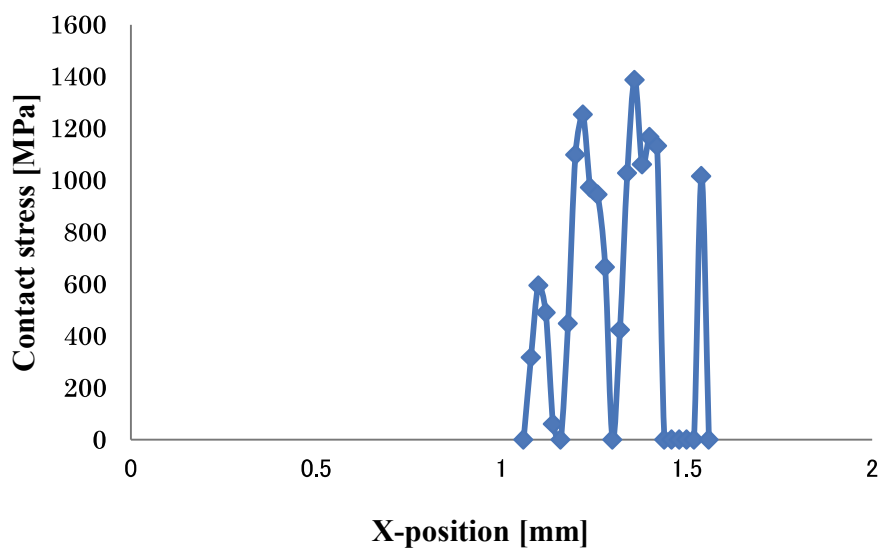


Fig. 5.7 Contact stress in X-position for gasket 400-MPa contact with flange having surface roughness $1.5\mu\text{m}$

Fig. 5.8 shows the real contact width between gasket and flange for real surface roughness model for the axial force 120 KN. The blue color is plastic contact stress condition, and red color is elastic contact stress condition. The plastic contact stress condition will deform the gasket, but the elastic contact stress condition will not deform the gasket because after unloading gasket will back to the initial condition. So our focus is in plastic contact stress condition. Figure shows that the contact width for plastic contact stress condition for metal gasket 400-MPa mode is longer than metal gasket 0-MPa mode. The gasket having surface roughness $1.5\mu\text{m}$ is longer for contact width than gasket having

surface roughness 2.5 μm and 3.5 μm .

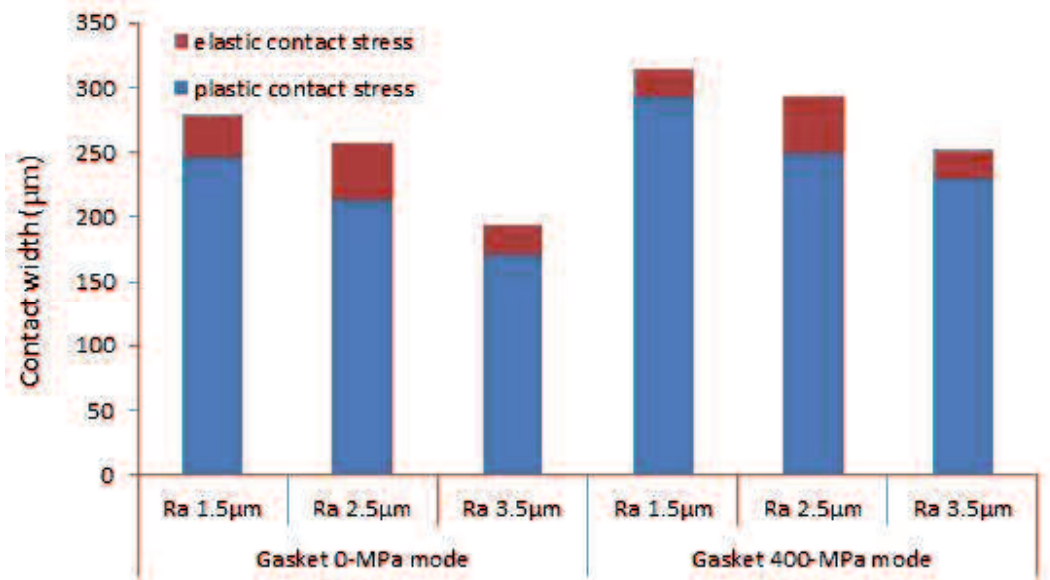


Fig. 5.8 Real contact width simulation result for all levels real surface roughness model of flange and all types of gasket when axial force 120 KN

Fig. 5.9 shows the width of contact width between gasket and flange for real surface roughness model when the axial force is 100 KN. Figure shows that contact width for plastic contact stress condition for metal gasket 400-MPa mode is longer than metal gasket 0-MPa mode. The flange has surface roughness 1.5 μm is longer for contact width than flange having surface roughness 2.5 μm and 3.5 μm . The contact width when axial force 120 KN is longer than 100 KN.

Fig. 5.10 shows the width of contact width between gasket and flange for real surface roughness model when the axial force is 80 KN. Figure shows that contact width for plastic contact stress condition for metal gasket 400-MPa mode is higher than metal gasket 0-MPa mode. The flange has surface roughness 1.5 μm is longer for contact width than flange having surface roughness 2.5 μm and 3.5 μm . The contact width when axial force 100 KN is longer than 80 KN.

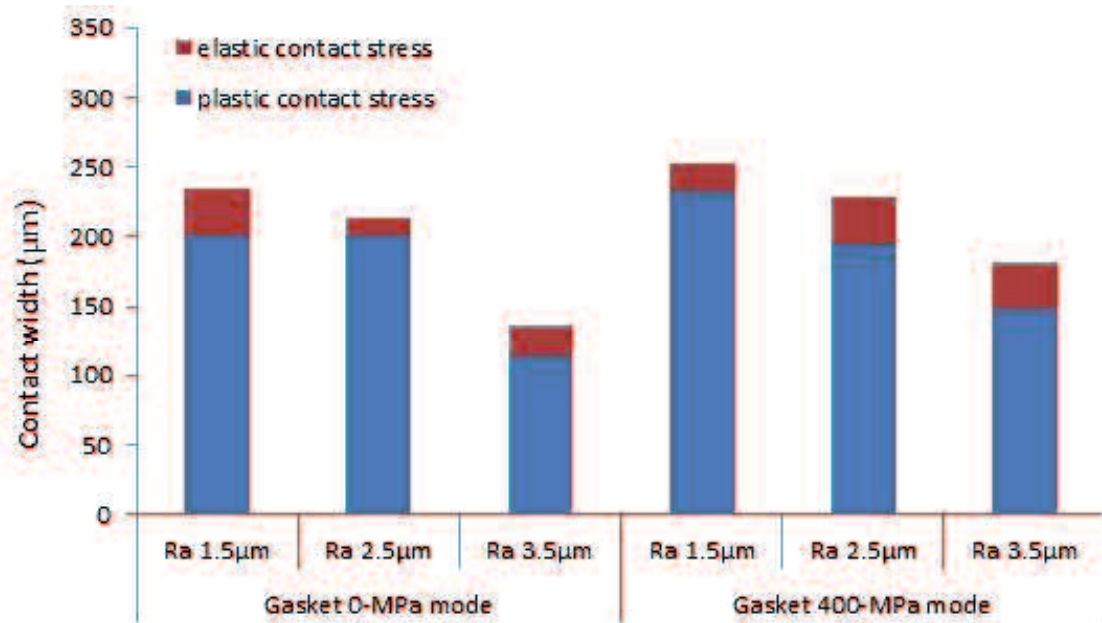


Fig. 5.9 Real contact width simulation result for all levels real surface roughness model of flange and all types of gasket when axial force 100 KN

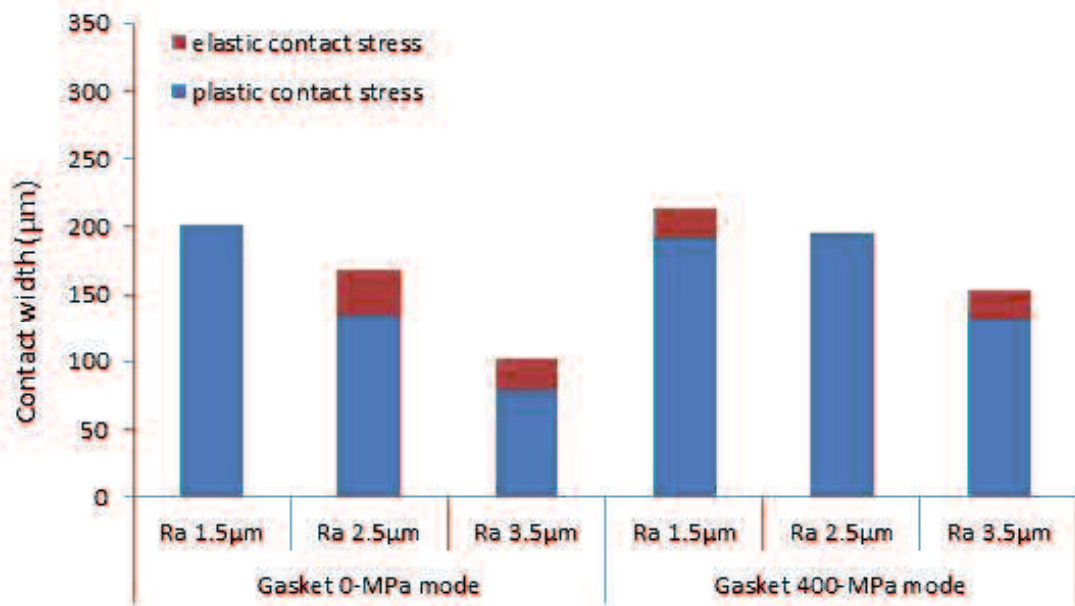


Fig. 5.10 Real contact width simulation result for all levels real surface roughness model of flange and all types of gasket when axial force 80 KN

Fig. 5.11 shows the width of contact width between gasket and flange for real surface roughness model when the axial force is 80 KN. Figure shows that contact width for plastic contact stress condition for metal gasket 400-MPa mode is higher than metal gasket 0-MPa mode. The flange has surface roughness 1.5 μm is longer for contact width than flange having surface roughness 2.5 μm and 3.5 μm . The contact width when axial force 80 KN is longer than 60 KN.

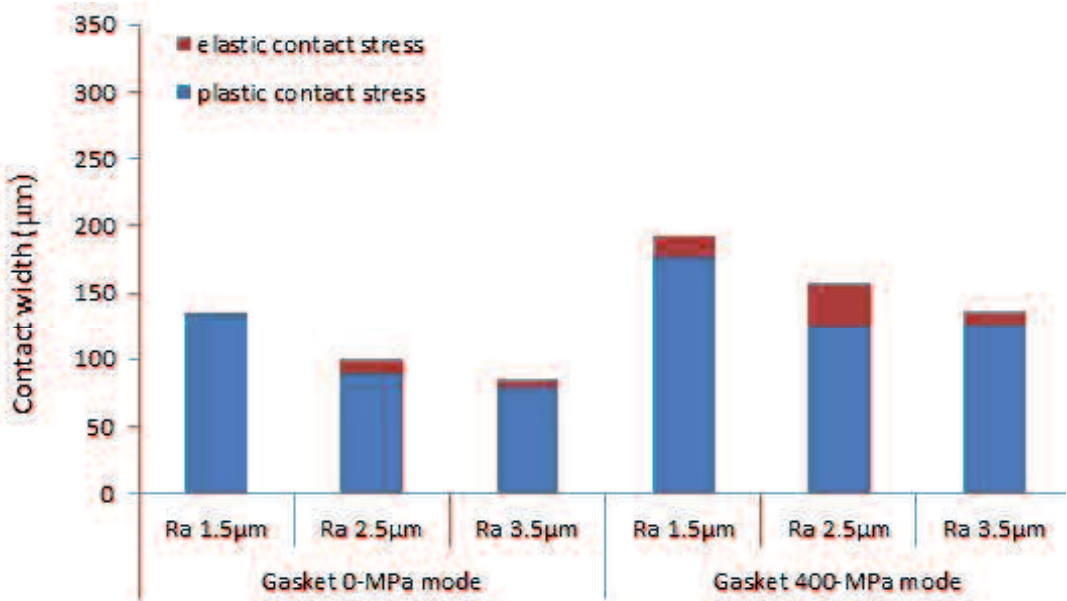


Fig. 5.11 Real contact width simulation result for all levels real surface roughness model of flange and all types of gasket when axial force 60 KN

5.2 Contact Width Experiment Analysis

After the axial force applied, the grooves will be formed in the gasket adjusted the shape of the flange roughness. Focus of this study, investigated the total number of grooves width formed in the gasket. The total number of grooves width is the real contact width during the tightening.

5.2.1 Material and Method

The gasket used in this research is circumference beads gasket. Using mold press, the shape of the gasket produced. The dimension of the gasket used is the standard dimension based on JIS B2404 [52] with 1.45 mm of gasket thickness. The gasket material was SUS304 due to its effectiveness in high-temperature and high-pressure environment.

The general-purposed flange based on JISB2220 with 10 K pressure and 25A diameter used in this test. The lower flange and the joint were welded carefully to avoid distortion. Types of flange based on the average surface roughness are 1.5 μm , 2.5 μm , and 3.5 μm . In this test, we used a new 25A-size metal gasket with corrugated shape. In this research, two types of gasket and three levels of flange surface roughness were investigated. Types of gasket, based on elastic and plastic design, are 0-MPa and 400-MPa mode.

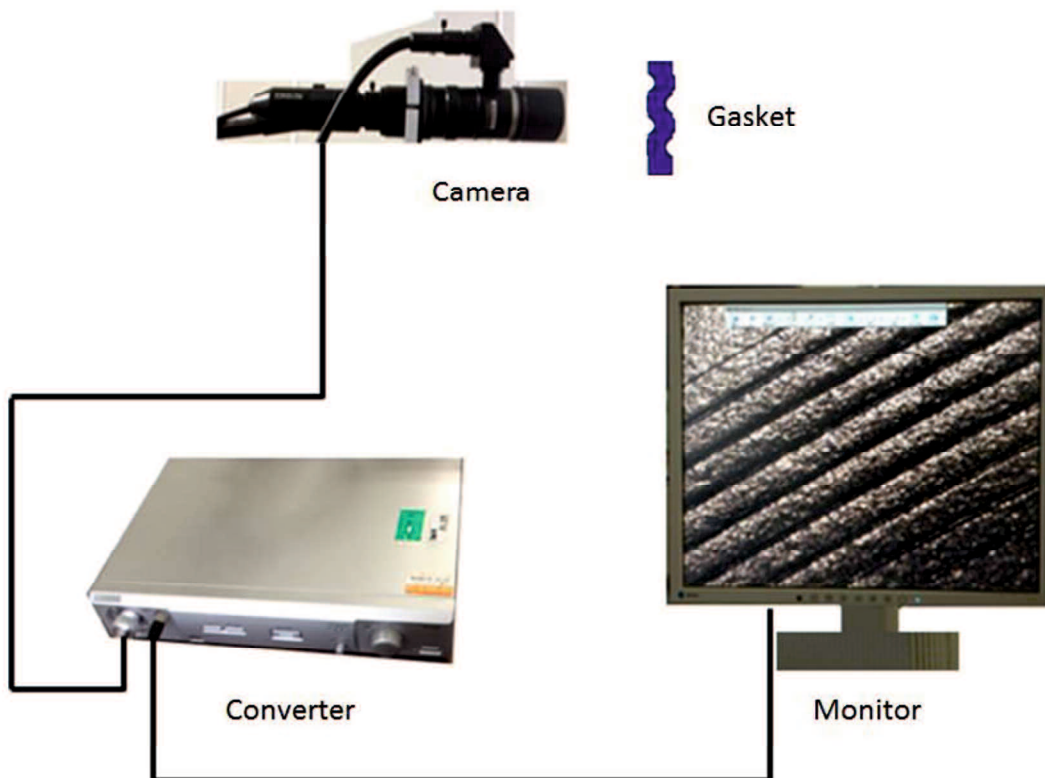


Fig. 5.12 Digital microscope VH-Z250

The previous study confirmed that if surface roughness increased the leakage will decrease. The simulation in the previous study proved that smoother of surface roughness will increase the contact width [49] and [50]. The digital microscope VH-Z250 series 500x in magnification was used to measure the contact width parameter of the proposed the 25-A size metal gasket, see Fig. 5.12. Using microscope we can measure the width of grooves that are the real contact width between the flange and the gasket.

$$CW = \sum_{i=1}^n h_i \tag{5.1}$$

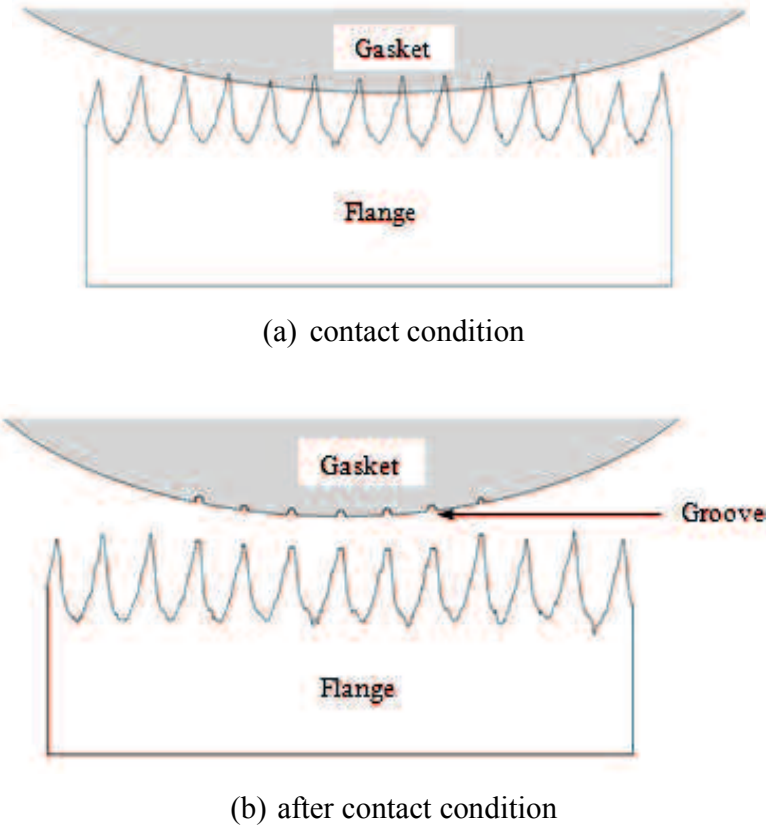


Fig. 5.13 Gasket and flange in contact and after contact condition

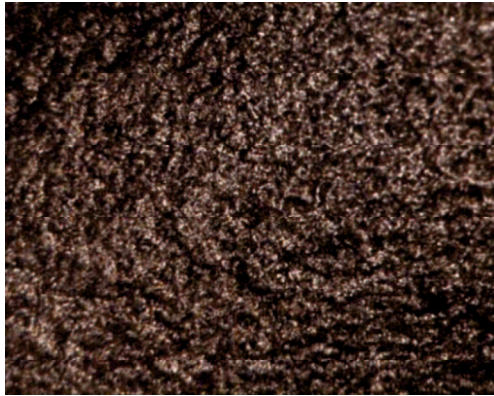
There are grooves in the gasket after contact with the flange, see Fig.5.13. The tightening process is carried out based on the axial force. Tightening the flange using bolts

can cause too high local contact stress on the convex section of the gasket. Groove will be formed in the gasket as an illustration of pressure distribution profile that occurred between the two surfaces. Focus of the current study was to observe the width of the groove formed in the gasket. The total number of grooves width is a real contact width between gasket and flange, see equation (6.1).

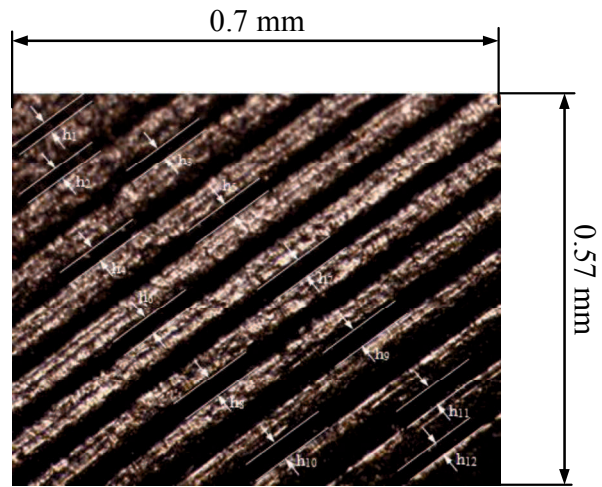
5.2.2 Results and Discussion

As a mentioned above, we measured two places of gasket, which are convex portion 2 and convex portion 3, because both convex were similar character and very influence for leakage process. Both of these convex have the higher contact stress and longer contact width compare with convex portion 1 and convex portion 4 [51].

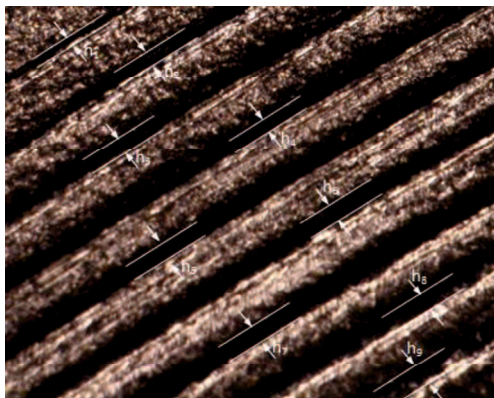
Fig. 5.14 shows the surface roughness condition of gasket 400-MPa mode before and after contact with the flange. Fig. 5.14(a) shows the surface roughness of gasket before contact with the flange. There were no grooves in the gasket surface. The surface roughness of gasket after contact with flange having surface roughness $1.5\mu\text{m}$, $2.5\mu\text{m}$, and $3.5\mu\text{m}$, respectively, are shown in Fig. 5.14(b), (c), and (d). There were grooves in the gasket surface. The grooves formed because of the tightening process between upper and lower rough flange. Based from the figures, we got the real contact width between gasket and flange. The real contact width is the total number of grooves width as described in equation (1). More detail for the real contact width for gasket 400-MPa mode contact with the flange shown in Table 6.1 [51].



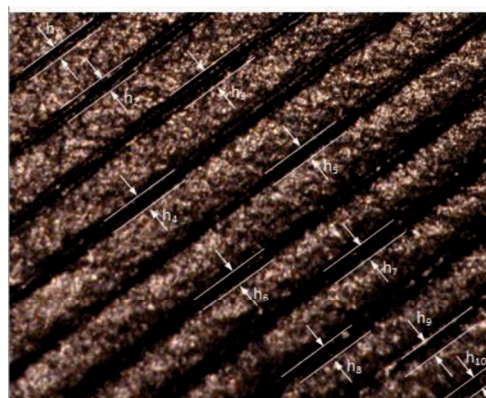
(a) Surface roughness of gasket before contact



(b) Surface roughness of gasket after contact with flange having surface roughness $1.5\mu\text{m}$



(b) Surface roughness of gasket after contact with flange having surface roughness $2.5\mu\text{m}$



(d) Surface roughness of gasket after contact with flange having surface roughness $3.5\mu\text{m}$

Fig. 5.14 Grooves formed conditions for gasket 400-MPa mode

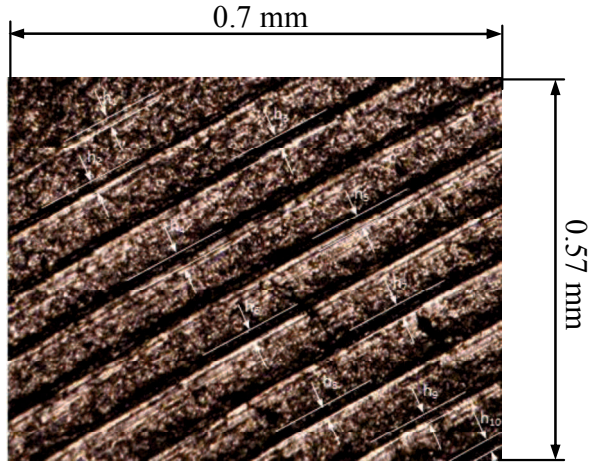
Table 5.1 Contact width result for 400-MPa gasket mode

Ra 1.5 μm		Ra 2.5 μm		Ra 3.5 μm	
Convex portion 2	Convex portion 3	Convex portion 2	Convex portion 3	Convex portion 2	Convex portion 3
17.49	19.67	24.04	13.11	8.74	21.86
25.14	26.23	26.23	14.21	17.49	20.77
21.86	32.79	30.60	18.58	19.67	19.67
26.23	20.77	28.42	32.79	20.77	19.67
21.86	27.32	26.23	30.27	21.86	18.58
24.04	26.23	31.69	28.85	19.67	18.58
27.32	28.42	29.18	22.13	21.86	20.77
29.51	26.23	25.90	28.85	21.86	20.77
25.14	27.32	22.62	20.27	18.58	19.67
29.51	28.42		30.60	15.30	15.30
25.14	32.79				
17.49	12.79				
273.24	308.98	244.91	239.66	185.80	195.64
Average: 291.11		Average: 242.28		Average: 190.72	

Table 5.1 shows the real contact width results for the gasket 400-MPa mode after contact with flange having surface roughness 1.5 μm , 2.5 μm , and 3.5 μm , respectively, for all levels surface roughness. The gasket contact with flange having surface roughness 1.5 μm shows the longest real contact width both for convex portion 2 and 3. The average contact width for convex portion 2 and 3 is 291.11 μm . The gasket contact with flange having surface roughness 3.5 μm shows the shortest real contact width both for convex portion 2 and 3. The average contact width for convex number 2 and 3 is 190.72 μm . This result is in line with the simulation result in [49] and [50]. Correspond the statement above and based on the real contact width measurement flange having surface roughness 1.5 μm is the best flange for decrease leakage and flange having surface roughness 3.5 μm is worst for decrease leakage. It means that the smoother surface roughness will decrease the leakage for the gasket 400-MPa mode.



(a) Surface roughness of gasket before contact



(b) surface roughness of gasket after contact with flange having surface roughness $1.5\mu\text{m}$



(c) surface roughness of gasket after contact with flange having surface roughness $2.5\mu\text{m}$



(d) surface roughness of gasket after contact with flange having surface roughness $3.5\mu\text{m}$

Fig. 5.15 Grooves formed conditions for gasket 0-MPa mode

Fig. 5.15 shows the surface roughness condition of gasket 0-MPa mode before and after contact with the flange. Fig. 5.15(a) shows the surface roughness of gasket before

contact with the flange. There were no grooves in the gasket surface. The surface roughness of gasket after contact with flange having surface roughness 1.5 μm , 2.5 μm , and 3.5 μm , respectively, are shown in Fig. 5.15(b), (c), and (d). There were grooves in the gasket surface. Based from the figures, we got the real contact width between gasket and flange. More detail for the real contact width for gasket 0-MPa mode contact with the flange shown in Table 5.2.

Table 5.2 Contact width result for 0-MPa gasket mode

Ra 1.5 μm		Ra 2.5 μm		Ra 3.5 μm	
Convex portion 2	Convex portion 3	Convex portion 2	Convex portion 3	Convex portion 2	Convex portion 3
14.21	20.04	25.14	22.95	20.77	28.42
16.39	20.77	30.80	29.51	22.95	22.95
20.77	20.77	34.97	25.14	21.86	25.14
29.51	20.77	26.23	31.69	19.67	27.32
27.32	25.14	27.32	26.23	21.86	18.58
27.32	25.14	20.77	26.23	20.77	20.77
24.04	31.69	12.02	12.02	16.39	22.95
26.23	32.79				
30.6	22.95				
16.39	18.58				
232.78	238.64	177.25	173.77	144.27	166.13
Average: 235.71		Average: 175.51		Average: 155.20	

Table 5.2 shows the real contact width results for the gasket 0-MPa mode for all levels surface roughness. The gasket contact with flange having surface roughness 1.5 μm shows the longest real contact width both for convex portion 2 and 3. The average contact width for convex portion 2 and 3 is 235.71 μm . The gasket contact with flange having surface roughness 3.5 μm shows the shortest real contact width both for convex portion 2 and 3. The average contact width for convex portion 2 and 3 is 155.2 μm . This result is in line with the simulation result in [49] and [50]. Correspond the statement above and based on the real contact width measurement, flange having surface roughness 1.5 μm is the best

flange for decrease leakage and flange having surface roughness $3.5\mu\text{m}$ is worst for decrease leakage. It means that the smoother surface roughness will decrease the leakage for the gasket 0-MPa mode.

Using Table 5.1 and 5.2, we compared the leakage performance of the gasket 400-MPa mode and the gasket 0-MPa mode based on the real contact width. The real contact width for the gasket 400-MPa mode is longer than the gasket 0-MPa mode for each gasket contact with flange having surface roughness $1.5\mu\text{m}$, $2.5\mu\text{m}$, and $3.5\mu\text{m}$, respectively. It means that the leakage performance for the gasket 400-MPa mode is better than the gasket 0-MPa mode.

Fig. 5.16 shows the contact width between gasket and flange for all levels surface roughness. It is very clear that the real contact width between flange and gasket 400-MPa mode is wider than gasket 0-MPa mode. As explanation above, for the same gasket, the real contact width between gasket and flange having surface roughness $1.5\mu\text{m}$ is longest than the others. The real contact width between gasket and flange having surface roughness $3.5\mu\text{m}$ is shortest than others [51].

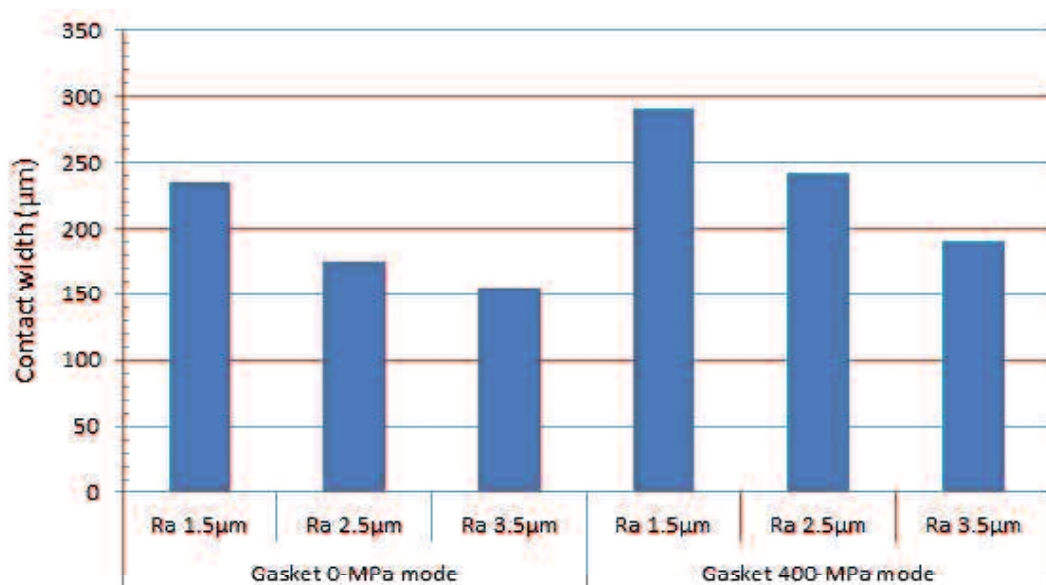


Fig. 5.16 Real contact width experiment result for all levels surface roughness of flange and all types of gasket

Comparison contact width analysis for the experimental result and simulation result see Fig. 5.8 and Fig. 5.24 shows that trend contact width is similar. The real contact width for the gasket 0-MPa mode contact with the flange was lower than the gasket 400-MPa mode contact with flange. The gasket contact with the flange having surface roughness 1.5 μm shows the longest real contact width both for the gasket 400-MPa mode and the gasket 0-MPa mode. The gasket contact with flange having surface roughness 3.5 μm shows the shortest real contact width both for the gasket 400-MPa mode and the gasket 0-MPa mode.

The total differences of measurement between simulation result for the real model of surface roughness and experimental result is 7.89 %. The differences of measurement between simulation result and experimental result for gasket 0-MPa mode is 8.71 % and for gasket 400-MPa mode is 7.07 %. Table 5.3 shows the differences of measurement between simulation result and experimental result.

Table 5.3 Differences of contact width between simulation result and experimental result

	Gasket 0-MPa mode			Gasket 400-MPa mode		
	Surface roughness 1.5 μm	Surface roughness 2.5 μm	Surface roughness 3.5 μm	Surface roughness 1.5 μm	Surface roughness 2.5 μm	Surface roughness 3.5 μm
Simulation result (μm)	246.18	201.48	170.53	293.67	250.18	230.26
Experimental result (μm)	235.71	175.51	155.20	291.11	242.28	190.72
Differences (%)	4.25	12.89	8.99	0.87	3.16	17.17
	8.71			7.07		
	7.89					

The result justifies the real contact width for gasket contact with the flange having small surface roughness is longer than gasket contact with the flange having big surface roughness. The surface roughness having two dimensions, which are roughness spacing and roughness height [19], see Fig. 5.17. The contacts width shown in Fig. 5.18 is not real

contact width. The real contact width is the sum of the real contact width, denoted by red circle in Fig. 5.19. Because of the number of real contact for small roughness more than big surface roughness, contact width for small surface roughness is longer than big surface roughness.

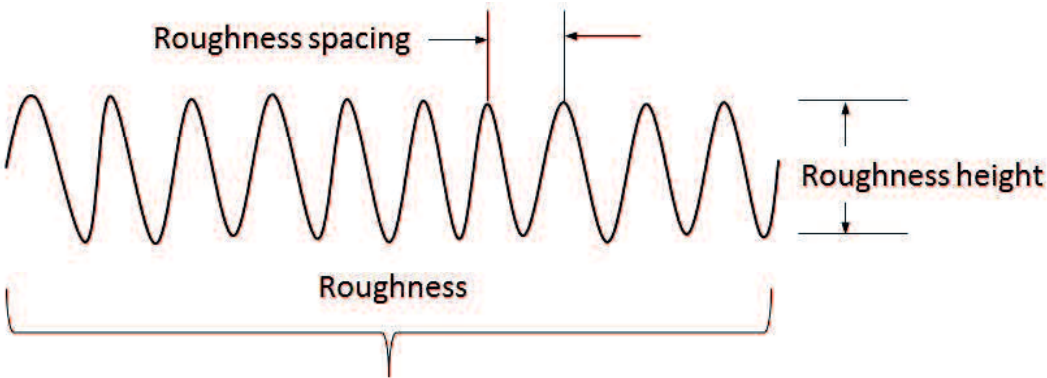


Fig. 5.17 Basic dimension of surface roughness

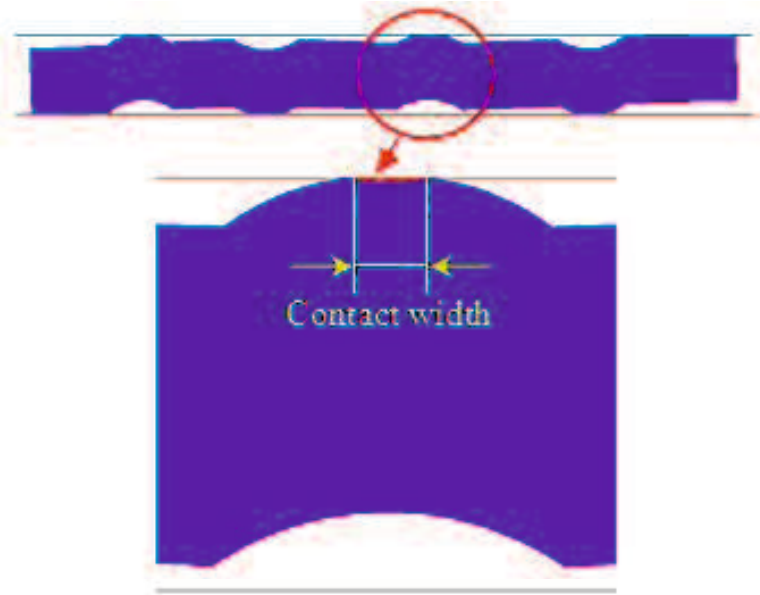


Fig. 5.18 Contact width

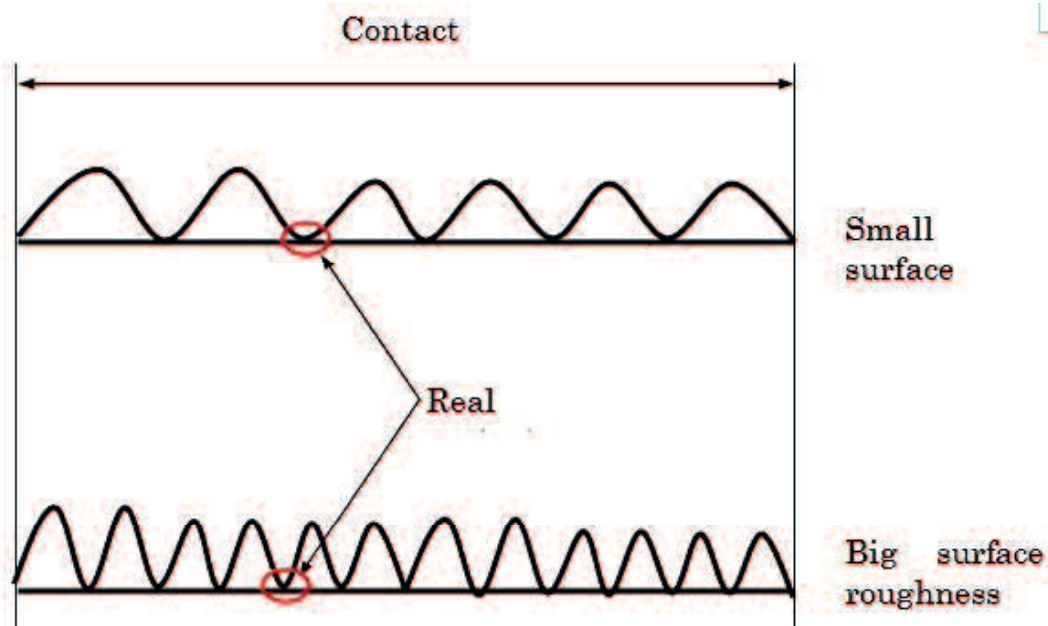


Fig. 5.19 Real contact width

The contact width for gasket 400-MPa mode was longer than 0-MPa mode. The design of the gasket 400-MPa mode based on contact width that considering plastic contact stress. The contact stress bellow 400MPa deleted, only contact stress ranging from 400MPa to top used to determine the contact width condition. The design of the gasket 0-MPa mode based on contact width that considering elastic and plastic contact stress. All contact stress used to determine the contact width condition. The contact stress for gasket 400-MPa mode is more easily to be plastic condition when the axial force more than 80KN.

5.3 Contact Area

When the gasket was tightened to the flange, the beads on both surfaces of gasket created an elastic effect. It can be generated high local contact stress on convex section of gasket to obtain a low loading metal gasket. There is contact between gasket and flange having variation surface roughness. The flanges will give the axial force to gasket in both upper and lower, see Fig. 5.20.

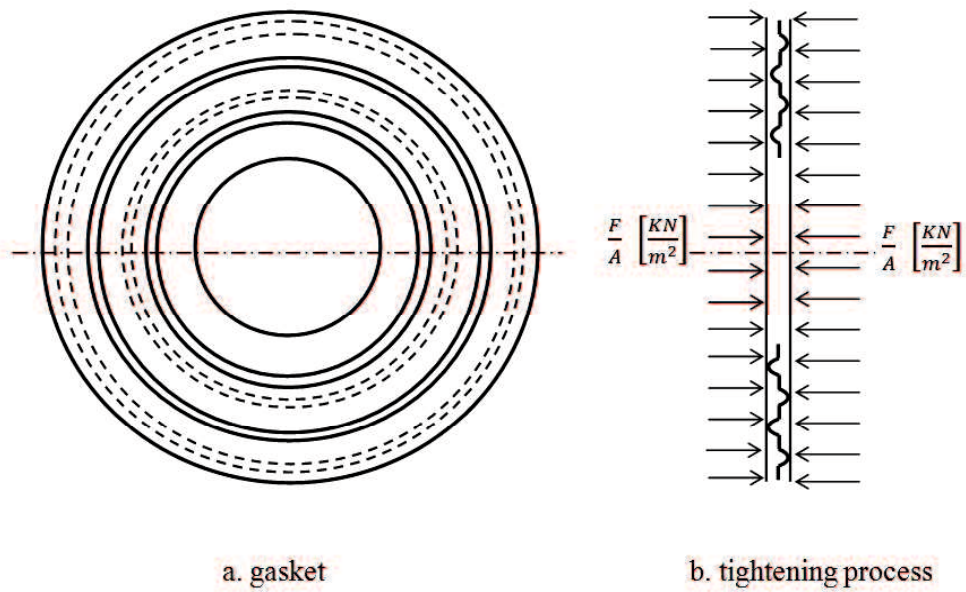


Fig. 5.20 Gasket in tightening process

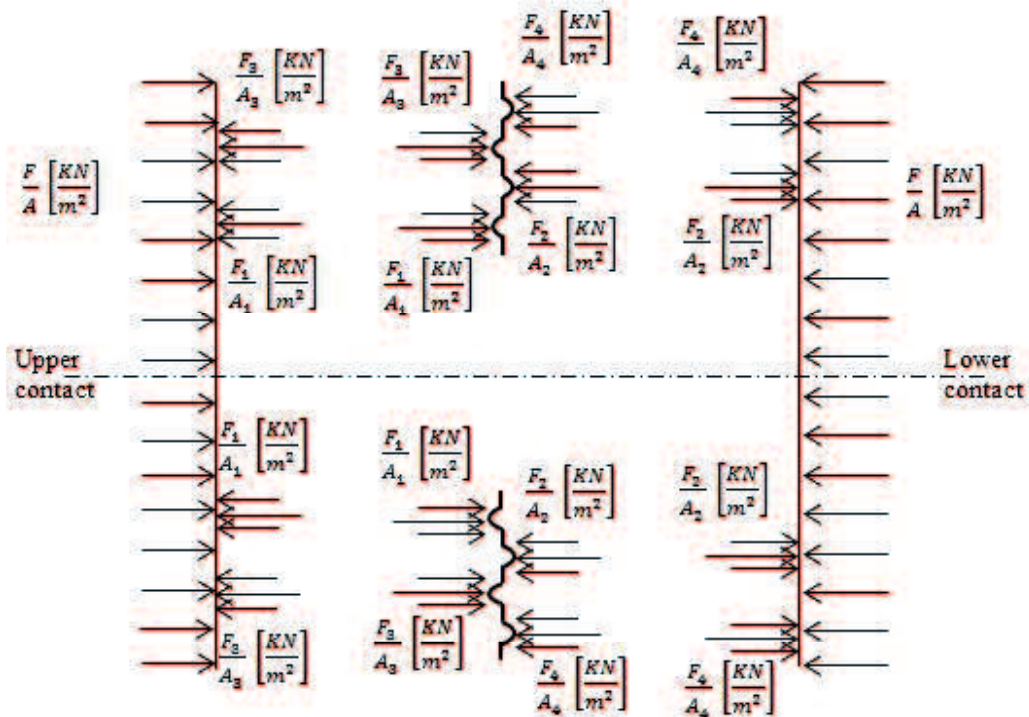


Fig. 5.21 Free body diagram for tightening process

The upper and lower flanges give same axial force to upper and lower gasket, respectively. Gasket will give the reaction force to the flange for upper and lower contact respectively. Fig. 5.21 shows the free body diagram for tightening process. The reaction forces of the upper contact are F_1 and F_3 , and the reaction forces of lower contact are F_2 and F_4 .

For lower contact

$$\frac{F}{A} = \frac{F_2}{A_2} + \frac{F_4}{A_4} \quad (5.2)$$

For upper contact

$$\frac{F}{A} = \frac{F_1}{A_1} + \frac{F_3}{A_3} \quad (5.3)$$

When A_1 , A_2 , A_3 and A_4 are contact area for convex portion 1, 2, 3, and 4 respectively.

The sliding contact occurred on all convex portions. The value of position change of the convex portion 1 and 4 are larger than convex portion 2 and 3 [53]. Fig. 5.22 and 5.23 shows the position change of the convex portion, respectively. Convex portion 2 and 3 works primarily to reduce leakage and convex portion 1 and 4 will support to realize it.

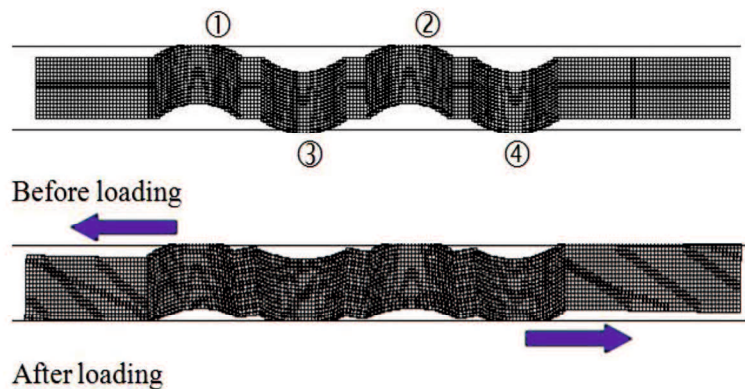


Fig. 5.22 Phenomena of sliding contact on the convex contact of the gasket

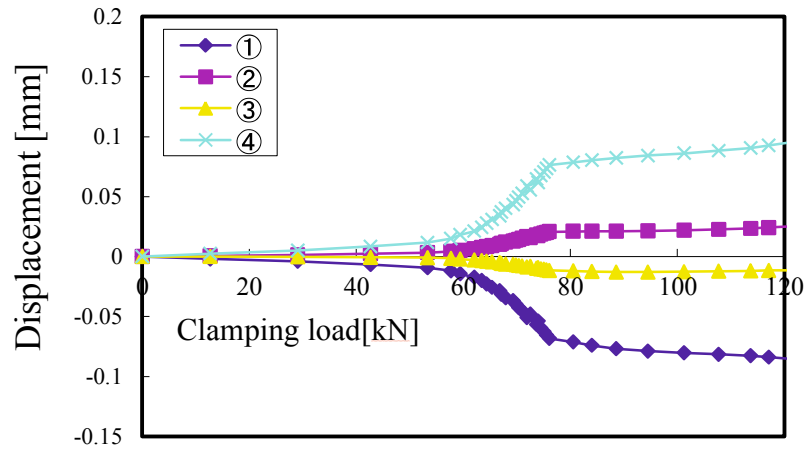


Fig. 5.23 Value of position change on the convex contact

As mentioned before, there are two types of gasket, which are 0-MPa mode and 400-MPa mode. Table 5.4 shows the average radius of contact width for each gasket mode.

Table 5.4 average radius of contact width

Average Radius	0-MPa mode	400-MPa mode
r_1 (mm)	$20.5-s_1$	$20.5-s_1$
r_2 (mm)	$25-s_2$	$24-s_2$
r_3 (mm)	$29.5+s_3$	$28.5+s_3$
r_4 (mm)	$34+s_4$	$32+s_4$

$$A_1 = \pi r_1^2 d_1 \quad (5.4)$$

$$A_2 = \pi r_2^2 d_2 \quad (5.5)$$

$$A_3 = \pi r_3^2 d_3 \quad (5.6)$$

$$A_4 = \pi r_4^2 d_4 \quad (5.7)$$

When d_1 , d_2 , d_3 and d_4 are contact width for contact area convex portion 1, 2, 3, and 4 respectively.

Based on convex radius average radius of contact as shown in Table 3 and the sliding distance is s , the contact area for convex portion 1, 2, 3 and 4 can be described as follows

Gasket 0-MPa mode

$$A_1 = \pi r_1^2 d_1 = \pi (20.5 - s_1)^2 d_1 \quad (5.8)$$

$$A_2 = \pi r_2^2 d_2 = \pi (25 - s_2)^2 d_2 \quad (5.9)$$

$$A_3 = \pi r_3^2 d_3 = \pi (29.5 + s_3)^2 d_3 \quad (5.10)$$

$$A_4 = \pi r_4^2 d_4 = \pi (34.5 + s_4)^2 d_4 \quad (5.11)$$

Gasket 400-MPa mode

$$A_1 = \pi r_1^2 d_1 = \pi (20.5 - s_1)^2 d_1 \quad (5.12)$$

$$A_2 = \pi r_2^2 d_2 = \pi (24 - s_2)^2 d_2 \quad (5.13)$$

$$A_3 = \pi r_3^2 d_3 = \pi (28.5 + s_3)^2 d_3 \quad (5.14)$$

$$A_4 = \pi r_4^2 d_4 = \pi (32 + s_4)^2 d_4 \quad (5.15)$$

5.4 Conclusion

This study investigates the real contact width for a flange with different surface roughness values through a simulation analysis using FEM and a contact width measurement. The following conclusions are derived from this study:

1. The real contact width for the gasket 0-MPa mode contact with flange was lower than the gasket 400-MPa mode contact with flange.
2. The gasket contact with flange has surface roughness $1.5\mu\text{m}$ shows the longest real contact width and $3.5\mu\text{m}$ shows the shortest for both the gasket 400-MPa mode and the gasket 0-MPa mode.
3. The total differences of measurement between simulation result for real model of surface roughness and experimental result is 7.89 %.

CHAPTER VI

DEFORMATION CHARACTERISTIC OF THIN STAINLESS GASKET MATERIAL

As a replacement for gaskets containing asbestos material, many researchers have studied the use of metal gasket materials. Saeed *et al.* studied a new 25A-size corrugated metal gasket that developed as an asbestos gasket substitute. The gasket had a metal spring effect and produced high local contact stress to create a sealing line with a flange. The results showed that the contact stress and contact width were important design parameters for optimizing the gasket performance [13]. Haruyama *et al.* [14] continued this research. The size limit of the contact width as a gasket design parameter investigated. Comparing the results of FEM analysis of the relationship between the clamping load of the flange and the contact width with experimental results for the clamping load and leakage clarified the contact width with no leak for the new 25A-size metal gasket. Based on this result, the contact width can be used as the main parameter to optimize the gasket design. The leakage can be reduced by increasing the contact width. Choiron *et al.* [15] studied a validity method for contact width measurement using simulation analysis, and the result was compared with the result of an experiment using pressure-sensitive paper. The contact width saw similar trends between the simulation and experimental results. Nurhadiyanto *et al.* [43] used FEM to study a gasket design optimization method based on elastic and plastic contact stress analysis that considered the forming effect. A helium leakage test showed that a gasket based on a plastic contact stress design was better than a gasket based on an elastic stress design. However, both types of gaskets could be used for seals because they did not leak in the helium leak test.

However, the 25-A size metal gasket requires a high axial force for the tightening process; moreover, a metal gasket has a tendency to corrode easily. To reduce the axial force and corrosion effect, we studied a thin stainless gasket material. This gasket will use for low pressure of the fluid. Ushijima *et al.* [54] studied the deformation mode of a thin

metal gasket based on an experiment and FEM. They compared the load and contact width-displacement curves obtained experimentally with those obtained analytically in a compression test, along with the deformed shape of the gasket. They classified the deformation modes into two types. In this paper, we present the results of numerical analysis using FEM and experimental analysis of thin stainless gasket material. We investigate the deformation modes and classify them into three types. In addition, we investigate the displacement-contact stress and width curves.

6.1 Material and Method

Stainless steel was used as a gasket material because of its effectiveness at high temperature and its resistance to corrosion. We used material gasket to reduce the axial force for tightening. This material also use for low fluid pressure. Its material properties determined through a tensile test carried out based on JIS Z2241 [40]. Based on the tensile test results, the nominal stress (σ) was 300.34MPa, the modulus of the elasticity (E) was 48.67GPa, the tangent modulus was 483.33MPa, and Poisson's ratio was 0.3. Fig.6.1 shows the dimensions of a thin stainless gasket material used in this study, which were as follows: convex portion length $D = 20$ mm; height $h = 4.0$ mm; thickness $t = 0.3$ mm; distance from the central axis $r = 100$ mm. The length of the flat portion varied, with the following values: $L = 1.5$ mm; 2.0 mm, and 4.0 mm.

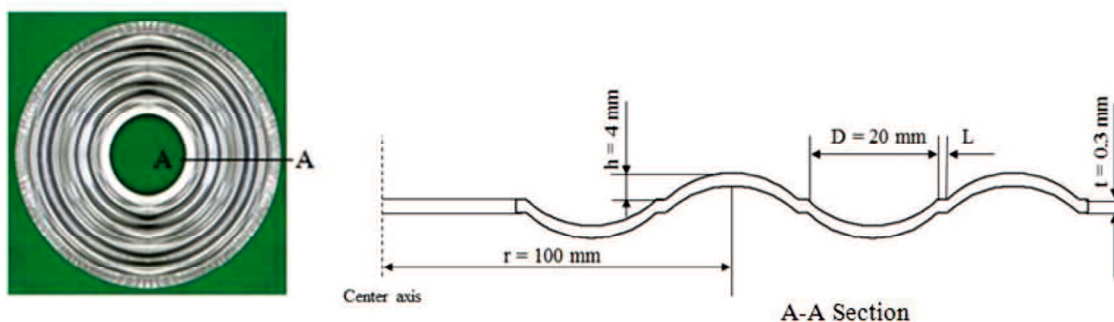


Fig. 6.1 Dimensions of thin stainless gasket material

6.1.1. Simulation Analysis

The deformation mode of the stainless gasket was investigated using an FEM analysis. The stages were modeled using the software MSC.Marc. The virtual gasket model with various designs was generated by using four basic steps. They were the parameterization the models, automatic meshing, computation of preprocessing and post-processing in batch mode and optimization. Firstly, 2-D parameter model is built by utilizing the Solid work software. To connect drawing data from Solid work (IGES file) and automatic meshing by using Hypermesh using batch command file built, and an NAS file produced by this procedure. Then the procedure file was configured to obtain preprocessing and running the model on MSC.Marc software. The graphic user interface (GUI) did not appear and the program run commands in the background. After the FEM analysis was complete, the output file, including analysis results could be generated in TXT file. The TXT result file was transformed to Microsoft excel by using MACRO commands. The output result contains the contact status, stress value, and body force at each time at every convex position. Calculation of the contact width versus axial force on convex position number 1 until 4 produced with several steps of MACRO command. Using two-dimensional assumptions, an axis-symmetric shell element model adopted for the tightening process simulation in the axial direction between the upper and lower flange. Fig. 6.2 shows the FEM analysis for the tightening simulation. The gasket material model compressed between the upper and lower rigid flanges using axial displacement to simulate the relationship between the load-displacement and contact width curves. Both the upper and lower flanges are assumed to be rigid bodies. The lower flange is assumed to have a fixed boundary condition. Further, the contact stress and the contact width an evaluation performed only for the convex portion of the gasket, which is effective at reducing the leakage. The deformation mode evaluation performed for the convex and flat portions.

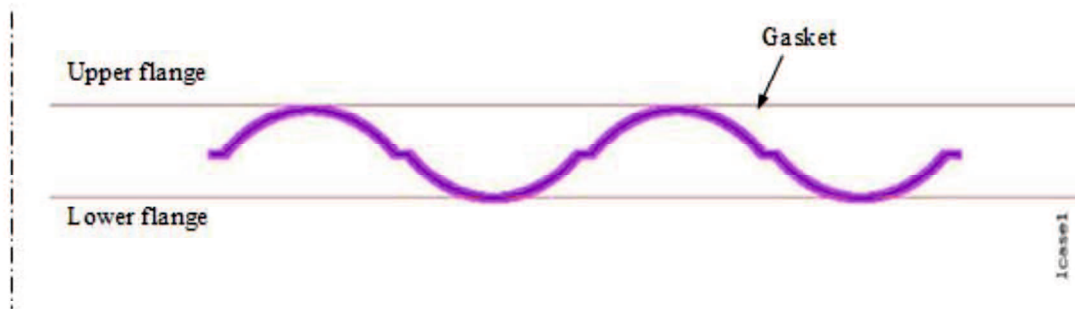


Fig. 6.2 FEM simulation model

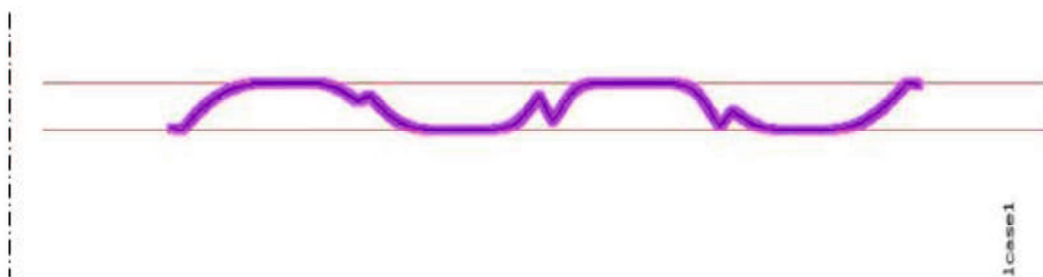


Fig. 6.3 Tightening simulation

6.1.2 Experimental Analysis

A tension large-sized testing machine (UTM-I-25000) used for the compression process and formed a gasket. Fig. 6.4 shows a schematic diagram of the experimental compression device. A load and displacement were monitored using a laser displacement sensor (SUNX HL-C135C-BK10) and sensor interface (Kyowa Electronic Instruments PCD300A) at a sampling speed of 20 Hz. The compression speed set at 5 mm/min.

The gasket manufactured using a mold press. The shape of the gasket is realized by using a punch to force the initial material to slide into a die. Hence, the forming effect was considered for assessing the modeling of gasket design. A tension large-sized testing machine (UTM-I-25000) used to perform the forming process. Fig. 6.5 shows a dies used to form a gasket. Fig. 6.6 shows a gasket that produced.

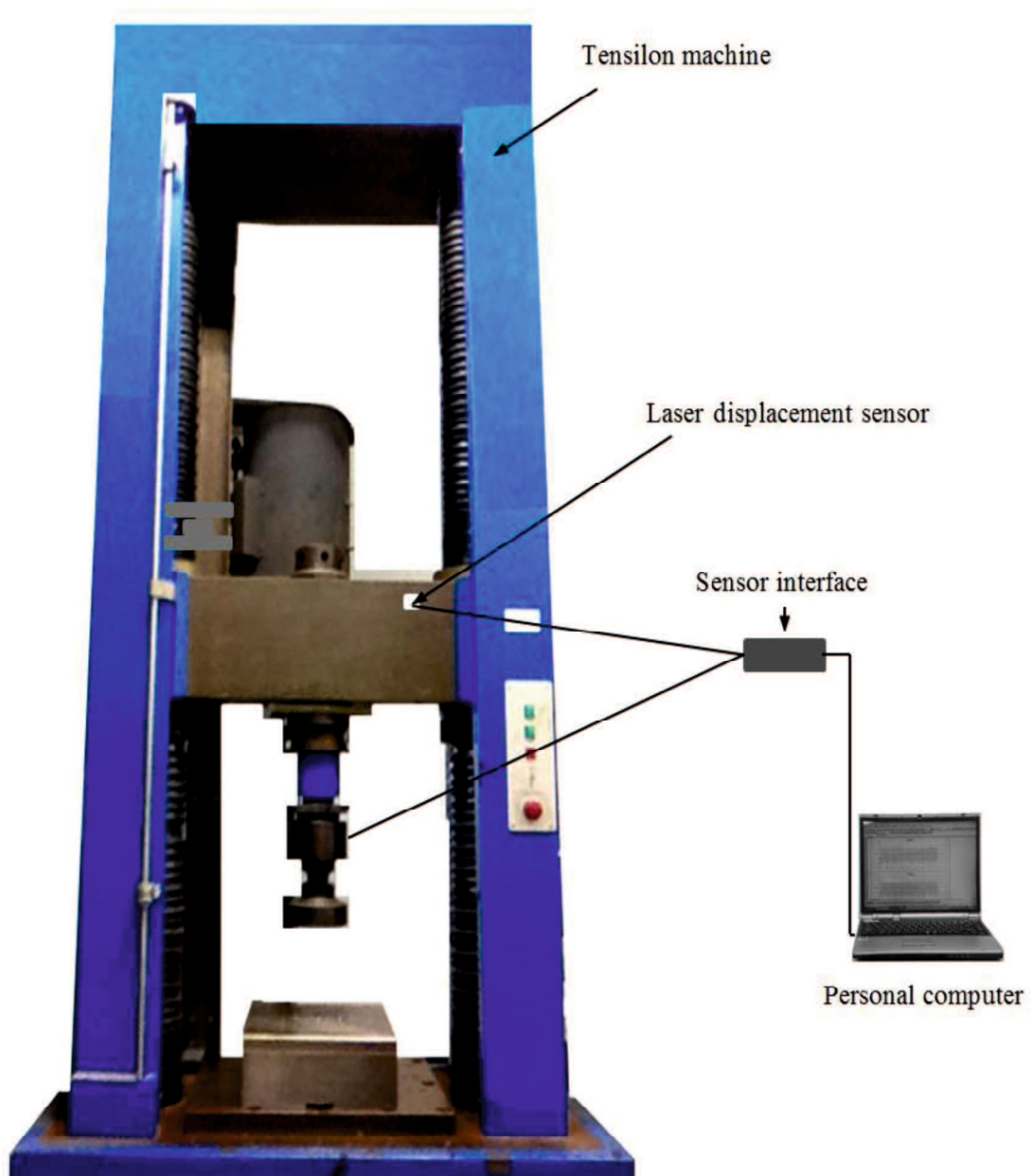


Fig. 6.4 Experimental apparatus



Fig. 6.5 Dies to produce a gasket



Fig. 6.6 Thin metal gasket

The deformation mode of the stainless gasket was investigated using a compression test. The gasket compressed between upper and lower rigid flanges using axial displacement. Both the upper and lower flanges were assumed to be rigid bodies. The lower flange has a fixed boundary condition. The upper flange moved in a downward direction and pressed the gasket. In order to verify the state of gasket deformation, we used silicone rubber. The silicone rubber was sandwiched and compressed between the gasket and upper flange as shown in Fig. 6.7. We did not use lubricating oil to simulate a dry contact condition in the actual environment.

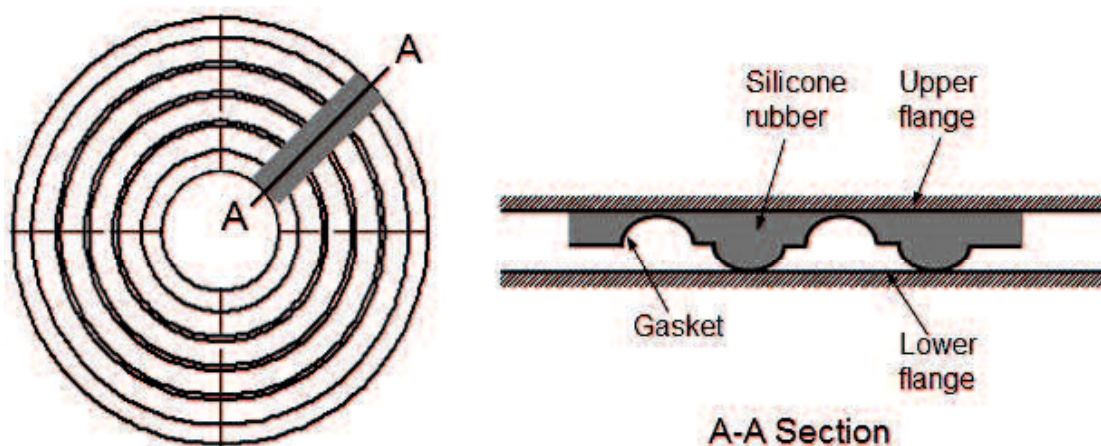


Fig. 6.7 The sandwiching silicone rubber

The experiment gasket deformation results denote using silicone rubber's deformation. Fig. 6.8 shows an example of silicone rubber deformation for the displacement 0 mm, 1 mm, 2 mm, 3 mm, 4 mm, and 5 mm. The characteristic of silicone rubber is very elastic, but the form is not easy to change after unloading condition.

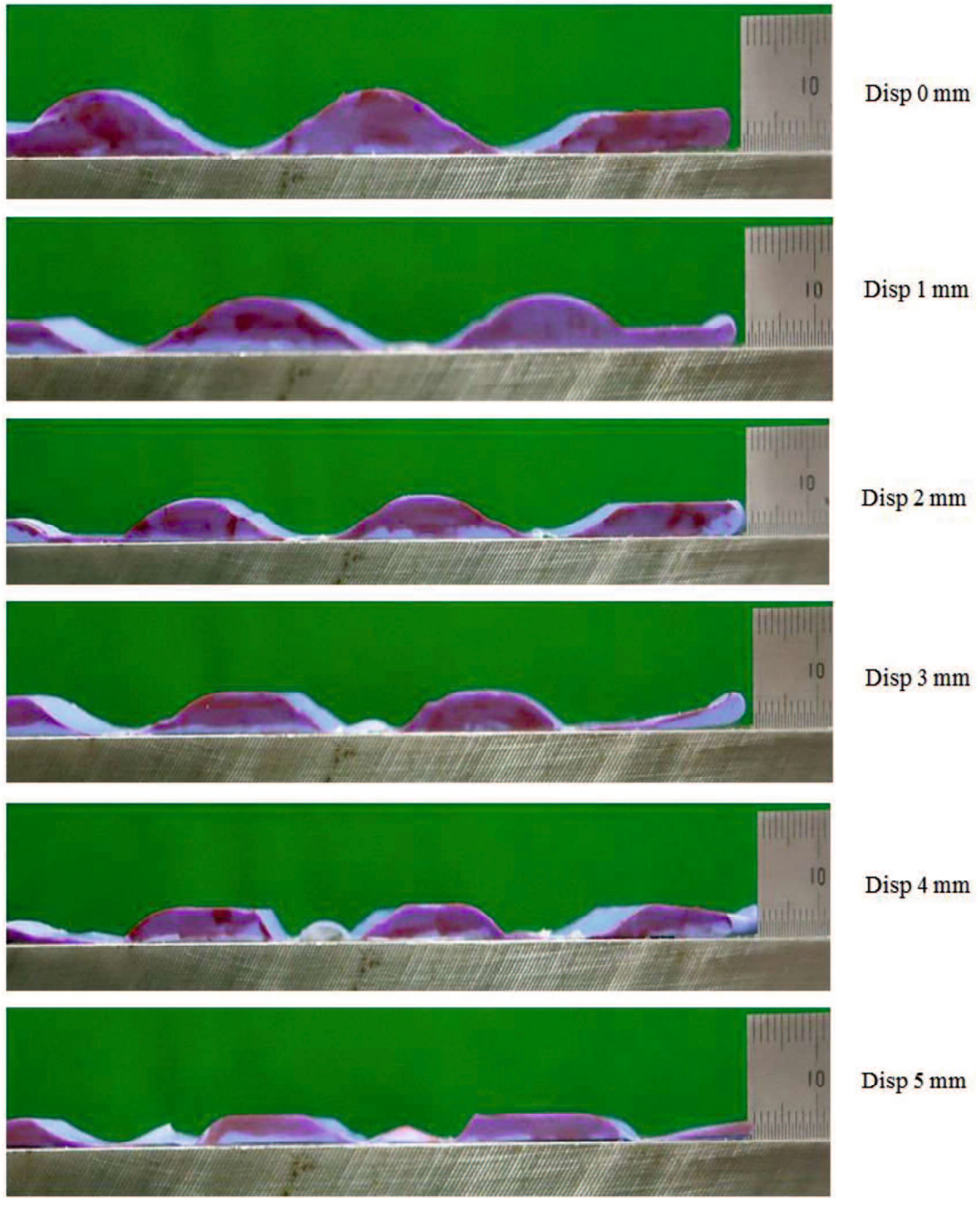


Fig. 6.8 Rubber deformation

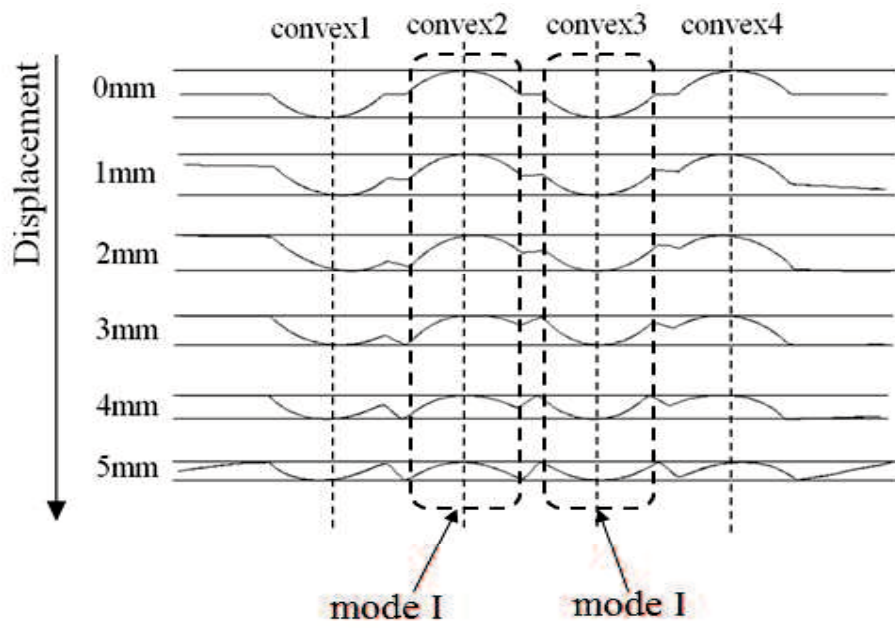
6.2 Results and Discussion

This study discusses of deformation shapes of gasket in the tightening process by an FEM and experimental analysis. Beside that the discussion will continue to curve correlation between the load and displacement in the tightening process for both an FEM and experimental analysis. The distribution maps of the deformation modes by simulation analysis also the important thing in this study. Finally, the displacement-contact stress and contact width curves in the tightening process by simulation analysis.

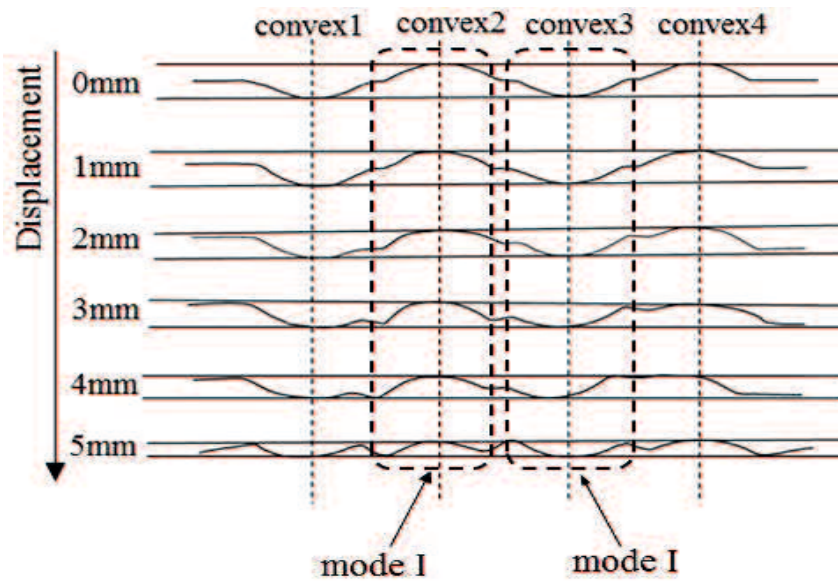
The deformation shapes founded by an FEM analysis and experimental analysis of a gasket having a flat portion $L = 4 \text{ mm}$, 2 mm , and 1.5 mm are shown in Fig. 6.9, 6.10, and 6.11, respectively [55]. Fig. 6.9 shows the deformation shape of the gasket with a flat portion of 4.0 mm . It could be determined that in this gasket, the deformation was concentrated in the flat portion, whereas most of the convex portion 2 and 3 remained un-deformed, we called this deformation mode I. The flat portion deformed because it includes long beam categories which not enough for bending load. This gasket did not provide a good seal because the contact width and the contact stress will not increase significantly.

Fig. 6.10 shows the deformation shape of the gasket with a flat portion of 2.0 mm . The convex portion 3 deformed and the contact width increased with the displacement, we called this deformation mode II. There is no buckling protrusion occurred; it is a good portion for decrease the leakage. Convex portion 2 deformed, but buckling protrusion occurred. We called this deformation mode III. Buckling occurred because the portion is not strong enough for bending load, and it will cause the contact width decrease.

Fig. 6.11 shows the deformed shape of the gasket with a flat portion of 1.5 mm . In the gaskets convex portion 3 deformed and the contact width increased with the displacement, we called this deformation mode II. There is no buckling protrusion occurred. We call the case where convex portion 2 deformed, and buckling protrusion occurred deformation mode III. Characteristic of gasket having flat portion 1.5 is similar with gasket having flat portion 2.0 mm .

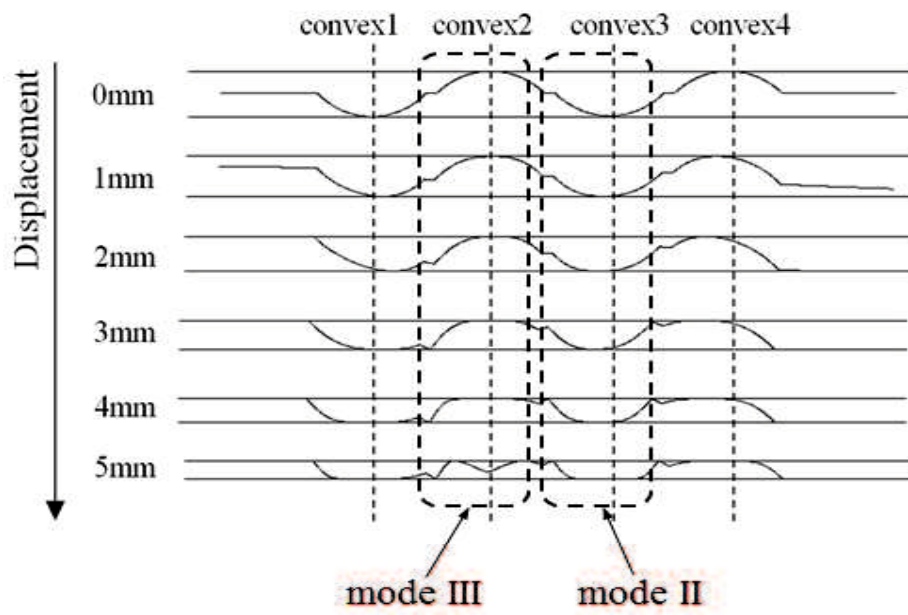


(a) FEM analysis

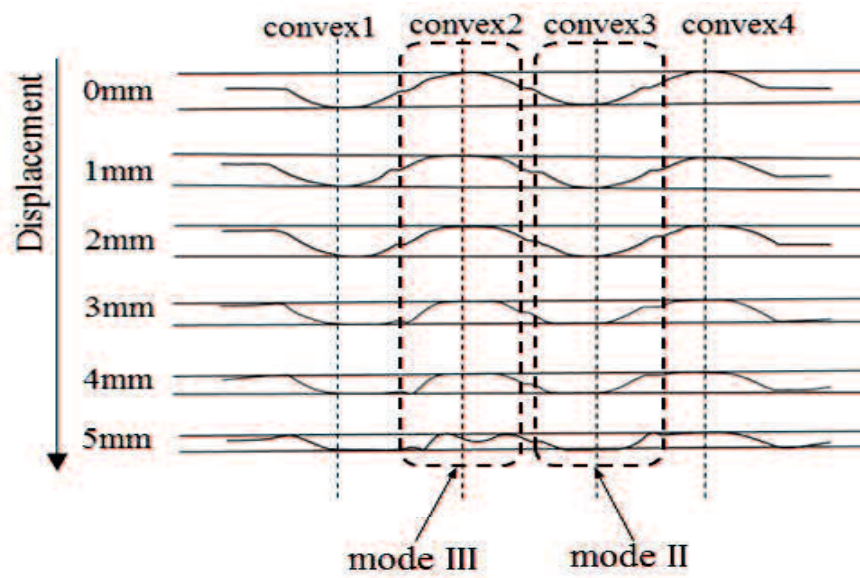


(b) Experiment analysis

Fig. 6.9 Deformation mode for gasket having flat portion of 4.0 mm

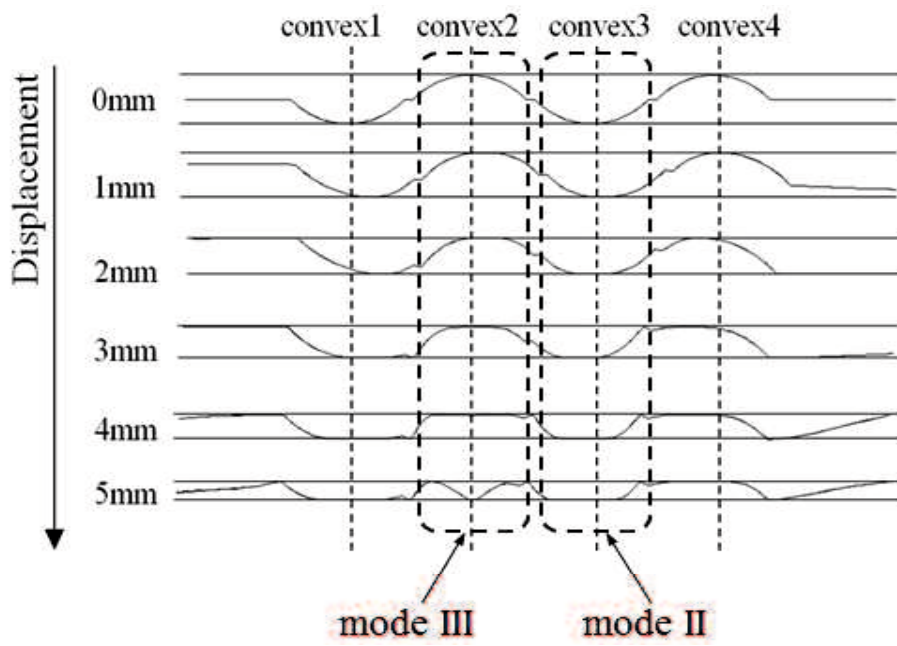


(a) FEM analysis

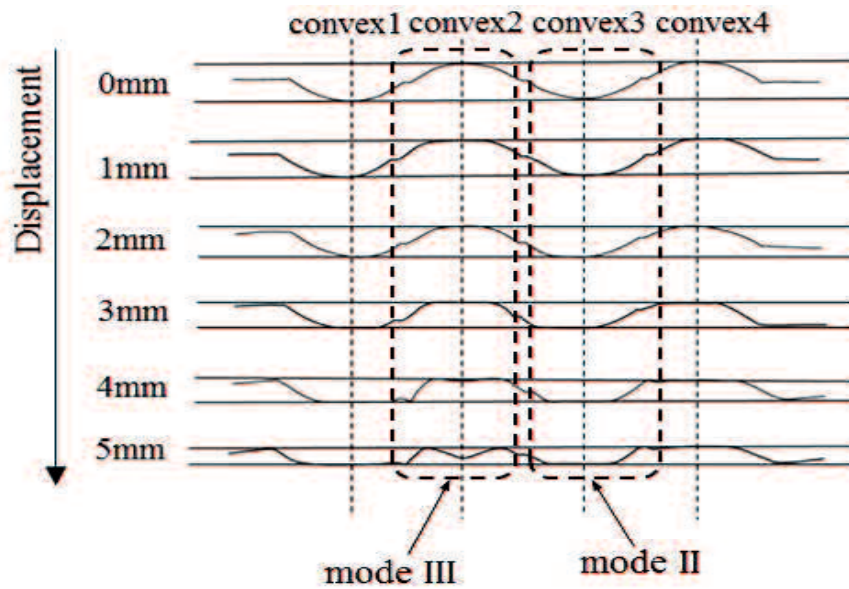


(b) Experiment analysis

Fig. 6.10 Deformation mode for gasket having flat portion of 2.0 mm



(a) FEM analysis



(b) Experiment analysis

Fig. 6.11 Deformation mode for gasket having flat portion of 1.5 mm

The deformation mode II is the best deformation mode because the contact width will increase with the displacement, and there is no buckling protrusion. The deformation mode III is better than deformation number I. It is important to design an optimum thin stainless steel gasket that convex portion 2 and portion 3 have a deformation mode II.

Fig. 6.12 shows a distribution map of the deformation modes of thin stainless metal gasket material. The vertical axis is the aspect ratio of the length of the flat portion to the length of the convex portion, L/D , whereas the horizontal axis is the aspect ratio of the height to the length of the convex portion, h/D . Here, the deformation mode of the thin stainless gasket material has a higher probability of deformation in mode I when L/D increases and h/D in low value. Deformation mode II will happen when L/D in middle value h/D in low value or L/D in high value and h/D in high value. The aspect ratio of the length of the flat portion to the length of the convex portion L/D in low value is the deformation mode III. The deformation maps of the thin stainless gasket material plotted in this study are very important in the design process of the gasket and could function as a key reference in the future [55].

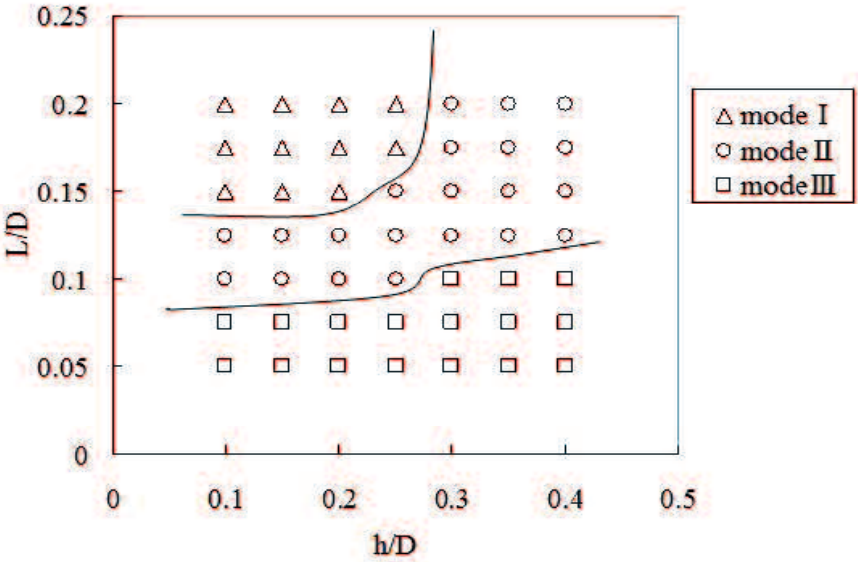


Fig. 6.12 Deformation map for thin stainless gasket material

Fig. 6.13 shows the curve correlation between the load and displacement for both the experimental and simulation analysis results. The load increase tended to be constant for a gasket having a flat portion of 4.0 mm with a displacement between 0–4 mm; after this, the load increased throughout the deformation. It means that the gasket system is not enough strong for bending load, especially for the flat portion. The flat portion deformed before the convex portion deformed. Moreover, for gaskets with flat portions of 1.5 mm and 2.0 mm, the load increased significantly. A relatively high value for the flat portion produced a decreasing load. There was good correlation between the simulation analysis results and experimental data.

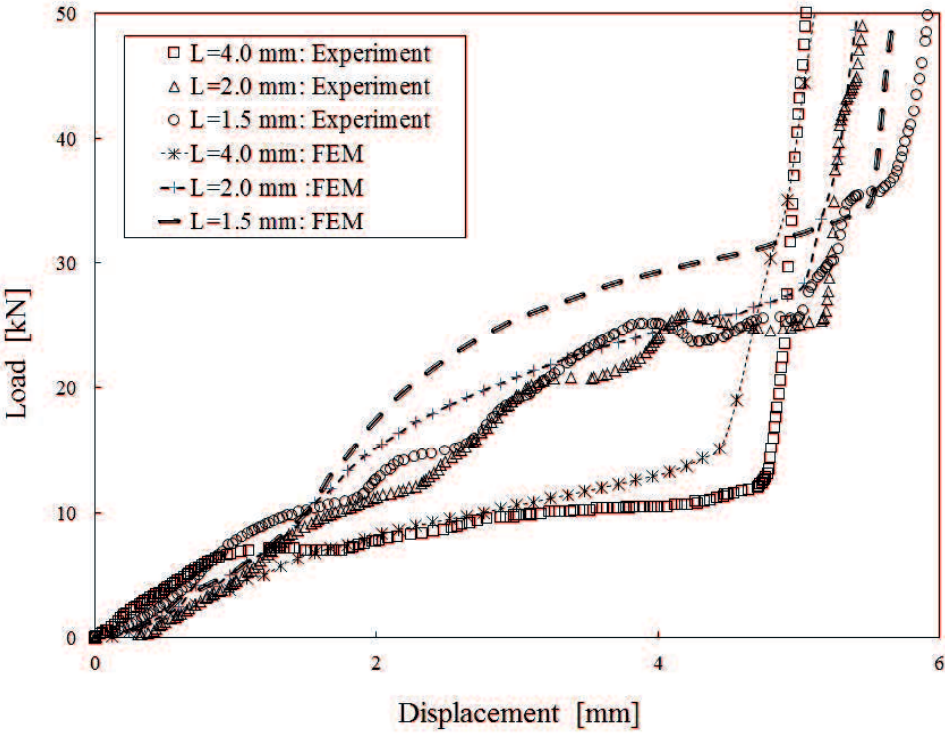


Fig. 6.13 Load–displacement curve

The simulation analysis obtained the displacement-contact stress and width curves.

Fig. 6.14 shows the relationship between the displacement and contact stress analysis results for flat portions of 4 mm, 2 mm, and 1.5 mm. A gasket having a flat portion of 4.0 mm did not provide a good seal because the contact stress did not increase. It is because the elastic portion not enough strong for beam load and deformed before convex portion deformed. In addition, an increase in the displacement increased the contact stress in convex portion 2 (deformation mode II) and convex portion 3 (deformation mode III) for flat portions of 2 mm and 1.5 mm. However, for gaskets with flat portions of 1.5 mm and 2 mm, there was a dent in convex portion 3, shape buckling occurred, and the contact stress decreased rapidly. Therefore, the deformation mode with the best sealing was deformation mode II.

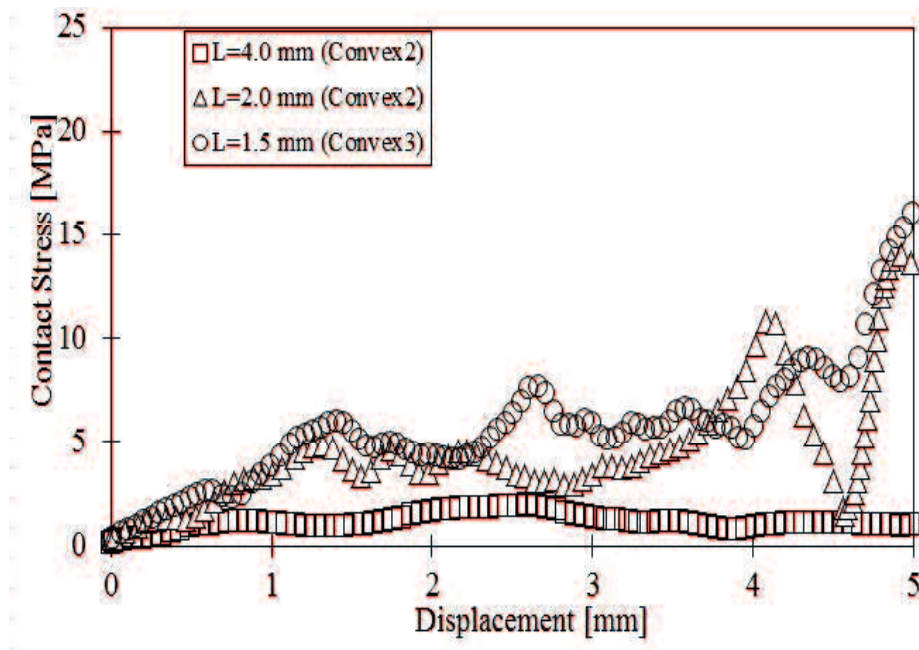


Fig. 6.14 Displacement-contact stress curve

Fig. 6.15 shows the relationship between the displacement and the contact width. In a gasket having a flat portion of 4.0 mm, the contact width in convex portion 2 did not increase when the displacement increased, because the deformation was concentrated in the

flat portion. The contact width in portion 2 for a gasket having a flat portion of 2.0 mm and the contact width in portion 3 for a gasket having a flat portion of 1.5 mm increased significantly when the displacement increase started from 3 mm [55].

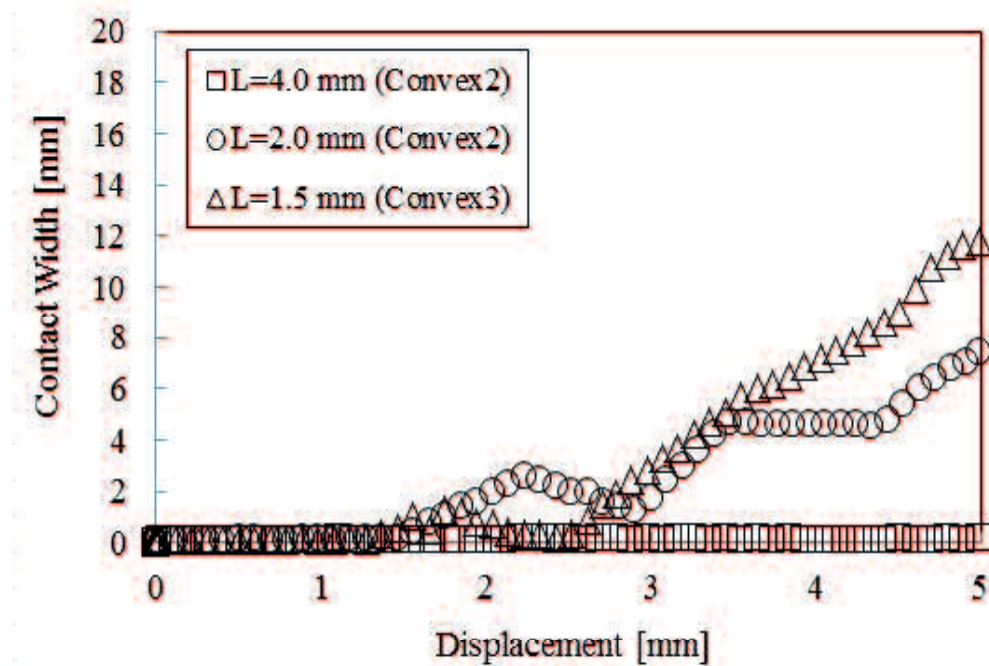


Fig. 6.15 Displacement-contact width curve

6.3 Conclusion

In this research, based on simulation and experimental analyses, we conclude that:

1. By comparing the analytical and experimental results, although some errors occurred, the validity of the finite element model was clarified.
2. Based on the FEM analysis results, the mode analysis could be divided into three types of deformation modes. In deformation mode I, the convex portion was un-deformed whereas the flat portion was deformed. In deformation mode II, the convex portion was deformed whereas the flat portion remained un-deformed. Deformation mode III was the same as deformation mode II, but dent geometrical buckling occurred. Therefore,

deformation mode II provided the best sealing.

3. Increasing the length of the flat portion decreased the load and caused deformation mode III to change to deformation mode II and then deformation mode I.
4. In deformation mode III, although it was possible to obtain both a high contact stress and high contact width, the contact stress rapidly decreased because there was a recessed protrusion.

CHAPTER VII

CONCLUSION

7.1 Summary of Result

The current work is dedicated to finding out the evaluation method of new metal gasket as asbestos substitution which uses a new approach of leak test results and the results of the FEM analysis concerning leakage performance. In this chapter, conclusions from the study are drawn and recommendations are presented for future research.

The three stage work is done to provide the result as follows:

1. The optimum design of the SUS302, 24A-size metal gasket by simulation based on an elastic and plastic contact stress was founded. Forming process for both metal gaskets mode can be done well. Final evaluation is determined by helium leak quantity to check leakage performance of both types of gaskets. According to the leaks that occurred, we find that the gasket 400-MPa mode was better sealing performances than 0-MPa mode. Both types of gasket can be used as a seal, because it did not leak in the helium leak test.
2. The average contact stress for a flange having surface roughness values of 1.5, 2.5, and 3.5 μm was similar. The contact width is a function of surface roughness of flange—it is increases with the surface roughness. The leakage did not occur when real contact width is 0.18 mm. For a low axial force, changes in surface roughness caused a significant change in the leakage; the same was not observed for a high axial force. The real contact width for the gasket 0-MPa mode contact with flange was lower than the gasket 400-MPa mode contact with flange. The gasket contact with flange having surface roughness 1.5 μm shows the longest real contact width both for the gasket 400-MPa mode and the gasket 0-MPa mode. The gasket contact with flange having surface roughness 3.5 μm shows the shortest real contact width both for the gasket 400-MPa mode and the gasket 0-MPa mode. The total differences of measurement between simulation result for real model of surface roughness and experimental result is 7.89 %.

3. Based on the FEM analysis results, the mode analysis could be divided into three types of deformation modes. In deformation mode I, the convex portion was un-deformed whereas the flat portion was deformed. In deformation mode II, the convex portion was deformed whereas the flat portion remained un-deformed. Deformation mode III was the same as deformation mode II, but dent geometrical buckling occurred. Therefore, deformation mode II provided the best sealing. Increasing the length of the flat portion decreased the load and caused deformation mode III to change to deformation mode II and then deformation mode I. In deformation mode III, although it was possible to obtain both a high contact stress and high contact width, the contact stress rapidly decreased because there was a recessed protrusion.

7.2 Future Consideration

Suggestions for future studies are:

1. Under high temperatures, the leak tightness of bolted joints is compromised due to the loss of the bolt load as a result of creep is not only on the gasket and bolt materials but also the flange material. Therefore the effect of creep-relaxation can be continued to maintain the performance of this gasket in the next project.
2. Development of corrugated gasket using material after treatment process.

REFERENCES

- [1] Asbestos is hard to replace as Japan heads for ban, *Sealing Technology* 1 (2006) 1.
- [2] Estrada, H., Parsons, I.D., Strength and Leakage Finite Element Analysis of GFRP Flange Joint, *International Journal of Pressure Vessel and Piping* 76 (1999) pp. 543-550.
- [3] Krishna, M.M., Shunmugam, M.S., Prasad, N.S., A Study on the Sealing Performance of Bolted Flange Joints with Gaskets using Finite Element Analysis, *International Journal of Pressure Vessel and Piping* 84 (2007) pp. 349-357.
- [4] Ross, E., Kockelmann, H., Hann, R., Gasket Characteristics for Design of Bolt Flange Connections of Metal-to-metal Contact Type, *International Journal of Pressure Vessel and Piping* 79 (2002) pp. 45-52.
- [5] Huang, J., Lee, W., Sealing and Mechanical Behaviors of Expanded PTFE Gasket Sheet Characteristic by PVRC Room Temperature Tightness Tests, *Materials Chemistry and Physics* 68 (2001) pp. 180-196.
- [6] Persson B.N.J., Albohr, O., Tartaglino, U., Volokitin, A.I., and Tosatti, E., On the Nature of Surface Roughness with Application to Contact Mechanics, Sealing, Rubber Friction and Adhesion, *Journal of Physics: Condensed Matter* 17 (2005) pp. 1-62.
- [7] Persson B.N.J., Bucher F., and Chiaia B., Elastic Contact between Randomly Rough Surfaces: Comparison of Theory with Numerical Results, *Physical Review Letter* Vol. 65.184106 (2002).
- [8] Persson, B.N.J. and Yang, C., Theory of the Leak-Rate of Seals, *Journal of Physics Condensed Matter*, 20 (2008) pp. 1-11.
- [9] Lorenz B. and Persson B.N.J., Leak-rate of Seal: Comparison of Theory with experiment, *Journal of Euro Physics Letter* 86: 4 (2009).
- [10] Person, B.N.J., Elastoplastic Contact between Randomly Rough Surfaces, *Physical review letters*, vol. 87, Number 11, (2001).
- [11] http://www.valqua.co.jp/products/download/catalog/zy03_1103.pdf, Nippon Valqua Industries Co., Ltd. (ASME data).
- [12] Bouzid A., Chaaban A., Bazergui, The Effect of Gasket Creep-Relaxation on the Leakage Tightness of Bolted Flanged Joints, *Journal of Pressure Vessel Technology* 117 (1995) pp. 71 – 78.
- [13] Saeed, H.A, Izumi, S., Sakai, S., Haruyama, S., Nagawa, M., Noda, H., Development of New Metallic Gasket and its Optimum Design for Leakage Performance, *Journal of Solid Mechanics and Material Engineering* 2: 1 (2008) pp. 105-114.

- [14] Haruyama S., Choiron M.A, Kaminishi K., *A Study of Design Standard and Performance Evaluation on New Metallic Gasket*, Proceeding of the 2nd International Symposium on Digital Manufacturing, Wuhan China, (2009) pp. 107-113.
- [15] Choiron M.A, Haruyama S., Kaminishi K., *Simulation and Experimentation on the Contact Width of New Metal Gasket for Asbestos Substitution*, World Academy of Science, Engineering and Technology, vol. 5, (2011) pp. 1182-1186.
- [16] Schafer B.W., Pekoz T., “Computational modeling of cold-formed steel: characterizing geometric imperfections and residual stresses”, *Journal of Constructional Steel Research* 47 (1998) pp. 193–210.
- [17] Santos Abel D., et.all, The Use of the Finite Element Simulation for Optimization of metal Forming and Tool design”, *Journal of Material Processing Energy* 119 (2001) pp. 152-157.
- [18] Choiron M.A, Haruyama S., Kaminishi K., *Optimum Design of New 25A-size Metal Gasket Considering Plastic Contact Stress*, *International Journal of Modeling and Optimization*, vol. 1, no. 2 (2011) pp. 146-150.
- [19] Widder, E., Gaskets: Surface Finish Effects in Static Sealing, *ASME B46 Seminar* (2004).
- [20] Toxicological Profile for Asbestos, *US Department of Health and Human Services, Public health Service Agency for Toxic Substances and diseases Registry* (2001).
- [21] Kenji Morinaga, Asbestos in Japan, *European Asbestos Conference* (2003).
- [22] The Gasket Company, ISO-9002 Certified. *Gasket Handbook*. Web: www.lamonsgasket.com.
- [23] Rao, S. S., *The Finite Element Method in Engineering*, Elsevier Science & Technology Books (2004).
- [24] Madenci, E. and Guven, I., *The Finite Element Method and Applications in Engineering Using Ansys*, Springer Science-Business Media, LLC (2006).
- [25] Cook, R.D., *Finite Element Modeling for Stress Analysis*, John Wiley & Sons, Inc. (1995).
- [26] Taguchi, G. and Konish, S. *Orthogonal arrays and linear Graphs*. ASI Press, Dearborn, Michigan (1987).
- [27] Person, B.N.J., Contact Mechanics for Randomly Rough Surfaces, *Surface Science Reports* 61 (2006) pp. 201-227.
- [28] Bottiglione, F., Carbone, G., Mantriota, G., Fluid Leakage in Seals: An Approach Based on Percolation theory, *Tribology International* 42 (2009) pp. 731–737.
- [29] Gao, Y.F., Bower, A.F., Kim, K.S., Lev, L., Cheng, Y.T., The Behavior of an Elastic-Perfectly Plastic Sinusoidal Surface Under Contact Loading, *Wear* (2006) pp.

- 145-154.
- [30] Valloire, F.R., Paffoni, B., Progi, R. Load Transmission by Elastic, Elasto-plastic, or Fully Plastic Deformation of Rough Interface Asperities. *Mechanics of Materials* Vol. 33 (2001) pp. 617-633.
 - [31] Greenwood, J.A., Williamson, J.P.B., Contact of Nominally Flat Surfaces, *Proc. Royal Soc. Lond., Ser. A* Vol. 295 (1966) pp. 300-319.
 - [32] Kadin, Y., Kligerman, Y., Etsion, I., Unloading an Elastic-plastic Contact of Rough Surfaces, *Journal of The Mechanics and Physics of Solid* Vol. 54 (2006) pp. 2652-2674.
 - [33] Toshimichi F., Tomohiro T., Finite Element Simulation of Bolt-Up Process of Pipe Flange Connections, *Journal Pressure Vessel Technology* 123 Issue 3 (2001) pp. 282-287.
 - [34] Zhou, H.Q., and GU, B.Q., Investigation into Leakage Behavior of Bolted Flange Connection with Octagonal Gasket, *Advanced Materials Research* 44-46 (2008) pp. 165-171.
 - [35] Lee, C.Y., Lin, C.S., Jian, R.Q., Wen, C.Y., Simulation and Experimentation on the Contact Width and Pressure Distribution of Lip Seals, *Tribology International* 39 (2006) pp. 915-920.
 - [36] Pressure measuring film-FUJI prescale film instruction manual.
 - [37] Noda, NA., Nagawa, M., Shiraishi, F., and Inoue, A., Sealing Performance of New Gasket Flange, *Journal of Pressure Vessel Technology*, vol. 124 (2002) pp.239-246.
 - [38] Fowlkes, W.Y., Creveling, C.M., *Engineering Methods for Robust Product Design*, Massachusetts, MA: Addison Wesley Longman, Inc., (1995).
 - [39] MSC Marc. *User manual* (2007).
 - [40] JIS Z2241, *Method of Tensile Test for Metallic Materials*, Japanese Standards Association (1998).
 - [41] Roy, Ranjit, *A Primer on the Taguchi Method*, Van Nostrand Reinhold (1990).
 - [42] Liu, H., Yuan, J.L., Jin, J., Visualization Simulations for a Cold Press Die, *Journal of Materials Processing Technology*, vol. 129, (2002) pp. 321 – 325.
 - [43] Nurhadiyanto D., Choiron M.A., Haruyama S., Kaminishi K., Optimization of New 25A-size Metal Gasket Design Based on Contact Width Considering Forming and Contact Stress Effect, *World Academy of Science, Engineering and Technology* Vol.6 (2012) pp. 661-665.
 - [44] Nurhadiyanto, D., Choiron, M.A., Haruyama, S., and Kaminishi, K., Contact width evaluation of New 25A-size Metal gasket Considering Forming Effect, *Proceeding of the 8th International Conference on Innovation & Management*, (2011) pp. 296-301.

- [45] JIS B2220, *Steel Pipe Flanges*, Japanese Standards Association, (2004).
- [46] JIS Z2330, *Standard Recommended Guide for the Selection of Helium Leak Testing*, Japanese Standards Association (1992).
- [47] JIS Z2331, *Method of Helium Leak Testing*, Japanese Standards Association (2006).
- [48] Handysurf E-35A/B User Manual, (2010).
- [49] Haruyama, S., Nurhadiyanto, D., Choiron, M.A., Kaminishi, K., Surface Roughness of flange Contact to the 25A-size Metal Gasket by Using FEM Simulation, *World Academy of Science, Engineering and Technology*, Vol. 7 (2013) pp. 565-569.
- [50] Haruyama, S., Nurhadiyanto, D., Choiron, M.A., and Kaminishi, K., Influence of Surface Roughness on Leakage of New Metal Gasket, *International Journal of Pressure Vessels and Piping*, 111-112 (2013) pp. 146-154.
- [51] Haruyama, S., Nurhadiyanto, D., and Kaminishi, K., Contact Width Analysis of Corrugated Metal Gasket based on Surface Roughness, *Advanced Material Research*, Vol. 856 (2014) pp. 92-97.
- [52] JIS B2404, *Dimensions of Gaskets for Use with the Pipe Flanges*, Japanese Standards Association (2006).
- [53] Choiron, M.A., Haruyama, S., Kaminishi, K., Optimization of New Metal Gasket Shape by using Simulation Experiment, *International Journal of Academic Research*, Vol 3 No. 3 (2011).
- [54] Ushijima, K., Haruyama, S., Kaminishi, K., Study on Deformed Mode of Metal Seal Materials Using Elastic Effect, *Proceeding of the 8th International Conference on Innovation and Management*, (2011). pp. 302-306.
- [55] Haruyama, S., Nurhadiyanto, D., Ushijima, K., and Kaminishi, K., and Chen, D.H., Deformation Characteristic of Thin Stainless Gasket Material, *Applied Mechanics and Materials*, Vol. 392 (2013) pp. 3-8.